The OPHELIE mock-up
Final report

H. Van Humbeeck, J. Verstricht, X.L. Li, P. De Cannière, F. Bernier and B. Kursten

EURIDICE report 09-134, January 2009

EURIDICE and its Members, SCK•CEN and ONDRAF/NIRAS, wish to thank all the companies involved, directly or indirectly, in the OPHELIE experiment and in the related research programme for their most valuable contribution to this enterprise.

Foreword and summary

Within the framework of the Belgian Research, Development and Demonstration Programme for final disposal of vitrified high-level radioactive waste in the deep Boom Clay layer, the EURIDICE EIG prepared, constructed, operated and dismantled the OPHELIE mock-up. The mock-up simulated, on the surface, a 2 m diameter (scale 1/1) and 5 m long section of a disposal gallery as considered in the SAFIR-2 design, the reference design valid in the 90s. In this design, 150 litre waste packages are inserted inside a 200 m long stainless steel disposal tube axially centred in the gallery. The space between the disposal tube and the concrete gallery lining is filled with a bentonite-based buffer material. The waste packages are inserted inside the disposal tube once the buffer material is saturated with water.
The function of the disposal tube is to provide full containment for the waste form during the thermal phase (about 500 years) by preventing its contact with water from the Boom Clay host formation. The buffer's role is to provide the disposal tube and the Boom Clay, the main barrier against migration of radio nuclides, with a favourable environment. Close in chemical compatibility with Boom Clay, the main requirements established for the buffer material are:

- a thermal conductivity at least equal to that of Boom Clay (λ_{BC} = 1.7 W/mK) to prevent excessive temperature in the engineered barriers;
- a hydraulic conductivity lower or equal to that of Boom Clay ($k_{H,BC} = 4\ 10^{-12}$ m/s) to avoid hydraulic pathways around the disposal tube, and;
- a sufficient swelling capacity to fill all physical gaps and an adequate swelling pressure (between 4 and 4.5 MPa) to prevent the collapse of the disposal galleries and minimise mechanical constraints on the disposal tube and the host formation.

The main objective of the mock-up was to prepare for the PRACLAY Experiment, which consisted in constructing and operating in-situ a fully instrumented 30 m long pilot gallery to simulate the behaviour of a disposal gallery as defined in the SAFIR-2 design. Except for the heat-emitting vitrified waste packages, which were replaced by electrical heaters, the materials and techniques used had to be as similar as possible to the real ones. More specifically, the initial objective of the mock-up was to verify some practical aspects like the robustness and performance of the sensors in harsh conditions over a period of several years, the specification, manufacture and placement procedures for the buffer material and the hydration process for this material. Taking advantage of such a large-scale infrastructure, the mock-up also served as a preliminary investigation into the buffer material's thermo-hydro-mechanical behaviour and an observation of its evolution, during and after 4.5 years of hydration and heating, through the monitoring and post-mortem analysis programme.

During the experiment's operational stage, unexpected processes and phenomena were observed: corrosion of sensor tubes, a lower than expected swelling pressure, and a high deduced apparent thermal conductivity value. High concentrations of chemical species potentially harmful to the corrosion resistance of metallic components (chlorides up to 1 g/L, reduced sulphur species,…) were also detected. Finally, many sensors failed quite rapidly after the heating phase began. In order to explain these unexpected phenomena and, if possible gain

greater insight into the influence of these phenomena on the performances of the different components of the disposal system, it was decided to carry out a scientific programme in association with the mock-up dismantling that was more extended than initially planned. This extended programme included:

- an investigation of the buffer material's thermo-hydro-mechanical (THM) behaviour, including execution of numerical simulations to help interpret the complex processes (saturation, desaturation, …) which took place in the buffer material. An extended laboratory hydro-mechanical characterisation of the initial material (and exposed for verification purposes) was also carried out, to obtain the parameters required to develop the constitutive law required for the simulations;
- an experimental programme studying the corrosion susceptibility of the different types of stainless steels that were in contact with the buffer material during the operational stage;
- an investigation of the chemical and microbial conditions prevailing in the mock-up to support the corrosion analyses;
- a mineralogical characterisation of the initial and exposed buffer material to verify whether some of the unexpected phenomena could be explained by mineralogical changes;
- a visual inspection of the state of the different types of sensors and an investigation of their failure mode;
- tests to verify whether operational conditions had influenced the mechanical properties of the concrete elements present in the mock-up.

The different stages of the OPHELIE experiment provided a lot useful information.

This allowed better understanding of the problems related to the buffer material. A material satisfying the requirements was developed which was composed of a mixture of FoCa clay (60 wt.%), sand (35 wt.%) and graphite (5 wt.%). Although this remains an expensive process, the manufacture of a large quantity of buffer blocks respecting close dimensional, mechanical and physico-chemical tolerances, their handling and accurate placement in representative conditions (a narrow space) were demonstrated.

Mineralogical changes observed on the exposed buffer material after 4.5 years of hydration and heating were very limited. The main modifications concerned the presence of gypsum where the buffer made contact with the central tube, at the interface with the stainless steel liner at the periphery and in the joints between blocks. The ubiquitous presence of gypsum crystals indicates that the redox conditions were globally still oxidizing in the centre of the mock-up and inside the bentonite blocks.

Overall, from a thermo-hydro-mechanical point of view, the buffer material fulfilled its role: it retained a low hydraulic conductivity/permeability and a high thermal conductivity. All physical gaps were filled by swelling. However, the swelling process was not homogeneous. The swelling mainly occurred close to the liner and the joints between blocks, although closed, remained visible.

In terms of stress-strain relationship, the laboratory THM characterisation programme clearly indicated that the "plasticity yielding" stress of the buffer material decreased upon hydration and heating and that the buffer material possessed a "collapse" potential upon hydration when approaching saturation. These properties explain the lower than expected swelling pressure and its evolution monitored during the experiment. However, the swelling always remained dominant as shown by the filling in of all initial physical gaps as observed during the dismantling. An optimal swelling pressure could be obtained by regulating the dry density of the blocks and optimising the volume and location of the initial physical gaps.

It is difficult to form a conclusion about the degree of saturation reached by the buffer material. According to the quantity of water injected and the numerical simulations, full saturation should have been achieved. However, direct measurements of the saturation degree after dismantling indicated incomplete saturation. Nevertheless, the material's high thermal conductivity values, even when unsaturated, combined with the material's rapid swelling make the installation of waste packages into the disposal tube before complete saturation of the buffer feasible.

One of the most important pieces of information gained through the OPHELIE experiment concerned the evolution of the chemical and microbial conditions with regards to the corrosion of the metallic components present in the mock-up or in an actual repository. The most unfavourable results observed during the experiment were as follows:

- enrichment of chemical species towards the central tube harmful for pitting corrosion (chlorides, …) were identified, combined with an impoverishment of chemical species well known to inhibit corrosion in chloride-containing solution like bicarbonate or sulphate towards the tube. Two mechanisms could explain such enrichment: an advective transport of salts by a water front migrating through the unsaturated buffer during hydration phase or the diffusion of solutes in a temperature gradient (thermo-diffusion or Ludwig-Soret effect);

- dissolved sulphides and, in some samples, thiosulphates, were detected in the hydration circuit water probably caused by a microbially-mediated sulphato-reduction mechanism. Microbial analyses of the water revealed the presence of sulphate-reducing bacteria, thiosulphate-reducing bacteria and methanogenic bacteria at high concentrations. No stringent conclusion can be drawn from the microbial analyses performed on the initial and exposed solid buffer samples: tests performed by two laboratories with different techniques gave contradictory results. The large amounts of dissolved organic carbon measured in the water could have contributed to fuelling the microbial activity. The source could be the organic matter naturally present in FoCa clay or hydrocarbons (a mixture of gasoline and oil) released by defective Glötzl cells as observed during the dismantling operations;

- pH values as low as 5 (instead of 8.5 for the fresh $NaHCO_3$ water used to hydrate the mock-up) were measured in the hydration system along with a high content of dissolved CO_2. The source of the CO_2, or conversely the reason for the acidification, remains unclear. Two mechanisms can be suggested: production by microbial activity in the

hydration system or decarboxylation by the thermal stress of the natural organic matter present in FoCa clay.

Despite these unfavourable chemical conditions, no significant signs of corrosion could be detected on the AISI 321 central tube in contact with the bentonite. The resistance of the AISI 304 used as a liner for the steel jacket was barely lower. It exhibited a corrosion resistance which was better than initially expected: corrosion spots were only detected at points with technological artefacts like welding points. These problems could be avoided in the future by applying appropriate techniques.
The most striking observation in dealing with corrosion in the mock-up was certainly the general corrosion of the AISI 316L hydration tube #7. A failed relative humidity sensor was discovered not far from this tube and it is very probable that the electrolysis induced by the direct current applied to this sensor for several years was the cause for this highly spectacular corrosion.
Nevertheless, the favourable behaviour of these varieties of stainless steel has to be confirmed over a longer time period.

The post-mortem tests performed on the concrete samples showed that mechanical resistance was not affected by the mock-up conditions.

The lessons learnt from the instrumentation programme will be taken into account in the framework of the PRACLAY Experiment. Except for the thermocouples, a large number of sensors failed during the experiment's operational stage. For some of them, the failure occurred quite rapidly. These issues may have been related to the design of the sensors themselves, the cables and their connection with the sensors or the installation operation. Most critical was the watertightness of the sensors and cables. Corrosion seemed to be the worst enemy in this critical aspect.
Another issue was the sensors' temperature range. Several sensor types could not cope with the temperatures prevailing in the mock-up.
Besides the loss of data, the OPHELIE experiment showed that the failure of the sensors may also jeopardise the performances of the engineered barriers (e.g., galvanic/electrolytic corrosion, or contamination by hydrocarbons, as observed in the mock-up).
For the PRACLAY Experiment, an extended preliminary selection of the sensors followed by a detailed test programme including corrosion aspects will be necessary to guarantee the long-term reliability of the sensors in harsh conditions with elevated temperature and pressure.

After the evaluation of the RD&D programme summarised in the second Safety and Feasibility Assessment Report (SAFIR-2 report) in 2001, ONDRAF/NIRAS decided to discard the reference design. Among other things, the results of the OPHELIE experiment, and more specifically the high concentration of chlorides observed influenced this decision. Consequently, the in-situ PRACLAY Experiment was redefined.

Having completed the OPHELIE experiment, EURIDICE has summarised the results, information and lessons learned through the different stages of the experiment in this document.

Table of content

1. INTRODUCTION 1

2. OBJECTIVES OF THE OPHELIE EXPERIMENT 7

2.1. PREPARATION OF THE PRACLAY EXPERIMENT 7

2.2. INVESTIGATION OF THE THM BEHAVIOUR OF THE BUFFER MATERIAL AND INTERACTIONS WITH THE OTHER COMPONENTS 8

2.3. EXTENSION OF THE SCIENTIFIC PROGRAMME ASSOCIATED WITH THE MOCK-UP DISMANTLING 8

3. DESIGN, MANUFACTURING AND ASSEMBLY OF THE MOCK-UP 11

3.1. THE METALLIC STRUCTURE 12

3.1.1. The main jacket and the covers 12

3.1.2. The central tube 13

3.2. THE HYDRATION SYSTEM 14

3.3. THE BUFFER MATERIAL 15

3.4. THE CONCRETE RING 16

3.5. THE HEATING SYSTEMS 16

3.5.1. The internal heating system 17

3.5.2. The external heating system 18

3.5.3. The thermal insulation 19

3.6. FINISHING THE MOCK-UP ASSEMBLY AFTER PLACEMENT OF THE BUFFER MATERIAL 19

4. REQUIREMENTS, SPECIFICATIONS, MANUFACTURING AND EMPLACEMENT OF THE BUFFER MATERIAL 21

4.1. ROLES AND REQUIREMENTS OF THE BUFFER MATERIAL 21

4.2. DEVELOPMENT PROGRAMME 22

4.2.1. Preliminary bibliographic studies 22

4.2.2. Choice of the buffer composition: the three phases of the development programme 23

4.3. BUFFER BLOCKS MANUFACTURE AND CONTROLS 24

4.3.1. Manufacturing of the buffer blocks 25

4.3.2. Dimensional and physico-chemical controls 25

4.4. PLACEMENT OF THE BUFFER MATERIAL TOGETHER WITH THE SENSORS 27

4.4.1. Objectives 27

4.4.2. Placement of the buffer blocks 28

5. THE OPERATIONAL STAGE AND THE ASSOCIATED INSTRUMENTATION PROGRAMME 31

5.1. THE INSTRUMENTATION PROGRAMME 31

5.1.1. Thermocouples 32

5.1.2. Internal strain gauges 33

5.1.3. Piezometers 34

5.1.4. Total pressure transducers 34

5.1.5. Relative humidity cells 35

5.1.6. Instrumented bolts 35

5.1.7. External strain gauges 36

5.1.8. Concrete pressure and load cells 36

5.1.9. Pressure sensors for the hydration system 37

5.1.10. Data acquisition system 37

5.1.11. Monitoring the movements of the central tube 38

5.2. MAIN PHASES OF THE OPERATIONAL STAGE 38

5.2.1. Preliminary test 38

5.2.2. Heating phase 38

5.2.3. Cooling phase 40

5.3. UNEXPECTED PHENOMENA AND PROCESSES OBSERVED DURING THE OPERATIONAL STAGE 40

5.3.1. Thermal and hydro-mechanical evolution of the buffer material 40

5.3.2. Corrosion of sensor tubes and presence of chemical and microbial species 42

6. DISMANTLING: PREPARATION AND OPERATIONS 45

6.1. DISMANTLING DOSSIER 45

6.2. ESTABLISHMENT OF THE SCIENTIFIC PROGRAMME ASSOCIATED WITH THE DISMANTLING 46

6.2.1. Reduction of the initial programme: context and criteria 46

6.2.2. Content of the dismantling programme 47

6.3. DISMANTLING OPERATIONS 48

6.3.1. Work organization 48

6.3.2. Sampling methodology 48

6.3.3. Packaging, labelling and interim storage 50

6.3.4. Documentation, QA/QC aspects 50

6.3.5. Dismantling operations 51

6.3.6. Preliminary buffer core drilling 51

6.3.7. Removal of internal components 51

6.4. MAIN CONCLUSIONS 52

7. GLOBAL BEHAVIOUR OF THE BUFFER MATERIAL: OBSERVATIONS MADE DURING DISMANTLING 55

7.1. MAIN OBSERVATIONS MADE JUST AFTER THE REMOVAL OF THE COVER: FILLING SAND MOVEMENT AND STATE OF THE CONCRETE SEGMENTS 55

7.2. GLOBAL BEHAVIOUR OF THE BUFFER MATERIAL 56

8. MINERALOGICAL AND CHEMICAL EVOLUTION OF THE EXPOSED BUFFER MATERIAL 59

8.1. INTRODUCTION 59

8.2. MATERIALS AND METHODS 60

8.3. MINERALOGICAL ANALYSIS OF THE INITIAL AND EXPOSED MATERIALS: MAIN RESULTS 61

8.4. CHEMICAL ANALYSES AND MOBILITY OF ELEMENTS IN A THERMAL GRADIENT 63

8.5. CATION EXCHANGE CAPACITY AND EXCHANGEABLE IONS POPULATION 65

8.6. REDOX FRONT – REDOX STATES IN THE MOCK-UP 66

8.7. MICROSCOPY STUDIES AND CHARACTERISATION OF THE JOINS 67

8.8. COMPARISON WITH THE HEATING TESTS MADE AT THE STRIPA MINE 69

8.9. CONCLUSIONS 70

9. PORE WATER CHEMISTRY AND MICROBIAL ACTIVITY 73

9.1. INTRODUCTION 73

9.2. MAIN RESULTS 74

9.2.1. Movement of solutes in a thermal gradient 74

9.2.2. Sulphides and microbially-mediated sulphate reduction 78

9.2.3. Microbial activity and perturbation of the water chemistry in the hydration system 81

9.2.4. Source of organic carbon in the mock-up 82

9.2.5. pH, E_h and pCO_2 conditions 83

9.2.6. CO_2 production 85

9.2.7. Origin of the water chemistry perturbation 86

9.2.8. Microbial reductive perturbation 86

9.2.9. Decomposition of organic matter exposed to moderate thermal stress 87

9.3. IMPLICATIONS OF THE PORE WATER CHEMISTRY FOR THE METAL CORROSION 88

9.3.1. Lessons learnt for the chemistry and the microbiology of the bentonite buffer. 88

9.3.2. Potential consequences for the corrosion studies 89

9.3.3. Implications for long-term monitoring instrumentation 90

9.3.4. Recommendations for the PRACLAY in-situ Experiment 91

9.3.5. Recommendations for the design of a deep repository 91

9.4. CONCLUSIONS 92

10. CORROSION OF THE METALLIC COMPONENTS 94

10.1. INTRODUCTION 94

10.2. CONTENT OF THE CORROSION ANALYSIS PROGRAMME 94

10.3. INVESTIGATIONS DURING DISMANTLING 94

10.3.1. Visual inspection 95

10.3.2. E_{CORR} and pH measurements 98

10.4. POST-DISMANTLING ANALYSES 98

10.5. CONCLUSIONS 109

11. PERFORMANCES OF THE MONITORING EQUIPMENT 109

11.1. INTRODUCTION 112

11.2. SENSOR PERFORMANCES 112

11.2.1. Table of performances 112

11.2.2. Thermocouples 112

11.2.3. Internal strain gauges TML 113

11.2.4. Geokon piezometers 115

11.2.5. Kulite total pressure cells 115

11.2.6. Rotronic relative humidity cells 117

11.2.7. RocTest segment pressure cell 118

11.2.8. Glötzl segment pressure cell 119

11.2.9. Glötzl segment load cell 120

11.2.10. External strain gauges 121

11.2.11. Bolt load cells (Bienfait) 121

11.3. PERFORMANCE OF OTHER MONITORING EQUIPMENT 122

11.3.1. Druck external pressure transmitters 122

11.3.2. E+H differential pressure transmitter 122

11.3.3. Electric power transducers 122

11.4. CONCLUSIONS 122

12. THERMO-HYDRO-MECHANICAL BEHAVIOUR OF THE BUFFER MATERIAL 124

12.1. INTRODUCTION 124

12.2. CHARACTERIZATION OF THE BUFFER MATERIAL 125

12.2.1. Outline of the laboratory tests 125

12.2.2. Conclusion of the laboratory tests ... *125*

12.3. NUMERICAL SIMULATIONS OF THE MOCK-UP ... 126

12.3.1. LAGAMINE finite element code: main principles ... *127*

12.3.2. Hypothesis and modelling procedure ... *127*

12.4. TEMPERATURE EVOLUTION IN THE MOCK-UP ... 129

12.5. HYDRO-MECHANICAL BEHAVIOUR ... 132

12.5.1. Hydraulic behaviour: analysis of the saturation state of the mock-up ... *132*

12.5.2. Mechanical behaviour: swelling performances ... *138*

12.5.3. Movements of the central tube ... *141*

12.6. CONCLUSIONS ... 142

13. BEHAVIOUR OF THE CONCRETE SEGMENTS ... 144

13.1. EVOLUTION OF THE MECHANICAL PROPERTIES OF THE CONCRETE SEGMENTS: RESULTS 144

13.1.1. Overview of the different tests ... *144*

13.1.2. Original specifications ... *144*

13.1.3. Sampling ... *145*

13.1.4. Compressive and tensile strength results ... *146*

13.1.5. Elastic modulus Ec ... *146*

13.2. CONCLUSION ... 146

14. CONCLUSIONS ... 148

14.1. DEVELOPMENT AND IMPLEMENTATION OF THE BUFFER MATERIAL ... 148

14.2. HYDRATION PROCESS AND THERMO-HYDRO-MECHANICAL BEHAVIOUR OF THE BUFFER MATERIAL ... 149

14.3. MINERALOGICAL EVOLUTION OF THE BUFFER MATERIAL ... 150

14.4. CHEMICAL AND MICROBIAL BEHAVIOUR OF THE MOCK-UP AND INFLUENCE ON THE METAL COMPONENTS ... 150

14.5. PERFORMANCE OF THE MONITORING EQUIPMENT ... 152

14.6. GENERAL/PRACTICAL LESSONS OF THE EXPERIMENT – PROJECT MANAGEMENT ... 152

LIST OF ABBREVIATIONS 154

APPENDIX 1 DESIGN AND COMPOSITION OF THE MOCK-UP METALLIC STRUCTURE 160

APPENDIX 2 ESTABLISHMENT OF THE THERMAL CONDITIONS 162

APPENDIX 3 POSITIONS OF THE INTERNAL SENSORS 166

APPENDIX 4 CHARACTERISTICS OF THE BUFFER MATERIAL..... 170

REFERENCES..... 182

1. Introduction

For more than a quarter of a century, Belgium has been studying the long-term management of long-lived intermediate level waste (ILW-LL) and high-level waste (HLW). The studies have focussed primarily on final disposal in Boom Clay, a 100 m thick poorly indurate clay formation present, notably at a depth of between 180 and 280 m, under the Mol/Dessel nuclear area.
The Research, Development and Demonstration (RD&D) Programme was launched in 1974 by the Belgian Nuclear Research Centre, SCK•CEN. In 1985, management of the programme was taken over by ONDRAF/NIRAS, the Belgian Agency for Radioactive Waste and Enriched Fissile Materials.

Since the programme began, different designs for vitrified HLW have been developed. The reference design valid in the 90's was the so-called SAFIR-2 design (Figure 1-1). In this design 150 litre waste packages are disposed of in a network of 2 m diameter and 200 m long horizontal galleries lined with 25 cm thick concrete segments. The disposal gallery is firstly fitted with a stainless steel disposal tube approximately 50 cm in diameter. The space between the disposal tube and the gallery lining is then filled with a clay-based buffer material made up of pre-fabricated blocks installed in three concentric rings. Once the buffer material has been saturated with water, the waste canisters are pushed into the disposal tube one by one. The thermal conductivity of the buffer material is therefore optimal when the waste is installed because of the water uptake and the associated swelling process limiting the presence of voids. Once the waste installed over the entire length, a sealing plug and welded cover are installed to isolate the disposal gallery from the main gallery.

The waste concerned is vitrified HLW coming from the reprocessing by COGEMA at La Hague (France) of spent fuel used in the Belgian nuclear power plants. In the beginning of the 90s, direct disposal of spent fuel was not considered. The vitrified HLW was thus considered to be the most difficult as regard disposal because of thermal and radiological aspects.

The role of the disposal tube is to provide the waste form with a perfectly watertight surrounding during the thermal phase (typically during the first 500 years) avoiding contact with the water from the Boom Clay host formation. The buffer provides a favourable environment for the disposal tube and host formation to allow these barriers to fulfil their respective roles.

In 1989, ONDRAF/NIRAS initiated the PRACLAY Project (PReliminAry demonstration test for CLAY disposal). This was aimed at demonstrating the technical and economic feasibility of the repository design on a large scale and using a direct experiment. Among other things, the PRACLAY Project involved the construction (from the URF HADES) and operation of a fully instrumented pilot gallery geometrically identical, except with the length limited to 30 m, to a disposal gallery, as defined in the SAFIR-2 design. Except for the heat emitting vitrified waste canisters which were replaced by electrical heaters, the materials and techniques used had to be as similar as possible to the real ones. This large scale in-situ experiment was known as the 'PRACLAY Experiment'.

To conduct the PRACLAY Project, ONDRAF/NIRAS and SCK•CEN joined their efforts and created an Economic Interest Group (EIG, a special form of consortium under European Union regulations) called the EURIDICE EIG (European Underground Research Infrastructure for DIsposal of nuclear waste in Clay Environment) to handle the extension of the URF with a second access shaft and a connection gallery.

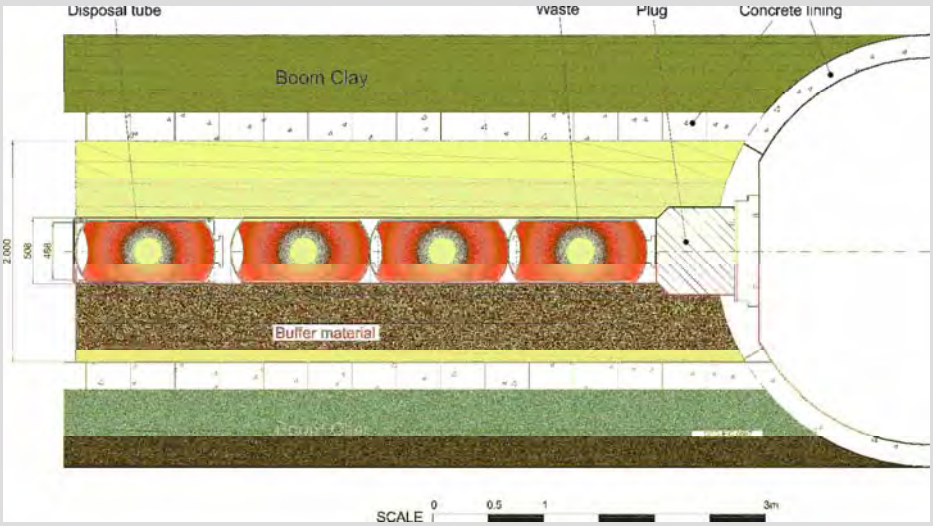

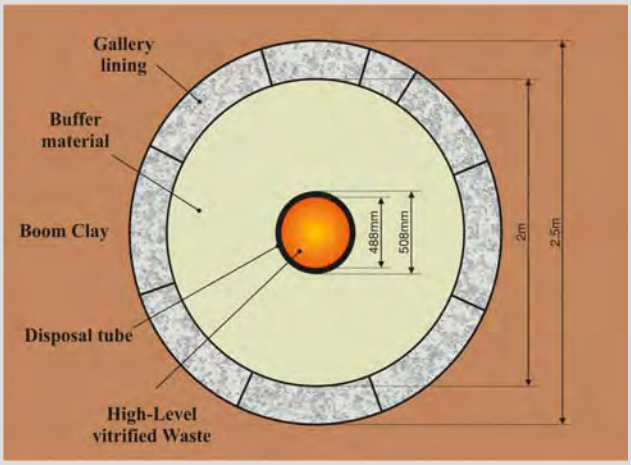

Figure 1-1: Longitudinal (TOP) and cross (BOTTOM) sections of a disposal gallery as defined in the SAFIR-2 design.

As several technical aspects of the in-situ test had not yet been worked out in detail, in 1995 ONDRAF/NIRAS and EURIDICE decided to first construct and operate a large scale surface mock-up called OPHELIE (On-surface Preliminary Heating simulation Experimenting Later Instruments and Equipments).

The mock-up simulated the engineered barriers of the disposal system as far as the disposal tube and the buffer material are concerned. Its design (except for the length which was limited to 5 m, and the gallery lining and host formation which were simulated by a cylindrical steel jacket) and the temperature, hydration and pressure conditions were as similar as possible to the in-situ ones.

The mock-up was constructed and put into operation in 1997 for about 4.5 years. The initial objective of the mock-up was to prepare for the PRACLAY Experiment. More specifically, it was intended to verify some practical aspects like the robustness and performance of the sensors in harsh conditions over a period of several years, the manufacture and placement procedure for the buffer material and the hydration process for this material. Taking advantage of such large scale infrastructure, the mock-up also served as a preliminary

investigation into the buffer material's thermo-hydro-mechanical (THM) behaviour and an observation of its evolution after several years of hydration and heating.

These objectives have been satisfied through the different stages of the OPHELIE experiment, the preliminary studies, the construction and assembly stage, the operational stage, the dismantling operation and the post-dismantling analysis programme and modelling work. A schedule of these different stages is given in Figure 1-2.

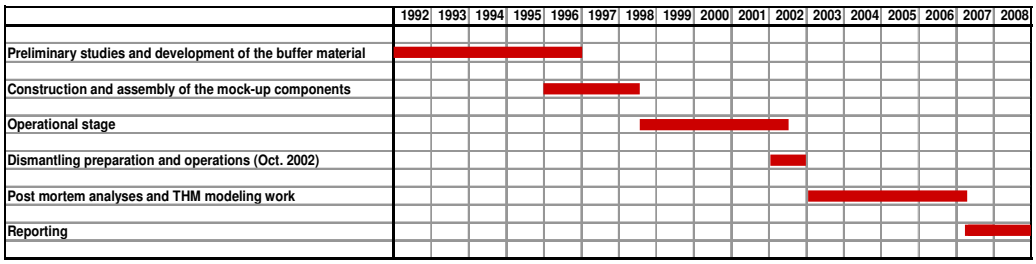

Figure 1-1: Schedule of the OPHELIE mock-up experiment.

Initially, a limited post-mortem analysis programme was envisaged including measurements of the physico-chemical and basic THM properties of the exposed material for comparison with the values of the initial material.
Some unexpected phenomena were observed during the experiment's operational stage. In order to explain these phenomena and to assess the ability of the buffer material and disposal tube to play their roles more fully , the dismantling programme was extended.

Many important results were acquired during the different stages of the experiment. The mock-up experiment made it possible to review the options chosen for the reference design.
In 2001, after evaluating the RD&D programme summarised in the second Safety and Feasibility Assessment Report (SAFIR-2 report, ONDRAF/NIRAS, 2001), ONDRAF/NIRAS decided to discard the reference design. The results of the OPHELIE experiment significantly influenced these decisions. Consequently, the objectives and design of the in-situ PRACLAY Experiment were redefined.

To avoid the loss of knowledge and know-how, it is essential to ensure the traceability of all the steps in the OPHELIE mock-up experiment and gather all the data collected in a final report.

This final report is structured as follows:

- chapter 2 presents the objectives of the mock-up experiment;
- chapter 3 describes the design of the mock-up and the component manufacture and assembly;
- chapter 4 describes the development programme and the manufacture and placement of the buffer material;

The term **"initial material/block"** is used for buffer blocks that were not exposed to the experimental conditions of the mock-up test. Other terms like "reference", "as-compacted" or "as-fabricated" material/ blocks can be found in this report and appended documents.

The term **"exposed material/blocks"** is used for the material subjected to the mock-up conditions.

- chapter 5 presents the experiment's operational stage. It describes the associated instrumentation programme, the main phases of the operational stage and the unexpected phenomena observed;
- chapter 6 describes the dismantling operations. It also gives an overview of the content of the scientific programme associated with the mock-up dismantling and the procedure for establishing it;
- chapter 7 summarises the main observations made during the dismantling operations on the buffer material's overall behaviour and performance.

Chapters 8 to 13 are dedicated to the results of the scientific programme associated with the experiment. They bring together the information gained during the operational stage, the dismantling operations and the post-dismantling programme. More specifically:

- chapter 8 presents the main results of the mineralogical and physico-chemical analyses performed on the initial and exposed buffer materials;
- chapter 9 presents the chemical (pore water) and microbial conditions prevailing in the mock-up. It discusses the influence of these conditions on the corrosion resistance of the metallic components;
- chapter 10 gives the results of the programme dedicated to the corrosion analysis of the steel components;
- chapter 11 summarises the performances of the different types of sensors installed in the mock-up;
- chapter 12 presents the THM behaviour of the buffer;
- chapter 13 gives the results of the tests performed to verify the evolution of the mechanical properties of the concrete segments;

Finally, chapter 14 provides the general conclusions and the lessons learnt throughout the entire experiment.

There are detailed reports for the studies related to chapters 8, 10, 11 and 12. The information given in these chapters constitutes a summary of these detailed reports. There is no such detailed report for the studies dedicated to the chemical and microbial behaviour of the buffer material (chapter 9). For this reason, there is a greater level of detail in this chapter.

Four appendixes are appended to this report:

- appendix 1 gives a schematic view of the metallic structure of the mock-up with the chemical composition of the components;
- appendix 2 describes how the thermal conditions were defined and reproduced in the OPHELIE mock-up;

- appendix 3 gives the positions of the sensors installed inside the mock-up;
- appendix 4 is specifically related to the characteristics of the buffer material. So, it complements chapters 8, 9 and 12 by presenting the mineralogical composition of the FoCaPr clay and the physico-chemical and THM (intrinsic) properties of the buffer material obtained from the laboratory characterisation programme.

2. Objectives of the OPHELIE experiment

The main objectives of the OPHELIE experiment were to prepare the in-situ PRACLAY Experiment (NIROND 97-06) and investigate the THM behaviour of the buffer material and its interactions with the other components, especially the disposal tube on a large scale. During the experiment, the objectives were extended.

2.1. Preparation of the PRACLAY Experiment

The OPHELIE experiment had to confirm several choices initially made for the in-situ PRACLAY Experiment in order to boost confidence in the successful outcome of this important milestone for the Belgian RD&D Programme for final disposal of HLW.

With regards the buffer material, the objectives of the mock-up were as follows:

- to develop a material that complied with the requirements established for the buffer;
- to verify the possibility of manufacturing a large quantity of buffer blocks using a (semi) industrial technique and respecting the tolerances set for the dimensions, physico-chemical and mechanical properties;
- to verify the placement procedure for the blocks and simultaneously with the various sensors without damaging measurement wires or tubes.

Another important objective of the OPHELIE experiment was to fine tune the hydration and heating phases. In an actual repository, the waste canisters are inserted inside the disposal tube once the buffer material has been saturated. In the case of the PRACLAY Experiment, the waste insertion was simulated by switching on the heating system. The following information was expected from the OPHELIE experiment:

- the time needed for the buffer material to reach saturation in order to verify whether it was compatible with the schedule for the PRACLAY Experiment and the optimised operation period of an actual repository. No set limit for the saturation time was fixed beforehand. A period of less than two years was considered acceptable;
- if the saturation period was longer than the acceptable limit mentioned above, to verify whether satisfactory conditions were met to install the waste canisters inside the disposal tube before saturation without risking the system's safety. The main two fixed conditions were sufficient overall heat transfer including the filling by swelling of all initial physical gaps.

Verifying the robustness and performance of the sensors in harsh conditions over several years was also one of the OPHELIE experiment's main objectives. Once installed in and around the future PRACLAY gallery, the instruments have to work for the entire test period in harsh pressure and temperature conditions and in contact with the saturated medium without any possibility of retrieval for repair or recalibration. The correlation between measurements, resistance to leakage and corrosion, the risk of component disturbances induced by sensor failures, and the influence of the location were the expected outcomes from the mock-up test.

Proving the feasibility of placing a disposal tube in a narrow disposal gallery by checking that a tube segment (of around 3 m in length) could be positioned accurately and welded to a previous one was initially considered as one of the experiment's objectives. However, this was skipped when drawing up the list of specifications in order to limit the complexity (quality control) and delivery time of the mock-up structure. It was decided that this aspect could be tested more effectively in a separate set-up that would not interfere with the mock-up experiment.

2.2. Investigation of the THM behaviour of the buffer material and interactions with the other components

This was the first time that such a large quantity of the developed buffer material was hydrated and heated under conditions similar to those expected in-situ. The mock-up constituted a unique opportunity to investigate the THM behaviour of the buffer subjected to these conditions coupled with the interactions with the central tube (simulating the disposal tube) and other components on a large scale. This investigation was carried out by:

- monitoring, during the experiment's operational stage, both the time and space evolution of parameters like the temperature, pore water pressure, relative humidity, swelling pressure in the buffer, total stress on the jacket as well as on the central tube, and the volume of water injected. Special attention was paid to the temperature profile in the buffer material to determine the overall heat transfer mechanism, the evolution in the degree of saturation and the values and uniformity of pressure on the jacket liner and the central tube induced by buffer swelling. Movement of the central tube, which can be a consequence of a non-uniform swelling pressure, was monitored in order to relate it to potential problems that could occur when inserting the waste canister in an actual repository;

- observing, during the dismantling operations, the swelling performance of the buffer material and more particularly the presence of physical gaps, contact between the buffer and the central tube and between the buffer and the jacket liner, and the homogeneity of the buffer (e.g. presence of an enriched zone in clay or sand). It was particularly important to verify the presence of the joints between blocks and, if present, their state; if open, they can be preferential pathways for the movement by advection of water and radionuclides in an actual repository;

- assessing the evolution of the physico-chemical, thermal, hydraulic and mechanical parameters of the buffer material through post-mortem analyses.

2.3. Extension of the scientific programme associated with the mock-up dismantling

During the operational stage, unexpected processes and phenomena were observed. They were related to the thermal and hydro-mechanical behaviour of the buffer material. Corrosion of sensor tubes allowed the discovery of chemical species which are potentially harmful to the corrosion resistance of the metallic components.

In order to explain these unexpected phenomena, and, if possible to gain greater insight into the impact of these phenomena on the performances of the different components of the disposal system, it was decided to conduct a scientific programme which was more extended than initially planned as part of the dismantling. A programme studying the corrosion susceptibility of the different types of stainless steels present in the mock-up was included as well as an investigation of the chemical and microbial conditions prevailing in the mock-up.

A decision was also made to perform numerical THM simulations to explain the complex THM processes the buffer was subjected to. To obtain the required information for the verification and validation of the mathematical model and their numerical implementation, a complete laboratory characterisation programme on the initial and exposed material was performed.

An extended mineralogical characterisation of the initial and exposed buffer material was carried out to verify potential changes which could explain some of the unexpected phenomena observed during the operational stage.

3. Design, manufacturing and assembly of the mock-up

The OPHELIE mock-up simulated, full scale with respect to the diameter and with a length of 5 m, a section of a disposal gallery of the SAFIR-2 reference design as far as the buffer material and the disposal tube were concerned. The mock-up principally simulated the cross-section part of the reference design. The longitudinal (or axial) aspects were not considered when designing the mock-up. The limited length did not allow the experimental study of this aspect in detail. The mock-up mainly represented the middle part of a heated gallery, corresponding with the monitored zone that was put forward in the design for the PRACLAY Experiment (Verstricht, 1995).

The main components of the mock-up were (Figure 3-1):

- the metallic structure with the main jacket, two covers and the central tube;
- the hydration system;
- the heating and insulation systems;
- the buffer material;
- the concrete ring;
- the monitoring equipment.

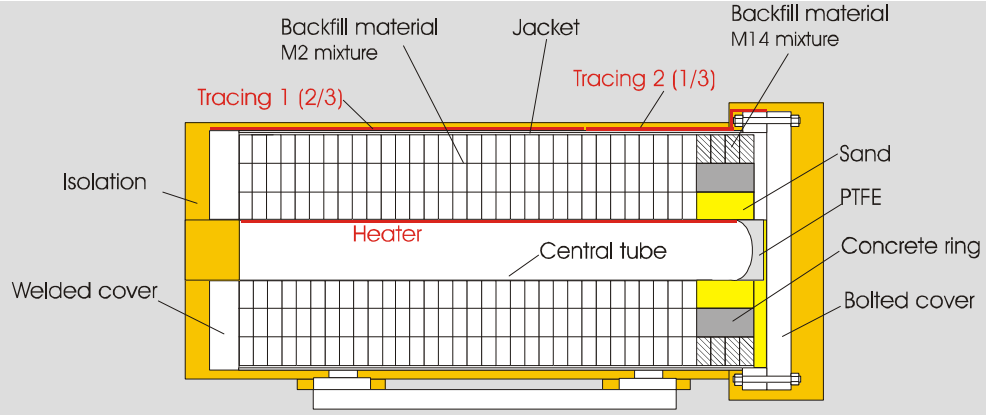

Figure 3-1: Schematic view of the mock-up and its components.

The construction and assembly of the mock-up components was compiled in the Technical Specifications (Verstricht & Dereeper, 1999). The instrumentation programme and monitoring equipment are detailed in section 5.1.

A general schedule of the construction and assembly tasks is given in chapter 5.

Table 3-1: General schedule of the construction and assembly tasks.

Date	Action
1996	Technical Specification, call for tenders for the metallic structure
Dec. 1996 – Mar. 1997	Levering, installation and assembly of the metallic structure
April – Mai 1997	Installation of the buffer blocks and internal sensors
June – July 1997	Manufacture and installation of the concrete segments
Aug. – Sept. 1997	Installation of the bolted and instrument covers. Connection of the
Oct. 1997	Installation of the external sensors and central heating system
Nov. 1997	Watertight test with N2
Jan. 1998	Installation of the external heating system and the insulation cover

3.1. The metallic structure

The mock-up's metallic structure was composed of a main jacket, two covers and the central tube simulating the disposal tube. Appendix 1 gives more details about the mock-up's metallic components and their chemical composition.

To design the steel structure, operating conditions were fixed at 5.0 MPa maximum internal pressure and 200 °C (the highest estimated temperature in the central tube was 170 °C – see appendix 2). All metallic components in contact with the buffer material were made of stainless steel.

The detailed design and data for the metallic structure was described in the Technical Specifications (Bergmans, 1996).

3.1.1. The main jacket and the covers

Design

The steel jacket simulated the confinement provided by the host formation. It consisted of a ~ 5 m long, 2 m internal diameter and 55 mm thick carbon steel cylinder (Figure 3-2, LEFT) protected against corrosion by a 3 mm thick AISI 304 stainless steel cladding (on the intrados).

One cover (260 mm thick) was fixed by welding ("welded cover") to the jacket. It was provided with 16 connections for the hydration system and a central opening to allow the fixation of the central tube equipped with the heater and to make internal access to the tube possible even during the mock-up operation.

The second cover (265 mm thick), at the front of the mock-up, was fixed by bolting ("bolted cover") after installation of the buffer material and the other internal parts. It was equipped with two openings (and mating covers) to allow a hermetically sealed feed-through of some 150 cables and instrumentation tubes.

As for the jacket, the covers were made of carbon steel with a 3 mm thick AISI 304 stainless steel cladding on the internal part.

Manufacture and installation

Based on different criteria (Brosemer et al., 1996), the order (after a call for tenders) was awarded to COEK Engineering N.V. (Geel, Belgium) in May 1996. Delivery took place in December 1996. The entire manufacturing process for the steel structure is described in the construction file (Aerts, 1997).

The manufacturer was responsible for the final design (including dimensioning) and approval of the structure. The global dimensions (lengths, diameters,…), materials and connections (e.g. hydration system) were specified in the Technical Specifications. Manufacturing was performed under a QA programme, as defined in a List of Fabrication Control (LOFC), with both internal checks by the manufacturer and external checks by SCK•CEN and a control body (AIB-Vinçotte). In January 1997, the final hydrostatic pressure test (7.5 MPa, i.e. 1.5 times the nominal pressure of 5.0 MPa) was successfully performed.

The actual installation of the steel jacket took place at the end of January 1997 (Figure 3-2, RIGHT).

Figure 3-2: Carbon steel body of the jacket (LEFT) and installation of the jacket in January 1997 (RIGHT).

3.1.2. The central tube

The central tube (Figure 3-3) consisted of a 4,696 mm long, 508 mm external diameter and 25 mm thick AISI 321 stainless steel cylinder (a Ti-stabilised variant of AISI 304 stainless steel). This type of steel was chosen because of the large axial load that the tube would be subjected to, especially at the flexible joints, resulting in elevated localised pressures. The specifications of the alloys to be used (including heat treatments, forming, welding procedures,...) were prescribed by the relevant standard for pressure vessels. The weight of the central tube was about 1,500 kg.

One end of the tube was welded to the rear side of the mock-up, while the other end (with a hemispherical shape, protected with PTFE piece) could move vertically (within limits) through

a hinge within an articulated joint (AISI 316Ti) near the welded tube end. Some vertical movement was expected due to the swelling of the buffer material, and this hinge therefore allowed some idea of the magnitude of such a movement to be obtained.

The central tube was constructed and installed by the manufacturer as an integral part of the whole structure.

Figure 3-3: Central tube installed in the steel jacket

3.2. The hydration system

The hydration system had to perform the flooding of the mock-up (i.e. fill all internal voids with water in a short period) and saturation of the buffer under controlled pressure during the experiment's operational stage.
The hydration pressure was fixed at 1 MPa, which is lower than the expected pore water pressure in-situ. A higher pressure would however have made the mechanical construction much heavier and more expensive.

Figure 3-4: A part of a hydration tube (LEFT). They were fitted to the cover connections (RIGHT).

This configuration, with the hydration pipes installed at the buffer's periphery, allowed simulation of the hydration that would take place in an actual repository if only a natural process had to be considered (the use of an artificial hydration system was proposed but not formally considered in the SAFIR-2 design).

Based on CEA experience and on the drawings by SCK•CEN, the hydration tubes were manufactured at the workshop of the LPS – Constructions Thermiques Européennes company in Monsempron/Libos (France). Over the mock-up's entire length, 4 tubes were connected to each other to form a continuous hydration line source. Sixteen of these lines were installed in the mock-up (fixed on the inside of the jacket) – each line coincided with the joint between two buffer blocks in the outer ring. Each line was connected to the distribution manifold of the hydration system through a cover connection (Figure 3-5, LEFT).

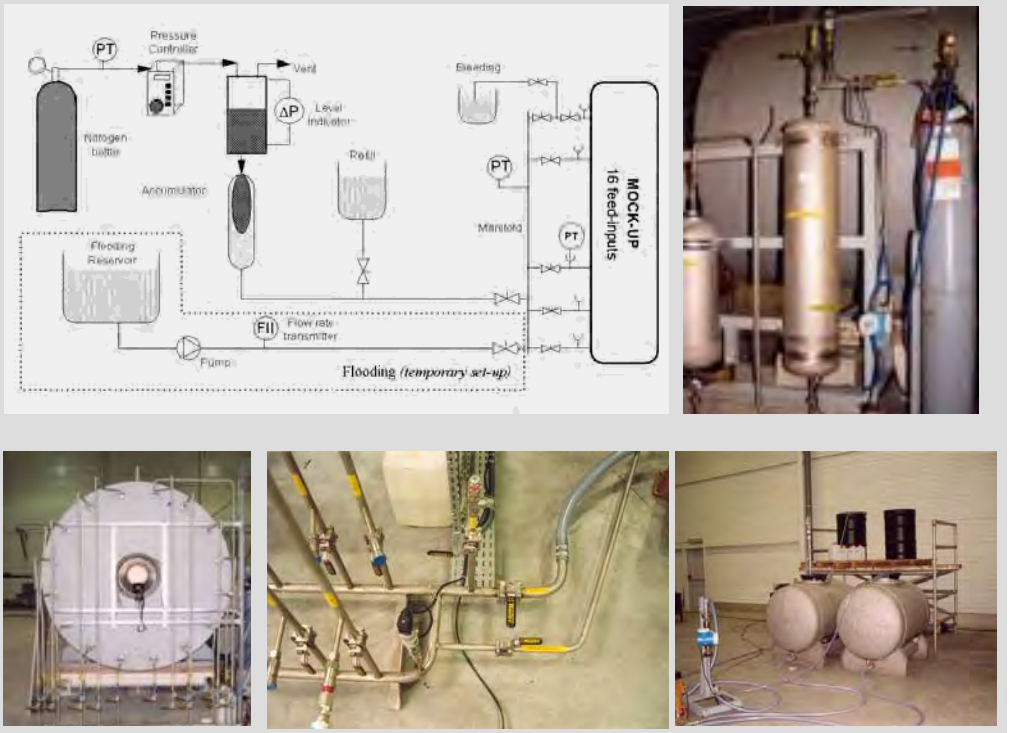

Figure 3-5: schematic view of the hydration system (TOP LEFT). The distribution manifold (BOTTOM LEFT) and flooding reservoirs with pump and flow rate meter (BOTTOM RIGHT). Detail of the manifold with pressure transmitter (BOTTOM LEFT) and the accumulator (BOTTOM MIDDLE).

Externally, a distribution manifold connected each hydration tube to the water supply. This supply initially used a centrifugal pump for flooding purposes. The distribution manifold allowed individual control of the flow in each hydration tube, while a quick release coupling allowed for individual pressure monitoring and taking samples. The gas pressure in the reservoir was controlled by a pressure controller (powered by N2-gas bottle). The volume injected into the mock-up over time could be monitored by measuring the level variations in this reservoir.

3.3. The buffer material

The buffer material consisted of pre-fabricated blocks of a mixture of 60 wt.% FoCa clay, 35 wt.% sand and 5 wt.% graphite uniaxially compacted at 61 MPa. This material was labelled "M2".

A complete buffer section consisted of three concentric rings (Figure 4-3 BOTTOM RIGHT) formed by 6 blocks (inner ring), 12 blocks (middle ring) and 16 blocks (outer ring). The internal diameter of the inner ring was 512 mm, 4 mm larger than the external diameter of the central tube to account for its dimensional tolerances. Between the rings, a tolerance of 1 mm in the radius was also added to ensure smooth assembly of the blocks. The eternal diameter of the buffer was smaller than the planned internal diameter of the gallery. That way, an annular physical gap of some 36 mm was present to facilitate the installation of the buffer blocks and, in the case of an actual repository, to allow for tolerances in the gallery lining. This annular void also limited the swelling pressure by allowing some expansion of the buffer.

The development programme and manufacture and installation (together with the sensors) of the buffer material are considered in chapter 4.

Thirty-six sections, each with a thickness of 130 mm, were installed across the entire length of the jacket.

The middle rings of the last four sections were replaced by a ring made of 6 concrete segments. For the buffer blocks around the concrete ring (outer rings), an increased content of FoCa clay was chosen to compensate for the lower overall swelling capacity. A composition of 85 wt.% of FoCa clay, 10 wt.% of sand, and 5 wt.% graphite was established; this mixture was labelled "M14". The inside was filled with SIBELCO M32 type sand due to the instrument tubes, pre-compacted blocks were difficult to use.

3.4. The concrete ring

A concrete ring, which consisted of 6 segments, was installed at the end of the mock-up (near the bolted cover) to test the behaviour of measuring instruments in the concrete that would be installed in and around the PRACLAY gallery lining (Figure 3-6). To be compatible with the buffer assembly, the segmented ring coincided with the middle buffer ring (outer and inner diameter of respectively 1 452 mm and 960 mm), over a length of 4 sections (520 mm).

The concrete was specified in accordance with the Belgian standard NBN B 15-001, with a strength class of C50/60 (Van Cauteren, 1996).

3.5. The heating systems

The thermal conditions for the OPHELIE mock-up were implemented using:

- an internal heater, simulating the heat generated by the HLW canisters (464 W/canister or 350 W/m);
- an external heating and insulation system simulating the boundary conditions imposed in an actual repository by the host formation.

The temperature conditions to be applied in the mock-up were studied in 1995 and 1996 by SCK•CEN (appendix 2). The approach was firstly to consider the thermal conditions of the in-situ PRACLAY Experiment, which was regarded as the reference case.

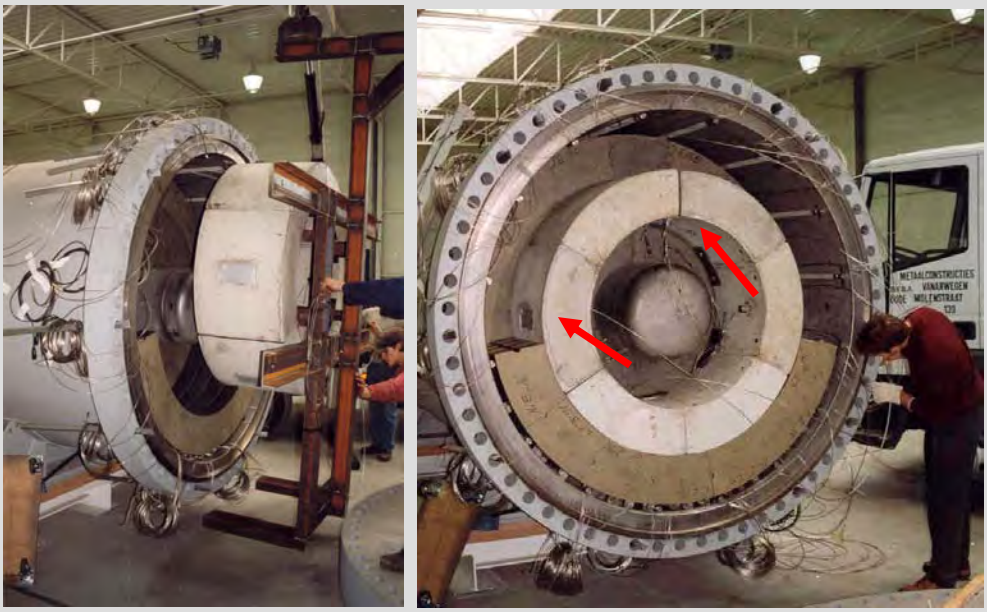

Figure 3-6: Installation of the concrete ring (LEFT) and concrete ring after placement partially surrounded by M14 buffer blocks (RIGHT). An extrados pressure cell is mounted, and at the top interface, two load cells are installed between the segments.

3.5.1. The internal heating system

The main heater, installed inside the central tube, consisted of 3 resistance cables mounted between 2 concentric aluminium tubes. The overall length of the heated part was 4.5 m.

ISOPAD GmbH supplied the heating cables, based on the study performed for the PRACLAY Experiment in 1995. The cables (model KMV-6), each 40 m long, consisted of a NiCr core (Cu for the cold part of the cable), insulated by MgO powder and enclosed in a stainless steel sheath with an outer diameter of 3.5 mm.

The cables were installed on the extrados of an aluminium tube (438 mm diameter and 4 565 mm long, made from 3 mm thick aluminium sheet, Figure 3-7), and covered by a second outer aluminium pipe (450 mm diameter, same length). Along with the heating cables, 6 thermocouples were also installed to monitor local temperatures inside the heater assembly. The whole assembly was then pushed into the central tube.

The resistances of the 3 cables were powered by variable autotransformers (variacs), delivering an output of 678 W/cable, or 450 W/m. The parameters of each cable (voltage, current and power) were also monitored using power transducers.

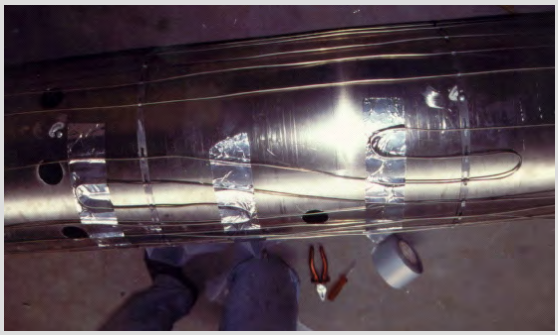

Figure 3-7: Installation of the heater cables on the extrados of the inner aluminium tube (TOP). The inner aluminium tube was then inserted in an outer aluminium tube to protect the heating cables. These two aluminium tubes were then inserted inside the central tube (BOTTOM).

3.5.2. The external heating system

The external heating system allowed the application of well-controlled conditions on the outside of the steel jacket by fixing the temperature at a set level (Figure 3-8, LEFT). They also compensated for the edge effects (due to the end covers), and prevented seasonal temperature variations in the demonstration hall being transferred to the mock-up itself.

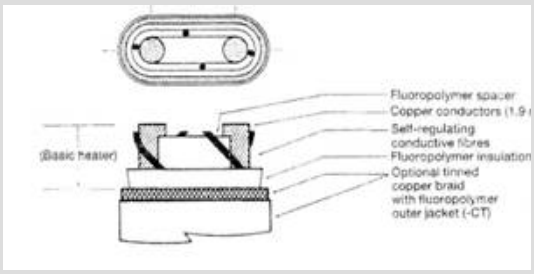

Figure 3-8: Installation of the external heat tracing and insulation (LEFT). Self-regulating heating cable type Raychem 20 XTV2-CT (RIGHT).

The system consisted of 2 heating cables with a length of 30 m and 20 m, installed at both ends of the mock-up (Dereeper, 1998). The heating cables were of the self-regulating type (Raychem model 20XTV2-CT – Figure 3-8, RIGHT) to obtain a more uniform temperature: their power dissipation at each location depended on the local temperature (power dissipation at 120 °C was 30 W/m). The overall temperature was controlled by a temperature controller

(one for each cable), with each controller getting its input from a Pt100 temperature sensor on the jacket.

3.5.3. The thermal insulation

Based on the thermal simulations, a thermal insulation of 60 mm of Rockwool was specified on the outside of the jacket.

To obtain a radial heat flow, the axial heat flow was limited as much as possible. In thermal simulations, adiabatic conditions were assumed at the covers. By applying thick thermal insulation (300 mm of Rockwool) heat loss at the covers was kept to a minimum. The insulation was installed by the Hertel Company in January 1998 (shortly after the hydration phase had started). The Rockwool insulation was finished with a metal outer sheet (Figure 3-9).

Figure 3-9: Mock-up after installation of the metal outer sheet (LEFT). Metal outer sheet on the welded cover (RIGHT)

A support structure of wooden beams (130 mm high) separated the steel structure from the floor structure to limit heat loss along this path.

3.6. Finishing the mock-up assembly after placement of the buffer material

The main activities performed after installation of the buffer material were:

- the filling of the volume between the concrete segments and the central tube with SIBELCO M32 type sand (Figure 3-10, TOP);
- installation of the bolted cover (Figure 3-10, BOTTOM LEFT);
- connection of the 16 hydration tubes to the external equipment of the hydration system;
- passing of the instrumentation cables through the instrumentation covers (Figure 3-10, BOTTOM RIGHT), and connection to the data acquisition system;
- installation of the external strain gauges and thermocouples;
- installation of the internal heating system;

- the watertightness test by pressurizing with N2 up to 10 bar;
- installation of the external heating system and insulation cover.

Figure 3-10: The mock-up just before the installation of the bolted cover (TOP). The volume between the concrete segments and the central tube was filled with sand type SIBELCO M32. The white piece is the PTFE protecting the hemispherical end of the central tube. Installation of the bolted cover (BOTTOM LEFT). About 80 instrumentation cables and tubes were fed through each of the two instrumentation covers (BOTTOM RIGHT).

4. Requirements, specifications, manufacturing and emplacement of the buffer material

Development, manufacture and placement of the buffer material were among the main objectives of the OPHELIE experiment as a preparatory step for the PRACLAY Experiment.

4.1. Roles and requirements of the buffer material

During each phase of the repository's life, the operational and long-term radiological safety of the disposal system is ensured by the different barriers that have specific roles and/or functions ("multi-barriers/functions" concept) during specific periods. With regards the components concerned by the OPHELIE mock-up, i.e. the disposal tube and buffer material, these roles were as follows:

- the stainless steel disposal tube provided the waste forms with a watertight surrounding, avoiding contact with water from the host formation during the thermal phase (typically during the first 500 years for vitrified HLW). The disposal tube also had operational safety functions and functional roles:
  - it dissociated the development of the disposal gallery and the waste placement. The buffer was therefore installed in a radiation and heat free environment and consequently, did not require remote techniques;
  - it facilitated the retrieval of the waste canisters for an adequate period.
- the buffer material provided a favourable environment for the disposal tube and the host formation to allow these barriers to fulfil their respective functions and roles.

Given the buffer material's role, the requirements regarding the choice of material were primarily compatibility requirements in terms of the disposal tube and the Boom Clay. The buffer material had to have:

- a well-known and controlled chemical composition compatible with the host formation (its composition must not substantially affect the retention properties of the Boom Clay) and without unfavourable chemical species detrimental to the corrosion of the disposal tube;
- a low hydraulic conductivity avoiding hydraulic pathways around the disposal tube. Limiting the quantity of water close to the disposal tube also limits gas formation through anaerobic corrosion and radiolysis. A value lower or equal to that of Boom Clay was expected ($4\ 10^{-12}$ m/s);
- a thermal conductivity sufficient and at least equal to that of Boom Clay (1.7 W/mK) to prevent excessive temperatures in the engineered barriers. Good heat dissipation is needed to minimise chemical processes detrimental to the corrosion of the disposal tube and to enhance the durability of the glass matrix. It also limits thermal expansion of the disposal tube (and the stress induced in the tube, buffer and sealing components),

mineralogical and chemical changes in the buffer material and changes in the concrete lining properties;

- a sufficient swelling capacity to fill the initial physical gaps (avoiding, in the event of a collapse of the gallery lining, the creeping of Boom Clay into the disposal galleries with the risk of destabilizing the host formation and limiting microbial activity and associated phenomena such as gas generation - e.g. methane - and corrosion of the disposal tube) and generate an adequate swelling pressure. A value of at least 4 MPa but no higher than 4.5 MPa was expected. Such a value limits the risk of the disposal galleries collapsing and minimises the mechanical constraints on the disposal tube and host formation.

Depending on the quantity of buffer material required for an actual repository, it had to be easily applicable on an industrial scale and with limited costs.

4.2. Development programme

The objective of the development programme was to select a composition for the buffer material and a design for the hydration system.

4.2.1. Preliminary bibliographic studies

ONDRAF/NIRAS decided to focus its investigation on clay-based materials because this had been the subject of many studies and research in several foreign countries (France, Sweden, Canada, Switzerland...). Bibliographic studies (Van Miegroet, 1991, ONDRAF/NIRAS, 1991b) concluded that:

- Boom Clay was not suitable for buffer purposes because of its low swelling capacity due to a low smectite concentration;

- smectite-rich bentonites and bentonite-based materials featured an adequate permeability/swelling potential. Such materials also had other necessary or interesting properties such as sufficient thermal conductivity, high ion exchange and absorption capacity, sufficient mechanical resistance, low shrinkage, suitable deformability and physical and chemical stability and are flexible to use. By mixing them with different inert aggregates (sand, graphite, zeolytes, etc…) some of their properties could be regulated/increased in order to satisfy the required criteria (swelling pressure, thermal conductivity, retention capacity, mechanical strength);

- use of water-saturated materials was excluded so as not to compromise the swelling capacity;

- calcium bentonite was preferred over sodium bentonite because of its superior chemical compatibility with the concrete lining of the galleries.

- from a geometrical point of view, pre-fabricated blocks of the desired density were preferred to pellets because they guaranteed better homogeneity of the buffer and they

could more easily be placed in a horizontal configuration. A maximum weight of 25 kg per block was specified for handling reasons.

4.2.2. Choice of the buffer composition: the three phases of the development programme

The specification of the buffer material, a mixture of FoCa clay (60 wt. %), sand SIKA type MX123 (35 wt. %) and graphite TRIMREX T 140-600 (5 wt. %), and the development of the hydration system were the result of a development programme carried out by CEA (1993 - 1996). This development programme was conducted in three phases.

The **FoCa bentonite** is a marine sedimentary clay coming from the Paris basin (France) and is extracted in an area between the two municipalities of Fourges and Cahaignes (Fo Ca) in the Vexin region (Eure department).

First phase

The first phase (1992-1993) aimed to:

- select a hydration system and buffer material based on laboratory information and tests on the industrial uniaxial compaction of blocks;
- define the buffer layout, i.e. conduct pre-mock-up tests and refine the placement procedure and hydration system.

The outcome of the first phase (Dardaine et al. 1994) was the selection of a buffer block composed of FoCa clay, sand and graphite combined with a simplified hydration system, i.e. hydration pipes placed at the buffer's periphery.

The FoCa clay gives the mixture its swelling property and low permeability. Sand reduces the swelling ability of the buffer blocks and guarantees their mechanical stability. Graphite improves the thermal conductivity of the blocks.

Second phase

The second phase (1995-1996) aimed to optimise the buffer material selected during the first phase (Dardaine et al., 1996). Good mechanical cohesion of the blocks to ensure easy handling and placement was added as a requirement (Van Cauteren and Van Miegroet, 1995). The optimisation was conducted in 3 phases:

- the study of the swelling pressure of several FoCa clay/sand/graphite mixtures at saturation;
- validation of a procedure for measuring the block strength, and;
- the manufacture of blocks and realisation of strength measurements.

The second phase allowed the selection of the final composition of the buffer material. The Brazilian test was selected to assess the mechanical characteristics of the blocks during production.

Third phase

The third phase (1996) included, before adapting the moulds and manufacturing the buffer blocks for the OPHELIE mock-up experiment, a run of pre-mock-ups (Figure 4-1) to verify, on a large scale, whether the swelling of the chosen buffer material was sufficient to fill a major peripheral void and whether the buffer material retained its symmetry around a central tube after hydration (Dardaine & Gatabin, 1996).

The pre-mock-up tests concluded that the layout chosen for the OPHELIE mock-up could be successfully hydrated. The voids were completely filled and the buffer kept its axial symmetry.

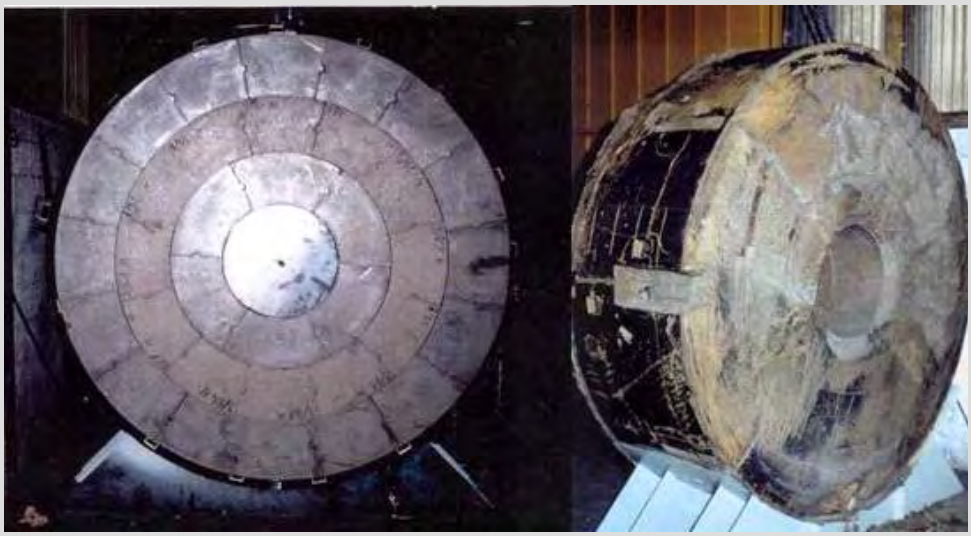

Figure 4-1: Completed mock-up before flooding (LEFT). The buffer material after removal of the steel structure (RIGHT).

4.3. Buffer blocks manufacture and controls

Earlier experiments, for instance BACCHUS 1 (Neerdael et al., 1992), demonstrated the possibility of manufacturing pre-fabricated blocks on a laboratory scale (small quantity, specific equipments and tools) with specific dimensions and physico-chemical properties. For the PRACLAY Experiment, and more generally for an actual repository, the quantity of buffer blocks required would be much larger, meaning the use of industrial manufacturing techniques. In addition to causing difficulties when placing these blocks, significant variations in block dimensions and physico-chemical properties might also have led to inhomogeneous behaviour in the buffer material when hydrated. In particular, the swelling pressure generated depends greatly on the initial density and water content of the blocks and the physical gaps resulting from the block placement. Inhomogeneous swelling pressure might induce differential stresses on the disposal tube and movement of this tube that could create problems when inserting waste canisters during the repository's operational stage.

With regards the block manufacturing criteria, the target values for the tolerances were a precision of 1 mm for the block dimensions and 1 % for the dry density.

A total of 1,505 blocks were manufactured for the OPHELIE mock-up. Manufacturing controls (density, water content, weight, dimensions and mechanical resistance) were performed on 3 % of the production of each type of block to verify compliance with the set tolerances.

4.3.1. Manufacturing of the buffer blocks

The blocks were manufactured by the "LPS – Constructions Thermiques Européennes" company, located in Monsempron/Libos, France. The FoCa clay (about 20 tons) was homogenised and, after the addition of sand and graphite, prepared in a mixing tank (type EIRICH DE 22) in batch sizes of almost 2 297 kg for the M2 mixture: 1,440 kg FoCa clay, 750 kg sand, 107 kg graphite. The moisture in the FoCa clay (13.6 % before blending with the other components) was taken into account to determine the total mass to be added as the composition of 60/35/5 refers to dry masses. For the M14 mixture, the batch size was 2,204 kg (1,904 kg FoCa clay, 200 kg sand, 100 kg graphite). After mixing, the appropriate amount of buffer powder was placed in the mould and compacted using an 800-ton hydraulic press (type LAEIS 1). Each block was given its own unique identification. Table 4-1 gives the manufacture dates and numbers for each type of block.

It was remarkable to observe that a 'film' of graphite formed on the surface of the blocks (except on 'pressed' surfaces) due to the manufacturing process. As mentioned in chapter 7, this hydrophobic film had an influence on the hydration process during the OPHELIE experiment.

Table 4-1: Manufacture number and date of the different types of buffer blocks.

Date	Type of blocks	Quantity	Identification
14-15/10/1996	inner ring, M2	277	2I/1 – 2I/277
16-17-18/10/1996	middle ring, M2	496	2M/1 to 2M/496
7-8-9-10-11/11/1996	outer ring, M2	660	2E/1 to 2E/660
12/10/1996	outer ring, M14	72	14E/1 to 14E/72

The blocks, grouped according to their type, were put on wooden pallets and packed carefully to protect them during transport.

4.3.2. Dimensional and physico-chemical controls

Blocks of each ring were subjected to manufacturing controls that consisted of verifying several parameters such as dimensions, water content, weight, density, mechanical resistance by Brazilian tests (Gatabin & Dardaine, 1997). The principle results are given in Table 4-2.

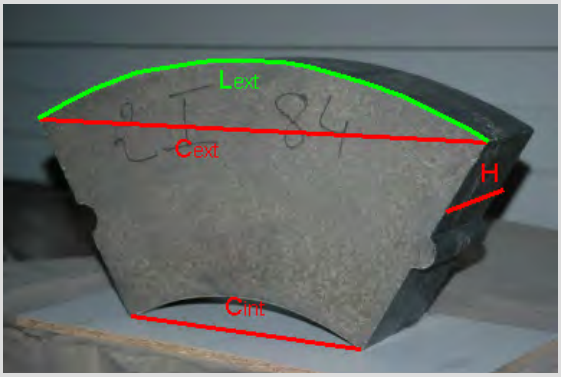

Figure 4-2: View of a pre-fabricated block from the middle ring.

As demonstrated by the low values of the standard deviations, the buffer blocks were manufactured according to the set dimensional tolerances (accuracy of 1 mm). From the physico-chemical (density, water content) and mechanical property values, it was also clear that highly homogeneous blocks had been manufactured.

Table 4-2: Theoretical values based on mould (red), average values and standard deviation (between brackets) of several parameters measured after the blocks manufacturing (N = number of measurements).

Rings	H [cm] thickness	L_{ext} [cm] External arc	C_{ext} [cm] External cord	C_{int} [cm] Internal cord	M [g] mass	W [%] Water content	ρd [g/cm³] Dry density	Mechanical resistance [MPa]
Inner ring, M2 N = 10	13.00 13.01 (0.02)	49.80 50.10 (0.04)	47.50 47.84 (0.04)	25.40 25.51 (0.2)	25 220 (38.99)	7.65 (0)	2.09 2.10 (0.01)	0.34 (0.02)
Middle ring, M2 N = 16	13.00 13.06 (0.03)	37.30 37.60 (0.02)	37.00 37.17 (0.02)	24.70 24.80 (0)	22 041 (13.17)	7.51 (0)	2.09 2.09 (0.01)	0.34 (0.02)
Outer ring, M2 N = 21	13.00 13.05 (0.04)	37.50 37.75 (0.04)	37.30 37.51 (0.04)	27.90 28.17 (0.03)	23 386 (40.79)	8.01 (0)	2.09 2.10 (0.02)	0.33 (0.07)
Outer ring, M14 N = 4	13.00 13.08 (0.05)	37.50 37.76 (0.02)	37.30 37.52 (0.02)	27.90 28.17 (0.02)	22 545 (32.79)	11.70 (0)	1.95 1.95 (0.01)	0.159 (0.03)

In 1999, the blocks in stock were subjected to a basic mineralogical, physico-chemical (water content and density) and THM (swelling pressure, and thermal and hydraulic conductivities) characterisation programme (Gatabin & Rodrigues, 1999 – see also chapters 8 and 12, and appendix 4). The main objectives were:

- to compare the composition of the FoCaPr clay used to manufacture the blocks (FoCa 7 and FoCa 21 were no longer available, at least in the required quantity) with the composition of FoCa7 (CEA laboratory reference material) and FoCa21 used for the development programme. Indeed, although originating from the same quarries, slight variations in the mineralogical composition of the clay may occur, inducing variations in the macroscopic properties such as the swelling capacity;

- to confirm that the thermal and hydraulic conductivities complied with the target values.

The analyses showed that FoCaPr contained more secondary minerals than FoCa21 and FoCa7, including calcite and sand, and less irons, implying a slight increase in the swelling pressure (about 15 % higher than the swelling pressure calculated for FoCa21 using the empirical law developed during the buffer material development programme).

The thermal conductivity measurements indicated values that were always higher than 2 W/mK, with an average value of 2.5 W/mK. The measurements also confirmed the expected dependence of the thermal conductivity on the water content: a decrease of 0.4 W/mK was measured for a sample whose water content had decreased from 7.7 % to 6.9 % after drying.

Hydraulic conductivity measurements were performed on reconstituted material (after crushing the blocks) and on samples directly bored from blocks. In the first case, hydration was carried out parallel to the compaction axis; in the second case, perpendicular to the compaction axis (representative of the mock-up hydration conditions). The results were similar, 8.10^{-14} m/s and 2.10^{-13} m/s (average values) respectively indicating limited preferential pathways. An increase in the hydraulic conductivity with temperature due to a decrease in the water viscosity was also observed. At 120 °C and 150 °C, the hydraulic conductivity of the buffer (samples bored from blocks) was about 4.10^{-12} m/s (similar to the hydraulic conductivity of Boom Clay at ambient temperature) and 1.10^{-11} m/s respectively.

A more extended mineralogical characterisation of the (initial) buffer blocks was also performed within the scope of the post-dismantling programme (chapter 8).

4.4. Placement of the buffer material together with the sensors

4.4.1. Objectives

When the OPHELIE mock-up was launched, the placement on of prefabricated buffer blocks a large scale had only been tested in a vertical configuration (BACCHUS 1, Buffer Mass test, …). The OPHELIE experiment constituted the first opportunity (with the FEBEX mock-up) to verify the placement procedure for the buffer material and verify whether an accurate placing of the buffer blocks could be carried out in a confined environment and in a horizontal configuration. In view of the in-situ PRACLAY Experiment, verification was also needed that the blocks could be placed simultaneously with the various sensors (installed on the central tube, the intrados of the jacket liner, and between and inside the buffer blocks) without damaging the measurement wires or protective tubes. In particular, answers were required for the following questions:

- were the initial joints between blocks, sections and rings regular enough? In other words, were the dimensional tolerances set for the bocks narrow enough?
- was the external (initial) physical gap of 36 mm large enough for handling and installing the blocks simultaneously with the instruments and hydration tubes?

FEBEX mock-up (Full-scale Engineered Barrier EXperiment) project was conducted by ENRESA (Spain). One of its objectives was to test the placement of blocks on a large scale and in a horizontal configuration. Chronologically, the OPHELIE mock-up experiment and the FEBEX Project were operated in parallel (around 1996).

- were the shape, weight and mechanical cohesion of the bocks suitable or did they need to be adapted?
- what changes did the blocks require in order to allow the passage of the sensor wires?

No quantitative criterion was defined for the placement of the buffer. However, general criteria such as the overall aspect of the buffer once installed, the time needed to install a section and the percentage of failed sensors due to installation damage were considered.

4.4.2. Placement of the buffer blocks

The actual installation started in mid-April 1997 with the installation of the internal strain gauges on the outside of the central tube. One week later, the first buffer section was installed. Only when one section was completely finished, was the installation of the next one started. Common tasks were the installation and fixing of the hydration tubes, cutting/adapting the buffer blocks (Figure 4-3, TOP LEFT) to fit internal obstacles (internal strain gauges,…) or instrumentation (holes for inserting sensors), fixing instrumentation cables, and weighing each block before installation. The installation was performed manually (Figure 4-3, BOTTOM LEFT).

Figure 4-3 BOTTOM RIGHT shows the completed section #30 with the grooves to guide the instrumentation cables along the outside. It took less than one hour to install a buffer section (including weighing the block) when no special intervention (adapting blocks, installing sensors …) was required. More time however was spent on installing the instruments. At the end of May 1997, the 32 buffer sections of M2 buffer had been installed.

The buffer blocks were manufactured to close tolerances, and therefore accurate placement with minimal additional void space was achieved. This required the use of spacers in the lower part to set the outer gap to exactly 36 mm. The overall section thickness, as derived from the position measurement along the jacket wall, was only a maximum of 1 mm larger than the block thickness (131 versus 130 mm). Open joints between the blocks were only noticed in the upper blocks of the outer ring. The gap of 36 mm between the outer ring and jacket would therefore only serve to accommodate tolerances in the diameter of the gallery. If the buffer blocks alone had to be considered, a much smaller tolerance (a few mm) would have been sufficient.

To maintain this dimensional accuracy, many blocks had to be adapted when the normal geometry had to be modified due to sensors (with sensor cables), block/central tube joints, hydration tube connections,… As already mentioned, most of the installation time was devoted to these block adaptations. In a real repository (without monitoring devices), a similar way (i.e. also manual) of installing the buffer would require far less time – a conservative estimate by installation staff was 30 minutes of installation time per section.

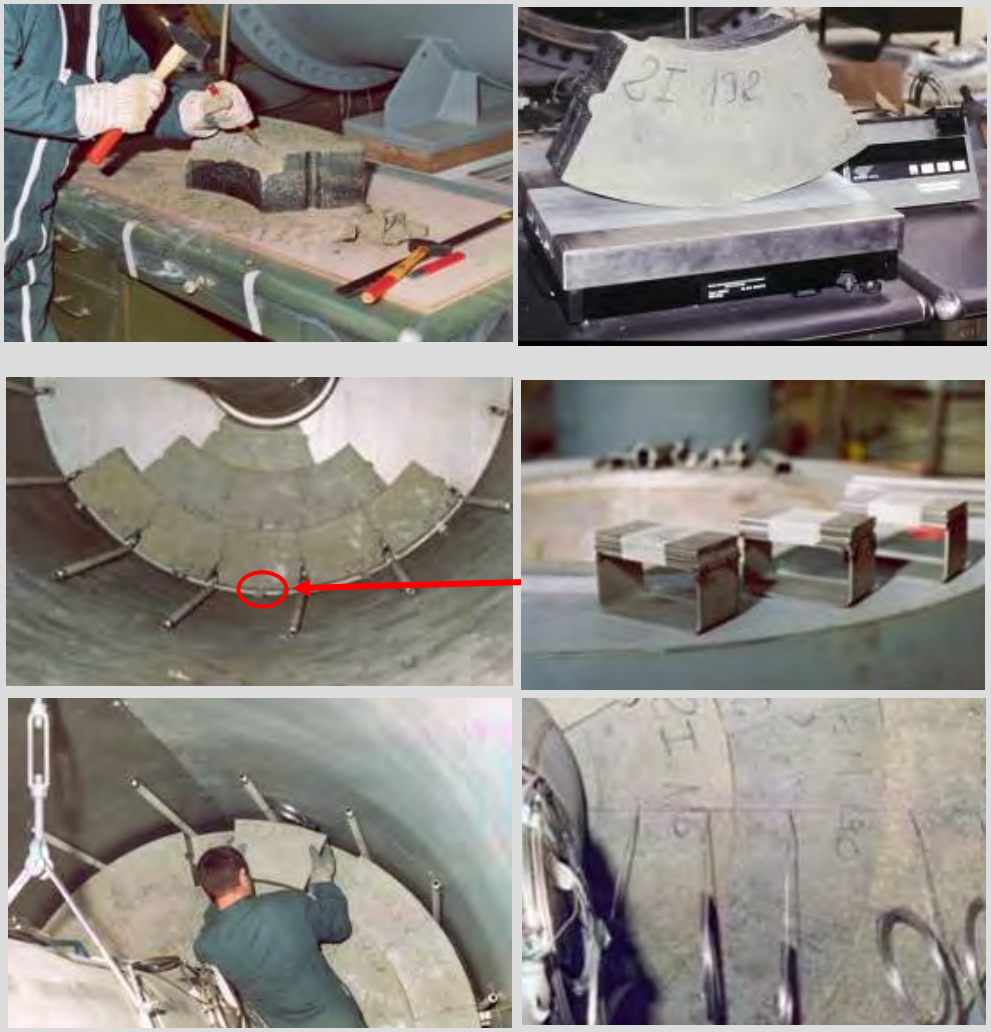

Figure 4-3: Cutting a buffer block to fit internal obstacles (TOP LEFT). Every block was weighed just before installation (TOP RIGHT). Block configuration when beginning the placement of section #1 (MIDDLE LEFT). Spacers were placed between the outer blocks and the jacket in the lower part (MIDDLE LEFT and RIGHT). The block placement was performed manually (BOTTOM LEFT). The close dimensional tolerances allowed a reduction in the thickness of the joins between blocks (BOTTOM RIGHT).

5. The operational stage and the associated instrumentation programme

The experiment's operational stage started in December 1997 and lasted about 4.5 years. The associated instrumentation programme allowed the monitoring of several parameters mainly dealing with the buffer material's THM behaviour and verification of the robustness and performance of different types of sensors in harsh pressure and temperature conditions and in contact with the saturated medium.

During this stage, unexpected phenomena and processes were observed when dealing with the thermal, hydraulic and mechanical behaviour of the buffer material and the chemical conditions prevailing in the mock-up. Corrosion problems were also identified in the sensor tubes.

The evolution of the thermal, hydraulic and mechanical parameters are given in chapter 12, where they are interpreted along with the information gained during the dismantling operations and the results of the post-mortem analyses.

5.1. The instrumentation programme

Instrumentation is an important aspect of the PRACLAY Experiment, in order to obtain data relating to the behaviour of the buffer and other engineered barriers constructions, as well as gain greater knowledge about the feasibility and reliability of long-term in-situ monitoring, which will be needed when designing the monitoring plan for an actual repository. Within the scope of the technical preparation for the PRACLAY Experiment, the OPHELIE experiment allowed the installation of sensors that were planned for the in-situ set-up.
The sensors were selected based on previous studies (Noynaert et al., 1991) and experience.

With the selected sensor types, the instrumentation layout was designed in such a way that a basic view of the buffer material's THM behaviour could be obtained. The main phenomena observed were the development of the hydration and associated swelling pressure, evolution of the temperature field, and couplings between the thermal, hydraulic and mechanical effects. The hydration evolution was monitored primarily by the external hydration system (monitoring the injected volume and pressure in the hydration tubes), complemented by relative humidity cells and some pore pressure transducers. The thermal pulses method (Dereeper, 1998 a) was also considered to follow the hydration of the buffer qualitatively but did not give conclusive information. Swelling due to hydration was monitored through the deformation of the steel structure, and was complemented by total pressure cells and load cells on the bolted cover. Also movements in the central tube due to the swelling process of the buffer were monitored. The pressure and load cells on the concrete ring were only installed to test their performance in representative conditions.
However, the bulk of the instrumentation consisted of temperature sensors within the buffer. Most sensors were installed at specific measurement sections to allow a clear picture of the radial profiles in different orientations.

Thermal pulse method can be used to follow quantitatively the hydration process. It consists in applying a heat source long enough to obtain a steady state temperature. The measurement of temperature profile, associated with the knowledge of the applied heat power, allows to determine the thermal diffusivity or thermal conductivity which depend on the saturation state of the material.
Eight pulses (one before flooding and the other during the first three months after the flooding) were applied. However, and with exception of the first thermal pulse, no significant difference between the seven pulses after the flooding was observed. It is a consequence of the addition of graphite and the pre-compacted nature of the blocks making the thermal properties less dependent of the saturation state.

A total of 147 sensors were installed inside the mock-up, complemented by 42 sensors on the outside.

Most of them were thermocouples (100), but there were also 54 strain gauges, 9 total pressure cells, 9 relative humidity cells, 6 piezometers, and the instruments for the concrete ring. An overview of the sensor positions is shown in Figure 5-1. More specific positions of the sensors are given in appendix 3.

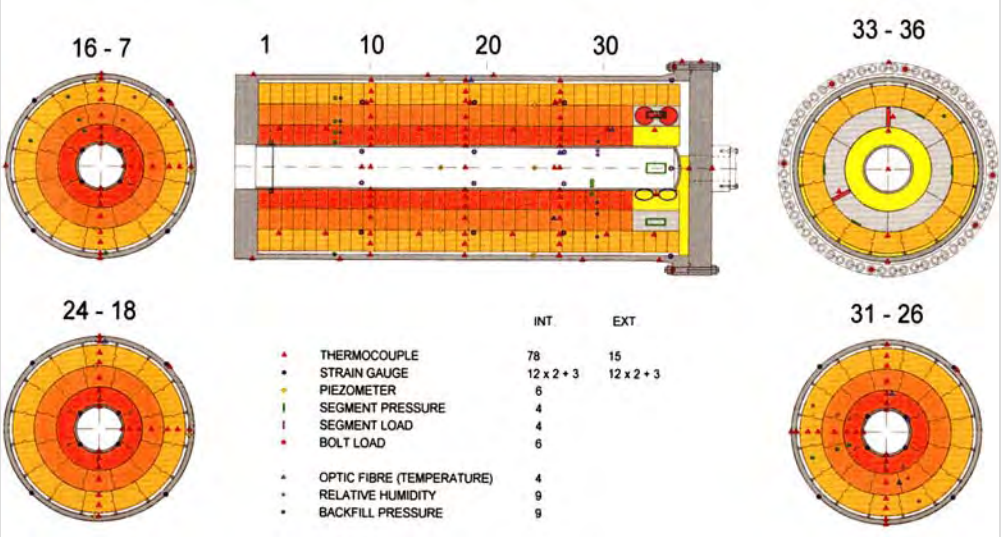

Figure 5-1: The instrumentation inside and outside the mock-up; the sensors were installed according to radial and longitudinal profiles.

5.1.1. Thermocouples

For the temperature measurements, thermocouples were selected due to their robustness, simplicity, and self-powered output signal. Stainless steel sheathed (2 mm OD), mineral insulated type K thermocouples from the Specitec company (France) were chosen.

Figure 5-2: Thermocouple profile in the middle of the mock-up (section #18, 90° orientation).

Inside the mock-up, 78 thermocouples were installed, distributed over 3 sections (each section with three radial profiles in different directions to investigate radial heat flow) and two longitudinal lines to check the uniformity of the temperature field. Inside the heater assembly,

six thermocouples were installed to monitor the heat source term. The remaining 16 thermocouples were installed on the outside of the steel jacket to monitor the boundary conditions. Figure 5-2 shows the thermocouple profile (vertical upwards) installed in section #18.

5.1.2. Internal strain gauges

Strain gauges were installed on the extrados of the central tube, as well as on the intrados of the steel jacket to monitor their mechanical deformation (both axial and orthoradial directions) due to the buffer swelling. Three sections of both the central tube and steel jacket were instrumented. Each section contained four locations with 2 strain gauges each (axial and circumferential direction), complemented by an additional dummy gauge per section for temperature correction purposes. This dummy gauge was fixed by spot welding at only one end, allowing for free expansion, independent of the structure. In total, 54 gauges were installed.

Due to the difficult working conditions (saturated medium, elevated pressure), hermetically sealed strain gauges type AWC-8 from the TML Company (Japan) were selected (Verstricht, 1996) for the central tube. This type of strain gauge can be installed by spot welding, and also has a stainless steel sheathed connection cable (three-wire configuration to allow for compensation of lead wire errors). Spot welding required careful preparation (very little roughness), obtained by careful grinding of the tube surface at the gauge positions. After spot welding the gauges, were covered by a stainless steel cap for mechanical protection during installation of the buffer blocks and filled with a silicone coating and sealant (Figure 5-3).

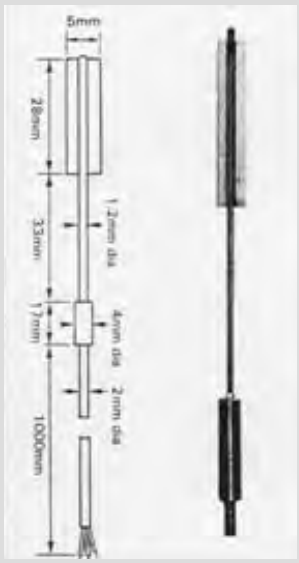

Figure 5-3: "TML" internal strain gauge (TOP LEFT); installed on the central tube, protected by a cap (TOP RIGHT) and before fitting of the protective caps (BOTTOM).

5.1.3. Piezometers

Vibrating wire pressure sensors from the Geokon company (USA), model 4500C-HT, were selected to monitor pore water pressure (Figure 5-4). Each sensor was equipped with a sintered stainless steel filter and a stainless steel sheathed signal cable. Each sensor was also equipped with a temperature sensor (thermistor). This type of sensor was specified for high temperatures, up to 200°C.

Two sensors were installed inside the buffer material, while four others were installed on the outside border of the buffer.

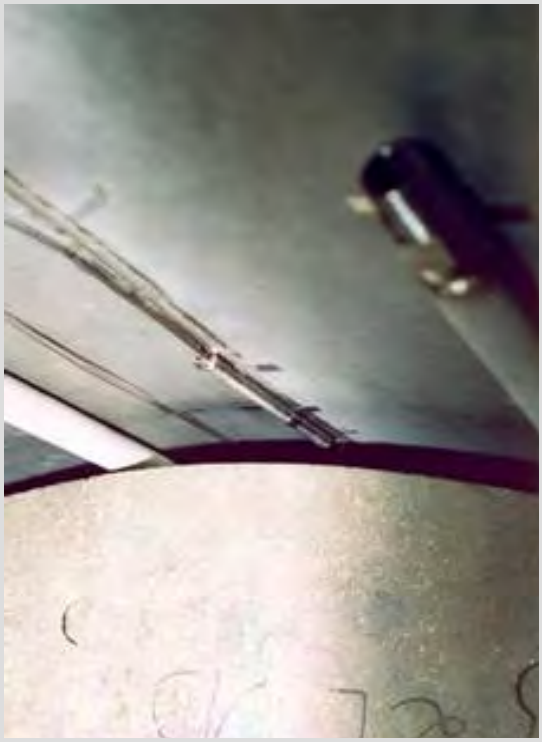

Figure 5-4: Piezometer (LEFT) installed in the void between buffer and jacket at the top of section #16 (RIGHT).

5.1.4. Total pressure transducers

To measure the swelling pressure of the buffer, CEA designed pressure sensors based on a Kulite (USA) pressure transducer, model HEM-375M (Figure 5-5). The transducers were equipped with a rubber cap filled with de-aired silicone oil to transmit the swelling pressure to the transducer membrane. A stainless steel sheathed signal cable was connected to the sensor. The transducers were placed in predrilled holes in the blocks.

Three sections were equipped with these transducers, arranged in radial configurations.

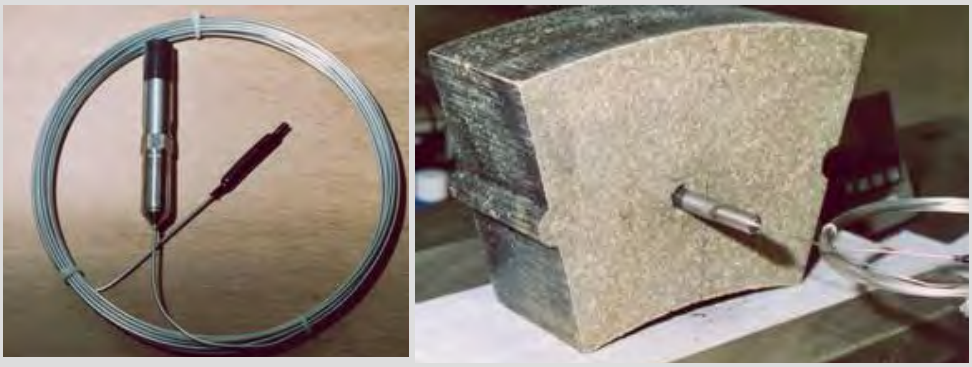

Figure 5-5: Total pressure sensor (LEFT); installed in hole in the buffer block (RIGHT).

5.1.5. Relative humidity cells

To measure the hydration of the buffer, relative humidity cells from Rotronic (CH), model Hygromer I-400, were adapted by CEA for installation in the buffer (Figure 5-6). These sensors had to measure the relative humidity in the buffer pockets formed by a sintered stainless steel filter cap. CEA had established a relationship between the moisture content of the buffer and the relative humidity in the pores. The original signal cable was replaced by a stainless steel sheathed cable (7-conductor), and this cable carried the signal from the capacitive measuring element and the Pt100 temperature sensor. The sensors were placed in predrilled holes in the blocks; due to their length, each sensor needed a hole drilled in two consecutive blocks. An external processing unit conditioned these signals into two 4-20 mA signals.

Two buffer sections were equipped with relative humidity cells, arranged in radial configurations.

Figure 5-6: Relative humidity sensor with cap and stainless steel cable sheath (extended with flexible cable).

5.1.6. Instrumented bolts

To measure the effect of the swelling buffer on the bolted cover, six bolts on this cover were instrumented. Of the different options available (bolts with integrated strain gauges, external strain gauges, and bolt load cells), the load cell option was chosen due to the ease of

installation (Verstricht, 1996). The bolt load cells consisted of ring-shaped load cells to measure the bolt load (Figure 5-7), both of the pre-stress applied during fastening and load development due to swelling of the buffer material.

Figure 5-7: Bolt load cell to monitor the load increase due to the buffer swelling.

5.1.7. External strain gauges

On the outside of the jacket, 27 strain gauges were installed in a configuration similar to the central tube. Conventional foil strain gauges, pre-mounted on a metal (Inconel) carrier were chosen, which could be installed by spot-welding to the mock-up jacket. In May 1998, after the first measurements were analysed, the dummy gauges (for thermal compensation) were replaced by an improved set-up with separate steel carriers (Figure 5-8).

Figure 5-8: External strain gauges, with dummy gauge mounted on separate carrier.

5.1.8. Concrete pressure and load cells

Two types of sensors were installed in the concrete ring: pressure cells at the extrados of the segments to measure the external pressure on the concrete ring, and load cells between segments to measure the load developed due to external pressure between the segments (Figure 5-9). Both types consisted of a pressure pad connected to a pressure transducer. Differences were based on the type of pressure pad (rectangular steel sheet for the pressure cells vs. heavy steel plates for the load cells), and measurement principle of the pressure transducer (compensating valve versus vibrating wire).

Four pressure cells were installed: two Glötzl type and two RocTest type sensors. All sensors consisted of a mercury-filled pressure pad (100 x 200 mm) installed in a recess at the segment extrados. The mercury pressure is measured by a pressure transducer: compensating valve type for the Glötzl type sensors (with a pressurizing and return line), and vibrating wire type (with a stainless steel sheathed signal cable) for the RocTest sensors. The pressure transducer was integrated into the concrete segments.

Four load cells (all Glötzl type) were also installed. At two interfaces between segments, two cells were installed in each of the recesses.

Figure 5-9: Segment pressure cell (LEFT); and segment load cell (RIGHT); all from Glötzl.

5.1.9. Pressure sensors for the hydration system

The hydration system was equipped with pressure sensors to measure gas pressure in the intermediate reservoir and water pressure at the hydration manifold inlet and the hydration tube inlet (Figure 3-5). A differential pressure transducer measured the level in the transfer reservoir. A mass flow rate transducer measured the water volume being injected into the mock-up during flooding.

5.1.10. Data acquisition system

The data acquisition system was built around a supervisory PC. Several data acquisition front-ends were connected to this PC:

- three Campbell CR10X dataloggers with appropriate multiplexers for logging the thermocouples, 4-20 mA transmitters (relative humidity and pressure transmitters), vibrating wire sensors, and Wheatstone bridge sensors (total pressure and bolt load cells);
- one system (Peekel Autolog 2100) for conditioning the resistive strain gauges (internal and external);
- electrical power transducers to monitor the electrical parameters of the heater cables.

All data was written to local files, which were then copied to a central database.

Manual measurements consisted of a manual read-out pump for the Glötzl type devices, and also a vibrating wire read-out for the RocTest sensors.

5.1.11. Monitoring the movements of the central tube

Movements of the disposal tube may be a consequence of a non-uniform swelling pressure. During an actual repository's operational phase, such displacements could induce difficulties when introducing waste canisters into the disposal tube.

Within the scope of the OPHELIE experiment, optical survey measurements with a theodolite were performed during the entire operational stage period to determine the vertical displacements of the central tube. Only vertical movements were possible due to the hinge design that connected the tube to the welded cover. Thermal expansion of the tube was not measured.

To monitor the movements of the central tube, a target point was established inside, at the end, of the central tube. Three other reference points were also established to check the overall mock-up position with respect to the demonstration hall (on the welded cover, on the handle of the bolted cover, and on the floor of the demonstration hall). These additional points helped to ensure the general accuracy (including reproduction due to repeated mounting of the measurement station) of the measurement set-up, and could also take into account small displacements of the mock-up, e.g. caused by the settlement of the wooden blocks between the mock-up structure and the jacket.

The measurement results are given in chapter 12.

5.2. Main phases of the operational stage

The operational stage of the mock-up consisted of the following phases: hydration at ambient temperature, heating with continuing hydration and cooling phase. This sequence was similar to the sequence that would occur in an actual repository where the waste canisters are installed after saturation of the buffer material. Table 5-1 lists the key dates of the mock-up tests.

5.2.1. Preliminary test

Preliminary to the buffer hydration, the tightness of the mock-up was tested by pressurizing with nitrogen (10 bar). This allowed leaks from a few feed-throughs and the piezometers to be repaired. Two load cells also appeared to leak, but could not be repaired and therefore had to be taken out of service.

5.2.2. Heating phase

The heating phase started six months after the start of the hydration. It was a compromise between the hydraulic conditions (complete saturation as planned in the reference design) and the test conditions (limited duration of the experiment). Given the status of the hydration (the amount of water injected had reached a high value in comparison to the global void and pore

volume calculated, the hydration system inflow rate had fallen back to a low value, swelling in the peripherical void was established based on the hydraulic isolation of the hydration tubes), it was concluded that the main hydration conditions had been met; full saturation would not significantly change the behaviour of the mock-up. Furthermore, a high thermal conductivity was measured using the thermal pulse method (about 3.8 W/mK). The minimum thermal conductivity criterion was therefore satisfied as a part of the decision to start the internal heating system at 678 W (Dereeper, 1998 b, Dereeper and Verstricht, 2000 a).

Table 5-1: Chronology of the main actions performed on the mock-up.

Date	Action
1997-12-02	start of hydration phase with flooding
1998-06-02	start of heating phase with central tube heater switched on
1998-11-04	start of external heating
2002-08-26	start of cooling phase with all heaters switched off
2002-10-02	start of dismantling phase with removal of bolted cover

In November 1998, the external heating system was switched-on (Verstricht, 1998 b). In the second half of January 1999, the thermal insulation, as specified by the thermal modelling (60 mm of Rockwool around the jacket, 300 mm at both end covers), was applied. The day-night cycles disappeared from the temperature data almost completely.

Table 5-2 lists the key dates related to the mock-up heating systems.

Table 5-2: Main heating settings of the mock-up.

Event	Date	Action
I	1998-06-02	central heater switched on; power of each heater set at 678 W
II	1998-11-04	external heating (tracing 1 and 2) switched on; temperature set at 90°C
III	1998-11-23	tracing 2 : set-point 90°C → 95 °C
IV	2000-01-24	tracing 1: 90°C → 100°C ; tracing 2 : 95°C → 105°C
V	2000-05-15	tracing 1: 100°C → 104°C ; tracing 2 : 105°C → 109°C
VI	2000-05-22	tracing 1: 104°C → 107°C ; tracing 2 : 109°C → 112°C
VII	2000-05-29	tracing 1: 107°C → 110°C ; tracing 2 : 112°C → 115°C
VIII	2002-08-26	cooling (all heaters switched off)

The thermal conditions strongly influenced the hydration and pressure conditions (section 12.3.3). To investigate this in more detail, the hydration circuit (with pressure regulation) was disconnected from the mock-up when switching on the heater. For piezometers PT4, this resulted in a pressure increase from 1.0 MPa to over 2.6 MPa, before decreasing back to 1.0 MPa (after some 75 days), after which the hydration system was connected to the mock-up again.

A similar procedure was followed when increasing the external temperature in January 2000. Probably due to the higher degree of saturation , the pressure increase for PT4 was even higher,

up to 4.5 MPa.
Although the hydration system remained connected during the remainder of the heating period, each temperature variation was followed by a pressure change due to the low permeability of the buffer.

5.2.3. Cooling phase

The mock-up was cooled down rapidly by switching off all heating elements six weeks before the dismantling began (end August 2002), and by removing the thermal insulation a few days later. Ambient temperatures were reached after only two weeks. Rapid cooling allowed the actual physico-chemical state (e.g. chemical and hydraulic heterogeneities) of the buffer to be better preserved than with a gradual temperature decrease. The hydration system kept the pressure at 1.0 MPa relative as long as temperatures above 100°C were observed. Once all the thermocouples were under 100 °C, the hydration tubes were disconnected from the supply until a pressure of 0.01 MPa relative was reached, after which the supply was connected again to avoid desaturation caused by gravitational effects. Due to the thermal contraction, a significant volume of water (~ 100 L) had to be injected.

5.3. Unexpected phenomena and processes observed during the operational stage

During the operational stage, unexpected phenomena and processes were observed when dealing with the thermal and hydro-mechanical behaviour of the buffer material and the chemical conditions prevailing in the mock-up. Corrosion problems were also identified.

5.3.1. Thermal and hydro-mechanical evolution of the buffer material

With regards the thermal and hydro-mechanical behaviour of the buffer, the following unexpected observations were made.

Dependence of the temperature gradient on the direction and the high apparent thermal conductivity.

The maximum temperature reached at different points within the buffer material and the radial temperature gradient were dependant on the direction (section 12.3.3). This resulted in a thermal conductivity between 4.0 and 5.0 W/mK considering a heat flow of 450 W/m, which was quite higher then the calculated (based on material characteristics) and measured values for the individual blocks during production (average value of 2.5 W/mK).

Temperature difference between hydration tubes

During the thermal phase, an increased temperature on some external tubes connected to the hydration system distribution manifold was observed. As not all tubes had the same temperature, this could not be due to thermal conduction – instead this it indicated water flow in these tubes. A temperature gradient was the only explanation for the driving force behind this water flow, indicating a hydraulic connection between some hydration tubes. Because the

connection between some hydration tubes was tested during the hydration phase, indicating a hydraulic cut off due to the buffer swelling, this conclusion did not come immediately after the observation and it was only in 2002 that this led to a more detailed investigation.

Three temperature sensors were attached to a hydration tube connected to valve #4 as shown in Figure 5-10, LEFT. The highest temperature was measured at the top of the tube, and the lowest near the valve (next to the distribution manifold near the floor). After closing this valve, an significant temperature decrease was noticed. Figure 5-10, RIGHT shows the temperature evolution of the different sensors.

The temperature difference after the valve closure can only be the result of thermal conduction. From the temperature drop and difference, heat loss due to water flow in the pipes was estimated (section 12.3.3).

The valves remained closed for the remainder of the heating period; due to the reduced heat loss, the thermocouples showed a small temperature increase.

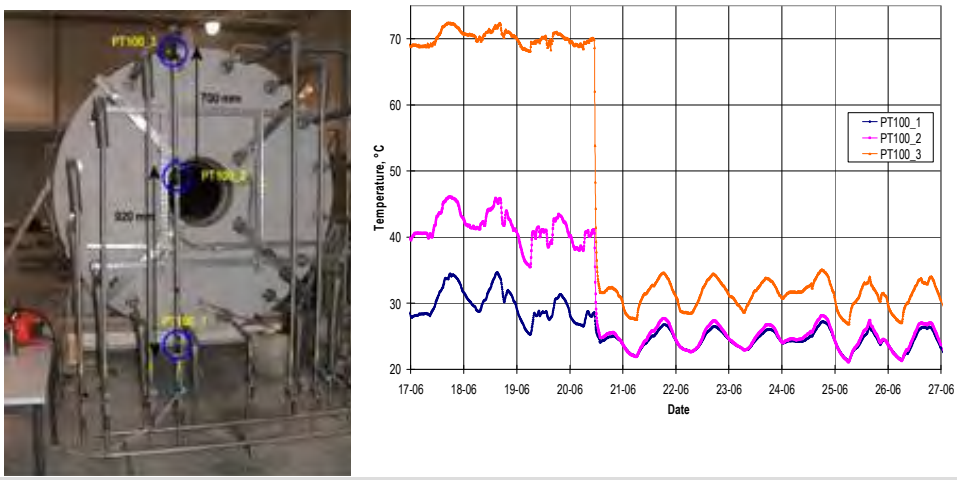

Figure 5-10: Positions of the three temperature sensors installed on the feed tube connected to valve #4. This picture was taken after the external insulation had been removed, but the actual test took place during the heated phase (LEFT). The temperature on the hydration tube before and after closing the feed valve (RIGHT). Daily temperature variations can be noticed.

Evolution of the swelling pressure

In January 2000, the temperature of tracings 1 and 2 of the external heating system was increased (event IV in Table 5-2) at the same time as the closure of the hydration system to impose undrained conditions. This resulted in an increase in the total pressure of about 3.5 Mpa. However, after this pressure peak, a continuous decrease in the total pressure up to the hydration pressure (1 MPa) was noticed (Figure 12-16), interrupted, temporarily, by new temperature increases (events V, VI and VII of Table 5-2). Firstly the Kulite sensors' reliability was examined to rule out the possibility of a sensor malfunction. However, the similar behaviour of the different sensors, and also a similar observation made in other sensors (external strain gauges), proved this phenomenon to be the case.

5.3.2. Corrosion of sensor tubes and presence of chemical and microbial species

Several stainless steel tubes, which were used as protective shielding for the lead wires from the strain gauges, presented evidence of leaks just outside the mock-up (Figure 5-11). Surface analyses indicated that the leaks were caused by pitting corrosion. The most likely scenario explaining perforation of the tubes outside the mock-up was that they were corroded from the outside to the inside somewhere inside the mock-up due to interaction with the buffer material. This allowed the buffer pore water to seep into tubes and, due to the high pressure, to be transported through them.

Chemical analyses of the composition of the water sampled from the leaks in the steel tubes (Dereeper et al., 2000 b) revealed significant anomalies in terms of the expected composition of the M2 mixture pore water (Table 9-1):

- an eleven times increase in the chloride concentration (~ 1 000 mg/L instead of 90 mg/L) was measured, about 40 times higher than in Boom Clay water. Other major components such as dissolved silica and dissolved organic matter were also anomalously high;
- unexpectedly low pH values (5.5 in the hydration circuit water and 3.7 in the water seeping from a strain gauge leak) were measured instead of the value of 8.5 relating to the solution used to saturate the buffer materials.

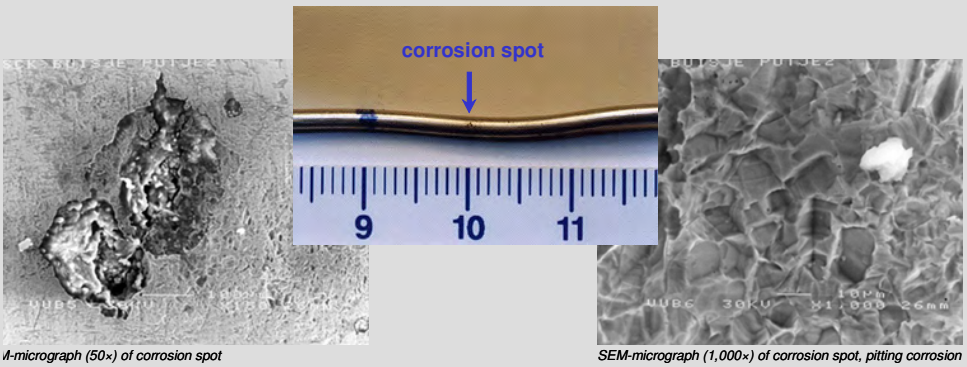

M-micrograph (50×) of corrosion spot

SEM-micrograph (1,000×) of corrosion spot, pitting corrosion

Figure 5-11: View of a defective steel tube used as a protective shielding for the Teflon® insulated electrical wires of a strain gauge. At a higher magnification (1,000×, RIGHT), cristallographic evidences of pitting corrosion was clearly visible.

In August 2000, dissolved sulfides (~ 20 mg/L – 6.5×10^{-4} mol/L) and thiosulfate (~ 10^{-5} mol/L) were measured in the hydration system water analyzed after finding a precipitate of zinc sulfide (ZnS, wurtzite) in a transparent tube located between the water accumulator and an external reservoir. The presence of dissolved sulfides was due to a microbially-mediated sulfate reduction process which could induce stress corrosion cracking (SCC) of stainless steel.

These chemical species can be detrimental to the corrosion resistance of the stainless steel components present inside the mock-up and inside an actual repository. Consequently, the decision was made to investigate these aspects in more detail by including chemical analyses

and measurements during the remaining period of the operational stage and by extending the post-mortem analysis programme to geochemical and microbial analyses of the buffer material (pore water and solid phase) and to an analysis programme studying the corrosion susceptibility of the different stainless steel components.

6. Dismantling: preparation and operations

The OPHELIE mock-up was dismantled in October 2002. The dismantling constituted an essential step in the experiment.

The main objective of the dismantling and associated post-mortem analyses was to better characterise and understand the phenomena occurring during the experiment's operational stage and more particularly to explain the unexpected phenomena and processes that took place in the mock-up.

The dismantling operations provided a unique "hands-on" experience of the engineered barrier by observing the different materials after hydration and heating over several years. As the barrier becomes accessible, the dismantling operation was the opportunity to investigate the processes that had influenced the performance of the different mock-up components.

The dismantling also provided useful information for the THM modelling work. The characterisation of the material exposed to the experimental conditions of the mock-up test allowed the parameters to be adjusted and the numerical model to be validated.

More generally, the dismantling provided additional data for optimising the PRACLAY Experiment from both a scientific (e.g. which processes need be monitored), and technical point of view (e.g. which sensors will give the most reliable measurement results) as well as for reviewing the reference design for disposal of HLW.

6.1. Dismantling dossier

Particular attention was paid to the dismantling preparation. As a preparatory step to the mock-up dismantling operation, a dismantling dossier (Dereeper et al., 2002) was established. This dismantling dossier was subdivided into two main parts:

- the first part described in detail all the activities to be done prior and during the dismantling, from preparations prior to switching off the heating elements to the final destination of the different components and samples. It specified the guidelines and procedures for the dismantling and sampling operations (including packaging, labelling and interim storage). The dismantling scenario was divided into four main phases. The first concerned the actions to be performed before the start of the cooling phase. The second one listed the preparations to be made during the cooling phase. The third phase dealt with the actions immediately before the removal of the bolted cover. Finally, the fourth phase concerned the activities to be performed once this cover had been removed;
- the second part presented the scientific programme associated with the dismantling including the inspections and tests to be performed during the dismantling itself, post-mortem analyses to be performed on samples of each mock-up component as well as the characterisation programme to be performed on the initial material. Alongside the different planned tests and analyses (and their number) and their objectives were

After the decision in 2001 to revise the reference design, ONDRAF/NIRAS investigated three new designs:

- the **Supercontainer** design which considers the placement of a carbon steel overpack containing two waste canisters inside a thick (about 70 cm) concrete buffer;

- the **Sleeve** design which considers the placement of a carbon steel overpack containing two waste canisters in a thick bentonite buffer;

- the **Borehole** design which considers the placement of a carbon steel overpack containing two waste canisters in a stainless steel envelope and directly placed into Boom Clay.

In 2003, ONDRAF/NIRAS selected the **Supercontainer** design as the new reference design.

descriptions of the test procedures, measurement techniques and the sampling plan[1] (number of samples to be taken, their position …).

This document also contained the forms, checklists and procedures to be used during the dismantling work.

6.2. Establishment of the scientific programme associated with the dismantling

The scientific programme associated with the mock-up dismantling ('The dismantling programme') was established by a working group composed of scientists and engineers from ONDRAF/NIRAS, EURIDICE EIG and SCK•CEN. It was reviewed by a committee of experts from the SAC (Scientific Advice Committee of EURIDICE), DAC (Departmental Advice Committee of the SCK•CEN Waste and Disposal Department), Andra (Agence Nationale pour la gestion des Déchets Radioactifs, France), EdF (Electricité de France, France), CEA (France), and CIEMAT (Centro de Investigaciones Energéticas, Medioambientales y Tecnológicas, Spain).

A (very) large dismantling programme was first proposed by engineers from the EURIDICE EIG (dismantling dossier version 0 – Dereeper et al., 2000 a – and dismantling dossier version 1 – Dereeper et al., 2000 b). For budgetary reasons (a maximum budget of ~1.2 MEUR had been fixed) ONDRAF/NIRAS had asked for these to be reduced. Among other things, the working group was responsible for the reduction of the proposed programme to an acceptable level.

6.2.1. Reduction of the initial programme: context and criteria

To reduce the dismantling programme initially proposed, several criteria were established.

The transferability of the results (or methodology) and their relevance for other repository designs was a first important criterion considered. Indeed, in 2001, before the preparation for the mock-up dismantling, ONDRAF/NIRAS decided to thoroughly revise the reference design for disposal of vitrified HLW, not only because of the chemical observations made during the operational stage of the OPHELIE mock-up (mainly the high chloride concentration), but also because of technical difficulties highlighted during the preparation of the PRACLAY Experiment and the preparation of the SAFIR-2 report (ONDRAF/NIRAS, 2003)

The transferability criterion was therefore set in order to make the information gained from the dismantling programme as useful as possible in the development of the three designs. Applied

[1] The proposed sampling plan was not restrictive. Depending on the observations, additional buffer samples could be taken for specific analysis i.e. buffer material in contact with the corroded zone of the metallic components, …

to these designs, the transferability criterion was mainly related to the roles and functions of the steel 'overpack' and more specifically to its resistance against corrosion.

The other criteria taken into account in establishing the final post-dismantling programme were:

- the added value for the PRACLAY Experiment;
- the understanding of the unexpected observations made during the operational stage;
- the contribution of the disposal tube and the buffer material to the confinement safety function;
- the unique character of the experiment and the impossibility of obtaining the results by other means.

6.2.2. Content of the dismantling programme

The outcome was a final version of the post-dismantling analysis programme that focused on the following topics:

- a visual inspection of the swelling process during dismantling operations (presence of voids, state of the joints, presence of zones enriched in clay or sand …) and investigation of the thermal, hydraulic, mechanical and coupled THM behaviour of the buffer material, including execution of numerical simulations to help interpret the complex processes (saturation, desaturation, …) experienced by the material. An extended hydro-mechanical characterisation of the initial materials (and the exposed one for verification) was carried out in order to obtain the parameters required to develop the constitutive law needed for the numerical simulations;
- a visual inspection of the state of the different metallic components during dismantling and an experimental programme studying the corrosion susceptibility of the different types of stainless steels present in the mock-up and that were in contact with the buffer material;
- an investigation of the chemical (pore water) and microbial conditions prevailing in the mock-up to support the corrosion analyses;
- a mineralogical and physico-chemical characterisation of the initial and exposed buffer material to support the THM studies and the corrosion analyses and to verify whether some of the unexpected findings could be explained by mineralogical changes;
- a visual inspection of the state of the different types of sensors and an investigation of their failure mode.

Taking advantage of the presence of concrete segments in the mock-up, tests to verify whether the operational conditions had influenced their mechanical properties were included in the post-mortem analysis programme.

6.3. Dismantling operations

6.3.1. Work organization

To perform the dismantling of the internal of the mock-up without interruption, two teams of seven people worked in continuous 12-hour shifts. Each team consisted of:

- two technicians for the sampling and dismantling operations, working in front of, or inside, the mock-up;
- one person for the observations and visual inspections during the dismantling, leading and documenting the sampling operations;
- three people (two technicians and one engineer) for the packaging, storage and codification of samples and sensors;
- one person for the general co-ordination of the dismantling operations;
- two people from CEA to carry out analyses (mainly determination of water content and density and mineralogical observations).

An overlapping of the shifts was planned to avoid interruption and to allow a short briefing between subsequent shifts.

Once the mock-up was empty, removal of the disposal tube and subsequent sampling of the metallic parts was performed according to a timetable of 8 hours per day.

All the dismantling operations were carried out under the supervision of the Operations and Safety Manager of the EURIDICE EIG.

6.3.2. Sampling methodology

Samples were taken from the buffer material, the different types of metallic components in contact with the buffer and the concrete segments.

Buffer material

The buffer material was sampled in two main zones in the middle of the mock-up (Figure 6-1), where the highest and the most uniform temperature fields were obtained during the heating phase. These central zones were most representative of the mock-up.

The samples for the mechanical, hydraulic and hydro-mechanical characterisations were taken from the same or several neighbouring sections in the zone A and/or B. It allowed the analysis and comparison of samples subjected to the same paths during the experiment. The variations in the hydro-mechanical properties were expected to be greater following a radial profile rather than a longitudinal one.

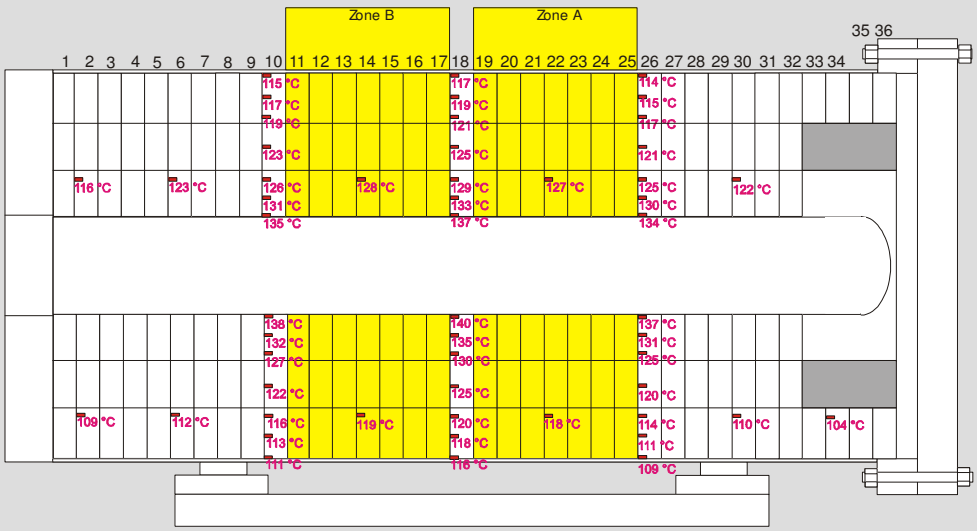

Figure 6-1: The main sampling zones and the temperature distribution inside the buffer (values from 6th of April 2001).

Samples for other investigations were not limited to these two zones. Samples were taken following a radial and a longitudinal profile, such as samples for:

- density and moisture content determination: the sample distribution was independent of temperature field but was only based on a geometrical criterion;
- chemical and mineralogical investigations;
- thermal conductivity measurements performed on three sections close to the section largely instrumented with thermocouples.

For each post-mortem analysis, a sample procedure specified the sampling process, such as sampling tools (core drilling, pushing tube, electrical saw, …), packaging and the sampling plan, specifying the exact location of the samples. The samples were located exactly using a theodolite.

A distinction was made between the sampling plan and the analysis programme. The dismantling was a unique opportunity to obtain samples of various components subjected to similar HLW disposal conditions. It was therefore decided to take a large number of samples which were not directly analysed but remained available as back-ups or, if required and financially possible, for further analyses. The additional samples were carefully packaged and stored to guaranty the quality of their long-term preservation.

The proposed sampling plan was not restrictive. Depending on the observations made during the dismantling, additional buffer samples were taken for specific analysis (for instance buffer material samples in contact with the corroded zone of the metallic components,…).

Steel components

The position and quantity of the samples for corrosion analyses were decided during the dismantling operations, after visual inspection and depending on their relevance. The position of the analysed samples is given in section 10.4.

Concrete segments

Two exposed and one non-exposed concrete segments were sampled for mechanical tests (section 13.1.3).

6.3.3. Packaging, labelling and interim storage

For the other post-mortem analyses, and to limit the risk of oxidation or desiccation as much as possible and prevent all gas diffusion and disturbances, the buffer samples and pieces of hydration tubes and sensors (for corrosion tests) were wrapped in plastic foil and vacuum packed in a PE/PET aluminium coated bag immediately after removal and inspection (dimensions and photos). For geo-chemistry analysis samples, a specific combination of inert gas filling (argon) and vacuum was used.

Bags with samples for geomechanical post-mortem analyses were immobilized in a container with plaster. Each package was assigned a unique code.

Before being delivered to the various laboratories, the samples for chemical and microbial analyses were stored in a cold room (4°C) to slow down kinetics and microbial growth.

6.3.4. Documentation, QA/QC aspects

Two different records were planned for the dismantling operations: the dismantling logbook and the sample track record:

- the dismantling logbook contains all the observations and actions made during the dismantling and sampling operations. Each record in this logbook contains the date and time, and the name of the operator(s) in addition to a detailed description of the observations and/or actions, and the work procedure applied (if any). For some procedures, specific forms had to be completed. For regular sampling activities, a copy of the sampling section was completed, while for particular observations and unplanned actions (material heterogeneities, localised corrosion, damage due to operations, …) section templates were available for documenting purposes (e.g. to indicate exact positions);
- the sample track record ensured the complete traceability of each sample. This record detailed the sampling conditions (date, time, operator, environmental conditions, dimensions, location …), the packaging and storage conditions, and finally the delivery conditions as well as every incident that occurred during these various steps. The record was completed by the person in charge of the sampling operations, the leader of the

packaging team, and the person responsible for the sample's delivery to its final destination.

Written notes were complemented by photographs and video footage. Video footage was planned for all main operations (removal of the different covers, the concrete segments, the buffer and the central tube...). These were identified by production date, combined with a sequential number. Each record (sample track record, sampling section record, record in dismantling logbook) contains a list of the photographs and video footage related to it.

6.3.5. Dismantling operations

The dismantling operations were conducted according to the main steps mentioned in Table 6-1.

Table 6-1: Chronology of the main actions performed on the mock-up.

2002-08-26	Switch off the heating elements – start of the cooling phase
2002-08-27	Removal of the thermal isolation
2002-09-24	Preliminary buffer core drilling
2002-10-02	Start of bolted cover and internal components removal (buffer, sensors and hydration
2002-10-11	End of internal components removal
2002-10-16	Removal of central tube
2002-11-15	Sampling of metallic components

6.3.6. Preliminary buffer core drilling

To obtain an as undisturbed (non oxidised) sample as possible, and to get an idea of the state of the buffer material prior to the actual dismantling, a core drilling through the steel jacket was carried out during the cooling phase. With a pushing tube, a large core from the buffer of the radial profile (from jacket to the central tube) was obtained (Figure 6-2, TOP LEFT and BOTTOM LEFT). However, the total length could not be retrieved because there was a spacer element in front of the pushing tube.

6.3.7. Removal of internal components

Before the instrumentation covers were removed from the bolted cover, the hydration system was purged to remove the remaining water, and filled with nitrogen gas to avoid early oxidation of the buffer.

The removal of the buffer material and all sampling operations lasted about 10 days. It progressed at a rate of two sections per 12 hour shift (including all the related sampling analyses and other measurements – e.g. pH and Ecorr), except for the first part. The area of the concrete ring, extending over the first four sections (sections #33 to #36) also had to be removed in one shift.

Figure 6-2: Core boring operations (TOP and BOTTOM LEFT). Sampling operations of the stainless steel liner (RIGHT).

W si ne
ja d ill
se m

A n ns
al n of
th o 0)
af

After removal of the central tube, stainless steel re
6-2 RIGHT) were taken for further corrosion inv

6.4. Main conclusions

The systematic preparation for the dismantling ed
scenarios - resulted in the smooth progress of to
account are the time required (a continuous ope nd
human resources (at least 2 shifts are needed du),
laboratory facilities (analyses), and logistical and technical possibilities in general. In particular,

a detailed sample programme proved to be essential, specifying the sampling method, packaging requirements, etc… for each sample.

Although a detailed work programme is essential, flexibility has to be built in to deal with unexpected observations (and for example taking additional samples). Equipment such as microscopes – together with qualified operators - was available on site. Maybe more sophisticated analytical facilities would have been useful for performing immediate, on site determination of unusual substances for example. A stricter (faster) procedure for determining the water content and degree of saturation was also proposed in order to limit the experimental artefact's impact on the degree of saturation measurements as much as possible and thus the doubts on the results obtained as discussed in section 12.3.4.

The work schedule was based on dismantling two buffer sections each shift. In the beginning this was quite tight, while at the end it was rather relaxed and maybe an additional section could have been dismantled.

7. Global behaviour of the buffer material: observations made during dismantling

The dismantling operations for the OPHELIE mock-up allowed the global behaviour of the buffer material after it was subjected to operational conditions to be observed, as along with the state of the concrete segments and the metallic components.

All the observations made during dismantling were the subject of a detailed report (Raynal and Jullien, 2002, parts 1 and 2).

Information relating to the state of the metallic components (corrosion) and the sensors is mentioned in chapters 10 and 11 respectively.

7.1. Main observations made just after the removal of the cover: filling sand movement and state of the concrete segments

On opening of the cover, it was be observed that the SIBELCO M32 sand, added to the mock-up after the cover was bolted to fill the remaining voids, had penetrated the lower zone between the buffer blocks and the lining (Figure 7-1, LEFT). This penetration occurred before the swelling of the buffer took place, probably during the flooding of the mock-up. The presence of the sand is also the only explanation for the hydraulic connection between some hydration tubes, which was observed during the operational stage (section 5.3.1). This sand was still visible further on, until section #25, that is to say over a length of about 1.5 m. On the other hand, the buffer at the deep end of the concrete ring (section #32) had penetrated the central part (Figure 7-1, RIGHT). The sand that initially filled this zone had been compacted by the swelling buffer.

Figure 7-1: Initial view of the mock-up after cover is removed (LEFT). SIBELCO M32 sand (white) had penetrated the lower zone up to section #25. Concrete ring after removal of PTFE discs at end of the central tube and removal of excess sand (RIGHT). The buffer material had penetrated the central part (blue arrows).

Th g ght
tilt t een
du id ved
on re the

concrete segments. Black colouring on the upper intrados of the concrete ring was observed. This consisted of mercury coming from a leaking load cell; also a cavity some 40 cm wide was observed at this location. The lower intrados showed no contamination.

7.2. Global behaviour of the buffer material

When the complete buffer sections were reached (between section #32 and section #1), some general characteristics relating to the M2 buffer material were observed:

- no empty spaces were left in the mock-up; the swelling buffer had closed all initial voids, Figure 7-3 TOP). The spacers, placed in the lower part of the mock-up to observe the initial annular gap (36 mm wide) during the buffer block placement, were completely filled and lost within the material; there was also strong (mechanical) contact buffer/central tube, buffer/steel liner and buffer/hydration tubes;

- expansion had mainly taken place in the outer ring, which was verified by measuring the geometry of the blocks and by determining the water content and the dry density during dismantling (chapter 12). The increase of the block volume through swelling was assessed between 4 % and 6 % for the outer rings and between 1.5% and 2.5 % for the middle and inner rings (Figure 7-2). A beige colour on the blocks of the outer rings confirmed the swelling of the clay platelets. In this location, the material appeared to be more plastic. The thickness of the clearest part was in the order of 6 to 7 cm. At the level of the joints opposite the hydration tubes, this thickness was between 10 and 15 cm (Figure 7-3, BOTTOM LEFT);

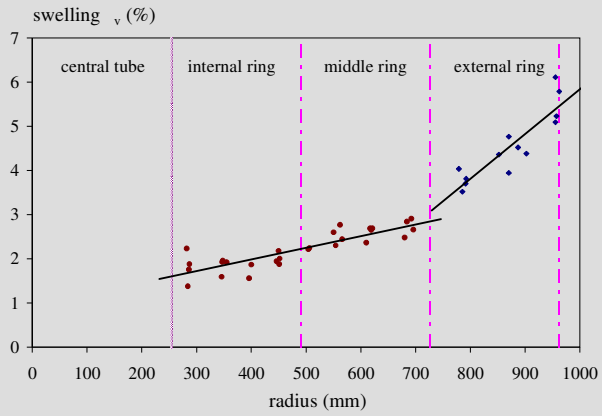

Figure 7-2 : Increase of the block volume through swelling.

- except for the colour change mentioned above, the texture of the initial material did not change visually. On the interface with the central tube, no fissuring under thermal load was observed. As for the outer ring, however, the material directly in contact with the central tube showed lighter coloration (some millimetres) and seemed slightly more plastic. Generally, it was not possible to detect an overall mineralogical zoning/evolution between the central tube and the liner visually that could be attributed to the thermal gradient;

- the joins between the blocks (of a same section) were still clearly visible, although the buffer did not easily break along them; however, between subsequent sections the blocks separated easily. Even the marks on the blocks were still perfectly legible. These observations tend to prove that the hydration process was not homogeneous. The joins between blocks formed preferential hydration paths (channel effect). The presence of the hydrophobe graphite film on the contact surfaces between blocks of a same section probably amplified the role of the joints in this heterogeneous process. It can logically be assumed that the hydration process developed as follows: penetration of water in all the joints followed by diffusion within the blocks ;

Figure 7-3: The buffer material filled all initial physical gaps (TOP). The swelling mainly occurred near the hydration tubes (BOTTOM LEFT); the joints between the blocks, and even the identification marks were still clearly visible although closed. The sections separated quite easily during the dismantling works (BOTTOM RIGHT).

- e …sor
  ll …tial
- …the
  …by
- …M2
  …e to

contamination while manufacturing the blocks of the central crown at the CTE plant in Libos, which uses this material on an industrial scale to produce heat-resistant bricks.

With regards the aforementioned observations, no longitudinal anisotropy was observed except for the presence of sand between section #36 and section #25 as discussed above.

Contrary to the M2 material, the swelling process of M14 seems to have been homogeneous because of the higher clay content and the larger accessible void in its immediate neighbourhood. Therefore, no colour zoning was observed and it was no longer possible to distinguish the joints between the blocks. Moreover, the material's plasticity was higher than that of the M2 material.

8. Mineralogical and chemical evolution of the exposed buffer material

8.1. Introduction

Before and during the experiment's operational stage, the initial M2 pre-fabricated buffer blocks (mixture with 60 wt. % FoCa clay, 35 wt. % sand SIKA type MX123 and 5 wt. % graphite TRIMREX T 140-600) were subjected to a basic mineralogical and physico-chemical analysis programme (section 4.3.2). At the time, the main objective was to confirm that the developed material properties met the requirements fixed for its development in terms of thermal conductivity, hydraulic conductivity, etc. Following the unexpected phenomena and processes observed during the operational stage (section 5.3), it was decided, in the scope of the dismantling programme, to carry out a more detailed mineralogical and physico-chemical characterisation of the initial and exposed materials. The main purpose was to verify whether these unexpected phenomena and processes could to some extent be explained by the mineralogical and physico-chemical evolution caused by the operational conditions of temperature, pressure and hydration the material was subjected to. For instance, it was of interest to verify:

- possible mineralogical changes affecting the texture of the buffer material exposed to heat or mass transfer and which could explain the lower than expected swelling pressure and/or the apparently high thermal conductivity observed;
- if the elevated concentrations of chloride, dissolved organic matter, and dissolved silica measured in the water from leaked strain gauges close the central tube were due to technological or sampling artefacts, or really related to the mobility of these elements – under the effect of a thermal gradient;
- if precipitated sulfide (ZnS, FeS_2) observed in the water accumulator (which was a first sign that microbially-mediated sulfato-reduction was at work and where high concentrations of dissolved sulphides were also measured – see chapter 9), was also present in the buffer material itself and to see if a redox-front could be detected in the buffer material around the hydration tubes.

The mineralogical and chemical analyses were contracted to the 'Service Analyse et Migration des Radioéléments' (SAMRA) of CEA Cadarache (France). The following three technical documents present the results of the chemical and mineralogical analyses:

- NT SAMRA 01-0056 (characterisation of the initial material, Raynal and Jullien, 2001);
- NT SAMRA 03-045 (characterisation of the exposed material, Raynald and Petronin, 2003);
- NT SAMRA 03-043 (characterisation of the joins, Pozo and Petronin, 2003).

8.2. Materials and methods

The characteristics of the initial buffer blocks were studied first. The same mineralogist team performed the analyses of the exposed material using the same analysis techniques[2]:

- X-ray Diffraction (XRD) conducted by the 'Laboratoire Environnement et Minéralurgie' (LEM) of CNRS Nancy (France) ;
- Fourier Transform Infra-Red Spectroscopy (FTIR) conducted by the LEM and the LTCR (CEA);
- Thermo-Gravimetric Analyses (TGA);
- Differential Scanning Calorimetry (DSC);
- Chemical analyses (major and trace elements);
- Cation exchange capacity (CEC) and population of exchangeable cations.

The chemical analyses (conducted by the CRPG Nancy) consisted of the following analyses on the bulk rock (after block crushing) and clay fraction < 2µm (after granulometric separation):

- major elements by Inductively Coupled Plasma – Atomic Emission Spectrometry (ICP-AES): SiO_2, Al_2O_3, Fe_2O_3, MgO, MnO, CaO, Na_2O, K_2O, TiO_2, P_2O_5;
- trace elements by Inductively Coupled Plasma – Mass Spectrometry (ICP-MS): As, Ba, Be, Bi, Cd, Ce, Co, Cr, Cs, Cu, Dy, Er, Eu, Ga, Gd, Ge, Hf, Ho, In, La, Lu, Mo, Nb, Nd, Ni, Pb, Pr, Rb, Sb, Sm, Sn, Sr, Ta, Tb, Th, Tm, U, V, W, Y, Yb, Zn et Zr on the bulk rock;
- others elements by chemical methods: Cl, S, F, H_2O, Fe^{2+}, C_{org} and C_{tot} (by measurement of the gaseous CO_2 flux after combustion at 800 °C).

Most of the samples analysed[3] for mineralogy and the physico-chemical characterisation were taken from section #19 (Figure 8-1), located in the middle of the mock-up and considered as representative of the overall functioning of the buffer material. As no texture or colour change was observed, the choice of the 27 samples to be analysed was based only on their spatial distribution: in the vicinity of the central heating tube, near the peripheral liner, or at joins between the rings and blocks, …. For the chemical analyses, some samples taken in section #1

[2] No mercury porosimetry measurements, nor BET specific surface determinations (method of Brunauer – Emmett – Teller), although initially planned, have been applied to the buffer materials because the clay porosity was strongly affected by the desiccation of the samples, and because nitrogen gas could not access all the surface interlayer sites.

[3] 48 samples taken with an electrical saw from section 19 and 27 were analysed. 21 others were retained for potential future analyses.

(coldest part of the mock-up) and from section #12 have also been analysed to verify the measurements at section #19.

The joins at the interfaces between blocks and between rings of section #19 were also examined by optical microscopy, Scanning Electron Microscope (SEM) and Transmission Electron Microscopy (TEM).

Several hundred bentonite buffer samples were taken from particular areas (interface buffer/concrete, interfaces buffer/corroded metallic elements …) but not analysed as part of this project.

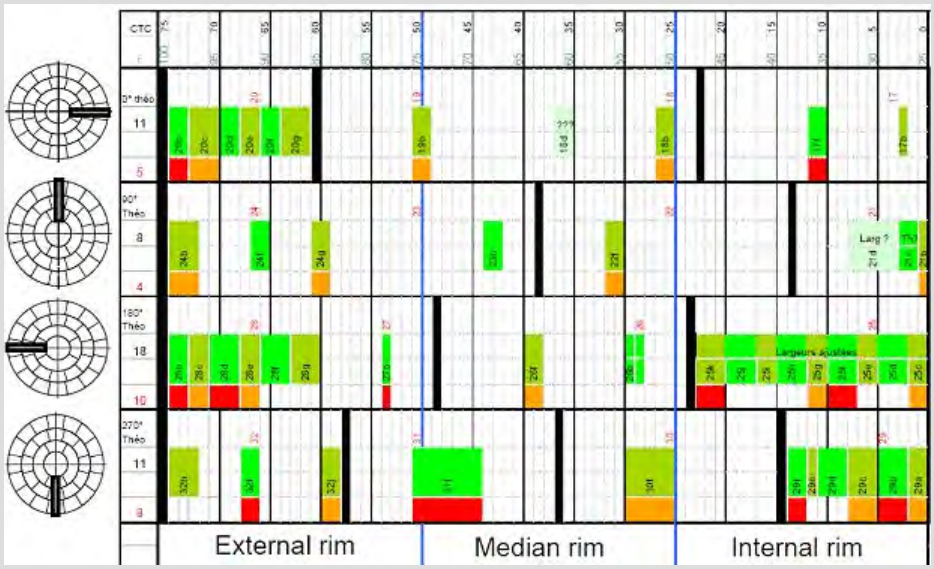

Figure 8-1: Position of the 48 samples from section #19 pre-selected for mineralogical and physico-chemical analyses. Samples highlighted in orange and red are those analysed.

8.3. Mineralogical analysis of the initial and exposed materials: main results

From the mineralogical and chemical analyses of the initial material, it stands out that:

- after verification and as expected, no significant differences could be seen between the M2 mixture and the pure FoCaPr (in all cases, the XRD and FTIR spectra of the FoCaPr and the M2 mixture are very similar, especially for what is dealing the argillaceous phases). The only differences arise quite logically from the XRD response (Figure 8-2) of the only adjuvant and their associated accessory minerals. As the quartz sand and graphite are considered as inert additives, the FoCaPr bears all the chemical reactivity of the blend;

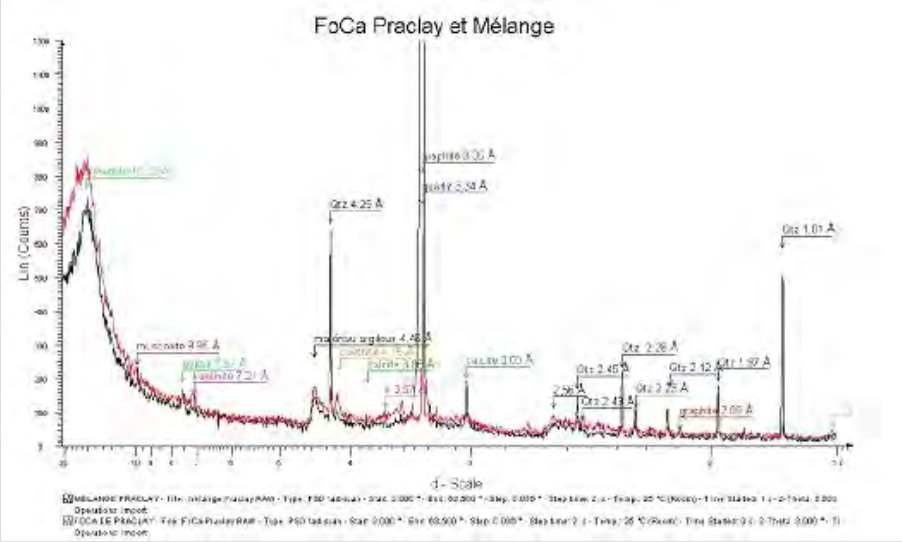

Figure 8-2: Comparison between DRX spectra of FoCaPr (red line) and (non exposed) M2 mixture (black line). From this figure it appears that FoCaPr also contains quartz.

- among the trace elements in the M2 mixture, zinc, up to 360 ppm, is certainly the most dominant. It could explain why wurtzite precipitate was observed in water tubing connected to the mock-up's water accumulator when the product solubility of ZnS was exceeded at the higher pH imposed by $NaHCO_3$. So, the zinc source could have been in the buffer material itself, and not only in the galvanised steel drum containing the reserve bicarbonate solution as assumed;

- about 28 ppm of chloride (mg/kg) was measured in the dried solid phase FoCaPr. This point is important in the mass balance calculations dealing with the transport of chloride towards the heating source;

- the total sulphur concentration in the material is not the same in the M2 mixture and the FoCaPr. There was more total sulphur in the M2 mixture than in the FoCaPr. This discrepancy could be attributed to some extra gypsum accompanying the quartz sand provided by SIKA;

- the gypsum content in the M2 mixture is estimated to be ~ 0.34 wt. % and 0.56 wt. % in FoCaPr (value consistent with the data obtained on the FoCa7 batch material which was about 0.4 wt. %). The total mass of buffer material in the mock-up (~ 23.5 tons) therefore contains about 80 kg of gypsum. If this quantity was to be distributed in the volume of injected water, it would represent 53 g/L of gypsum. This value is 22 to 24 times higher than the solubility limit of gypsum in pure water (2.4 g/L in cold water, and 2.2 g/L in water at 100 °C). So, the water inside the mock-up was always saturated in terms of gypsum;

- the calcite ($CaCO_3$) content of the FoCa Pr is estimated to be about 6 wt. %. This is unexpectedly higher than in the (very) well characterized FoCa7 batch (1.4 wt. %).

The analyses of the exposed material indicated that no important, or substantial, mineralogical changes could be evidenced between the initial and the exposed buffer materials but also spatially inside the mock-up. The M2 buffer material seemed to be very stable under the temperature and pressure conditions encountered in the OPHELIE mock-up, at least for the duration of the experiment. Thus:

- all the XRD spectra (on total rock samples and clay fraction < 2µm after the different steps[4] of the sample treatments) show very similar patterns. The non-clayey secondary minerals present on all the XRD spectra of the clay fraction are calcite and goethite (FeO(OH)). Anatase (TiO_2) is visible on some diffraction spectra, indicating that this mineral is present in small amounts close to the detection limit. This confirms the former data on the initial material. No formation of new minerals was observed in the exposed buffer material after the OPHELIE experiment: no trace of nahcolite ($NaHCO_3$) which should have precipitated from the hydration water, was detected;

- as for XRD, no significant variation was observed between the different samples from the FTIR analyses. The M2 material appeared to be homogeneous over the entire section #19: no singularity was apparent on the spectra of samples taken at the contact with the central tube, nor on those in contact with the liner at the periphery of the mock-up;

- TGA and DSC analyses showed that the bentonite remained calcic. No sign of supplementary pyrite oxidation was evidenced.

8.4. Chemical analyses and mobility of elements in a thermal gradient

In spite of the initial heterogeneity of the M2 material which is a mixture of three phases, the results of the chemical analyses on the M2 mixture of samples from section #19 were relatively homogeneous (Raynal and Petronin, 2003). It is difficult to comment on the SiO_2 evolution because its content strongly depends on the abundance of sand grains in the analysed sample. This is reflected by the inverse evolution of Al_2O_3 and Fe_2O_3 whose concentrations depend only on the clay component of FoCa Pr. The Fe_2O_3 values measured in the exposed material seemed lower than those of the initial reference mixture, although it is difficult to claim that this reduction is significant.

The CaO profile (Figure 8-3, TOP LEFT) followed that of calcite, gypsum, and interfoliar calcium of FoCa clay. The CaO content was also in the same order of magnitude as that of the initial M2 reference mixture. This behaviour is extremely consistent with the observations made by Karnland et al., (2000) on an in-situ heating experiment at Stripa which also: "suggest transport of Ca^{2+}, SO_4^{2-} and HCO_3^- ions toward the heat source, where gypsum and calcite precipitate because of their retrograde solubility, and Ca^{2+} exchanges for Na^+ in smectite"… ."The presence of precipitated gypsum is observed in bentonite near the central tube surface". This quotation could also be applied directly to the OPHELIE mock-up.

[4] Naturally oriented section, after saturation with ethylene glycol and then after heating at 550 °C.

A moderate enrichment in inorganic carbon related to $NaHCO_3$ can be evidenced on radial profiles as a function of the distance to the central heating tube (Figure 8-3, TOP RIGHT).

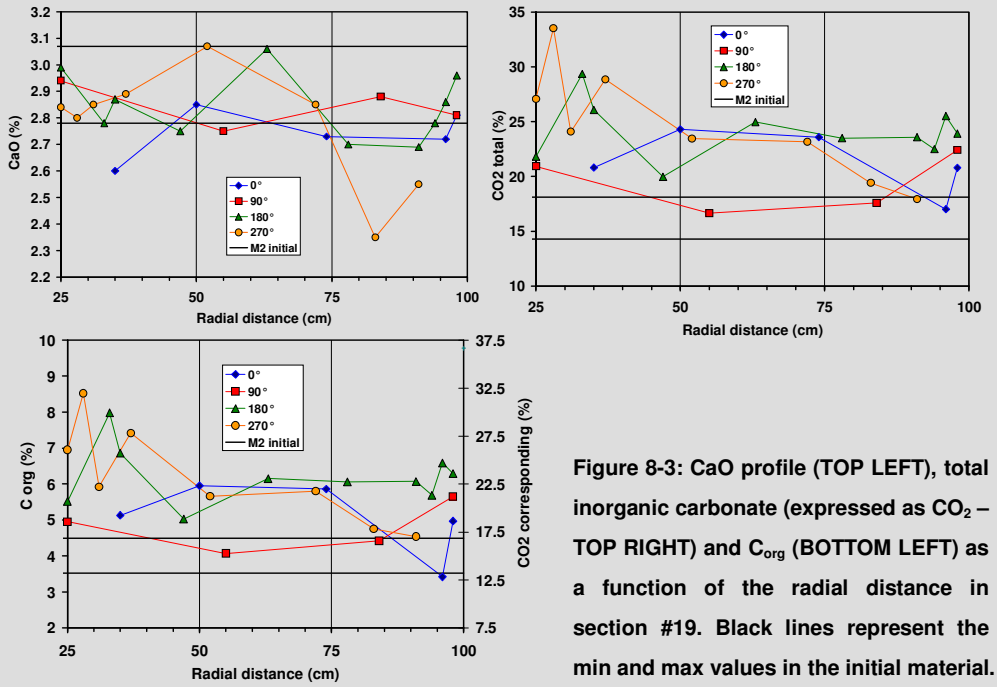

Figure 8-3: CaO profile (TOP LEFT), total inorganic carbonate (expressed as CO_2 – TOP RIGHT) and C_{org} (BOTTOM LEFT) as a function of the radial distance in section #19. Black lines represent the min and max values in the initial material.

A similar enrichment was also observed for organic carbon (C_{org}) near the heating tube (Figure 8-3, BOTTOM LEFT). The contents of other major elements are below the detection limit (MnO, Na_2O, K_2O and P_2O_5), affected by important uncertainties (> 10 % for MgO), or do not significantly change (TiO_2).

The chlorine content is systematically higher than in the initial M2 mixture (Figure 8-4, LEFT). An enrichment of chlorine towards the central tube (confirmed by the analyses of samples from sections #1 and #12) was also observed. This agrees with the measurements of the same elements in pore water extracted from the buffer material by rehydration/squeezing. A tentative explanation for this phenomenon is given in chapter 9.

It is also worth mentioning an unexpected correlation between organic carbon and chlorine (Figure 8-4, RIGHT) although this currently remains unexplained. A parallel could also be drawn in the correlation observed between organic carbon and dissolved silica (chapter 9).

Among all the chemical profiles, that of total sulphur shows a highly characteristic evolution as a function of the radius (Figure 8-5). The sulphur concentration strongly decreased in the zone close to the external liner suggesting a lower quantity of gypsum in that location. A first explanation is that this zone was initially empty, and strongly influenced by hydration, giving rise to gypsum dissolution. Another tentative explanation is that, because of the microbial activity observed in the water hydration system, dissolved sulphates were reduced and reprecipitated as insoluble sulphides very close to the hydration tubes at the periphery.

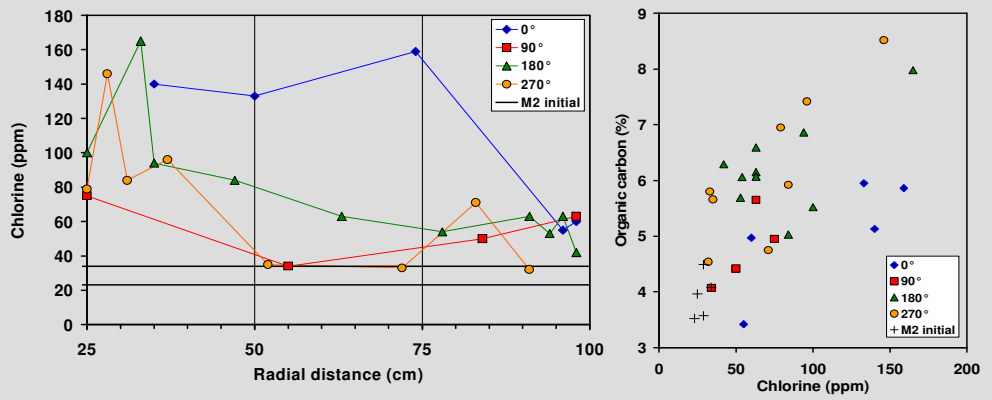

Figure 8-4: Profile of chlorine as a function of the radial distance (LEFT) and correlation between chlorine and organic carbon at section #19 (RIGHT). Black lines represent the min and max values of the initial material.

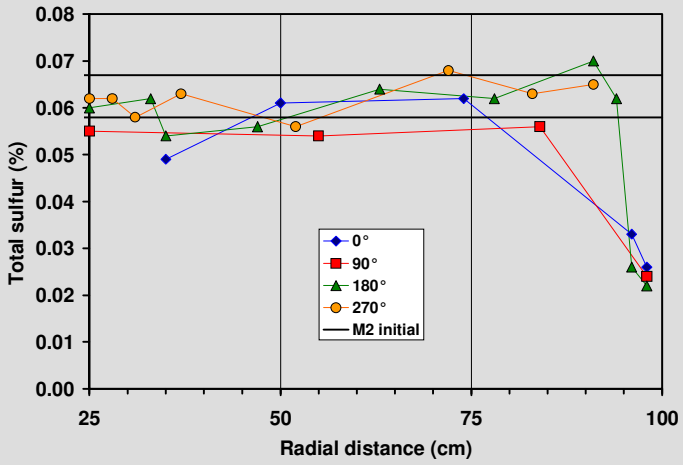

Figure 8-5: Profile of total sulphur as a function of the radial distance at section #19. Black lines represent the min and max values of the initial material.

For the trace element contents, it was noticed that these are generally higher in the exposed material than in the initial material (except for Cd and Ga) without clear trends. It is likely that this difference arises from the reproduction of the analysis techniques themselves because the samples were not analysed at the same time. Conversely, for the exposed buffer samples, no spatial difference is observed.

8.5. Cation exchange capacity and exchangeable ions population

The analyses (determination by the copper ethylene diamine method) indicated that the cation exchange capacity (CEC) of the exposed M2 material did not significantly vary with respect to the reference unexposed M2 material. Variations were within the error range of the method estimated at ± 2 ceq/kg. As shown in Figure 8-7, the CEC profiles of the exposed material did

not exhibit major trends as a function of the radial distance. Similarly and consistently, Na^+, K^+, and Mg^{2+} did not significantly change.

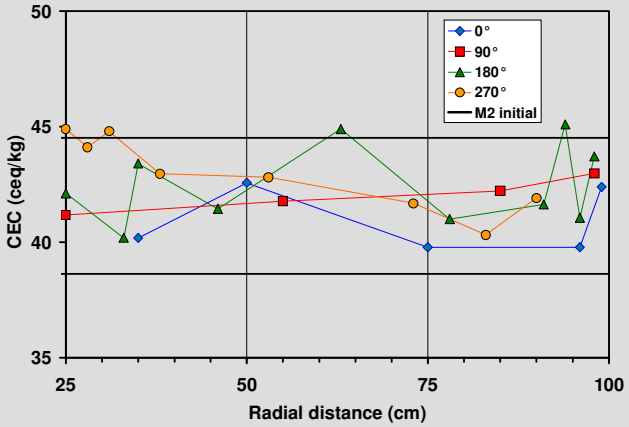

Figure 8-6: Profile of CEC as a function of the radial distance.

The sum of the exchangeable cations (~ 77 ceq/L) was almost twice as high as the cation exchange capacity (~ 42 ceq/L). This was mainly due to calcium (~ 70 ceq/L) released by the dissolution of gypsum and calcite during exchange with copper ethylene diamine. As a consequence, the value of exchangeable calcium cannot be estimated. However, the values obtained for the other exchangeable cations (Na^+, K^+, and Mg^{2+}) can be considered as representative (Σ = 7.5 ceq/L). The values for Mg^{2+} (~ 4 ceq/L) and K^+ (~ 0.9 ceq/L) determined on the exposed material were around the same magnitude as for the initial reference material. For exchangeable Na^+, (~ 2.6 ceq/L) the exposed samples exhibited a slightly higher proportion of Na^+. This cannot be explained just by the influence of the nature of the solution (1.173 g/L $NaHCO_3$) used to hydrate the buffer material, because the total quantity of sodium injected (only 480 g of Na^+ were present in the total volume of injected water) was too small with respect to the 23.5 tons of M2 mixture. This corresponds to 0.1 ceq/L of exchanged sodium, well below the accuracy of the copper ethylene diamine method. This explains why the formation of a sodic clay could not occur in the case of the OPHELIE mock-up.

8.6. Redox front – redox states in the mock-up

The persistence of gypsum and the formation of sulfides have allowed information on the redox state of the engineered barrier at the end of the OPHELIE experiment to be obtained.

Two totally opposite redox-conditions were detected in the OPHELIE mock-up, in the buffer material inside the mock-up, and in the hydration system water outside the mock-up respectively. On the one hand, several mineral phases, such as goethite, hematite, and gypsum, observed in the buffer material, both in the initial and exposed, indicate the preservation of oxidizing conditions within the buffer blocks. On the other hand, in the meantime, the significant concentration of dissolved sulfides, the wurtzite precipitate and the negative redox potential (E_h between -250 and -400 mV, SHE, depending on the pH conditions, varying from 5 to 8.5) clearly revealed slight to strong reducing conditions in the hydration system water (chapter 9).

However, no redox front was clearly observed in the buffer material as was previously noticed on FoCa clay samples from an in-situ heating experiment conducted at the Stripa mine (Jullien et al., 2000). It was not possible to distinguish a clear redox-transition zone in the buffer material along the radius from the outer side of the mock-up towards the central tube: most of the bentonite blocks retained their original ochre/brown colour typical for Fe(III) oxy-hydroxides, and gypsum was predominating.

It is likely that a very steep transition zone (~ mm) existed in the periphery of the hydration tubes, where the graphite-rich, grey coating, the oil released by defective Glötzl cells (section 11.2.9), and organic mater would have provided chemical conditions favourable for the growth of the sulfato-reducing and methanogenic bacteria observed in the hydration system. Because of the low solubility of metal sulfides (FeS, FeS_2, ZnS, …) precipitation should have occurred quickly after the diffusion of sulfides from the hydration tubes to the surrounding clay material. The transition zone remained undetected on the level of general macroscopic observations (this is also the zone where the blocks swelled after their desegregation by flooding due to the presence of the large annular initial void) and microscopic analyses of this zone were not carried out, these analyses[5] not being a priority of the Belgian Programme.

8.7. Microscopy studies and characterisation of the joins

Microscopic analyses (Optical, SEM and TEM) were performed on join samples selected from section #19 (Figure 8-7):

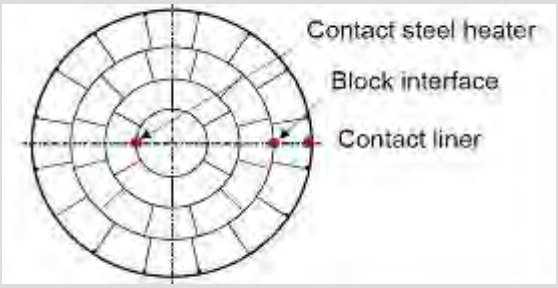

Figure 8-7: Position of the joins analysed in section #19.

The main information obtained from the analyses was as follows:

- a small relatively disturbed zone was observed at the join contact with the central tube (Figure 8-8). Analyses on the micrometric scale did not reveal any difference in the overall clay composition. This seems to be due to a number of small silica crystals spread throughout, as if sand grains had been fragmented (Beaucaire, 2003);

[5] Nevertheless, in spite of these limitations, the presence of small neoformed crystals of pyrite in the lens of sand initially formed by the water flooding below the buffer material at the bottom of the mock-up was noticed. Small cubic crystals rich in iron and sulphur, and dispersed throughout the sand samples were observed by SEM analyses.

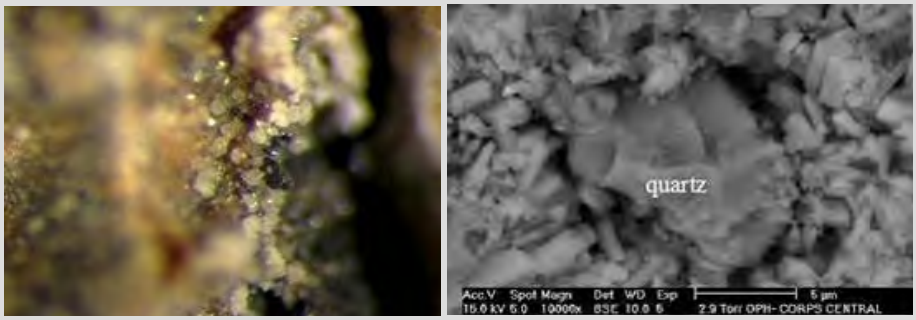

Figure 8-8: New crystallisation of silica grains at the contact with the heater underline the partial alteration of silica rich minerals. The pictures were taken with an environmental OM (LEFT) and a SEM (RIGHT).

- the joins between blocks were filled by graphite with a thickness of ~ 0.1 mm and delimit zones less homogeneous than the reference material (Figure 8-9, TOP). The presence of a graphite foil was also visible on the external surface of the initial blocks which was probably due to the manufacture process (chapter 4). The presence of the partially hydrophobic, graphite foil, prevented homogenisation of the material during the hydration process. This explains why the joins between blocks were still visible after the operational stage. It should be noted that at the level of the interface with the liner, the graphite film has been recovered by clay thanks to the presence of the large initial annular void which allowed the material to swell. In some places however, uncovered graphite foils subsisted (Figure 8-9, MIDDLE). There was no clay on the surface of the graphite grains, but there was some clay on the surface of the sand grains.

- recrystallised gypsum was found everywhere in the mock-up in the locations of initial physical gaps: on the interface with the central tube and the liner and in the joins between blocks (Figure 8-9, BOTTOM). The important dissolution of calcium sulphate present in the FoCa clay during the re-hydration phase was likely to have caused the precipitation of this substance in some well-hydrated points when the mock-up was heated-up. Indeed, gypsum solubility decreases with temperature. Gypsum precipitation was also observed in the frame of the in-situ heating test conducted with FoCa clay at Stripa (Pozo et al., 1997; Poinssot et al., 1997 a,b). The gypsum had indurated the FoCa clay by precipitating in the pore space close to the heated zone;

- On contact with the liner, an enrichment in iron (percentage in atoms between 32 and 35%) with traces of chromium (0.15 to 0.6 %) and lead (0 to 0.6 %) was observed. It probably originated from pieces of metal pulled out by corrosion at the level of the welds.

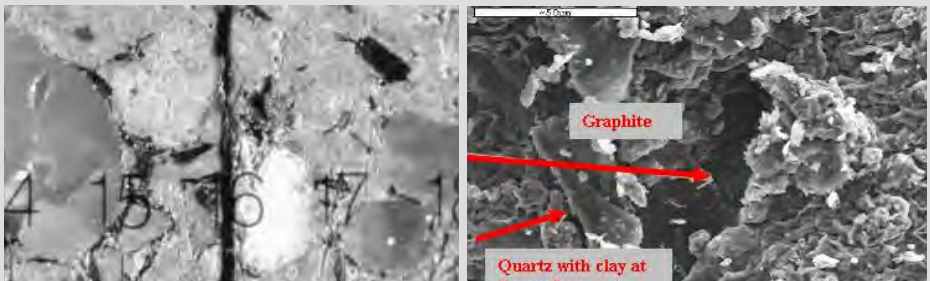

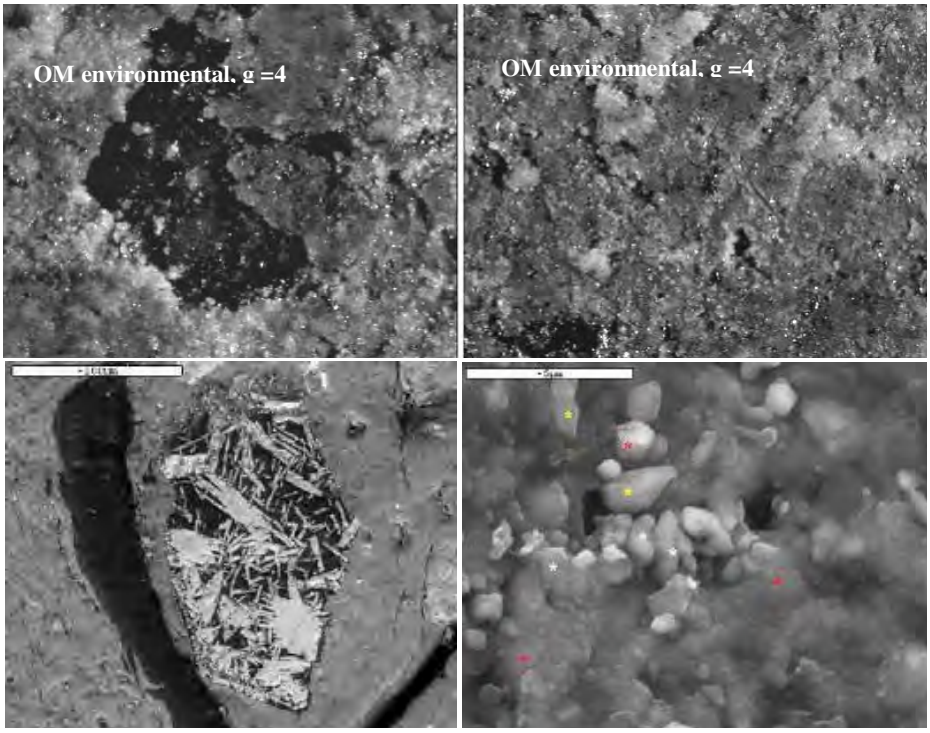

Figure 8-9: Join (about 0.1 mm thick) between two buffer blocks filled by graphite (TOP LEFT). On contact with the liner, the graphite was covered by swelled clay (TOP and MIDDLE RIGHT, pictures taken with an environmental OM and SEM respectively). However, some uncovered graphite foils subsisted (MIDDLE LEFT). Gypsum crystals close to the heater (BOTTOM LEFT). At the interface with the liner, gypsum (yellow crosses) combined with calcite (white crosses) was frequently observed (BOTTOM RIGHT). Red crosses represent quartz.

8.8. Comparison with the heating tests made at the Stripa mine

Because FoCa clay was also used in an in-situ heating experiment conducted at Stripa (former iron mine, Sweden), it is interesting to compare these results with those of Stripa and to verify the similarities and differences between the results of both experiments.

At Stripa, high mobility was observed (Jullien et al., 2000) for several elements under a strong thermal gradient (3 °C/cm):

- enrichment in Fe, Al and Si towards the cold zone, and;

- enrichment in S, Ca and Mg towards the hot zone.

At Stripa, the iron was highly mobile and precipitation of iron sulfide occurred in reducing conditions. At the iron/clay interface located between the metal heater (carbon steel) and the FoCa clay, the neoformation of berthierine, a variety of green rust (i.e., Fe^{2+} bearing iron oxy-hydroxide), was also observed.

The results obtained from the OPHELIE mock-up under a tenfold lower thermal gradient (0.3 °C/cm) essentially differs from those of Stripa on the following points:

- Si dissolved in the pore water was enriched towards the heating zone (as was also observed for chlorine and dissolved organic matter). The trend for the silicon enrichment was exactly opposite to the observations made at Stripa. A possible explanation is that the aforementioned Si enrichment only covers dissolved silicon which was analysed in the pore water recovered after rehydration/squeezing of the exposed M2 mixture at BGS, while at Stripa the silicon profile was measured directly in the solid FoCa samples. No significant changes for Si were noticed in the profile made directly on the M2 mixture solid samples (total silica);

- no stringent trends could be drawn for Fe and Al;

- no significant iron/clay interfaces were observed in the mock-up because no carbon steel was contacted with the M2 mixture. As stainless steel was the only source of iron at the interface with the central tube and the liner in the periphery of the mock-up, no substantial amounts of iron were released into the buffer material from these metal components. So the iron/clay interaction in the mock-up was not a relevant process from the point of view of the chloritisation reaction of smectites, i.e. the transformation of swelling smectite into non-swelling chlorite upon the formation of brucite-like $Fe(OH)_2$ bridges in the interlayer.

However, as observed in Stripa, calcite and gypsum seem to precipitate near the heating zone as would be expected from thermodynamical solubility calculations, because the solubility of these salts decreases with temperature.

8.9. Conclusions

Overall, no significant chemical or mineralogical changes were evidenced in the M2 mixture exposed to a temperature up to 140 °C at ~ 1MPa hydraulic pressure over approximately 4.5 years. The M2 buffer material correctly fulfilled its main roles: to fill all the gaps and interstices present just after the placement of the engineered barrier system, while providing a sufficiently low hydraulic conductivity to prevent preferential pathways for water circulation and a thermal conductivity high enough to dissipate heat.

However, some potentially aggressive chemical species in terms of metal corrosion, such as chlorine (accompanied by organic matter), demonstrated a local enrichment towards the heating element. This unexpected finding must be taken into account when defining the chemical boundary conditions for corrosion of the metal barrier. This enrichment of some

elements towards the central tube also agrees with the measurements of the same elements in pore water extracted from the buffer material by rehydration/squeezing at the British Geological Survey (BGS).

Neoformed calcium sulfate crystals were observed at the buffer's contact with the heating element in the centre of the mock-up, and at the interface with the stainless steel liner at the periphery. Gypsum crystals ($CaSO_4 \cdot 2\ H_2O$) were ubiquitous in the mock-up after dismantling indicating that the redox conditions remained globally oxidizing in the centre of the mock-up and inside the bentonite blocks. No important iron sulfide recrystallisations were observed inside the buffer blocks, or in the joins between them. No steep redox-gradient could be evidenced in the mass of the buffer materials. Reducing conditions, related to sulfate-reducing bacteria were only observed in the hydration circuit water. Some crystals of iron sulfide were only observed by scanning electron microscopy in the sandy lens extending below the bentonite buffer and where water had circulated in loops because of thermo-convection. Thermochemical sulfato reduction with graphite does not seem to have played a significant role in the centre of the OPHELIE mock-up, even in the heated zone.

Finally, no major change, or spatial variation, was really observed in the buffer material. This confirms the observations made during the dismantling operations. It appears that the nominal functioning of the mock-up did not lead to a significant evolution of mineralogy and physico-chemical properties of the buffer material.

9. Pore water chemistry and microbial activity

9.1. Introduction

The study of the geochemical and microbial evolution of the buffer material was not included in the initial objectives of the experiment. Nothing was foreseen in the original design of the mock-up for multidisciplinary researches related to the geochemistry of the buffer, water-rock interactions at elevated temperature, microbial perturbation, or their implications for the metal corrosion. For this reason, the mock-up was not equipped with simple instruments like piezometers enabling water sampling. Similarly, the initial chemical state and properties of the reference materials were not systematically characterized before starting the experiment. This limits in some case the interpretation of the results obtained.

In June 1999, during the operational stage, leaks observed in the stainless steel tubing of the strain gauges provided the opportunity to collect and to analyze pore water samples[6]. These analyses revealed important anomalies (section 5.3.3) with respect to the expected composition of the M2 mixture pore water given in Table 9-1 (Dereeper et al., 2000).

Table 9-1: Estimated composition range of the FoCa M2 pore water extracted by squeezing. This water composition was also used by SCK•CEN for diverse corrosion experiments.

Species (—)	Concentration (mg/L)	Concentration (mol/L)
Cations		
Ca^{2+}	600	1.5×10^{-2}
Na^{+}	180 – 260	$7.8 \times 10^{-3} – 1.1 \times 10^{-2}$
Mg^{2+}	35	1.5×10^{-3}
K^{+}	8.4	2.1×10^{-4}
Anions		
SO_4^{2-}	1 600	1.7×10^{-2}
HCO_3^{-}	70 – 160	$1.1 \times 10^{-3} – 2.6 \times 10^{-3}$
Cl^{-}	90	2.5×10^{-3}
F^{-}	1.6	8.5×10^{-5}

These chemical conditions representing an increased risk for the corrosion of the metallic barriers, especially for the disposal tube, if one considers the safety of the disposal system, it was decided to further study the chemical and microbial processes taking place in the mock-up.

The chemical and microbial characterization programme mainly consisted of analyses performed at three different periods:

[6] One of the main motivations was to verify the composition of water in contact with FoCa clay because at the same period the corrosion team wanted to know the exact composition of FoCa clay water in order to start new corrosion tests under representative conditions.

- during the operational stage: mainly time series of chemical analyses to follow the aqueous concentrations of major or critical elements (concentration in chloride, bicarbonate, sulphate, total organic carbon (TOC), dissolved silica, and major cations: Na^+, K^+, Ca^{2+} and Mg^{2+}). Two locations were sampled: water leaks from defective strain gauges installed on the central tube and the hydration system, at the periphery;
- just before dismantling (cooling phase), specific analyses of:
  - dissolved sulphides by polarography and capillary electrophoresis;
  - dissolved CO_2 and other gases by gas chromatography after recovery by water out gassing;
  - volatile and dissolved organic compounds present in the water of the hydration system by gas chromatography coupled to mass spectrometry;
  - on-line measurements of pH and Eh from a hydration tube at the periphery of the mock-up and the leak of strain gauge SG23, and;
  - microbial analyses of water samples from the hydration system to search basically for sulphate-reducing bacteria (SRB) and for methane-producing bacteria (MPB).
- post-dismantling analyses:
  - squeezing of bentonite samples to extract pore water to determine the radial profile of the concentrations of the major or critical elements (e.g., Cl, S, Si, TOC);
  - mineralogical and total chemical analyses of the solid samples (related in chapter 8), and;
  - microbial analyses of the solid samples taken in the middle of bentonite blocks from the outer, the median and the inner rings to search for thermophilic micro-organisms.

9.2. Main results

9.2.1. Movement of solutes in a thermal gradient

The chemical analyses performed during the operational stage on water leaks from defective strain gauges installed on the central tube confirmed high concentrations of chloride (~ 1 000 mg/L) and of other solutes (Figure 9-1). Bromides follow the change in chloride as a function of time and are present between 8 and 16 mg/L.
Simultaneously, the concentration of TOC (~ 850 mg/L) and dissolved silica (~ 1 000 mg/L), much higher than the expected ones, were also measured in the same water samples. Dissolved silica and TOC seem to be correlated ($R^2 = 0.85$). The reason for this correlation is unclear but a contamination from organic silicone mastic used to protect the gauges cannot be ruled out; indeed, during dismantling, this mastic was found to be severely altered.

Bicarbonate progressively increases with time up to 400 mg/L. A similar behaviour is observed for sulphate increasing to 500 mg/L (without taking into account the erratic measure at strain gauge SG9). Finally, nitrate (not shown on Figure 9-1), normally below the limit of detection in Boom Clay and in reduced clays is also present and enriched up to 25 mg/L and follows the trends of chloride and bromide.

No clear trends can be drawn from the change in the major cations: Na^{+}, K^{+}, Mg^{2+} and Ca^{2+} (not shown on the pictures).

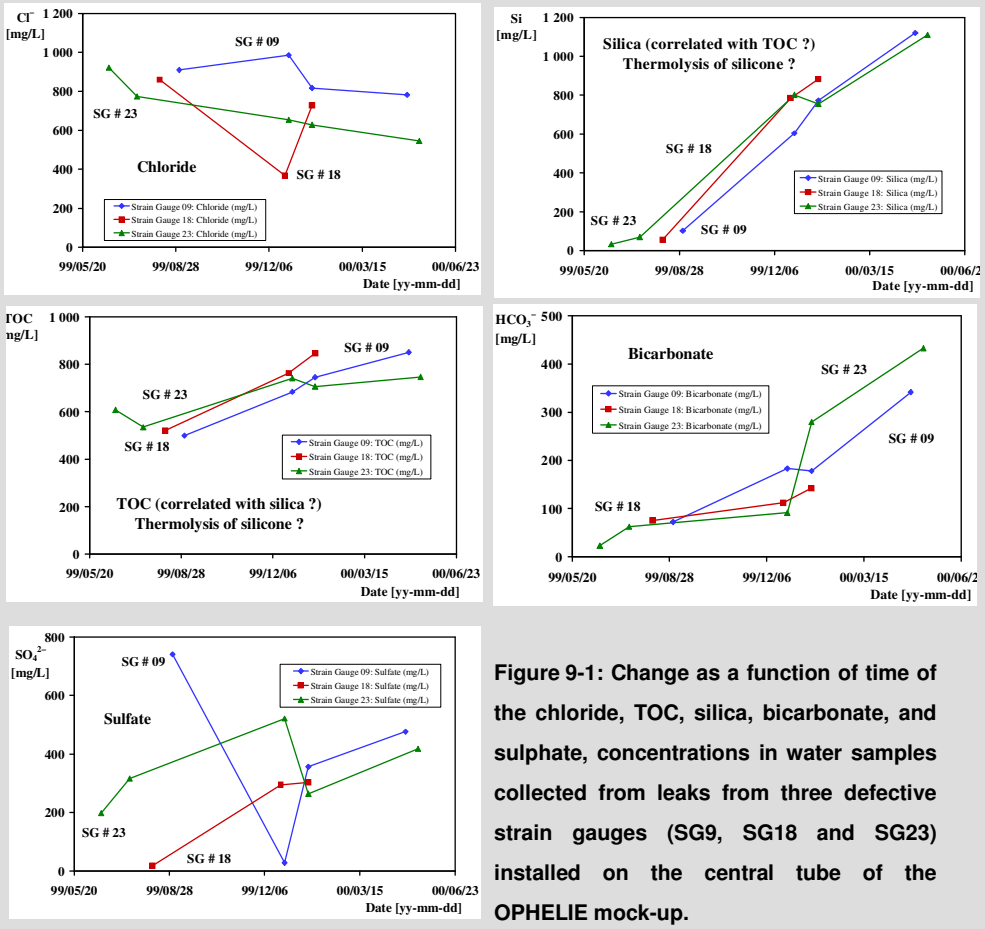

Figure 9-1: Change as a function of time of the chloride, TOC, silica, bicarbonate, and sulphate, concentrations in water samples collected from leaks from three defective strain gauges (SG9, SG18 and SG23) installed on the central tube of the OPHELIE mock-up.

The chemical analyses of pore water extracted by rehydration/squeezing at BGS (Charlton et al., 2004) from exposed sampled from section #19 (Figure 9-2) confirmed the high concentrations previously measured in the water collected from the strain gauges leaks. It also clearly showed higher concentrations of chlorides, TOC, and dissolved silica near the heating tube. In contrast, bicarbonate and sulphate profiles follow an opposite trend with higher concentrations close to the external liner. Here also no stringent trends can be drawn from the profiles of pH and major cations.

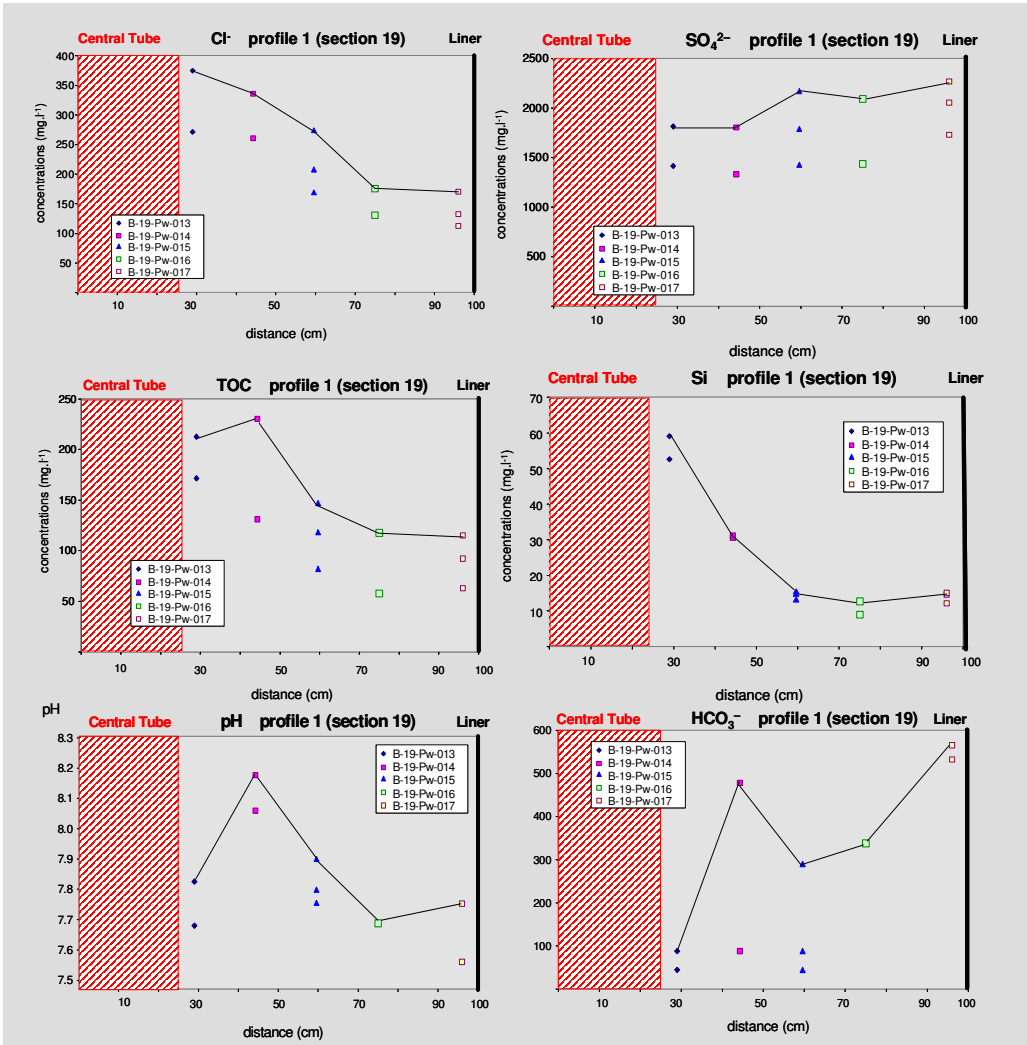

Figure 9-2: Radial profile (as a function of distance from the central heating tube) of chloride, pH, TOC, silica, bicarbonate, and sulphate, in water extracted by rehydration/squeezing at BGS from bentonite blocks sampled at section #19 during the dismantling.

An apparent movement of solutes towards (or from) the heating source can be observed due to the combination of several processes difficult to distinguish from one another.

Regarding the chlorides, two mechanisms could explain the enrichment towards the hottest point:

- off-diagonal Onsager effects between temperature gradient and ion flux, as thermo-diffusion (Soret Effect) and thermo-osmosis could have provided a driving force for their diffusion in the porous medium;
- advective transport of salts by the water front moving in the unsaturated buffer material during the hydration phase. Water moving at the head of the hydration front would have progressively dissolved the crystallized salts present in the dry buffer and slowly increased its concentration during the progression of the water front in the medium. This hypothesis has been independently confirmed by laboratory hydration experiments of reconsolidated FoCa clay plugs. Similar observations have also been performed in the

frame of an European Project on the thermo-hydro-mechanical and geochemical behaviour of the clay barrier (Volckaert et al. 1996 a and b) and have also been reported in the final report of the FEBEX project (Huertas et al., 2000).

The retrograde solubility of calcite and gypsum at elevated temperature caused the precipitation of $CaCO_3$ and $CaSO_4 \cdot 2\,H_2O$, and thus decreased the concentrations of Ca^{2+}, HCO_3^-, and SO_4^{2-} near the central heated tube. It created a chemical concentration gradient in the system from the periphery towards the centre. This gradient could have been responsible for the diffusion of the corresponding ions towards the hot zone where they combined to precipitate poorly soluble salts.

The increase in solubility of silica with temperature created a concentration gradient from the hot zone to the colder zone, causing a global mass transfer of silica towards the periphery[7]. However, it is to be mentioned that:

- this enrichment in silica towards the outer and colder zone was not clearly evidenced by the mineralogical analyses made on the total rock samples (chapter 8);

- the analyses at BGS could not be performed at the temperature prevailing in the mock-up but were made at room temperature after the cooling phase. For this reason, the measured silica concentration is probably a "relic" or an "after-effect" reflecting the silica concentration gradient during the operational stage of the mock-up. Two explanations can be envisaged to explain the profile. After cooling down, (i) the silica concentration could have remained oversaturated with respect to room temperature, or (ii) new silica-bearing amorphous phases could have been formed. In this case, the concentration of silica in pore water could be controlled by various amorphous phases with different solubility. The water extracted by rehydration/squeezing was probably enriched in soluble silica near the heat source because of the higher solubility of the secondary amorphous phases precipitated along the thermal gradient after the cooling of the mock-up. In this case, the "relic" Si concentration gradient measured in the pore water of the buffer materials is thus not the consequence of a solute enrichment by thermo-diffusion towards the heating source, but the cause of the solute movement towards the cold zone as observed in the solid phase in the in-situ heating experiments of the Stripa mine (Jullien et al., 1997, 2000). The main merit of this explanation is that it reconciles all the observations made in the pore water and in the solid phase. The contradiction is only apparent, but the whole picture is coherent and quite logical.

In the same way, it is also possible to envisage two conflicting explanations to account for the apparent enrichment of total organic carbon (TOC) towards the hot zone:

- TOC could be considered as an anion (non-solubility limited and conservative tracer) behaving as a chloride. In this case, the enrichment of TOC towards the heating element

7 Evidence of this phenomenon has been reported by mineralogical observations (Pozzo et al., 1997, Poinssot et al., 1997 a and 1997 b, Jullien et al., 1997 and 2000) of clay texture in the buffer materials in the in-situ heating tests made at the Stripa mine (Sweden) where silica recrystallized in the outer rim.

would be explained by thermo-diffusion or by accumulation in a hydration front during the buffer resaturation;

- natural organic carbon decomposes under the effect of temperature (Deniau et al., 2005a,b) and thus undergoes a stronger thermal stress near the heat source. So, the thermal decomposition of the FoCa kerogen would be greater near the hot zone (Lorant et al., 2008) and a larger number of small molecules soluble in water would be formed. Then, these small mobile molecules produced by the thermal degradation of insoluble kerogen would migrate along the concentration gradient towards the cold zone.

The movements of the different solutes in the OPHELIE mock-up and their tentatively associated driving forces are summarized in Table 9-2.

Table 9-2: Overview of the movements of solutes in the OPHELIE mock-up and the corresponding driving forces.

Solute	Solid Phase	Movement direction	Driving Force / Process
Chloride	—	Cold —> Hot zone	Thermo-diffusion
DOC as soluble anion only	—	Cold —> Hot zone ?	Thermo-diffusion or hydration front
TOC	Kerogen	Hot —> Cold zone ?	Thermal decomposition
Dissolved silica	SiO_2 / TOT	Hot —> Cold zone	Solubility increase with T
Bicarbonate	$CaCO_3$	Cold —> Hot zone	Solubility decrease with T
Sulphate	$CaSO_4 \cdot 2\ H_2O$	Cold —> Hot zone	Solubility decrease with T
Calcium	$CaCO_3$	Cold —> Hot zone	Solubility decrease with T

TOT: Tetrahedron-Octahedron-Tetrahedron structure of the clay minerals: tetrahedron = silica; octahedron = gippsite, alumina.

9.2.2. Sulphides and microbially-mediated sulphate reduction

At the end of August 2000, a precipitate of zinc sulphide (wurzite, ZnS) was discovered in the water injection system of the OPHELIE mock-up. This finding has motivated more detailed investigations on sulphides present in the water of the hydration system, and on the mechanism of the sulphides production. The existence of dissolved sulphides at relatively high concentration was not expected and raised the fear of possible risks of stress corrosion cracking (SCC) of the stainless steel disposal tube.

During the handling of the water accumulator to adjust the hydraulic pressure in the mock-up, the formation of a grey precipitate was observed in a transparent plastic tubing connected between the reserve drum containing 200 L of 1 170 mg/L $NaHCO_3$ solution and the water accumulator of the mock-up. During the sampling of water from this tubing a characteristic H_2S smell was noticed. The chemical analyses of the precipitate made by UCL (Vandevelde and Thomas, 2000) revealed the massive presence of zinc. XRD (Naud, 2000a) showed that

this grey substance was nearly pure wurtzite. The most plausible explanation for the formation mechanism of this wurzite is given in Figure 9-3.

Figure 9-3: Mechanism of formation of ZnS in the hydration circuit of the OPHELIE mock-up (September 2000).

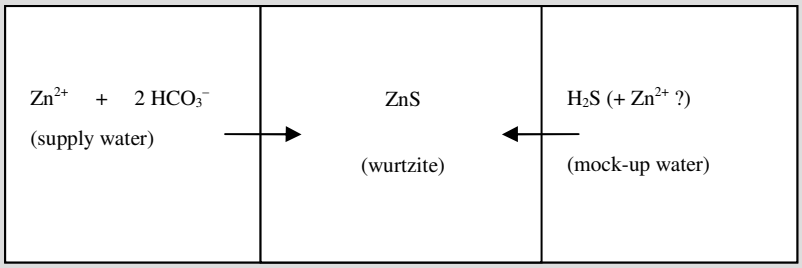

The precipitation reaction of wurzite could be consistently explained by the combination of the following reactions:

$$H_2S + 2\ HCO_3^- \rightleftharpoons S^{2-} + 2\ H_2CO_3$$

$$Zn^{2+} + S^{2-} \rightleftharpoons ZnS$$

$$Zn^{2+} + 2\ HCO_3^- + H_2S \rightleftharpoons ZnS + 2\ H_2CO_3$$

The water of the mock-up enriched in H_2S or in sulphides was allowed to flow back to the bicarbonate solution contained in the galvanized 200 L drum. The zinc coating of this water reservoir was likely the main source of Zn^{2+} although the FoCa clay mixture also contains zinc traces. The hydrogen sulphide was neutralized by the Zn^{2+} bearing bicarbonate solution inside the water tubing. As a consequence, the sulphide anions concentration increased above the solubility product of Zn^{2+} and S^{2-} gave rise to the precipitation of ZnS inside the transparent tubing.

Later, some months before the mock-up dismantling, new fresh water samples were taken from the mock-up water injection system under strictly anaerobic conditions to specifically analyze dissolved sulphides (HS^-). The results of these sulphide analyses performed independently by two laboratories (ULB and CEA) with two different methods (polarography and capillary electrophoresis) are presented in Table 9-3.

These analyses confirmed the presence of reduced sulfur species in the water, more particularly free dissolved sulphides at concentrations as high as $6.5\ 10^{-4}$ mol/L (ULB, polarography: Pourbaix, 2002; 2003, and Schmitz, 2002; 2003) and thiosulphates at $2\ 10^{-5}$ mol/L (CEA, capillary electrophoresis: Descostes and Meier, 2002). No sulphides could be detected by CEA in their water sample, but only thiosulphate. The capillary electrophoresis (CE) method used at CEA was developed by Motellier et al. (1997) and by Motellier and Descoste (2001). Although chlorides present in the solution interfere with the detection of sulphides, the failure to detect sulphides by CE is probably due to an uncontrolled oxidation of sulphides during the transport, storage or handling of the water samples during the analyses. However, the concentration of thiosulphates measured by CEA was of the same order of magnitude as that of the sulphides detected by ULB. This is coherent and quite logical because thiosulphates are a labile

intermediate species appearing in the process of oxidation of sulphides, or in the reduction of sulphates (Xu and Schoonen, 1995).

Two different pathways can be envisaged to explain the formation of sulphides in the mock-up:

- a thermochemical-sulphate reduction (TSR) (Cross et al., 1998, 2000, 2004) by graphite or organic matter (at higher temperature close to the central heating tube), and;
- a microbially-mediated sulphate reduction by chemotropic bacteria (SRB) from the sulfur cycle (Stroes-Gascoyne et al., 1996, 1997, 1998, 2002, 2004, 2005, 2007) at lower temperature near to the hydration tubes.

Table 9-3: Comparison between the values of sulphides and thiosulphates measured in the hydration circuit of the OPHELIE mock-up by polarography at Cebelcor/ULB and by capillary electrophoresis at CEA.

Laboratory	Analytical	Hydration	Leaks
Cebelcor (Aug 02)	Polarography (1st measurements)	1.80×10^{-4} M HS^-	Only SO_4^{2-}
Cebelcor (Jan 03)	Polarography Iodometry	6.50×10^{-4} M HS^- 4.12×10^{-4} M HS^-	(—)
CEA (Aug 02)	Capillary-Electrophoresis	2.00×10^{-5} M $S_2O_3^{2-}$	Only SO_4^{2-}

BGS did not detect thiosulphates (ion chromatography) in the pore water extracted by rehydration squeezing from the bentonite blocks recovered after the OPHELIE mock-up dismantling.

The first hypothesis of TSR into sulphide by simultaneous oxidation of graphite into CO_2 at high temperature is not supported by experimental evidence found in the mock-up. However, it can also not be ruled out. Major precipitation of pyrite in the immediate surrounding of the central heating tube was not observed. The industrial FoCa clay is "in principle" strongly oxidized at the beginning, if not entirely. The initial pyrite content of FoCa is very low and below the limit of detection of X-ray diffraction. Mineralogical analyses (Raynal and Petronin, 2004) after the dismantling of exposed bentonite blocks showed that FoCa remained oxidized in the core of the mock-up and inside the bentonite blocks. Large amounts of gypsum were also observed everywhere in the joints between the bentonite blocks. No neoformed pyrite could be observed near the central heating tube. The reason is probably that the TSR reaction rate was too slow at the temperature prevailing in the mock-up. It seems that the TSR reaction only occurs at a significant rate at temperatures higher than 350 °C, as is often the case in oil and gas fields (Cross et al., 1998, 2000, 2004). However, the question is unclear, because publications from Trudinger et al. (1985) and Worden et al. (1995) also indicate that the thermochemical reduction of sulphate could already occur in the temperature range of the mock-up (115 – 140 ° C), but at the scale of geological time.

In the second hypothesis, SRB could have been at work in the mock-up. During the initial six month hydration phase of the mock-up, SRB bacteria could have easily developed at room temperature in the free water, or in the decompacted bentonite blocks of the outer ring. During

the heating phase, bacteria could also have lived in the water of the injection system kept at room temperature outside the mock-up. Micro-organisms might have even survived in the tailing of the temperature gradient in water pipes heated up to 80 °C or 110 °C. Indeed, papers in the literature (Jørgensen et al., 1992) (Stroes-Gascoyne et al., 2002, 2004, 2005) indicate that many sulphate-reducing bacteria (SRB) are thermophilic and can survive at high temperature as observed in hydrothermal vents in the deep ocean, or in the Yellowstone thermal ponds (Wyoming, USA).

9.2.3. Microbial activity and perturbation of the water chemistry in the hydration system

To verify this second hypothesis dealing with the microbially-assisted sulphate reduction, water from the hydration circuit and solid bentonite samples recovered in aseptic conditions after the dismantling operations were analyzed by two different microbiology laboratories (Companie Française de Géothermie, CFG, Marseilles, and SCK•CEN). An overview of the main results of the microbial analyses is presented in Table 9-4.

Table 9-4: Comparison between the results of microbial analyses made at CFG – BRGM and SCK•CEN on fluids and solids from the OPHELIE mock-up.

Nature of the Sample	CFG – BRGM (Daumas, 2000, 2003) Numeration	SCK•CEN (De Boever, 2003a,b, 2004a,b) Enrichment at 80 °C
Water from the hydration circuit	> 150 000 SRB / mL > 150 000 TRB / mL > 150 000 MPB / mL	Enrichment cultures show limited activity
Solid of reference (non heated)	250 SRB / g clay 130 MPB / g clay 0 TRB / g clay	Enrichment cultures show limited activity
Solid exposed (heated)	Quasi Sterile No SRB, no TRB 25 MPB / g clay	Activity: 5×10^3 CFU/g of thermophilic bacteria!

The CFG lab found more than 150 000 bacteria per ml of water for each of the following species: sulphate reducing bacteria, thiosulphate reducing bacteria, and methanogenic bacteria. The SCK•CEN lab did not immediately detected such a microbial activity in the water, but surprisingly also found some activity for thermophilic bacteria in the solid samples recovered from the mock-up after the dismantling. However, the CFG lab failed to detect any microbial activity in the exposed solid. Although discrepancies still exist between the results obtained by the two labs using different methods, microbial activity has certainly been at work in the OPHELIE mock-up during the initial hydration phase, or afterwards during the thermal phase

at least in the cold part of the water injection system, or in the tail of the thermal gradient. Traces of iron sulphides have also been detected in grey and green coatings formed in the buffer material around the hydration tubes (Kursten, 2004) and also in the sandy lens below the bentonite blocks (Beaucaire, 2003). These not abundant sulphides precipitates are also an indication of sulphate-reduction in the hydration system of the mock-up.

The preferred explanation for the presence of sulphide in the water of the hydration system is the activity of SRB. Advective water circulation was fortuitously observed in the hydration tubes of the mock-up a few months before the dismantling when part of the insulation material covering some tubes was removed. Some hydration tubes were much hotter than other ones as simply felt accidentally with the fingers and later confirmed with thermocouple measurements. These differences in temperature were due to cross-connection between the ends of the hydration tubes near the cover of the mock-up where sand was used as backfill material. During the dismantling, other connections between hydrations tubes were discovered beneath the clay-based blocks, where a large triangular lens of sand was formed by the collapse of the sand put near the cover when the mock-up was flooded at the beginning of the hydration phase. So, preferential water paths have certainly existed during the whole thermal phase of the mock-up making possible heat and matter (mainly organic carbon and sulphate) transfers between the mock-up and the hydration system. It could explain that organic matter and nutrients have been continuously exchanged between the bentonite mixture and the water of the hydration system. Simultaneously, thermophilic sulphate-reducing bacteria and methanogenic bacteria might have developed in the hydration tubes inside the mock-up where the temperatures could have been lower than expected. Anyway, it is not impossible that thermophilic bacteria could have grown in the tailing of the thermal gradient inside the hydration tubes at temperatures in the range of 80 – 110 °C.

Finally, a last question arises as to the exact nature of the source of carbon needed for fuelling the observed microbial activity. Organic matter is the most plausible electron donor in the mock-up because the dissolved organic carbon measured in the water from the strain gauges was very high: circa 1 g/L. According to Daumas (2000, 2003), there was no competition for "food" between the different strains of bacteria detected because the amount of nutrient available for microbial growth was not the limiting factor. The question of the origin and degradation of organic carbon in the mock-up is treated hereafter and in the section on the pore water chemistry perturbation.

9.2.4. Source of organic carbon in the mock-up

As previously mentioned, the value of dissolved organic carbon measured in the water of the mock-up was surprisingly high (up to ~ 1 g/L at some places). This organic matter could have fuelled the microbial activity observed in the hydration circuit of the mock-up. Beside the presence of natural organic carbon in the FoCa clay itself, one can reasonably rule out the leaching of organic matter from graphite whose composition is only pure elemental carbon. X-ray diffraction (Naud, 2000b) have also revealed that graphite used for the M 2 mixture was highly crystalline and defracts X-rays very well with a minimum of diffusion due to amorphous carbon. Leaching tests made in the surface laboratory also failed to extract organic carbon from

this graphite. So, an unknown pollution of the buffer material was suspected. The source of the pollution could have occurred in the extraction of the FoCa clay from the Fourge Cahaine quarry (engine oil, gasoline spills, …), or from the industrial treatment process (drying, aggregation, compaction of the bentonite blocks, …). Another cause could arise from the instrumentation of the mock-up itself. Gas chromatography – mass spectrometry (GC-MS) coupled analyses made by VITO (2000, 2002) of water from the hydration circuit before the dismantling operations are presented in Table 9-5.

Table 9-5: Volatil organic carbon measurements on the water from the hydration circuit.

Organic compound	Concentration (µg/L)
Benzene	~ 500
Toluene	~ 500
Xylene	~ 500
MTBE (methyl-tertiary-butyl-ether)	2

These analyses revealed the unexpected presence of volatile organic carbon (VOC) mainly constituted of aromatic molecules (benzene, toluene and xylene, each at concentration of about 500 µg dm^{-3}) accompanied by traces of methyl-tertiary-butyl-ether (2 µg/L MTBE). MTBE is not a natural product, but a synthetic compound added since 1980 to gasoline as a substitute for tetraethyl lead: it is an oxygenated anti-detonating additive for reformulated gasoline. During the dismantling operation of the mock-up, the source of MTBE was clearly identified. The Glötzl hydraulic load cells used for the total pressure measurements were found totally destroyed during the dismantling as mentioned in chapter 11. The Glötzl cells were fabricated from Mn-steel (Kursten, 2004). As this low-alloy steel is easily corroded, these load cells could not withstand to the corrosion at elevated temperature and released their hydraulic fluid in the mock-up after their early failure.
All their oil content (~ 400 ml of a mixture of oil dissolved in gasoline) spread into the mock-up and was likely dispersed in the water of the hydration circuit through the sand backfill used for filling the residual dead space between the bentonite blocks and the cover of the mock-up. Because of the thermo-advection process observed inside the tubes of the hydration system, this mixture of oil and gasoline was evenly distributed overall and contaminated the mock-up hydration system, so contributing to an increase in the concentration of organic matter required to fuel the development of bacteria.

9.2.5. pH, E_h and pCO_2 conditions

On-line pH and E_h measurements were performed on the water tubing at two different locations in the OPHELIE mock-up: (i) on a tube of the hydration circuit at the periphery of the mock-up and (ii) on a water leak occurring from the electrical wire of strain gauge SG 23 installed on the central heating tube. Two flow-through cells equipped with pH and E_h electrodes were installed on-line at the two different places. It was possible to recirculate water with a gear-pump in the hydration circuit. Because of the high flow-rate and the large volume of water in the circulation loop, the system was well buffered chemically, and very stable E_h and pH values were

measured. However, on the leak originating from strain gauge SG23 on the central heating tube, no recirculation loop could be created because the leak was a one-way flow without the possibility to reinject water inside the mock-up. As a consequence, the flow-through measurements on this leak were made at a much lower flow-rate and on much smaller water volumes. The redox potential was therefore less well buffered and no negative E_h values could be measured. An overview of the pH and E_h conditions measured on-line in the OPHELIE Mock-up during the period June – September 2002 is given in Table 9-6.
As indicated in Figure 9-4 LEFT, negative values between -150 mV and -175 mV (with respect to the Standard Hydrogen Electrode, SHE) were measured on-line for the redox potential (E_h) in the water of the hydration circuit, confirming the restoration of reducing conditions by the microbial activity.

Table 9-6: Extreme values of pH and Eh measured on line in the OPHELIE Mock-up.

Hydration circuit: Flow-Through cell with constant recirculation (close loop)
pH = 5.5
E_h = -250 mV (SHE)
(strongly reducing + dissolved CO_2)
Strain gauge SG23: Flow-Through cell with one-way flow
pH = 3.7
E_h > + 0 mV (SHE)
(clearly oxidizing + acidic conditions)
Fresh injected water = 14 mM $NaHCO_3$
pH = 8.5
E_h > + 0 mV (SHE)

Simultaneously, the pH values were also very stable but unexpectedly low: pH about 5.6 in place of the expected 8.5 corresponding to the 1170 mg/L $NaHCO_3$ solution injected. The on-line pH measurements were verified in the lab by means of batch measurements made on water volumes of a few milliliters. Vigorous shaking of the vial containing the water sample was performed between successive pH measurements to expel oversaturated dissolved gases. After completing such a manual degassing of a water sample, the pH value could be restored to the value of the injected $NaHCO_3$ water (8.5). This observation probably indicates the presence of CO_2 or H_2S dissolved in the water and imposing a pH close to 5.6.

The pH value measured on-line on the leak from strain gauge SG23 installed on the central heating tube was even lower (pH = 3.7) progressively increasing up to 5, while the redox value always remained positive between +400 mV (SHE) at the beginning and +200 mV (SHE) at the end of the measurement campaign as shown in Figure 9-4, RIGHT. Such a low pH could have been induced by a corrosion phenomenon in progress in the strain gauge, or by an unknown artifact, such as the thermolysis of silicone mastic covering the strain gauge. In any case, at such a low pH value, the surface of steel, or stainless steel, is no longer passivated and corrosion is certainly a concern.

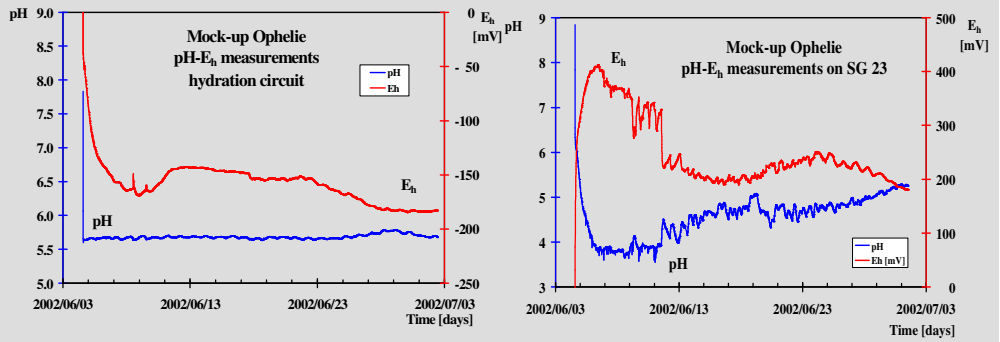

Figure 9-4: On-line pH and Eh (mV, SHE) measurements (June 2002) in the hydration circuit in (LEFT) and in the leak from strain gauge SG23 installed on the central heating tube (RIGHT).

9.2.6. CO_2 production

Gas analyses on water sampled from the hydration system of the mock-up (Jockwer, 2002) mainly revealed the presence of dissolved CO_2 accompanied by traces of O_2, H_2, and CH_4. The main results of these gas analyses are presented hereafter in Table 9-7.

The substantial production of CO_2 in the mock-up could be one of the explanations that account for the low pH of ~ 5 measured online in the water of hydration system. However, the exact nature of the CO_2 source remains unknown. Different CO_2 source terms can be envisaged. Various hypotheses are given hereafter by order of decreasing plausibility, starting from the most favorite:

Inorganic reactions:

- heating up of the $NaHCO_3$ solution at 120 – 140 °C with CO_2 outgassing;
- cation exchange, involving calcium carbonate precipitation:

$$2\ Na^+ + X{=}Ca \leftrightarrow 2\ X{-}Na + Ca^{2+}$$

$$Ca^{2+} + HCO_3^- \leftrightarrow CaCO_3 + H^+$$

$$H^+ + HCO_3^- \leftrightarrow H_2CO_3$$

$$H_2CO_3 \leftrightarrow H_2O + CO_2$$

$$2\ NaHCO_3 + X{=}Ca \leftrightarrow 2\ X{-}Na + CaCO_3 + H_2O + CO_2$$

Microbial and organic reactions:

- production of CO_2 by the microbial activity;
- thermolysis of organic matter naturally present in the FoCa (thermal stress of the kerogen present in the FoCa clay);

- oxidation of graphite by sulphate (TSR);
- degradation with temperature of the oil/gasoline mixture released by the defective Glotzl cells.

The pH decrease could therefore be explained by the following mechanisms:

- cation exchange, involving calcium carbonate precipitation:

$$2\ Na^+ + HCO_3^- + X{=}Ca \ \leftrightarrow \ 2\ X{-}Na + CaCO_3 + H^+;$$

- production of H_2S by SRB or TSR;
- production of acetic acid as observed in the Pore water Chemistry (PC) experiment at Mont Terri (Wersin et al., 2004 and 2007);
- however, if pyrite or sulphides oxidation cannot be ruled out, the production of H_2SO_4 could also explain the pH decrease.

In the absence of a complete and detailed study of the problem (with detailed geochemical modeling), it is very difficult to conclude what process was the dominant one to control the pCO_2 and pH.

9.2.7. Origin of the water chemistry perturbation

Two processes mentioned earlier in particular deserve more attention: a microbial perturbation and a possible thermal decomposition of organic matter present in the clay.

9.2.8. Microbial reductive perturbation

Microbial activity was clearly observed in the hydration circuit of the mock-up. The observations are very similar to those made at the Mont Terri rock laboratory (Switzerland) in the PC experiment and in the diffusion experiments (DIR) made at the Bure underground laboratory (France) (Poulain, 2006; Poulain et al., 2007a,b). All these experiments were also affected by an unexpected microbial growth.

The PC experiment was also affected by unexpected artifacts. Because of a contamination of the water by an undesirable source of organic carbon (most likely a residue of acetone used to clean the downhole filter screen), major microbial activity and sulphate reduction were observed to have developed in the water circuit. Some interesting features very similar to those occurring in the OPHELIE mock-up were noticed.

The pH in PC experiment was lower than normal by one unit (6.6 in place of 7.6) and a negative E_h value (-220 mV, SHE) was measured, while the first chemical analyses of the water samples showed strong deviations with respect to normal conditions: high alkalinity (12 mM), the presence of 278 mg/L of acetic acid, the presence of free dissolved sulphides (0.29 mM H_2S), a decrease of sulphate, a much too high pCO_2 value (0.3 bar), and a much too high DOC value (3 mM). The microbial analyses confirmed the presence of a large number of

sulphate reducing bacteria in the water of PC experiment. Bataglia (2004) observed 2 10^6 count/mL, a value in the range of ground water reported by Pedersen (1997, 1999).

Common points are that enough space and free water were available for the development of bacteria, with a major source of degradable organic carbon (electron donor), sulphate (electron acceptor), and enough nutrients to fuel major microbial activity.

Table 9-7: Composition of the main gases dissolved in the water from the hydration circuit.

Dissolved Gas				
Container Number	**Concentration in the Degassing Container**	**Released Amount**	**Specific Released Amount**	
##	C_0	g_m	S_m	
[—]	[vpm]	[ml]	[ml/g]	[L/1000 kg]
Carbon Dioxide, CO_2				
19	85 610	37.10	0.72	718.59
20	83 890	36.24	0.71	705.37
Oxygen, O_2				
19	1 900	0.82	0.02	15.95
20	2 200	0.95	0.02	18.50
Hydrogen, H_2				
19	880	0.38	0.01	7.39
20	0	0.00	0.00	0.00
Methane, CH_4				
19	115	0.05	0.00	0.97
20	100	0.04	0.00	0.84

Remark: no ethane (C_2H_6), or propane (C_3H_8) could be detected in the water of the hydration circuit.

9.2.9. Decomposition of organic matter exposed to moderate thermal stress

The second process to explain the formation of CO_2 inside the mock-up could be due to the effect of thermal stress on the kerogen present in the FoCa clay. The kerogen is the non-water-soluble and immobile fraction of organic matter intimately associated with the clay matrix. Recent studies (Deniau, 2004; Deniau et al., 2005a,b, 2006, 2008; Lorant et al., 2008) have demonstrated that when the natural and immature organic matter of a clay, such as Boom Clay, is exposed to moderate heating (80 to 100 °C) a large release of CO_2 occurs on a very small time scale. The activation energy of this early "Flash CO_2" production, related to preferential decarboxylation reaction of activated –COOH groups present in the organic matter, is only 20 kCal/mol, while CO_2 produced at higher temperature requires activation energy in the range 40 – 50 kCal/mol. According to Pitsch (2005) and Pitsch et al. (2007) calculations, this "Flash CO_2" could well explain the decrease of about one pH unit observed in the Cerberus experiment (Noynaert et al., 1997; 1998a,b; 2000) where Boom Clay was exposed to heating

and γ-radiation. A high CO_2 concentration was also measured in the Coralus experiment (Valcke et al., 2004) where the clay is also exposed to γ-radiation and heating. The question of a "Flash CO_2" production by the thermal decomposition of the organic matter at moderate temperature (80 to 140 °C, as in the mock-up) is important and certainly deserve further attention. Indeed, the quantity of CO_2 produced could alter the pH and the calco-carbonate equilibrium in the near-field of a deep repository of HLW or spent fuel. As recently modeled (Pitsch et al., 2007), the geochemical perturbation would result from the short-term pH lowering induced by the formation of CO_2 within the clay and the subsequent dissolution of carbonate minerals. After diffusion and reaction of CO_2 within the clay, durable changes in the mineralogical properties altering, among other things, the original calco-carbonic equilibrium and the population of exchangeable cations could subsist in the long-term. The resulting perturbation of the water-rock system may in turn affect the retention and diffusion properties of radionuclides within the clay barrier to an extent that remains to be consistently determined.

9.3. Implications of the pore water chemistry for the metal corrosion

A significant outcome of the OPHELIE mock-up was certainly the contribution to revealing to the Belgian programme the importance of the chemical conditions prevailing in the buffer materials as boundary conditions for the corrosion of the metallic barriers. So, one of the new objectives assigned to the mock-up at the mid-term of the experiment was to provide the corrosion specialists with sufficient insight into the chemical species and processes potentially harmful for the metal corrosion: Cl^-, HS^-, $S_2O_3^{2-}$. The finding of a significant microbial activity in the water of the hydration system also explains why reducing conditions were rapidly restored in free water. The sulphides produced in the water by SRB bacteria were progressively consumed by the oxidized minerals (iron oxides) present in the buffer materials around the hydration tubes. In the case of a real repository, sulphides will also react with pyrite oxidation products formed in the excavation disturbed zone (EdZ) around the galleries. However, if dissolved sulphides reach the nuclear waste containers, they could represent an increased risk for the localized corrosion of their metallic envelopes.

9.3.1. Lessons learnt for the chemistry and the microbiology of the bentonite buffer

The observations of the chemical conditions and of the corrosion phenomena made in the frame of the OPHELIE mock-up should be taken into account for the selection of the candidate metallic materials. Another approach to improve the life-time of the metallic overpack would also be to better control the chemical conditions prevailing in the buffer surrounding the waste packages by selecting buffer materials totally free of chlorides, sulphides, thiosulphates and sulphates. Moreover, the development of low pH in the near-field is not advised from the point of view of the metal corrosion. The addition of calcium carbonate or calcium hydroxide to the backfill materials could help to buffer the pH and to maintain alkaline conditions. A high pH is favorable to the passivation of metals and should contribute to suppressing the microbial activity. Furthermore, it also has the advantage of lowering the solubility of many radionuclides and enhancing the sorption of cations. Cement could be an advantageous

alternative to the use of swelling materials (bentonite, smectite-rich clay) and has been proposed for the supercontainer concept.

9.3.2. Potential consequences for the corrosion studies

The analyses of the water samples taken from the leaks from the strain gauges and the hydration system of the OPHELIE mock-up revealed the presence of sulphate-reducing bacteria and of chemical species potentially harmful for the metallic barrier at concentrations higher than those commonly expected by the corrosion studies. These species and their concentrations are listed in Table 9-8.

Chloride, thiosulphate, sulphide, elemental sulfur, and bacterial biofilm are known to induce localized corrosion (pitting or crevice corrosion) in the relatively low pH range encountered in the OPHELIE mock-up ($3.5 < pH < 5.5$). Moreover, the reduced species of sulfur (H_2S, HS^-, S^0, and $S_2O_3^{2-}$) can promote stress corrosion cracking (with inter, or intra, granular cracking). The sulphate reducing bacteria which have also been detected in the hydration system of the mock-up are likely responsible of the presence of sulphides and thiosulphate found in water and can also induce microbial corrosion by forming biofilms on metallic surfaces. The effects of the different forms of localized corrosion are discussed hereafter.

Table 9-8: List of the most aggressive chemical species found in the water samples from the OPHELIE mock-up and their potential detrimental effect for the corrosion of the metallic barriers.

Aggressive Species	Concentration (mol/L)	Expected Corrosion mechanim
Chloride (Cl^-)	2.8×10^{-2}	Pitting Corrosion
Thiosulphate ($S_2O_3^{2-}$)	2.0×10^{-5}	Pitting Corrosion + SCC
Sulphide (H_2S / HS^-)	6.5×10^{-4}	Pitting Corrosion + SCC
Sulphate-Reducing Bacteria (SRB)	1.5×10^5 CFU	Microbially Induced Corrosion →SCC

CFU: Colony Forming Unit.

Pitting and crevice corrosion induced by Cl^- and $S_2O_3^{2-}$

Stainless steel can suffer severe problems of localized corrosion (Laitinen et al., 2000) in environments containing chloride, thiosulphate, and sulphide (paper pulp industry, sour oil wells and petroleum refinery, sulphide ore processing, …), especially at a low pH in the range 3 – 5 as that precisely measured in the OPHELIE mock-up in the samples of water collected during the operational stage from the leaks for the strain gauges, or from the hydration circuit.

The effect of thiosulphate on localized corrosion has been explained by several authors in two different ways:

- thiosulphate is reduced to elemental sulfur (S^0), which adsorbs on bare metallic surface preventing passivation (Newman et al., 1982);
- thiosulphate is reduced to hydrogen sulphide (H_2S) which catalyses the anodic dissolution of stainless steel (Tromans and Frederick, 1984).

Thiosulphate and chloride also have a synergistic effect in inducing localized corrosion. Thiosulphate alone seems not to immediately initiate pits, but more likely to weaken the passive surface film and make it easier for chloride to initiate pits. In addition, thiosulphate accelerates corrosion in pits already initiated because its electromobility in solution is higher than that of chloride. Moreover, electromigration of divalent thiosulphate is faster than that of chloride, and its concentration is considerably enriched inside the pits by the same kind of electrokinetic mechanisms as those occurring in capillary electrophoresis.

Stress corrosion cracking induced by H_2S and $S_2O_3^{2-}$

Carbon steels are also sensitive to stress corrosion in environments H_2S, a widespread problem in oil refineries and desulfuration installations (Tuttle and Kane, 1981). Damage due to stress corrosion cracking is also frequent in oil wells and pipelines carrying sour gas. High steels can also be affected by SCC in the presence of 1 10^{-3} mol/L of thiosulphate, as reported by Zucchi et al. (2000) who used $S_2O_3^{2-}$ in their experiments as a simulant for H_2S in sour environments.

Microbially-induced corrosion and sulphate-reducing bacteria (SRB)

Pitting corrosion of iron and steel can also be induced by media containing SRB (Starosvetsky et al., 2000). The main difficulties in understanding the microbially-induced corrosion (MIC) of nuclear waste containers arise from the complexity of the chemical composition of these media (King and Stroes-Gascoyne, 1995; King et al., 1999). Apart from chloride ions, SRB media contain sulphides, whose role in the mechanism of pitting formation is of particular importance. It is known that sulphides can induce pitting on steel in solutions free of chloride ions. The activation of the metal surface could be caused by HS^- ion, and iron dissolution might occur through the formation of soluble $FeHS^+$ species.

In chloride containing solutions, sulphides also promote steel depassivation. So, the complex mix of chloride, thiosulphate, and sulphide with SRB biofilms is potentially very harmful for the metallic barrier in the low pH range (3.5 – 5.5) observed in the OPHELIE mock-up. The partial oxidation of sulphide in thiosulphate and the easy reduction of this latter by SRB bacteria developing in biofilms also complicate the understanding of the corrosion mechanisms and the long-term predictions of steel corrosion.

As a conclusion, if the chemical species detected in the water of the OPHELIE mock-up should be present in real repository conditions, it could jeopardize the integrity of the metallic overpacks and compromise the confinement function. So, the question of corrosion inside the OPHELIE mock-up is important. Therefore, an experimental programme was elaborated at SCK•CEN to study the corrosion behaviour of the different metallic components used in the mock-up. The results of these observations are summarized in chapter 10.

9.3.3. Implications for long-term monitoring instrumentation

In the same way, the materials used for the casing of probes and sensors should be carefully selected to avoid premature failure of instruments exposed to harsh chemical conditions and sensitive to corrosion at high temperature. Water intrusion inside the sensors and leaks from

internal fluids (oil, mercury, silicone grease, …) must be avoided, not only to protect the instruments themselves, but also to prevent the chemical contamination of interstitial water and to preclude the development of microbial activity (e.g., fuelled by organic carbon).

9.3.4. Recommendations for the PRACLAY in-situ Experiment

In the future, multidisciplinary studies should be better integrated from the start of the project. Indeed, geochemical measurements and microbiological analyses are particularly important for determining the chemical boundary conditions needed by the corrosion studies. They should be taken into account in the initial design of the experiment. Amongst others, the in-situ measurement of non-preservable parameters, such as pCO_2, pH and E_h, should be regularly performed in the pore water around the PRACLAY Heater Test to assess the effect of a thermal perturbation on these parameters, especially if a moderate heating of organic matter may produce a large quantity of CO_2 (Deniau et al., 2005b and Lorant et al., 2008).

9.3.5. Recommendations for the design of a deep repository

A non-negligible level of microbial activity can develop in deep geological environments in the absence of space and water restrictions, especially if organic carbon and mineral nutrients are present. It is difficult, if not impossible, to make a clear distinction between exogenous and endogenous bacteria. Allochthonous micro-organisms could develop from inevitable contaminations by human activities in the underground galleries, while dormant autochthonous microbes could "wake up" after some time if favorable conditions arise again.

On the one hand, the rapid restoration of reducing conditions in the near-field of a repository by the microbial activity could be favorable for the retention properties of the buffer material. Indeed, the solubility of redox-sensitive radionuclides is much lower in their reduced valence state, and their sorption is also enhanced.

On the other hand, reduced species of sulfur produced by the SRB bacteria, such as dissolved free sulphide (HS^-), elemental sulfur (S^0), and thiosulphate ($S_2O_3^{2-}$), can be very detrimental for the localized corrosion of the metallic barrier, especially for the lower grade varieties of stainless steel sensitive to pitting and stress corrosion cracking (AISI 304). Thiosulphate, like chloride, can induce severe problems of pitting corrosion, while sulphide can cause stress corrosion cracking under anoxic conditions. The presence of thiosulphate combined with high chloride concentrations induced by the movement of soluble salts towards the hot zone could cause severe localized damages to the stainless steel overpacks whose integrity must be guaranteed during the whole thermal phase.

If the presence of bacteria cannot be ruled out in the near-field of a repository for HLW, minimum precautions should be taken to minimize their activity:

- physical gaps has to be filled as much as possible to avoid microbial proliferation in free water and the development of biofilms on the walls of interstices, or small cavities, remaining in the engineered barriers, and;

- all sources of organic carbon and nutrients should be eliminated in the buffer materials.

In the case where encysted bacteria would subsist, blocked in the pores of highly compacted buffer materials, their metabolic activity would be restricted by the low water content, the absence of organic carbon, and the mass transfer of nutrients and metabolism toxins limited by diffusion in the compact clay (Stroes-Gascoyne et al., 1996; Kjartanson et al., 2003). If voids filled with water and enough nutrients would be left in the engineered barrier, they could constitute zones particularly favorable for the growth of extremophile microbes if radiation and temperature are not too high to inhibit their development.

9.4. Conclusions

Although, the OPHELIE mock-up was not designed to study the chemical and microbial evolution of the OPHELIE mock-up, important observations with potential implications for the metallic corrosion studies, the long-term monitoring, the design of the PRACLAY in-situ Experiments and the design of a future repository have been made.

The large scale of the OPHELIE experiment has enabled the comparison between the composition of the squeezed pore water and the mineralogy of the solid phase. It made it possible to obtain evidence both of the driving force and the effect of the movement of the solutes in the buffer materials exposed to a temperature gradient.

At least three processes potentially detrimental to the corrosion resistance of the metal elements have been highlighted:

- an enrichment process in chlorides towards the central tube associated with a depletion in species known to inhabit corrosion in chloride-containing solution such as bicarbonate or sulphate. Chloride concentrations up to 1g/L have thus been measured in contact with the central tube presenting a concern for its corrosion by pitting. Such a concentration was never previously considered for the corrosion studies. Two mechanisms could explain this enrichment process without it being possible to conclude which one actually acted or which one was predominant: advective transport of salts by a water front migrating through the unsaturated buffer during the hydration phase or the diffusion of solutes in a temperature gradient. Enrichment processes in other species like for instance dissolved organic matter or dissolved silica were also observed;

- the presence of microbial activity in the water of the hydration system pointed out the presence of dissolved sulphides and, in some samples, thiosulphates, and was confirmed by microbiological analyses which revealed the presence in high concentrations of sulphate-reducing bacteria, thiosulphate-reducing bacteria and methanogenic bacteria. The conditions encountered by the hydration system, namely the presence of free water and free space associated with an even temperature and the presence of nutrients (dissolved sulphate notably from the gypsum and dissolved organic carbon ‘renewed’ thanks to the convection loops and organic matter potentially released by defective Glötzl cells) have allowed sulphate-reducing bacteria to grow. The large amounts of dissolved organic carbon measured in the water could have contributed to fuelling microbial

activity. The source of dissolved organic carbon could be the organic matter naturally present in the FoCa clay or/and hydrocarbons (a mixture of gasoline and oil) released by defective Glötzl cells as observed during dismantling operations. Limiting free space in a disposal gallery is therefore required as much as possible.
No stringent conclusion can be drawn from the microbial analyses performed on the initial and exposed solid buffer samples. Tests performed by two laboratories with different techniques yielded contradictory results;

- A relatively low pH value (5 instead of 8.5 for the fresh $NaHCO_3$ water used to hydrate the mock-up) preventing or more or less limiting the formation of a protective passivation layer on the surface of the metal elements. One of the causes of this low pH is amongst others the high content of dissolved CO_2. The source of CO_2 remains unclear. Two mechanisms can be suggested: production by microbial activity or decarboxylation by thermal stress of the natural organic matter present in FoCa clay.

The finding of these chemical conditions potentially harmful for the metallic barrier has potential implications in different domains: for the selection of an adequate instrumentation for the long-term monitoring and for the design of the PRACLAY gallery or of a future repository. For a future repository, it would be well advised to control the chemical conditions prevailing in the buffer material to prevent chloride enrichment towards the heat-emitting waste.

It is also recommended to suppress the microbial activity responsible for the production of free sulphides and carbon dioxide lowering the pH. No technical voids would subsist in the compact buffer material around the waste canisters in order to create water and space restrictions to limit microbial growth and sulphate reduction. No organic carbon (natural or added by industrial processes) would be present in the buffer to avoid fueling the bacterial activity. Kerogen would ideally be removed from clay materials to avoid its thermal decomposition leading to the production of CO_2 and of small organic molecules available as a microbe nutrient and complexing agent.

Ideally, the buffer material should be free of Cl^-, HS^-, SO_4^{2}, and OM: if clayed material is used as buffer, it implies thus an industrial purification of to remove most of the pyrite, gypsum, kerogen, and soluble chloride. Such a process could be expensive and not easy to achieve on tens of thousands of tons of clay.

Another option is be to maintain strongly alkaline conditions in the buffer materials to avoid the depassivation of steel at low pH. The addition of limited quantities of alkaline compounds (e.g., $CaCO_3$, Na_2CO_3, $Ca(OH)_2$, NaOH) to clay-based buffer materials could help to maintain sufficiently high pH, to neutralize CO_2, and to suppress the microbial activity. Cement-based material, as used in the supercontainer design, is an alternative to swelling clays: it offers the advantage of imposing more favorable chemical boundary conditions to protect the metallic barriers in the very long term.

10. Corrosion of the metallic components

10.1. Introduction

During the experiment's operational stage, pitting corrosion problems in the stainless steel sensor tubes (strain gauges) were detected (section 5.3). Unfavourable chemical and microbial environments leading to the corrosion of metal components, confirmed by the post-mortem analysis programme, were also identified. If these conditions and the related corrosion processes should occur in an actual repository or during the PRACLAY Experiment, they could compromise the integrity of the metallic components, thereby jeopardizing the confinement function of the central tube or the success of the instrumentation programme due to sensor malfunctioning.
As a consequence of these observations, it was decided to extend the mock-up's dismantling programme to an experimental programme studying the corrosion behaviour of the different metal components and instrumentation devices used in the mock-up.

This chapter is a summary of the document "OPHELIE, Analysis of the metallic components" written by B. Kursten in June 2004.

10.2. Content of the corrosion analysis programme

The corrosion programme consisted of a twofold approach:

- tests performed during the dismantling of the mock-up. Attempts were made to measure the free corrosion potential (E_{CORR}) of the central tube. The pH of the buffer material in contact with the metallic components was also measured;
- post-dismantling analyses. Surface analyses techniques – optical microscopy (OM), scanning electron microscopy (SEM), energy dispersive spectrometry (SEM-EDS), X-ray photoelectron spectrometry (XPS), glancing incidence X-ray diffraction (GID) ... – were performed on the metallic components (e.g. the lining of the steel jacket, the lining of the welded and bolted covers, the central tube) and sensors (e.g. strain gauges, Glötzl hydraulic load cells, Rotronic relative humidity sensors and sheath tubes used as protection for the instrumentation devices' electrical wires) that were observed to have been attacked in order to study the type and extent of attack and the nature of the corrosion products.

It should be mentioned that the OPHELIE mock-up was not initially designed as a corrosion experiment. For this reason, a quantitative characterisation of the corrosion attack (e.g. uniform corrosion rate) could not be performed due to a lack of information on the metallic components at the time the mock-up was installed. Furthermore, it is also difficult to determine an uniform corrosion rate on stainless steel, since stainless steels are mostly prone to localised corrosion.

10.3. Investigations during dismantling

The investigations during dismantling consisted of a visual inspection of the corrosion state of the metallic components and measurements of some parameters (E_{CORR} and pH).

10.3.1. Visual inspection

The majority of the metallic components remained unaffected after exposure to the buffer material for 4.5 years and most of the attack was located on the steel lining of the jacket along hydration tube #7, as shown in Figure 10-1.

Figure 10-1: General view of the steel jacket lining. Most of the attack was located along hydration tube #7 indicated by a red arrow.

Th dration tube #7 had two entirely different (visual) ap

- mock-up, the corrosion resulted in the formation of
- mock-up, the corrosion resulted in the formation of orange-brown corrosion products.

A failed relative humidity sensor was discovered not far from this tube. It is very probable that the electrolysis induced by a direct current applied to this sensor over 4.5 years was the cause of this highly spectacular corrosion phenomenon.

Figure 10-2: View of the attack observed on the lining along hydration tube #7. Two distinct appearances could be observed, viz. green and orange-brown corrosion products.

During dismantling, it was also observed that several stainless steel tubes, which acted as protective shielding for the electrical wiring of the mock-up instrumentation sensors (e.g. thermocouples, strain gauges, pressure cells, relative humidity sensors, piezometers, ...), were in contact with hydration tube #7 (Figure 10-3). In some cases, the stainless steel protective tubes were completely destroyed, resulting in direct contact between the bare copper wiring and the hydration tube.

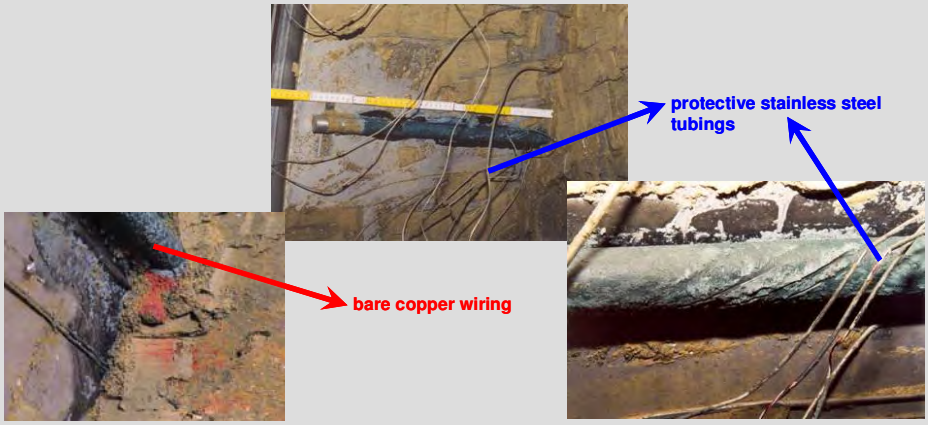

Figure 10-3: View of the corroded hydration tube #7.

Less than 5 % of the total surface area that was exposed to the saturated buffer material, which amounted to over 50 m², showed signs of attack (in one form or another and to whatever degree). Of this 5% of corroded material, more than 90% was located near hydration tube #7. The rest of the attack was situated on local and isolated spots (Figure 10-4). A remarkable observation was that many of the isolated attacks were situated near 'constructional anomalies' such as metal strips spot-welded to the lining, contact between the lining and protective steel tubes, ... (Figure 10-5).

Figure 10-4: View of the steel jacket lining showing an occasional isolated spot with minor attack.

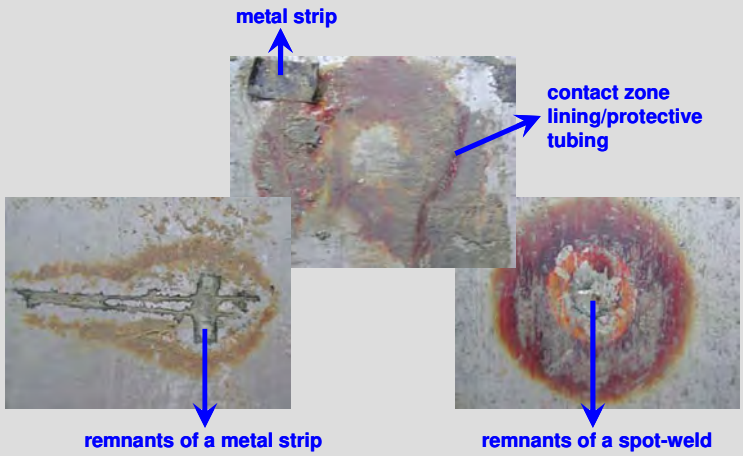

Figure 10-5: Photographs of isolated attacked spots near a 'constructional anomaly' (metal strip spot-welded to the lining, contact between the lining and protective steel tube, ...).

The central tube was found to be only slightly attacked near the weld that connected the hemispherical cap to the tube (Figure 10-6). This part of the central tube was, however, situated at the beginning of the mock-up and had not been in contact with the saturated buffer material but rather with a mixture of sand and bentonite. The shape of the attacked zone (marked with a blue line) suggests that the attack occurred along the zone filled with sand of coarse granulometry.

Figure 10-6: View of the central tube after dismantling. The (slight) attack was only situated near the weld that connected the hemispherical cap to the tube. This part of the central tube had been in contact with sand.

During the dismantling of the mock-up, it was observed that several sensors were severely attacked, as illustrated in Figure 10-7:

- several of the stainless steel sheath tubes, used to shield the sensors' electrical wires, had corroded through;
- many of the strain gauges had failed because the solder material (Sn-Pb-Ag) used to close the stainless steel sleeve was entirely corroded away;

- the plain surface of the ring-shaped discs of the Glötzl hydraulic load cells remained rather undamaged, while the ring-dovetail grooves, joint and connecting piece showed major corrosion (these parts were entirely covered with orange-brown corrosion products);
- the bodies of the Rotronic relative humidity sensors showed relatively little corrosion. The filter cap, however, was entirely covered with a green deposition layer.

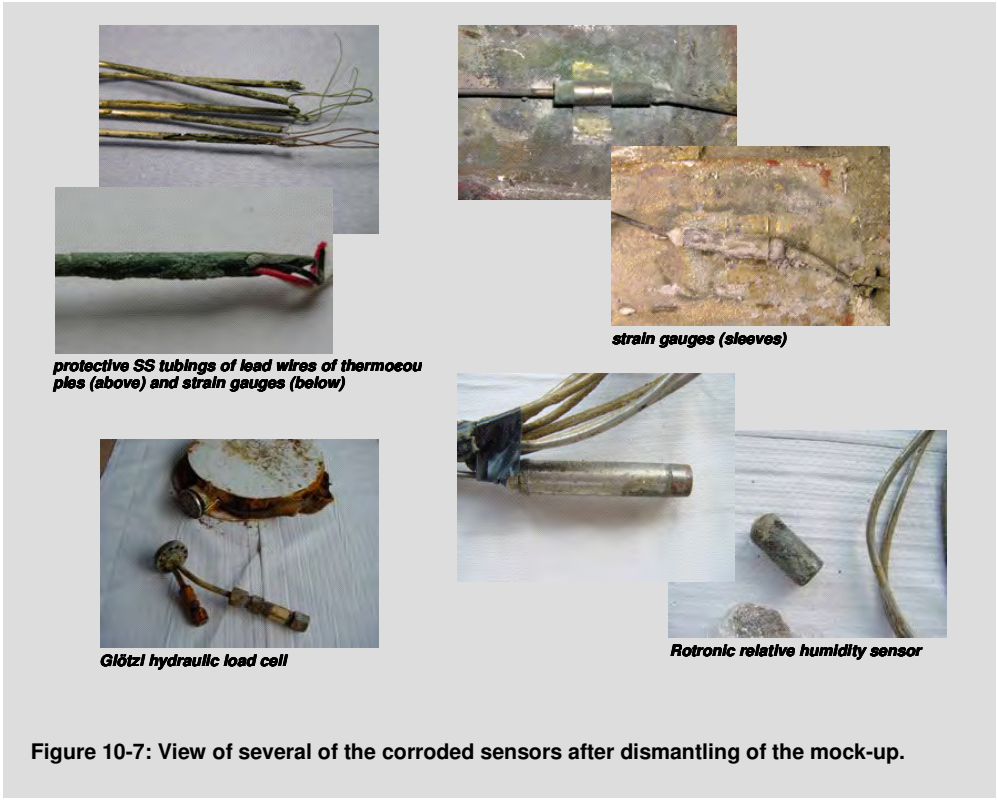

Figure 10-7: View of several of the corroded sensors after dismantling of the mock-up.

10.3.2. E_{CORR} and pH measurements

The OPHELIE mock-up provided the means to determine the free corrosion potential, E_{CORR}, of the central tube more accurately under conditions representative of long-term underground disposal (anaerobic conditions). Because of the long duration of the experiment (4.5 years, including 3.5 years at 140°C), it was considered that anaerobic conditions were established at the end of the experiment when all dissolved oxygen was consumed by microbial activity as evidenced by the presence of free dissolved sulphides observed in the water accumulator.

Knowledge of the accurate value of the free corrosion potential forms the backbone of the scientific approach, adopted by SCK•CEN (and other researchers worldwide), to study the long-term corrosion behaviour of the metallic barrier. The long-term corrosion behaviour of the candidate disposal tube materials (stainless steels) is established by comparing the values of the critical potential for pit nucleation (E_{NP}) and the protection potential (E_{PP}), which are determined from cyclic potentiodynamic polarisation tests, with the free corrosion potential:

- $E_{CORR} \geq E_{NP}$: immediate pitting problems;
- $E_{PP} < E_{CORR} < E_{NP}$:

- if E_{CORR} is close to E_{NP}, immediate pitting can occur if the separation between E_{CORR} and E_{NP} is reduced, e.g. by changing the oxidising power of the solution or by manganese sulfide (MnS) inclusions (i.e. a local site with a higher potential);
- if $E_{CORR} << E_{NP}$, the overpack material could suffer long-term pitting problems because localised attack, once initiated, will not be able to repassivate.

- $E_{CORR} << E_{PP}$: pits can neither grow nor nucleate.

The approach to determine the long-term corrosion behaviour is represented schematically in Figure 10-8. From this figure, it is evident that pitting (either immediate pitting or long-term pitting) cannot take place as long as the free corrosion potential, E_{CORR}, of the material concerned in the service environment considered remains lower than the protection potential.

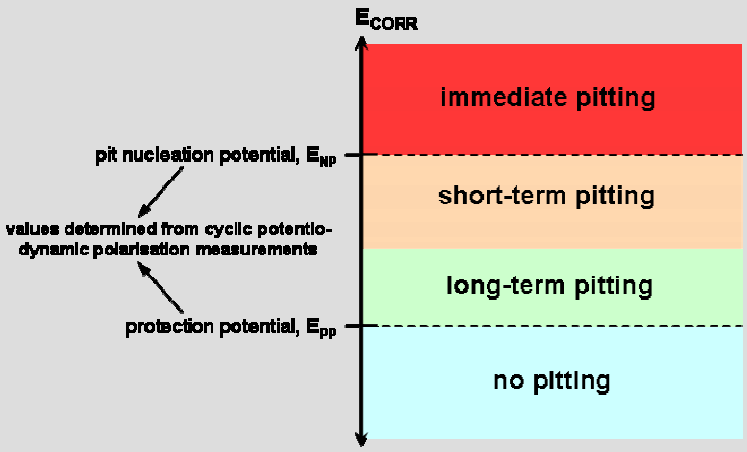

Figure 10-8: Schematic representation of the approach adopted to determine the long-term corrosion behaviour.

The free corrosion potential was determined during dismantling by measuring the potential difference between the central tube and a commercially available Ag/AgCl reference electrode.

In some cases, the pH of the saturated buffer material in contact with the central tube was measured for better characterisation of the environment surrounding the central tube. This was performed because unexpectedly low pH-values that differed widely from the expected pH-value of 8.5 (corresponding to the 1.17 kg/m³ $NaHCO_3$ solution injected) had previously been measured:

- a pH of 5.6 was measured in the water originating from the hydration circuit;
- a pH of 3.7 was measured in the water originating from a strain gauge leak.

Two methods were applied to measure the pH: (i) using a strip of litmus indicator paper (after wetting the buffer material with deionised water) and (ii) using pH and redox electrodes (after suspending the buffer material in deionised water).

An overview of the free corrosion potentials measured in the central stainless steel tube of the mock-up is given in Figure 10-9. The E_{CORR} values under laboratory[8] conditions are also given for comparison. It was not possible to draw an unambiguous conclusion concerning an absolute value for E_{CORR} under repository relevant conditions from these free corrosion potential measurements. Except for measurements conducted near the cover of the mock-up (central tube in contact with sand), all E_{CORR} values measured were in the range of +250 to +302 mV_{SHE}. A comparison of the E_{CORR} values measured in the mock-up with those measured in the laboratory (+265 mV_{SHE} under oxic conditions and -120 mV_{SHE} under anoxic conditions), indicates that the conditions inside the mock-up (within the time span of the measurements performed under air) were oxic..

The outcome of the E_{corr} measurements of the central tube are however contradictory compared to other observations from independent measurements. These independent measurements seem to indicate that anoxic conditions were attained inside the mock-up at the end of the operational phase:

- a negative redox potential measured on line at the end of the experiment (measured before and during the cooling phase);
- the presence of sulphide – H_2S, HS^- and ZnS (which are very sensitive to oxidation) – in the water injection system (chapter 9) and a charcateristic smell of rotten eggs during the dismantling of the mock up;
- the presence of microbial activity (SRB, TRB, MPB, anaerobic microorganisms);

This apparent discrepancy could be explained by the spatial variations of redox conditions inside the mock-up if a redox front developed from the injection tubes located at the periphery towards the centre of the mock-up: the mass of blocks remained largely oxidised (initial conditions) while a thin zone of buffer material was chemically reduced by sulfide immediately around the water injection tubes. Sulfate reducing bacteria were detected in the water injection system (chapter 9).

The free corrosion potentials measured from the middle to the end of the mock-up (contact with saturated buffer) were approximately 250-300 mV higher than those measured near the front cover of the mock-up (contact with sand). One possible explanation is the partial oxidation of the clay front with oxygen from air in the mock-up during the dismantling operations: between the measurements performed on opening the mock-up and in the middle, more than three days had elapsed.

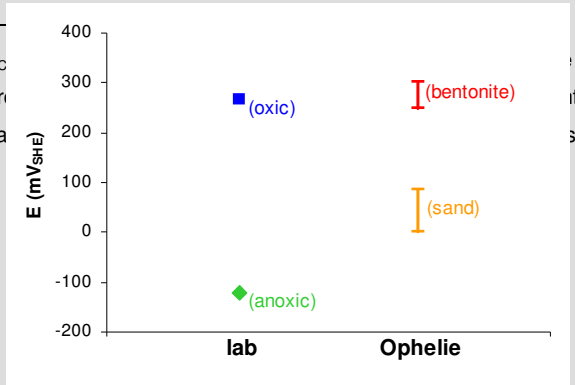

8 E$_C$ framework of a previous NIRAS corrosion pr tial of AISI 316L hMo grade stainless steel sa sed to buffer the OPHELIE mock-up.

Figure 10-9: Comparison of E_{CORR} values determined in the laboratory and during the dismantling of the mock-up.

The pH-values measured using litmus indicator paper were neutral to slightly acid (the pH was between 5 and 7). The pH values determined with a pH electrode were about 2 pH-units higher.

10.4. Post-dismantling analyses

Figure 10-10 shows the placement of the analysed samples. Effort was mainly focused on the central tube and stainless steel jacket lining. The reasons were as follows:

- the central tube was manufactured from AISI 321, the stainless steel grade that most closely represents the composition of the primary candidate overpack material (AISI 316L hMo) of all the metallic components used in the mock-up;
- the boundary environmental conditions (e.g. pore water chemistry and temperature) were different in the centre (central tube) and at the periphery of the mock-up (jacket lining). The corrosion of several sensors was also investigated to verify and prove their stability when exposed to the buffer material at high temperature and pressure in view of their long-term use in the PRACLAY gallery.

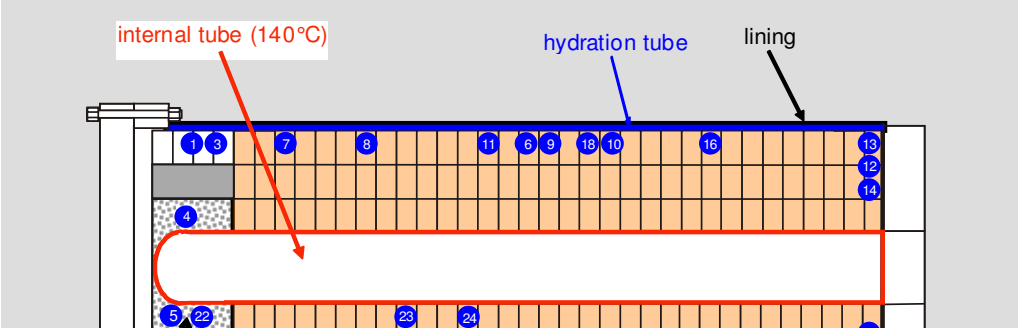

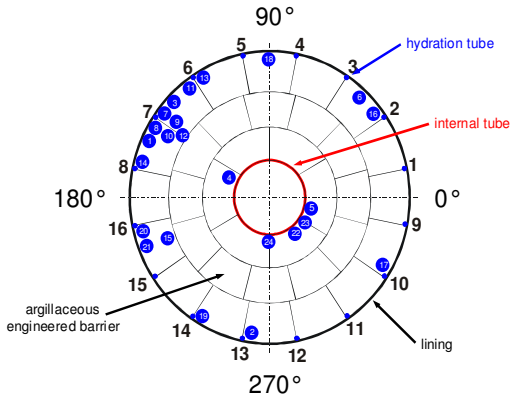

Figure 10-10: Placement of the samples for corrosion analyses (sensors not included).

Three types of corrosion products were encountered:

- green deposition products. These had a brick-like porous morphology and contained huge amounts of Cr and S (Figure 10-11). These products are composed of chromium oxide hydroxide [CrO(OH)] on the surface. Deeper in the layer, chromium sulphide is highly likely to be present (Figure 10-12);

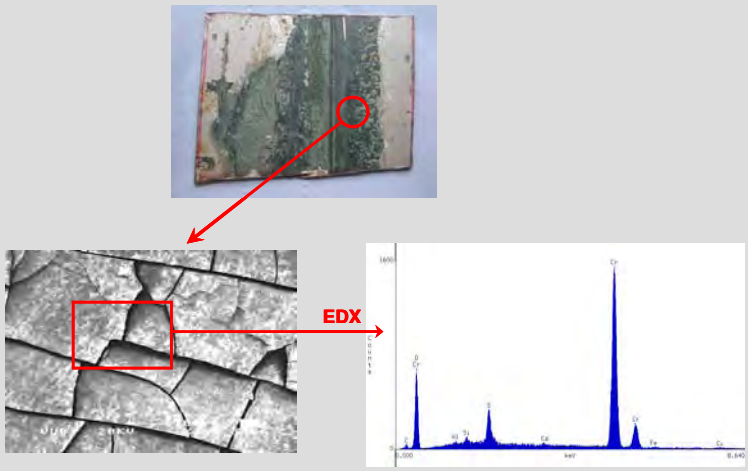

Figure 10-81: Characterisation of the chemical composition of the green deposition layer formed on top of the steel jacket lining.

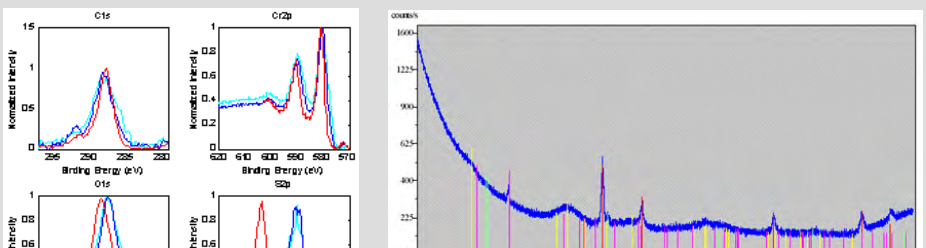

Figure 10-9: Surface analyses results of the green deposition layer formed on top of the steel jacket lining. XPS high-resolution scans acquired before (red curves), after 20 minutes (blue curves) and after 50 minutes (cyan curves) of ion sputtering. After ion sputtering, the single S-peak was split into two, indicating that sulfide compounds are highly likely to be present deeper in the layer (LEFT). XRD pattern at an incident angle of 0.5° (RIGHT). The broad peaks are the result of an amorphous phase present in the top surface layer. This is most likely to be composed of chromium oxide hydroxide (yellow lines).

- orange-brown deposition products, whose colour is usually associated with the rusting of Fe-containing materials. These layers had a granular morphology and were usually composed of a mixture of Fe oxides and clay components (Si and Al oxides, Ca, K). Two types of layers were observed:
  - a very thin layer with a thickness of 10-20 nm. This was not considered to be caused by corrosion attack but due to 'staining'. This is a modification of the passive layer resulting in the discoloration of the passive layer;
  - a thick layer with a thickness > 5-10 µm. However, on many occasions, the morphology of the surface beneath the deposit was found to be similar to that of the back side[9] of the sample (only slight signs of intergranular attack probably introduced during the production process for the metal sheets due to acid pickling, were observed). It is therefore likely that many of these products were not formed as a result of the corrosion of the stainless steel lining itself but due to the deposition of oxidation products of Fe-containing clay components.
- purple-brown deposition products. These layers also had a granular appearance and were composed of a mixture of Fe-O and Fe-S (Figure 10-13). These products were only found on the central tube (exposed to sand with a high oxygen content).

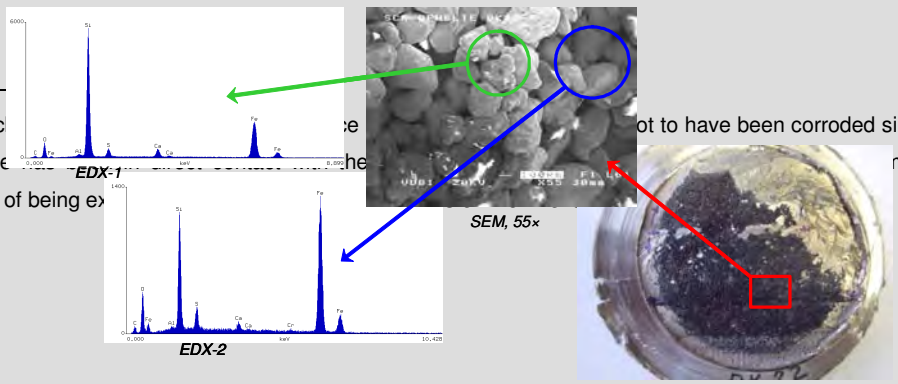

[9] The bac… ot to have been corroded since this side … nent instead of being ex…

Figure 10-103: Surface morphology and elemental composition (SEM/EDX-analyses) of the purple-brown deposition layer formed on top of the central tube. The grains were partly composed of sand particles (SiO_2) (EDX-1) and partly of a mixture of Fe-S and/or Fe-O compound and sand (EDX-2).

The central tube (AISI 321 grade) seemed to be more resistant to corrosion than the stainless steel lining (AISI 304 grade) of the steel jacket:

- the stainless steel lining showed development of several corrosion spots, some of which penetrated several hundred micrometers into the base metal, as illustrated in Figure 10-14;
- on the other hand, the central tube showed only some minor attacks near the weld that connected the hemispherical cap to the tube. However, this part of the central tube was exposed to a different environment, viz. sand, and much more aggressive environmental conditions (higher oxygen content, higher temperature, and increased chloride concentration).

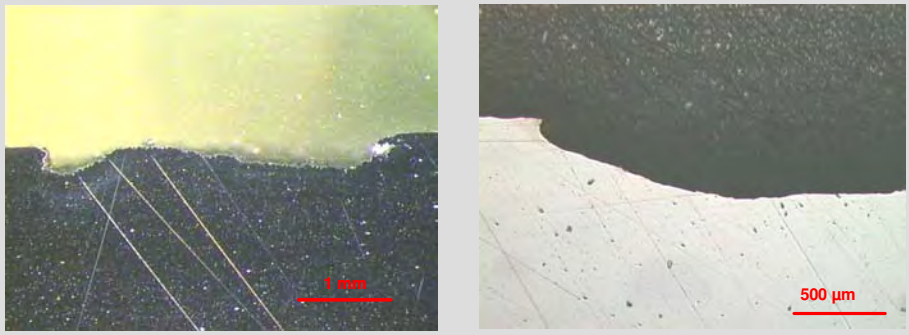

Figure 10-14: Corrosion spots developed on the AISI 321 grade stainless steel lining of the steel jacket. Binocular macrograph (magnification: 32×) of a polished and unetched cross section of the corrosion attack on sample BK2 - the attack was 3.5 mm wide and ~350 µm deep – (LEFT). Optical micrograph (magnification: 50×) of a polished and unetched cross section of the crater formed on sample BK19 - the attack was ~480 µm deep – (RIGHT).

Considering the high levels of chloride that were measured during the experiment's operation stage in water samples collected from leaks in defective stainless steel tubes, it was surprising that chloride was only detected in the oxidation products on rare occasions (and at relatively low levels). This could however have been caused by the sample preparation technique; since

chloride usually forms soluble salts, the chloride could have been washed away by the water coolant used for the abrasive cutting machine during sectioning.

Evidence of the presence of pyrite (FeS_2) was detected. Quantitative SEM/EDX analyses revealed that some of the deposition products consisted solely of Fe and S with a stoechiometric atomic ratio indicating the presence of pyrite (2 S atoms for 1 Fe atom). Figure 10-14 shows the results of the quantitative SEM/EDX analyses of deposition products formed on some of the welds on hydration tube #8.

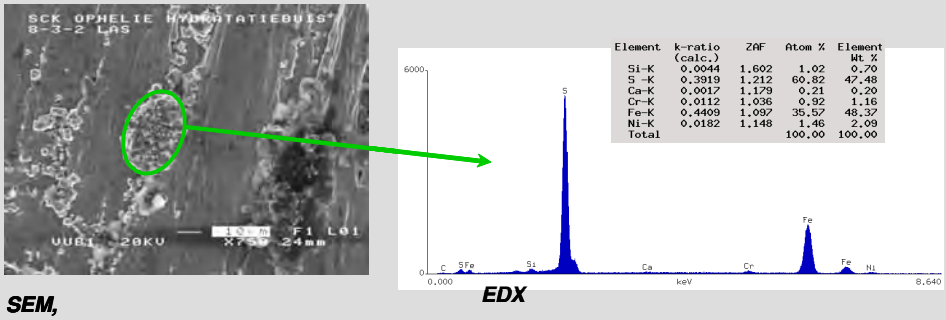

SEM, ***EDX***

Figure 10-15: Quantitative SEM/EDX analyses of deposition products formed on some of the welds on hydration tube #8, pointing to the presence of FeS_2 (stoechiometric atomic ratio Fe/S: 2 S atoms – 1 Fe atom).

This could point to an incomplete oxidation or a partial reduction of the FoCa clay. If this medium is to be considered, it would be advisable to re-assess the pre-treatment of the FoCa clay.

The existence of microbiologically influenced corrosion (MIC) cannot be excluded. Several indications have been encountered that could point to the occurrence of MIC in the mock-up:

- clusters of strings (Figure 10-16 LEFT) that were observed on the surface of the inner wall of some of the water supply-tubes for the hydration system could point to the presence of microbiological activity;
- some strain gauges showed signs of a ductile fracture in the vicinity of the contact zone between the part of the stainless steel protective tubing encasing the strain sensitive foil and the thin steel carrier base, which was used for connection (spot-welding) to the central tube (Figure 10-16 RIGHT). However, such a honeycomb-like shaped appearance of attack has also been attributed to MIC, especially in the vicinity of welds: the Cr-depleted austenite phase (δ-ferrite) in welds (and in heat-affected zones) of stainless steel can be attacked preferentially under the impact of microbiological activity.

To find out whether MIC had occurred in the mock-up, a more fundamental and detailed study of the microbial activity and water chemistry (presence of dissolved sulphides) was also performed (chapter 9).

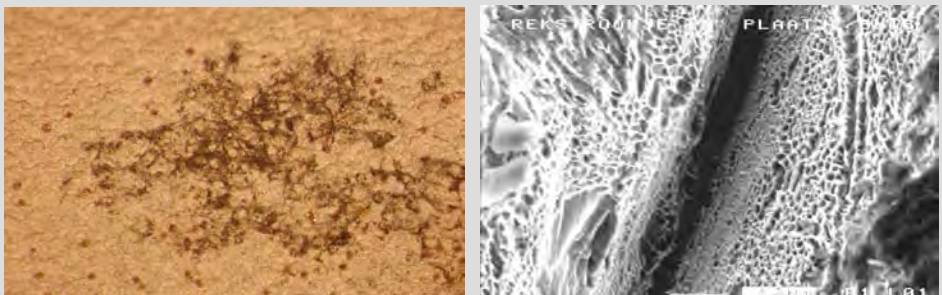

Figure 10-16: Binocular macrograph (magnification: 25×) of the surface of the inner wall of the water supply-tube of hydration tube #15 (part outside the mock-up) showing a cluster of strings (LEFT). SEM-micrograph (magnification: 1,500 ×) of strain gauge SG17 showing a honeycomb-like attack at the weld line (RIGHT).

The welds were not always properly performed:

- welding faults such as undercutting, weld bubbles, … were frequently encountered;
- on some occasions, the weld material was found to be much purer than the base material: the substrate and heat-affected zone contained the usual levels of the alloying elements (Fe, Ni and Cr) in AISI 304 grade stainless steel, while the weld consisted of a filler material with a much higher Cr-content. As a consequence, the weld remained unattacked but the heat-affected zone revealed severe signs of intergranular attack.

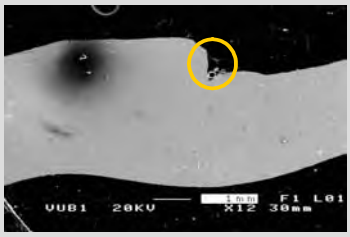

SEM-1, 12×

undercutting

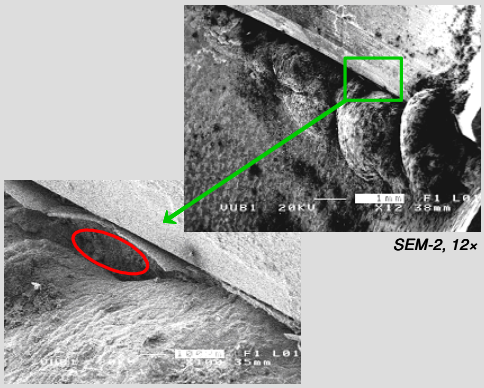

SEM-2, 12×

SEM-3, 100×

weld bubbles

Figure 10-17: Examples of weld flaws. Undercutting is a weld discontinuity that occurs when a groove is melted into the base metal adjacent to the toe or root of the weld and left unfilled by weld metal. Weld bubbles can create crevices, between the substrate and themselves, which can act as sites for corrosion initiation (enrichment of aggressive anions).

Most of the instrumentation devices (strain gauges, relative humidity sensors, hydraulic load cells) were found to have broken down prematurely:

- the strain gauges seemed to have been attacked at the parts connecting the sleeve with the strain tube on the one hand and with the stainless steel sheath on the other hand. For some of the strain gauges, the connecting parts were found to be entirely corroded (Figure 10-18). For the strain gauges where the connecting part was still present, evidence was found that the connecting part consisted of a stainless steel (machined) head that was soldered (Sn) to the stainless steel sleeve (Figure 10-19). Since such a stainless steel head cannot corrode entirely without leaving a single trace, it was assumed that some of the sleeves were mounted without a stainless steel head. In these cases, the sleeves were probably completely closed with Sn-solder. Evidence of a ductile fracture surface (honeycomb-like shaped appearance) due to overload was also observed (Figure 10-20). This could have been caused during the dismantling operations;

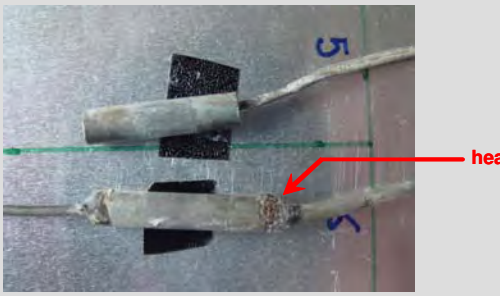

Figure 10-18: Close-up of the sleeves of strain gauges SG5 and SG6. The head of the sleeve of strain gauge SG6 was still present, while that of strain gauge SG5 had completely disappeared.

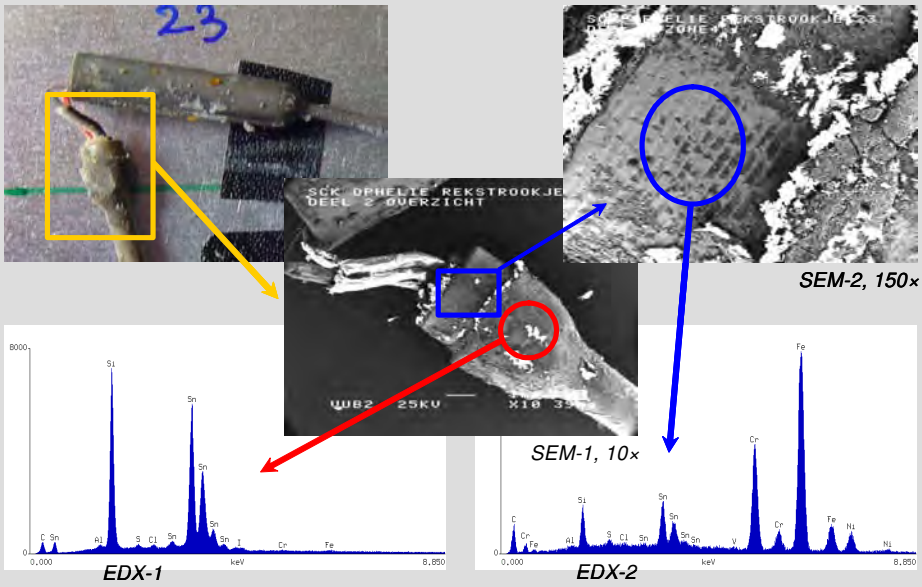

Figure 10-19: Close-up of the head of the sleeve of strain gauge SG23. The head was fabricated from stainless steel and showed signs of machining (SEM-2). The elemental composition of the head (EDX-2) mainly consisted of the typical alloying elements of stainless steel (Fe, Cr and Ni). The surface of the head was entirely covered with soldering material (Sn) (EDX-1).

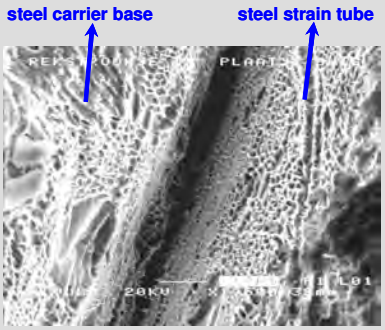

Figure 10-20: SEM-micrograph (magnification: 1,500×) of strain gauge SG17, showing a ductile fracture near the weld line between the steel strain tube and the steel carrier base.

- the design of the Rotronic relative humidity sensors promotes the risk of corrosion:
  - the sensing element was surrounded by a porous stainless steel filter cap that was coated on the inside with a thin copper foil (Figure 10-21, BOTTOM). The contact between two dissimilar metals (stainless steel/copper) could accelerate corrosion of the least noble metal ('galvanic coupling');
  - the filter cap was porous, which can lead to the existence of oxygen gradients, concentration gradients, … (Figure 10-21, TOP RIGHT). The filter cap was covered with a very thick dark greyish green to black layer, which was composed of Cr and S (Figure 10-21, TOP LEFT);
  - the use of a ceramic material for the cap could be a possible solution that needs to be investigated.

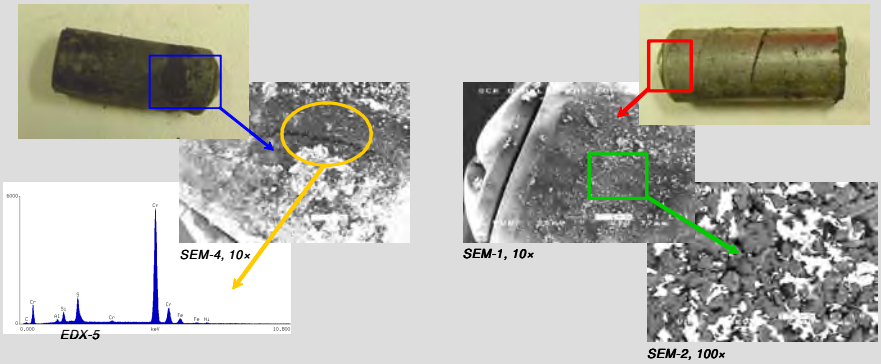

Figure 10-21: Surface investigations (SEM/EDX analyses) of the corroded filter cap of several relative humidity sensors. The filter cap was covered with a very thick dark greyish green to black layer, which was composed of Cr and S (TOP LEFT). The filter cap was porous (TOP RIGHT). Close-up of the interior of the filter cap of sensor RH8. The inner wall of the cap was coated with a thin copper foil (BOTTOM).

- most of the corrosion in the Glötzl hydraulic load cells was situated at the connecting head. Corrosion had propagated millimetres deep into the base metal of the connecting head. The head was found to be manufactured from ordinary Mn-steel. And filler materials (Ag, Cu and Zn based), which are much more noble than the substrate, were used to join (brazing) the two ring-shaped pressure plates (Figure 10-22).

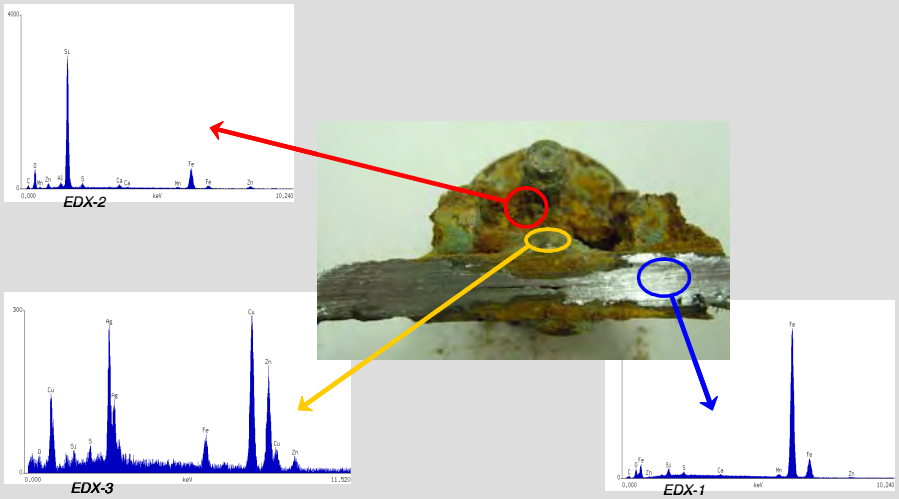

Figure 10-22: Surface investigations (SEM/EDX analyses) of the connecting head of a corroded Glötzl hydraulic load cell. The connecting head was manufactured from ordinary Mn-steel (EDX-1). The corrosion products were composed of a mixture of clay components and Fe-oxides, which accounts for the brownish colour (EDX-2). Brazing, based on noble filler materials (Ag, Cu, Zn), was used as a joining technique (EDX-3).

10.5. Conclusions

The 'OPHELIE' mock-up experiment was not initially designed as a corrosion experiment. As a consequence, quantitative characterisation of the corrosion attack (e.g. uniform corrosion rate) could not be performed due to a lack of information about the metallic components at the time the mock-up was installed.

It was not possible to draw an unambiguous conclusion concerning an absolute value for E_{CORR} under repository conditions. Furthermore, the free corrosion potentials measured in the mock-up have to be interpreted with caution because many uncertainties affected the measurements:

- a lack of information concerning the oxygen evolution (rate of oxygen consumption) inside the mock-up during the operational stage;
- uncertainties concerning the influence of the duration that air (O_2) had been in contact with the clay front during the dismantling stage (i.e. during the time span between the removal of a clay section and the E_{CORR}-measurement) such as:
  - how fast does oxygen diffuse through the argillaceous buffer environment ?

- was there a tight contact between the central tube and the argillaceous buffer material after saturation or did crevices exist along which oxygen could penetrate more easily once the mock-up was opened ?

While it is possible to explain the corrosion of hydration tube #7 (electrolysis induced by a direct current continuously applied over 5 years to a failed relative humidity sensor in the close vicinity of the tube), this is not the case for the colour change in the corrosion products formed along this tube, from green (Cr, Ni) to orange-brown (Fe).

The information gained from the OPHELIE mock-up experiment can be used to provide recommendations within the framework of the PRACLAY Experiment and the disposal concept:

- during the PRACLAY Experiment, it would be useful to conduct on-line E_{CORR} measurements in combination with monitoring the evolution of the O_2-content with time, at several locations in the gallery;

- during the design phase of the reference disposal concept, attention should be paid to avoiding situations that could lead to an increased risk of developing localised corrosion, such as crevices (contact between lining and protective tubes) and traps (spot-welds) where corrosive liquids could accumulate and create a locally more aggressive environment (‘occluded cell’);

- AISI 321 grade stainless steel is more resistant to corrosion than AISI 304 grade stainless steel. According to the SAFIR-2 concept, the elemental composition of AISI 321 grade stainless steel is quite similar to that of the reference candidate overpack material (i.e. AISI 316L hMo grade stainless steel), , except for the molybdenum content. The higher molybdenum content theoretically makes AISI 316L hMo grade stainless steel even more corrosion resistant than AISI 321 grade stainless steel;

- if welding is to be considered as a closure technique, an in-depth study should be performed into the application of post-weld treatments:

  - post-weld cleaning can be helpful in removing the heat-tinted metal formed during welding;

  - post-weld heat treatments are commonly applied to reduce the corrosion susceptibility of the heat-affected zone.

- furthermore, a detailed description of the welding procedure, in all its aspects (technique, atmosphere, pre-welding treatments, post-weld heat treatment, post-weld descaling procedure, non-destructive interim check-up,…) should be written to guaranty the quality of the work;

- the following points should be taken into account before the installation of instrumentation in the PRACLAY Experiment:

  - avoid the use of low-alloy steel (e.g. hydraulic load cells fabricated from Mn-steel);

- avoid contact between dissimilar metals (e.g. stainless steel/copper).

11. Performances of the monitoring equipment

11.1. Introduction

Assessing the performance of monitoring equipment was initially one of the main objectives of the OPHELIE experiment. This chapter summarises the experience with each sensor type, consisting of observations during installation, operation, dismantling and post-dismantling analyses.

Initially, several analyses, including recalibration were planned on the recovered sensors. Although specific attention was paid to the sensors and the instrumentation cables, it was not possible to obtain completely undamaged sensors during the dismantling operations (e.g. mineral insulated cables turned out to be fragile as even the slightest damage to the cable sheath renders the sensor unusable due to the hygroscopic nature of the MgO). Recalibrations were not therefore considered useful. In contrast, extensive analyses were performed on the corrosion behaviour of different sensor types (chapter 10).

Important lessons for the PRACLAY Experiment have been drawn from the OPHELIE experiment. Where relevant, the potential of each sensor type is mentioned.

The positions of the sensors mentioned in this chapter can be found in appendix 3.

11.2. Sensor performances

11.2.1. Table of performances

An overview of the performance during the operational stage according to sensor type is given in Table 11-1.

11.2.2. Thermocouples

Operational stage

From the 78 sensors installed in the backfill, only three failed; five other thermocouples showed decreased insulation resistance, but, except for TC58 (showing unstable values), the others showed normal temperatures.

Dismantling and post-dismantling analysis

Upon dismantling, all thermocouple readings were checked against a manual reading; no anomalies showed up. The cables of TC58 and TC59 were close to the severe corrosion of RH6 and therefore were also affected by this corrosion. This explains the zero insulation of sensors, the failure of TC59, and the instability seen at TC58.

Conclusion

This sensor type is well suited to the experimental conditions. An assessment of the corrosion resistance of the sheath material in the medium concerned (e.g. bentonite or concrete) is recommended. Some recommend a more resistant material, such as inconel or even titanium, to be specified for the sheath material, but switching to a more noble material must not put the stainless steel parts at risk. However, the overall mineral insulation causes more delicate and time-consuming interventions when connections are to be made or repaired.

Table 11-1: Performance of the different sensor types in the mock-up.

Sensor type	# installed	# Failed	Comments
thermocouples	100	3	corrosion due to nearby RH sensor
Internal strain gauges	27	27	corrosion drift effects
piezometer (vibrating wire)	6	5	overpressure (4 x rated) connection sensor – cable
"RocTest" segment pressure	2	2	After 1.5 years
"Glötzl" segment pressure	2	2	membrane rupture after 2 years
"Glötzl" load cells	4	4	tube connections, sensor corrosion
"Kulite" buffer pressure	9	6	sealing of sensor body mineral insulated cable
moisture content "Rotronic"	9	9	After flooding (100 % humidity) mineral insulated cable fragile at connector
external strain gauges	27	0	re-installation of dummy gauges
bolt loads	6	0	interpretation of measurements
hydration system sensors	4	0	one replaced at elevated pressure

11.2.3. Internal strain gauges TML

Operational stage

The measurement of the strain on the central tube by the hermetically sealed strain gauges did not lead to meaningful results. Firstly, the strains to be measured on this quite thick tube were expected to be very low. Furthermore, detection of these small mechanical strains was complicated by the large temperature variation.

The first measurements, after the start of the heating, showed large variations. The gauges typically showed strains of several 100's µstrain. After a few months, some strain gauges started to show erroneous signals.

At the end of 1998, half a year after the heating, several gauges started to leak through the signal cable. With time, most internal strain gauges had to be disconnected from the data-acquisition system.

The water that leaked out of the gauges showed high chloride content, pointing to corrosion as a possible cause of the failure.

Dismantling and post-dismantling analysis

During dismantling, it became clear that the soldered cable connections were the weak point: the stainless steel parts were intact, but in most gauges, the solder had completely disappeared (but not in all gauges – Figure 11-1, RIGHT). The cables from SI4, SI5, SI6 and SI16 were also attacked by the corrosion of RH6 (Figure 11-1, LEFT). A full corrosion analysis was performed (chapter 10). This dealt with the influence of the materials used, as well as the construction techniques (soldering, welding...), on the observed corrosion phenomena.

Figure 11-1: Corrosion of the metal sheath (LEFT) and corrosion of the soldered connection part between the sensor and cable (RIGHT).

Conclusion

In general, the resistive type of strain gauge is not recommended for long-term measurements due to inherent long-term drifts, complicated by the thermal influences and the saturated environment. If dynamic or short-term phenomena are to be observed, these types of gauges can be considered, provided some improvements are made (corrosion resistance, thermal compensation).

If strains must be monitored, the more robust vibrating wire type - or the more recent fibre optic based strain sensors- have more potential. In addition, deformation measurements could be employed to obtain equivalent data on the phenomenology investigated (e.g. deformation of long tubes).

The current disposal concept, and consequently the re-designed PRACLAY Experiment, no longer includes long (~ 200 m) disposal tubes; the effect on non-uniform swelling with respect to the gallery axis (the main reason for this type of measurements) on this tube is therefore no longer relevant.

11.2.4. Geokon piezometers

Operational stage

From the six sensors installed, PZ5 appeared to have failed during the installation work. All sensors had to be sealed at the cable sheath end as the connection between the sensor body and cable sheath was apparently not watertight. PZ1 and PZ3 failed in the first half of 1998. During the pressure peak at the start of 2000 (event IV in Table 5.2), values over 3.5 MPa were achieved. With the sensors specified for only 1.0 MPa, it is not surprising that two more sensors (PZ4 and PZ6) failed during this event, leaving PZ2 intact for the rest of the experiment. The value indicated by this instrument was lower than the pressure applied, indicating a possible zero drift.

In addition, unstable readings were sometimes obtained, probably due to the vibrating wire read-out technique.

Dismantling and post-dismantling analysis

Apart from the dismantling operation consequences, no visual damage (corrosion) was observed on the sensors. The connection between the sensor body and the stainless steel sheathed cable did not appear to be watertight.

Conclusion

Most problems were clearly due to the adaptations required (e.g. metal cable sheath). Also the vibrating wire sensor read-out needs some extra attention to obtain stable signals. Furthermore, a piezometer is delivered with a saturated filter and installing this filter in a non-saturated environment (e.g. bentonite with high suction) might also lead to negative initial pressures. The twin-tube type piezometer, the most common type of sensor used in HADES, with an accessible pressure transmitter (recalibration or replacement) and the possibility of determining other hydraulic parameters, remains the preferred option.

11.2.5. Kulite total pressure cells

Operational stage

The nine sensors installed showed good measurement data during the initial phase of the experiment. PT3 failed during the hydration phase, after four months. The initial pressure peak due to the start of the heating was recorded well by the other sensors. Three more sensors (PT4, PT6, PT7) failed in the second half of 1998, and one sensor (PT2) in 1999. PT5 failed at the end of 2000. Three sensors (PT1, PT8, PT9) were still functioning at the end of the experiment. Insulation resistance measurements and continuity measurements indicated that the sensor wiring of the broken sensors was affected. Water ingress was one of the most probable explanations.

Table 11-2 shows the chronology of events of the problems encountered.

Table 11-2: Chronology of events for the total pressure sensors.

Date	Sensor	Remarks
1998-02-13	PT3	readings not reliable, later broken
1998-08-19	PT4	readings not reliable, later broken
1998-09-22	PT6	readings not reliable, later broken
1998-11-13	PT7	readings not reliable, later broken
1999-05-12	PT2	readings become unstable
2000-10-12	PT5	sharp drop to zero

Dismantling and post-dismantling analysis

No particular damage could be seen on the sensors. The cable of PT4 was close to the corroded sensor RH6. The failure of this sensor is most probably due to its corrosion (Figure 11-2, RIGHT).

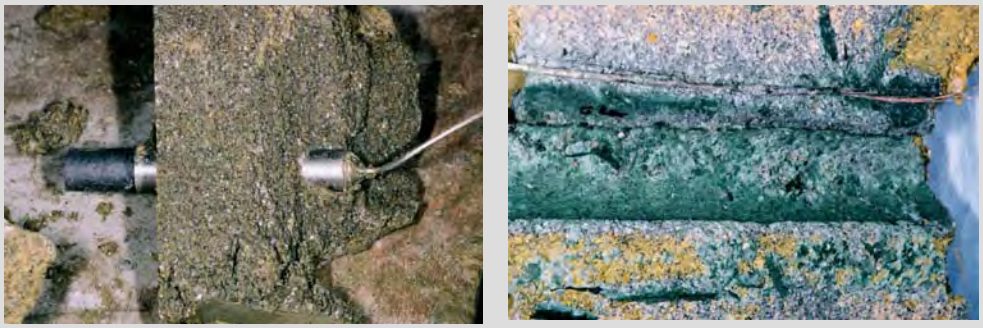

Figure 11-2: Kulite total pressure sensor retrieved during dismantling (LEFT) and corrosion of the signal cable (RIGHT).

Conclusion

The feasibility of measuring total stresses in swelling materials with this type of pressure sensor has been successfully demonstrated in other setups (e.g. RESEAL EC experiment).

This particular design therefore needs to be improved before it can be used again. This type of measurement will be needed to measure the swelling pressure of the bentonite in the PRACLAY Seal Test[10] in particular.

[10] The PRACLAY Seal Test is a specific test in the PRACLAY Experiment, as it is currently defined and designed. Its main objective is to verify the installation and performance of a bentonite-based annular seal as a hydraulic cut-off in the excavation disturbed zone.

11.2.6. Rotronic relative humidity cells

Operational stage

Apart from one sensor (RH6) that did not show valid data after the start of the hydration, most other sensors showed stable data during the hydration phase. One sensor (RH9) failed after indicating saturated conditions. After the start of the heating however, most sensors started to show unstable or invalid (far above 20 mA) signals (see Table 11-3 for the chronology of events). The capacitive sensing cell was not able to function properly in the presence of liquid water, but according to the manufacturer (Rotronic), the sensor should become operational again once the medium becomes desaturated.

Table 11-3: Chronology of events for the relative humidity cells.

Date	Sensor	Remarks
1998-02-23	RH9	out of range (38 mA) after plateau indicating saturation
1998-06-06	RH3	unstable readings
1998-08-15	RH5	out of range (signal > 20 mA)
1998-09-21	RH4	out of range (signal > 20 mA) after rapid increase
1998-09-30	RH2, RH7	out of range (signal > 20 mA)
1998-11-02	RH8	out of range (signal > 20 mA)
1999-01-08	RH1	out of range (signal > 20 mA)

Dismantling and post-dismantling analysis

During dismantling, heavy corrosion was observed on several sensors, probably due to galvanic corrosion. Several sensors broke apart during dismantling operations (the sintered stainless steel cap was not fixed to the sensor, Figure 11-3). Sensor RH6, which suffered wiring problems and had not shown valid data from the beginning, had also caused the corrosion of other cables in its neighbourhood. Maybe wrong wiring aggravated the corrosion of this sensor.

The corrosion analysis on this type of sensor also highlighted the use of different alloys; in particular, the copper foil on the inside of the stainless steel filter cap seemed to be a poor design in terms of corrosion performance.

Conclusion

The sensor design was not well suited to the experimental conditions. The sensor body, with several metals, was subject to galvanic corrosion. The sensor part (capacitive measuring element, as well as Pt100 temperature sensor) was damaged when the medium became saturated. Some measurement problems could also be related to the cable design. The mineral insulated cable (4 mm diameter) with no less than seven conductors required very delicate working when making or repairing connections. Also the conditioning box (to convert the capacitive signals into a standard 4-20 mA current signal) could deliver signals lying far outside these limits (e.g. negative current signals).

This type of measurement remains essential in the PRACLAY Seal Test. In non-saturated set-ups abroad, this type of sensor shows a reasonable performance. To increase the confidence in this type of measurement, other measurement principles will be explored further (such as the psychrometer, TDR, and thermal conductivity).

Figure 11-3: Fragile sensor-cable connection (LEFT) and sensor with exposed sensing element as the filter cap was not fixed to the sensor body (RIGHT).

11.2.7. RocTest segment pressure cell

Operational stage

Both pressure cells measured successfully for more than a year, but then both broke down at almost the same moment: PR2 at the beginning of March 1999, PR1 mid April 1999. It is not clear if the cause was related to the vibrating wire sensor or the cable connection. The low insulation resistance of the cables is an indication of deteriorated cable connections, probably due to water ingress.

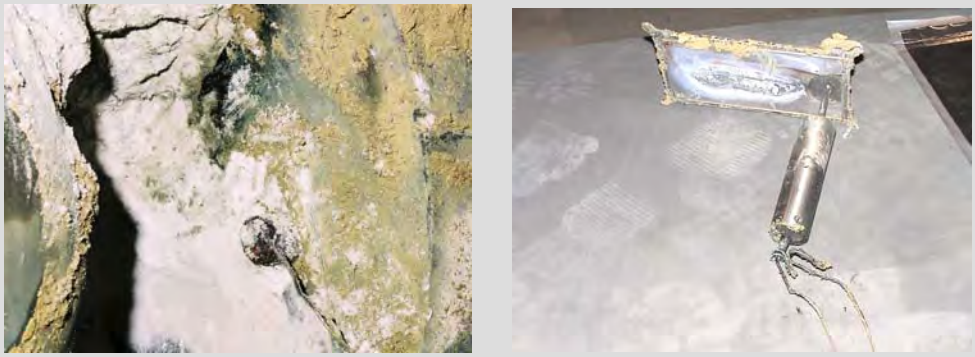

Figure 11-4: Uncovering the RocTest pressure cell (LEFT). The retrieved sensor clearly shows damage at the sensor-cable connection (RIGHT).

Dismantling and post-dismantling analysis

During dismantling, corrosion of the mineral insulated cables of PR1 was observed. The connection between the signal cables and the sensor body (resin potted) also showed serious

corrosion attack, including leakage of mercury (Figure 11-4). This means that it is not simply a signal cable problem, but also a problem with the sensors itself.

Conclusion

This cell clearly requires an improved design if it should be considered for use in the PRACLAY Experiment. However, a flatjack type cell is quite essential when large measurement surfaces are needed to minimize local heterogeneities. The hydraulic fluid could also be water, so that mercury or oil contamination of the medium is avoided.

11.2.8. Glötzl segment pressure cell

Operational stage

After the last successful hand-pump reading in October 1998, mercury showed up in PG1 during the reading in March 1999. This is a clear indication of a broken membrane in the compensating valve. This phenomenon was also observed earlier, especially at higher temperatures, and therefore seems to be inherent in the sensor design. PG2 gave a very low value (0.5 bar). A second measurement on 15 March 1999 also showed mercury in the return tube for this sensor.

Analyses of the mock-up water at the final stage, just before cooling, showed a further elevated concentration of organic components, which was most probably due to leakage/spillage of hydraulic oil when reading out broken sensors.

Dismantling and post-dismantling analysis

The sensor had completely broken down due to corrosion. The use of carbon steel fixing bolts resulted in the disintegration of the stainless steel sensor body. Moreover, the external protection was not resistant to the elevated temperatures. The pressure pad, made from carbon steel, was also analyzed by the corrosion team.

Conclusion

In addition to the complexity of the compensating valve technique (pressure and return tube, connections), the reliability of these sensors, especially at higher temperatures is questionable. Since these sensors use fluids that could significantly affect the buffer or backfill environment (oil or mercury in the flatjacks, and oil for the read-out lines) the use of this type of sensor is not recommended. For the PRACLAY gallery, flatjack pressure and load cells will be used, but the flatjack will be filled with water and the pressure will be measured with a more conventional type of pressure transducer (vibrating wire).

11.2.9. Glötzl segment load cell

Operational stage

Two cells (LG1 and LG2) showed a leak through the connecting tubes due to a bad connection between the sensor and the tube on installation. So, they could not be read-out. LG3 broke down in 2000 (the last successful reading at the end of December 1999 gave a value of 10 bar, while the reading in April 2000 showed water in the return tube).

LG4 broke down a few months later.

Dismantling and post-dismantling analysis

The sensor had completely broken down due to corrosion. The use of carbon steel fixing bolts resulted in the disintegration of the stainless steel sensor body (Figure 11-5, BOTTOM LEFT and BOTTOM RIGHT). Moreover, the external protection was not resistant to the elevated temperatures (Figure 11-5, TOP LEFT and TOP RIGHT). The corrosion analyses again highlighted the effect of using different alloys (stainless steel, carbon steel) and construction techniques (e.g. brazing, with noble metal filler materials attacking the carbon steel) on the corrosion performance. In particular the connection head, made of ordinary carbon steel, and connected by brazing to the pressure pad, suffered from this galvanic corrosion; corrosion penetrated several mm deep into this part.

Figure 11-5: Uncovering the load cells after removal of a concrete segment (TOP LEFT). The sensor body protection does not withstand elevated temperatures (TOP RIGHT). Fixing bolts for the sensor body had disappeared (BOTTOM LEFT). The two sensor halves came apart without any effort (BOTTOM RIGHT).

Conclusion

See Glötzl segment pressure cell .

11.2.10. External strain gauges

Operational stage

The sensors detected short term variations very well. Overall, thermal and long-term drift limit their use to short-term or dynamic measurements. Temperature variations not only influenced the strain gauges, but also the readout system (through, for example, the completion resistors in the signal conditioning). Day-night cycles were clearly observed in the measurement data. In the first months, during hydration, the following improvements were made:

- cable compensation (3-wire instead of 2-wire) by the signal-conditioning;
- improved mounting of compensation gauges (on separate carrier).

Dismantling and post-dismantling analysis

No specific analyses were performed. A systematic check of the measurements before dismantling did not reveal any anomalies regarding nominal resistance (350 ohm) or insulation resistance.

Conclusion

Although these sensors functioned reliably, their interpretation only yielded good results for short term events, such as the pressure increases during hydration or the pressure peaks during temperature increases.

These sensors are therefore envisaged for similar applications in the PRACLAY Experiment, where short term effects are to be monitored in accessible locations (e.g. steel support structure of the PRACLAY Seal).

11.2.11. Bolt load cells (Bienfait)

Operational stage

These cells delivered good quality measurement data, but their interpretation (load decrease at increasing internal pressure in the mock-up) was problematic. This was probably related to the installation of the bolts, with the instrumented bolts fastened at a lower torque than the other bolts. The load cells were dimensioned on the manufacturer's calculations of the mock-up structure. However, when pressure-testing the structure, it became apparent that the torque (and hence the pre-tension in the bolts) had to be much higher to guarantee the tightness of the bolted cover. This was based on the plastic deformation of the joint, and was not initially taken into account by the manufacturer.

Dismantling and post-dismantling analysis

No visual damage was observed.

Conclusion

The actual measurement performance was fine but interpretation was not straightforward due to the non-representative mounting. The direct measurement of loads requires a precise and well-prepared installation procedure, suited to the actual loading situation.

11.3. Performance of other monitoring equipment

11.3.1. Druck external pressure transmitters

Due to the elevated water pressures in the mock-up, the original transmitters had to be replaced by sensors with a higher range (3.5 MPa instead of 1.6 MPa). One of the two sensors broke down at a pressure of 3.9 MPa.

11.3.2. E+H differential pressure transmitter

This sensor functioned without problems during the whole experiment.

11.3.3. Electric power transducers

Apart from one failure (device replaced), these devices functioned without significant problems.

11.4. Conclusions

The OPHELIE experiment has identified several pitfalls for instrumentation in similar circumstances. These issues may be related to the design of the sensor itself, the cable and its connection with the sensor or the installation. Care also needs to be taken to ensure that the instrumentation does not affect or degrade buffer performance.

Most critical was the water tightness of the sensors (including cables). Corrosion seems to be the worst enemy in this critical aspect. A further discussion on corrosion is given elsewhere in this report, but the following issues are closely related to this:

- the hydration process leading to elevated salt concentrations at the hydration front;
- thermal-driven water flow in permeable media (e.g. sand filled "pockets") speeding up corrosion through a constant renewal of reacting agents;
- galvanic corrosion due to a sensor design incorporating different metals (e.g. the use of ordinary screws in a stainless steel environment);
- hydration with air-saturated (and hence oxygen rich) water;

- the current supply to broken sensors that may potentially worsen the corrosion.

Another issue was the temperature range of the sensors, as it became clear that several sensor types could not cope with the temperatures prevailing in the mock-up.

Finally, instrumenting heavily limited volumes of buffer material should not affect the actual behaviour of this material. An initial preferential water transport along cables was observed, which disappeared after a short time (a few hours). However, damaged sensors may once again have been the cause of water leakage along these cables or tubes. More problematic was the release of mercury and organic substances from flatjack sensors (mercury release was also a problem during the partial dismantling of the FEBEX in-situ set-up). Mercury and organic substances will therefore be banned from the PRACLAY Experiment.

As far as accessible sensors are concerned, normal quality measures should apply: keeping a stock of spare sensors for quick replacement, regular maintenance and recalibration.

12. Thermo-hydro-mechanical behaviour of the buffer material

12.1. Introduction

During the OPHELIE experiment, the buffer material was subjected to a complex coupled hydration and heating process and thus experienced a complicated saturation-desaturation process. The complexity is due to the strong coupling between the transient flow (gas and water flow, water phase changes such as vaporization and condensation, etc…), heat transport and swelling/collapse phenomena. It is also increased by the influence of the temperature on the hydro-mechanical properties of the low permeable buffer blocks and the role of the joints between the blocks.

The complex thermo-hydro-mechanical (THM) processes which took place in the mock-up were actively investigated by means of laboratory testing, numerical analysis and examination of the mock-up test itself.

Prior to and during the mock-up experiment, a systematic laboratory characterization programme was conducted to determine the fundamental physical properties of the initial material and blocks.

During the mock-up experiment, some unexpected phenomena were measured and observed (high apparent thermal conductivity, lower than expected swelling pressure generation, regular decreasing of the total pressure, etc...) which could not be explained with the available knowledge. This revealed that additional laboratory tests were needed to gain a deeper understanding of the material's THM behaviour further, especially in terms of the shear strength and deformability properties under different saturated states and temperatures. A systematic suction-controlled experimental programme was therefore planned. Indeed, small-scale laboratory tests under well-controlled conditions (controlled temperature-saturation/suction-stress paths) are very useful for identifying and quantifying processes in a short period of time.

In the meantime, it was felt that a numerical THM modelling of the mock-up could lead to a better understanding of the coupled THM behaviour of the buffer material and allow discrimination of the coupling between processes and detection of the dependencies among them. This numerical model should take into account the interactions between mechanical stresses, fluid flow and heat flow. The information required for the verification and validation of the mathematical models of the coupled processes and their numerical implementation also required the same systematic laboratory characterization programme.

Finally, dismantling the mock-up gave an excellent opportunity to investigate the processes that may influence the performance of the different mock-up components. The characterization of the exposed material allowed, on the one hand, to verify whether the initial physical properties of the buffer material had been altered by the long-term combined heating and hydration process in the mock-up, and on the other hand, to adjust the parameters and further

validate the numerical model. For this reason, a basic laboratory test programme was also performed on the exposed material.

The information mentioned in the present chapter and in appendix 4 (section A4.3) is a summary of the document "Thermo-hydro-mechanical analysis of the mock-up OPHELIE – Laboratory characterization and numerical modelling" (Li et al., 2005), which exhaustively reports on the THM results of the OPHELIE experiment.

12.2. Characterization of the buffer material

12.2.1. Outline of the laboratory tests

The THM laboratory characterization programme (Table A4-2 of appendix 4) was composed mainly of the following parts:

- **characterization of the fundamental physical properties of both the initial and exposed materials**: thermal properties (thermal conductivity), hydraulic properties (hydraulic conductivity, relative permeability for water, water retention curves) and mechanical properties (especially swelling pressure); for the most part these tests were conducted by CEA (France);

- **additional laboratory tests on the initial material consisting essentially of suction and temperature odometer and triaxial tests**. Some of them were carried out at two contrasting temperatures (room temperature and 80°C) to analyse the thermal influence on the hydro-mechanical behaviour, such as the volume change response (swelling capacity, compressibility), water retention capacity and hydraulic conductivity. Additional tests using Environmental Scanning Electron (ESEM) photomicrographs and mercury intrusion porosimetry (MIP) techniques were also carried out to characterize the multiple porosity network of the mixture in different states and to provide information about the mechanism influencing the hydro-mechanical behaviour of the material. The experimental programme was mainly commissioned to CIMNE of UPC (Spain), the laboratory Geomac of ULg (Belgium) and Laboratory Jacques Verdeyen of ULB (Belgium);

- **odometer and triaxial tests on the exposed material**. This post-dismantling test programme was jointly performed by CEA, CIEMAT, Geomac of ULg and laboratory Jacques Verdeyen of ULB;

- in addition, **on-site analysis of the water content and density** was conducted by CEA during dismantling.

12.2.2. Conclusion of the laboratory tests

Section A4-2 of appendix 4 presents the results of the THM characterization programme carried out on the initial and exposed buffer materials and blocks in more detail (see also Table A4-2) for the tests performed. The most important features are listed below:

- **thermal conductivity**: the measured average value of the thermal conductivity for the initial blocks was about 2.5 W/m.K (Sr = 72 %). Despite its high intrinsic thermal conductivity (due to the addition of graphite), the effect of the water content/saturation was still significant. It could reach values as high as 3 W/m.K at full saturation and with a porosity similar to that of the initial blocks. The measurements on exposed material confirmed this dependence;

- **hydraulic conductivity**: the hydraulic conductivity of the initial and exposed materials were, as expected, below that of Boom Clay (between 10^{-13} and 5 10^{-13} m/s vs. 4 10^{-12} m/s). The hydraulic conductivity of the exposed material is slightly higher than for the initial material. Hydraulic conductivity depends strongly on temperature. The decrease in the water viscosity alone does not explain the increase in hydraulic conductivity at higher temperatures. Wetting, enhanced by heating, also modifies the microstructure of the material (pore size distribution);

- **swelling capacity**: the swelling capacity is sufficiently high, notably in the low stress range. Swelling deformation is lower at the higher temperature. The swelling pressure on wetting largely depends on the density. In constraint conditions, the temperature essentially influences the swelling pressure build-up, but not its final values (at full saturation). Under non-constraint conditions, the temperature significantly influences the final value of the swelling pressure;

- **collapse potential**: some small collapse strains are observed during liquid transfer at elevated stresses. The occurrence of this collapse is limited to a very low suction range (less than 3 MPa). Collapse strains also do not appear to be greatly affected by temperature. In any case, the swelling strains dominate the volumetric deformation on wetting;

- **stiffness**: stiffness for changes in total suction under isothermal conditions increases with net stress. For a given net stress, it appears not to be greatly affected by temperature. Stiffness for changes in loading under isothermal conditions increased with suction. For a given suction, it increased with temperature;

- **a thermal softening behaviour** is identified;

- **shear strength and secant modulus** increase significantly with suction level.

- **the initial and exposed materials present similar THM properties**. The variations of swelling capacity, hydraulic conductivity and stiffness of the exposed material are mainly related to the dry density and water content (saturation) reached during the operation stage of the mock-up experiment. Only minor irreversible modifications are detected on the exposed material.

12.3. Numerical simulations of the mock-up

Numerical simulations, associated with the results of the laboratory characterization programme on the initial and exposed material, were conducted to better understand the THM

processes that took place in the OPHELIE mock-up and more particularly to provide support for the interpretation of the unexpected phenomena observed during the operational stage of the experiment. These simulations allowed the mechanisms present in the mock-up to be discerned.

12.3.1. LAGAMINE finite element code: main principles

The numerical simulations of the mock-up along with the numerical sensibility studies were carried out by the finite element code LAGAMINE, initially developed by the University of Liège (Belgium) to model the non-linear mechanical behaviour of a solid, taking into account large strain. It was later extended to simulate the coupled THM behaviour of a saturated-unsaturated porous media. The THM formulation for porous media uses a multi-phase, multi-species approach. The porous medium is assumed to be made up of three phases: solid, liquid and gas. The solid phase represents the inert mineral. The liquid phase contains water and dissolved air, whereas the gas phase is made up of dry air and water vapour. The compositional approach is used to write balance equations assuming the conservation mass of each chemical species. By combining the mass balance equations for water and air with the equation for the energy balance (non-isothermal problem) and momentum balance (mechanical equilibrium), the governing equations for the THM problem can be obtained. The finite element method is used for spatial discretisation while the finite differences method is used for temporal discretisation. The developed finite elements are iso-parametric elements with the following degrees of freedom: soil skeleton displacements, temperature, liquid water pressure, and gas (dry air + vapour) pressure.

The relevant constituent equations that describe the set of phenomena are incorporated into the THM formulation.

The motion of liquid water and gas is generally described by Darcy's laws. Their flow velocity depends greatly on temperature, saturation and porosity. Non-advective water vapour flow and dry air flow are assumed to follow Fick's diffusion law in a tortuous medium (Philip and De Vries, 1957). Heat transport is related to three effects: conduction, convection by fluids and phase changes. The unsaturated mechanical constitutive law developed is a refined model based on the BBM model (Alonso et al., 1990) in which the LC yield curve (Loading Collapse) permits modelling of the phenomenon of collapse upon wetting. Thermal elasticity is incorporated in the formulation. More details on the THM formulation are given in Collin et al., 2002.

12.3.2. Hypothesis and modelling procedure

The problem was idealized as a one-dimensional problem due to the limited time. Consequently only one representative section, in the middle of the mock-up, was considered. The following main hypotheses have been adopted:

- the jacket and the heater are not modelled explicitly and are supposed to be rigid and impermeable to water;

- the gas pressure is set at the atmospheric pressure (100 kPa);
- the initial annular gap has been taken into account, but not the joints between the blocks;
- the heat exchange between the mock-up and the environment was modelled with an equivalent heat change coefficient.

The modelling procedure approximately followed the experimental procedure:

- application of the hydration pressure progressively up to 1 MPa and keeping it constant during the test period;
- six months after hydration, the heater is switched on and kept constant during the test period;
- increase of the external temperature in steps up to the target temperature.

The following initial conditions were taken for the simulations:

- total stress $\sigma = 0$ kPa
- degree of saturation $S_r = 72$ %
- pore water pressure $P_w = -50.38$ MPa
- gas pressure $P_g = 100$ kPa
- net stress $\sigma^* = -100$ kPa
- temperature $T = 293$ K

The initial pore pressure was determined on the basis of the water retention curves determined in the laboratory.

The parameters used for simulations were obtained from the laboratory THM programme.

The dependency of the thermal conductivity on the degree of saturation of a mixture was calculated according to the following law:

$$\lambda_{mixture} = \lambda_{solid}^{(1-n)} . \lambda_{water}^{n.Sr} . \lambda_{air}^{n(1-Sr)}$$

For the buffer blocks, the results are plotted on Figure 12-1.

The water retention curve - only that of the wetting path was used - and the relative permeability curve were established from the laboratory test results (see appendix 4).

All parameters relating to the mechanical model (BBM model) were deduced from the systematic laboratory suction and temperature testing programme under odometer and triaxial conditions

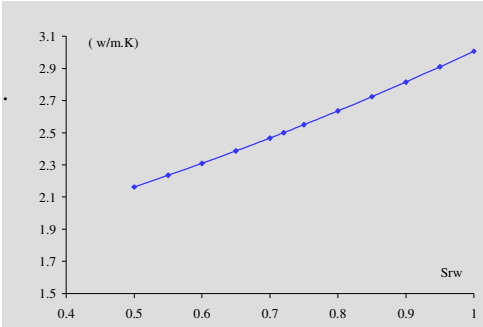

Figure 12-1: Thermal conductivity of the buffer material depending on the degree of saturation.

12.4. Temperature evolution in the mock-up

As mentioned in section 5.3.1, the temperature distribution inside the mock-up was asymmetric: the temperature and its radial gradient varied along different radial directions (Table 12-1). This resulted in a higher than expected apparent thermal conductivity when considering a constant linear heat power of 450 W/m and conduction only as a transfer mechanism.

Table 12-1: Maximum temperatures in the different direction for section #18.

Orientation	Temperature (°C) for section #18		
	central tube	jacket	ΔT
0° (horizontal)	137.5	118.0	19.5
90° (up)	138.0	118.0	20.0
270° (down)	141.5	117.0	24.5

Figure12-2 shows the temperature evolution in the middle of the mock-up. The heating conditions are mentioned in Table 5-2.

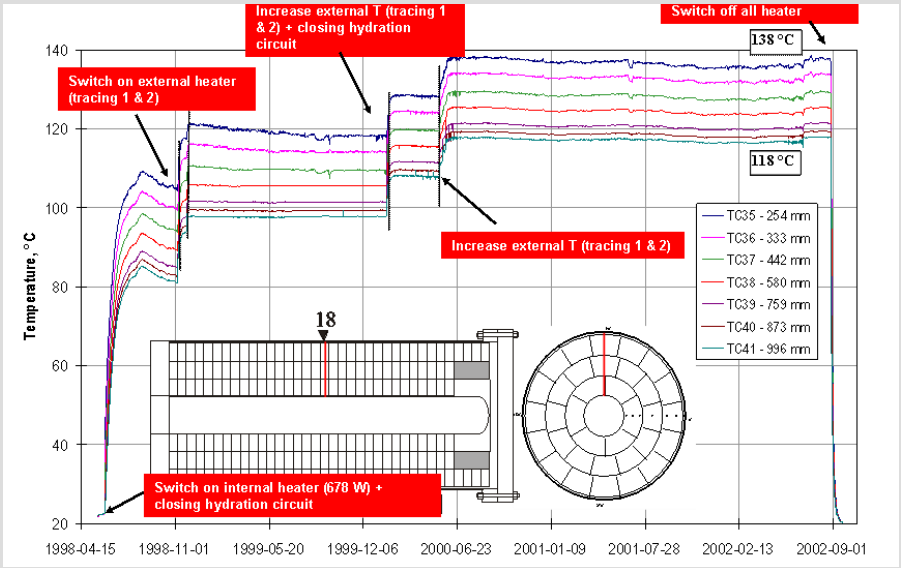

Figure 12-2: Temperature evolution in the middle of the mock-up (section #18, upward profile).

Figure 12-3 shows the axial distribution of the temperature as recorded by the thermocouple array above the central tube (at r = 439 mm). It shows that the end covers (the bolted cover in particular) influenced the temperature distribution.

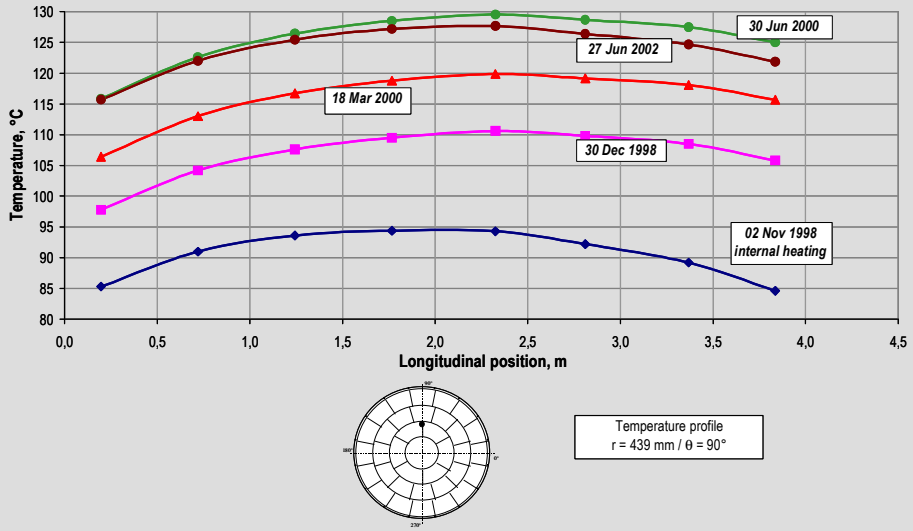

Figure 12-3: Axial temperature profile above the central tube.

The asymmetrical temperature distribution can be explained qualitatively as follows:

- the enhanced heat transfer by conduction due to direct contact between the heater and the central tube at the lower part of this tube only, as observed during the mock-up dismantling. This explains the higher temperatures in the downward direction. An analytical analysis assuming pure conduction demonstrated that a gap of only 1 mm between the buffer and the heating element would result in a drop of about 3.5 °C in the inner surface temperature of the buffer (considering a linear heat power of 450 W/m);
- the uplift of the central tube (Figure 12-19) led to a difference in the "effective thickness" of the buffer in the up and down directions and resulted in the asymmetrical temperature gradient.

The higher than expected apparent thermal conductivity can be explained by a reduced radial heat flow due to “leakage” of the heat through the end covers and the presence of other heat transfer mechanisms:

- a detailed analysis of the temperature measurements indicated that the two covers on the mock-up constituted the main sources of heat loss despite their insulation. The longitudinal temperature distribution inside the mock-up proved this phenomenon;
- a thermal convection loop created by a connection between hydration tubes through a sand lens in the lower part of the buffer (below the bentonite blocks) was evidenced by major differences in the temperature measured between the inlet of several hydration tubes at the rear of the mock-up (Figure 5-10). This thermal convection reduced the radial heat power.

In total, a loss of between 15 to 18 % of the heat was estimated.

In addition, the effect of the increasing saturation on the thermal conductivity also played a major role. Numerical simulation shows that the temperature difference in radial direction drops from 38 °C (assuming a constant thermal conductivity of 2.5 w/m.K for the blocks) to 26 °C (considering a thermal conductivity depending on the degree of saturation) and assuming a heat power of 450 W/m (Figure 12-4).

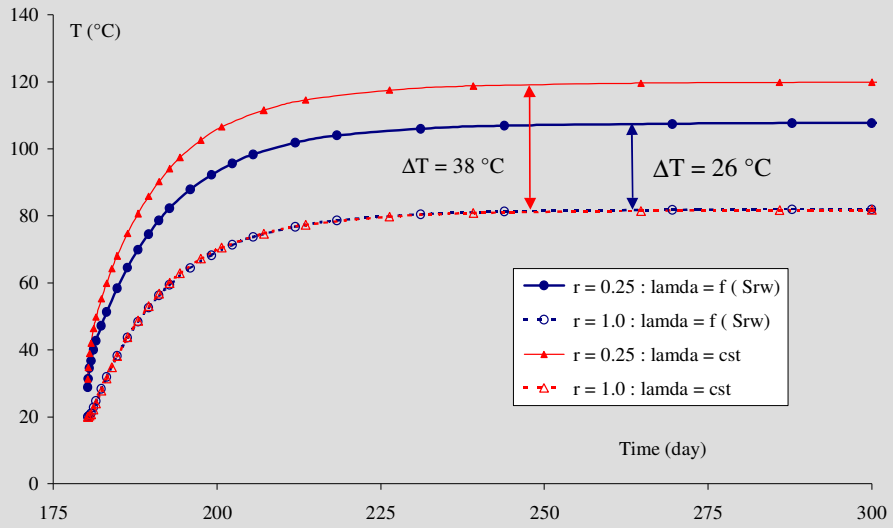

Figure 12-4: Effect of the degree of saturation on the radial temperature gradient.

Finally, in order to study the relative importance of the different heat transfer mechanisms in such a buffer material (without taking into account the 'experimental/design artefact' like the presence of a sand lens), a series of one-dimensional numerical simulations based on the THM properties obtained from the laboratory tests were carried out.

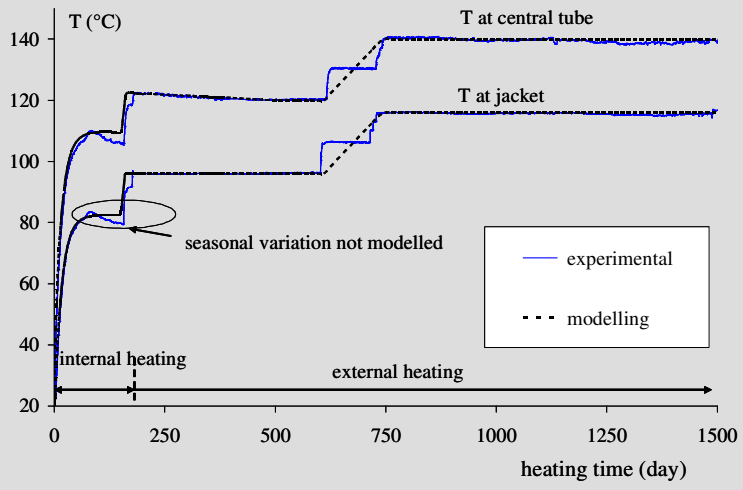

Figure 12-5: Temperature evolution: comparison between measurements and results of numerical simulations.

Numerical results showed that the heat transfer is dominated by conduction. The temperature change in the mock-up can be correctly reproduced by taking into account the dependence of the thermal conductivity, the saturation and heat loss estimation (Figure 12-5). This indicated that the heat transfer in the buffer is conduction dominant.

12.5. Hydro-mechanical behaviour

The hydro-mechanical behaviour depends not only on the properties of the material itself, such as hydraulic conductivity, water retention capacity, swelling capacity,… but also on the boundary conditions on local (presence of the joints between blocks, …) and global scales (temperatures, hydration pressure and peripheral annular void, etc.). The initial state of the material (saturation state, density, etc.) also influences the hydro-mechanical responses of the buffer during the operation phase.

12.5.1. Hydraulic behaviour: analysis of the saturation state of the mock-up

Whether the mock-up reached saturation or not during operation is an important aspect to be assessed in terms of the performance of the buffer material. The analysis of the saturation state of the buffer material was mainly based on the following information complemented by the numerical simulations:

- the measurement of the water volume injected;
- the data from the relative humidity sensors;
- post-mortem analyses of the exposed material: water content, dry density and thermal conductivity (due to the thermo-hydraulic coupling).

Normally, the pore pressure change in the mock-up would provide information on the saturation process. Unfortunately, most sensors failed after the most important pressure peak (chapter 11).

Water intake change

The estimated water volume to be injected was about 2 182 L (based on the calculation of the volume of physical gaps, pore volume of initial blocks …). Monitoring of the water volume actually injected during the operation stage indicated a value of 2 077 L (volume after a period of between 800 and 900 days after hydration start, Figure 12-6). The difference between these two values can mostly be explained by both water and solid dilatations under heating. This is confirmed by the additional volume of water (corresponding to this deficit) re-injected in the mock-up during the cooling phase.

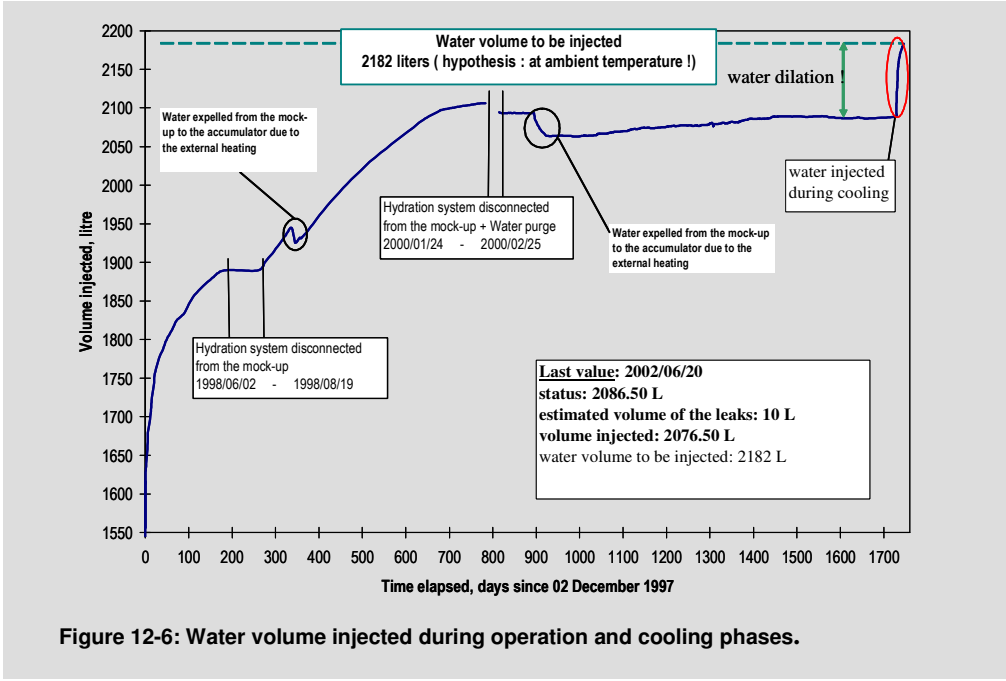

Figure 12-6: Water volume injected during operation and cooling phases.

Figure 12-7 shows the simulated and measured water volume injected during the hydration and heating phases. The final values align well with each other. However, due to the fact that the initial flooding of the initial physical gaps was not modelled, the numerical result indicates a more progressive injection process. The numerical results suggest the mock-up was fully saturated about 900 days after the start of the hydration.

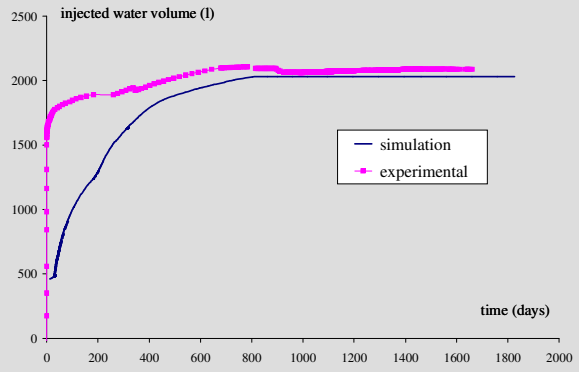

Figure 12-7: Simulated and measured water injected.

Relative humidity change

According to the relative humidity sensors (Figure 12-8), the saturation front reached the position r = 872 mm (RH9 near the external jacket) two months after the start of the hydration - this is a relatively rapid saturation process. This rapid saturation process near the external jacket was also observed numerically.

Other sensors indicated that the saturation front reached the position r = 439 mm about 400 days after starting the hydration of the mock-up.

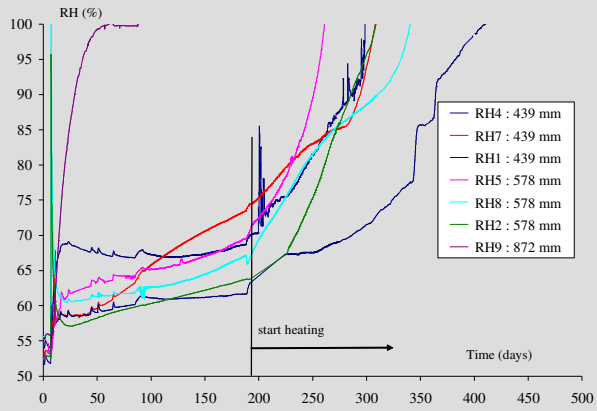

Figure 12-8: Evolution of the relative humidity in the mock-up.

Measurements taken during dismantling: water content, dry density and degree of saturation

More than 200 samples were taken from different sections of the mock-up during dismantling for on-site determination of the water content and dry density (Gatabin and Touzé, 2003). The influences of the presence of the M14 blocks, the concrete ring and sand were analyzed and commented on. Hereafter, only the results from the mid-section of the mock-up (section #17, the most representative of the performance of the buffer material because it was less affected by other such elements as mentioned above) are presented.

The results for water content and dry density depending on the radial coordinate are presented in Figure 12-9. The void ratio and consequently the volumetric swelling formation and the degree of saturation can be deduced.

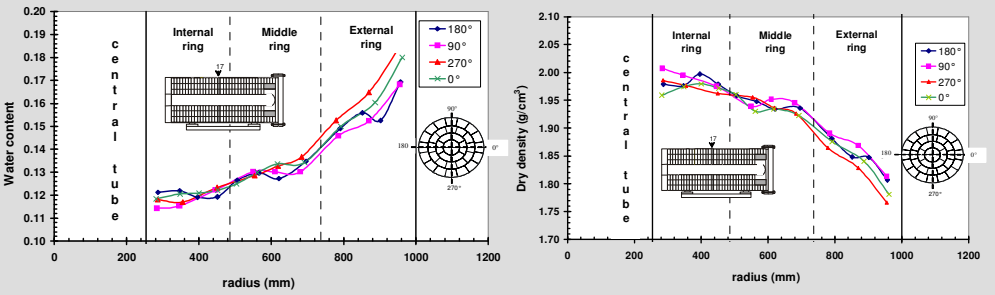

Figure 12-9: Water content (LEFT) and dry density (RIGHT) distribution in section #17.

The saturation profiles assuming ρs = 2.64 g/cm³ are given in Figure 12-10. They indicate saturation ranges of between 94 % (inner ring) and 98 % (outer ring). The results gave a higher degree of saturation in a block's centre than in its periphery. Accordingly, the mock-up was probably not fully saturated.

It's worth highlighting that the degree of saturation is not a directly measured propertyc but the result of a calculation sensitive to variations in some parameters, especially the sample volume. An error of about 1 % in the volume measurement may lead to an error of about 4 % in the

degree of saturation.

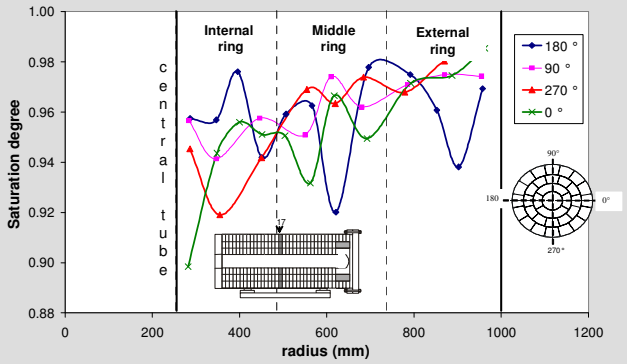

Figure 12-10: Spatial distribution of the degree of saturation in section #17.

In addition, a small error in the density value of soil particles ρ_s may also lead to a significant error in the degree of saturation calculation…. and some uncertainties exist about the solid density value of the buffer material components (Table 12-2). Moreover, a slightly non-homogeneous mixing of the three components may also result in some differences in the density of the solid particles in tested samples.

Table 12-2: Density of solid particles in the buffer material (g/cm³).

Component		FoCaPr	Sand	Graphite	Buffer material
Reference	RT DESD/99-56	2.64	2.65	2.09	2.61
	RT DESD/93.105	2.67	2.65	2.26	2.64
	RT DESD/96.139				

The direct consequence of these uncertainties concerning the density of the solid particles is an imprecision on the obtained degree of saturation value. As shown in Figure 12-11, there is a greater degree of saturation obtained (2 %) when considering a value of 2.61 g/cm³ for the dry density of the buffer material instead of 2.64 g/cm³.

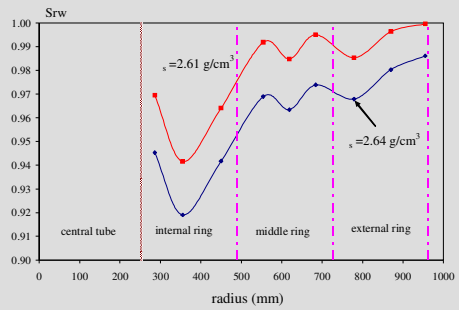

Figure 12-11: Evolution of the degree of saturation with dry density.

The above-mentioned remarks about the sensibility of the degree of saturation make the overall evaluation of the saturation state of the mock-up difficult. There is a conflict between the total water volume injected and the degree of saturation distribution. Regardless of the imprecision in the absolute value of the degree of saturation obtained, it is difficult to explain the

systematically increasing trend obtained from the inner towards the outer rings and the higher degree of saturation in a block's periphery.

Notwithstanding, the following aspects could, in all likelihood, influence the saturation profiles obtained:

- the unavoidable drying out of the samples during sampling and measurements, which lowers the saturation value obtained. It is difficult to quantify this effect;
- the unavoidable post-swelling of the samples provoked by releasing the stresses due to sampling, which leads to underestimation of the degree of saturation of the samples (assuming constant water content).

Figure 12-12 shows the post-swelling due to the release of the confined stresses estimated on the basis of the parameters deduced from laboratory test results and the swelling pressure measured in the mock-up. It indicates that samples extracted from the inner ring show higher post-swelling, which leads to a higher error when estimating the degree of saturation.

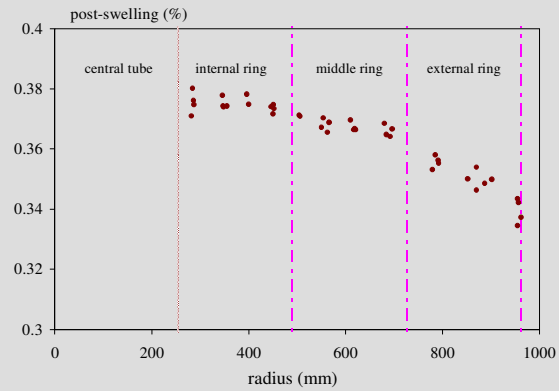

Figure 12-12: Estimation of the post-swelling process of tested samples.

By combining the water content and void ratio profiles (Figure 12-9 and Figure 7-2), the deviation in the degree of saturation obtained with regard to the "in-situ" one can be obtained. Figure 12-13 clearly shows the decreasing trend of the deviation (under-estimation) from the inner to the outer rings. To a large extent this explains the degree of saturation profiles obtained (Figure 12-10).

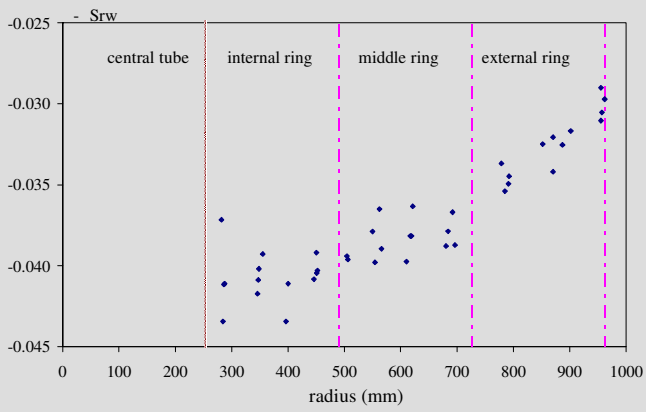

Figure 12-13: Under-estimation of saturation due to stress release when sampling.

By considering that this characteristic deviation will smooth over the increasing trend from inner to outer rings and lead to a more homogeneous "in-situ saturation" distribution, as shown in Figure 12-14, this suggests that the mock-up probably approached full saturation, if it was not fully saturated.

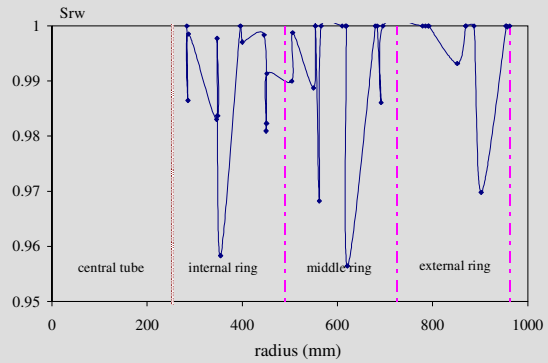

Figure 12-14: Corrected "in-situ saturation" profile.

Numerical simulations

Taking into account the information mentioned above, the numerical simulation suggested that the buffer material reached saturation about 900 days after the beginning of hydration (Figure 12-15).

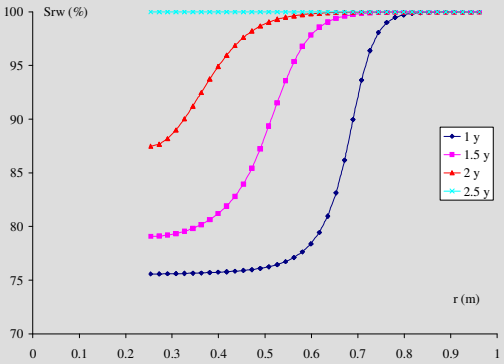

Figure 12-15: Saturation profiles (from the central tube to the steel jacket) for different time periods obtained by numerical simulation.

Concluding remarks on the saturation state of the mock-up

Direct measurement of the water content and dry density of the exposed material performed during dismantling indicated that the buffer material did not reach saturation (95 % close to the central tube and 100 % close to the external jacket). However, numerical simulations suggested that the mock-up had reached saturation about 900 days after the beginning of hydration.

This discrepancy between the simulations and experimental results still needs to be clarified. The following uncertainties require further investigation:

- from the point of view of saturation measurements, the inevitable expansion of the samples after their deconfinement from the mock-up, which further depends on the "in-situ" density; loss of water by evaporation before the on-site moisture measurements often led to underestimations in the degree of saturation;

- from the point of view of numerical simulation, considering hydraulic transfer at microstructure scale would be helpful in better understanding the hydration mechanism of the buffer material.

12.5.2. Mechanical behaviour: swelling performances

As related in chapter 7, during dismantling operations it could be observed that the buffer material had filled all initial physical gaps due to swelling by water uptake, thus fulfilling one of its key roles. However, the swelling process was not homogeneous. Swelling had taken place mainly in the outer rings. Furthermore, the joints between the blocks and rings were still visible.

Evolution of the swelling pressure

Figure 12-16 shows the evolution of the total pressure as recorded by the Kulite total pressure cells. The main (and unexpected) observations/phenomena are as follows:

- the evolution of the swelling pressure followed the hydration process: firstly generated in the outer rings (cells PT4, PT5 PT8 and PT9), then smoothly propagated towards the inner part (PT1 and PT2);
- the swelling pressure in the mock-up ranged between 1.5 and 2 MPa when, not considering the peaks due to artificial undrained heating events (closing of hydration circuit during an increase in temperature), a value of 4 MPa was expected;
- from November 1999 (i.e. 700 – 800 days after the beginning of the test), the swelling pressure showed a regular decreasing trend, which was enhanced after the large peak.

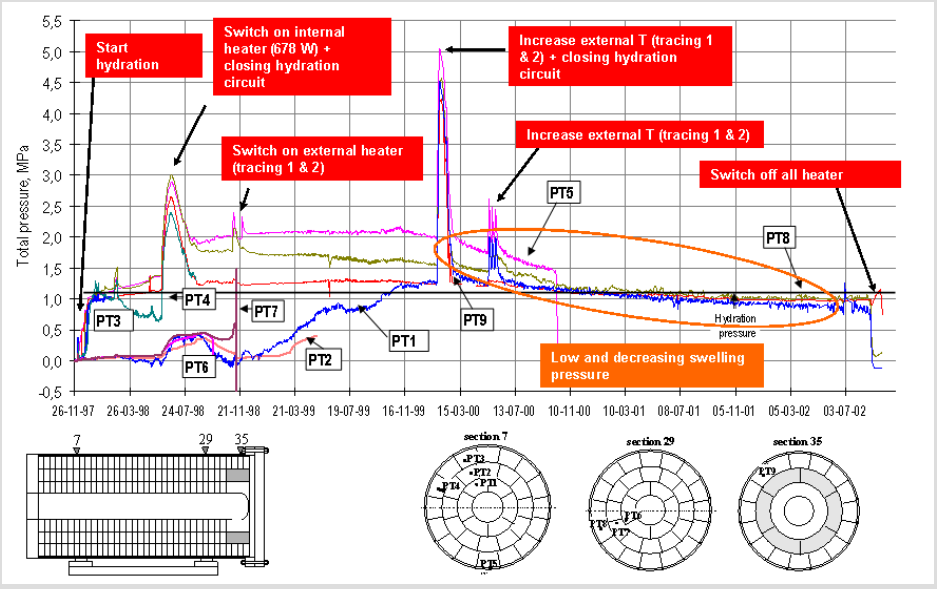

Figure 12-16: Total pressure evolution in the OPHELIE mock-up measured with piezometers.

Figure 12-17 shows the pressure inside the mock-up derived from the external strain gauges. An accurate (quantitative) comparison is complicated by the thermal influence and long-term drift in the strain gauge readings, which is a limiting factor in the interpretation of the absolute pressure values. Momentary and overall evolutions correspond very well with the data given by the Kulite total pressure sensors.

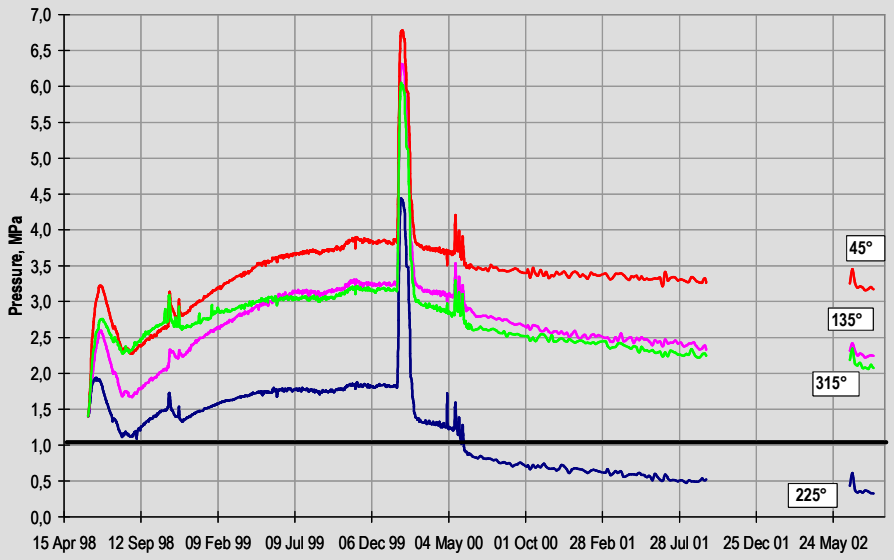

Figure 12-17: Pressure evolution inside the mock-up derived from the external strain gauge readings.

During the development programme for the buffer material, to determine the density necessary to achieve the target value of 4 MPa of swelling pressure, the initial physical gaps present in the mock-up after installation of the buffer material had been taken into account. However, these voids were homogenously 'distributed' across the entire volume of the buffer material. So the density defined in view of the construction of the blocks was an "averaged" density which was then applied to all the blocks.

The values and evolution of the swelling pressures observed during the OPHELIE experiment cannot be explained by taking into account this average density and the boundary conditions of the experiment (water pressure). The positioning of these initial technological vacuums (principally between the outer rings and the jacket) and the evolution of the intrinsic THM properties of the material should be considered within the conditions of the experiment as identified during the laboratory characterization programme (appendix 4).

Therefore, the smaller than expected swelling pressure and its evolution can be explained by:

- the presence of the annular gap and the joints between blocks that gave the material the freedom to swell and consequently generated a lower than expected swelling pressure;
- as indicated by the laboratory tests, the material shows a much lower "plasticity yielding stress" upon hydration, heating and loading. In addition, higher temperatures decrease this

yielding stress even more. This surprisingly high plasticity impeded the generation of the swelling pressure;

- the laboratory tests also revealed that the material shows some creep capacity (Romero, 2004). This viscosity behaviour may lower the total stress in the mock-up through a relaxation mechanism;

- the swelling capacity was decreased by the high temperature as observed in the laboratory.

The continual decrease in the swelling pressure since November 1999 was mainly due to the "collapse upon wetting" property of the material. This property was identified by the suction-controlled drying-wetting odometer tests: the material shows a collapse potential when the suction ψ is less than 3 MPa, i.e. close to saturation. The swelling pressure reaches values around 2 MPa. This corresponds with the condition in the mock-up: as full saturation approached (about 800 days after starting the test) the swelling pressure reached about 2 MPa. The mechanism for the collapse upon wetting is mainly due to the reorganization of the double porosity microstructure upon wetting and heating.

The decreasing trend in the swelling pressure can be perfectly reproduced (quantitatively and qualitatively) through digital simulations taking into account the parameters deduced from the suction-controlled laboratory tests (Figure 12-18). This indicates the reality of the collapse under wetting phenomenon.

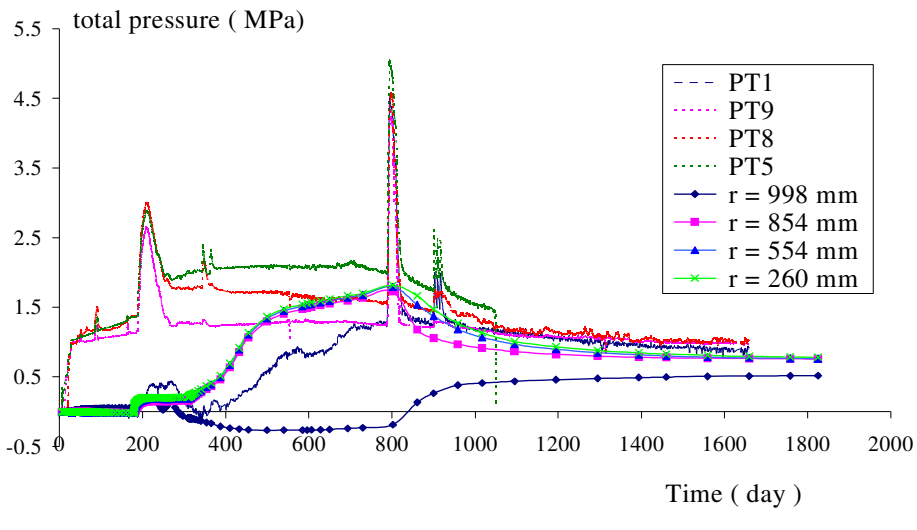

Figure 12-18: Comparison between measured (PT values) and numerically simulated (full lines) evolution of the swelling pressure. The large pressure peak was not modelled.

It is important to note that even if the material has a collapse potential, the swelling still remains dominant. This is demonstrated by both laboratory tests (Romero, 2004 and appendix 4) and the post-dismantling observation: all physical gaps were filled. Although the collapse induced a lower than expected swelling pressure, this latter can be adjusted by an optimisation of both the dry density of the blocks and the initial spacing between them (optimisation of the

joint thickness) since the swelling pressure mainly depends on these aspects. In addition, the swelling pressure should be more stable in the long term after saturation is attained.

12.5.3. Movements of the central tube

The movement of the central tube could be one of the consequences of a non-homogenous swelling of the buffer material. In the case of an actual disposal, any movement of the disposal tube could present difficulties during the installation of the vitrified waste canisters.

Figure 12-19 indicates the movement of the central tube (only vertical movements were possible due to the hinge design that connected the tube to the welded cover). The first measurement was taken just before flooding; a second one after completion of the flooding. Several more measurements were carried out during the following weeks. No measurements were performed during the heated phase, as there was no optical access due to the thermal insulation.

Right after switching off the heating elements, a few more measurements were carried out, with the last measurement being performed right before the removal of the bolted cover.

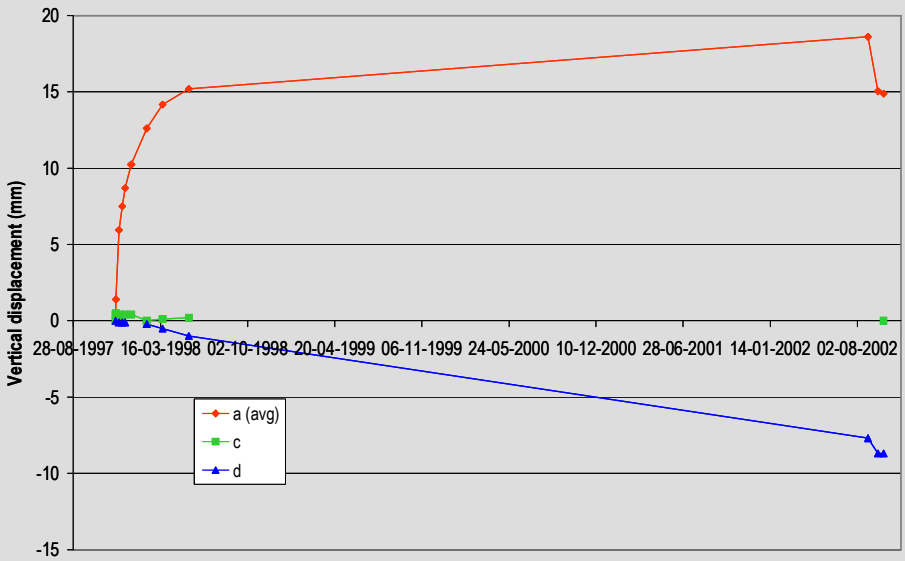

Figure 12-19: Vertical movement of the central tube during the experiment. Red line is an average of 3 measurement points at the end of the central tube, green line represents the movement of a reference mark on the welded cover at the entrance of the tube and blue line represents the movement of a reference mark on the handle of the bolted cover.

In the first weeks after the flooding (start of hydration), a steady uplift of the central tube end was observed which reached about 15 mm before the heating started. After the heater had been switched on, the uplift had further increased up to 18.6 mm. At that time however, a settlement of the mock-up structure of about 8 mm was also noticed (blue line on Figure 12-20). This could be attributed to the compression of the wooden blocks due to the weight of the mock-up.

Cooling of the mock-up increased this settlement by one more millimetre. Also the central tube showed a remarkable settlement of 3 mm during cooling.

The central tube uplift relative to the mock-up structure should take into account the settlement observed at the bolted cover. For the final uplift, a value of 24 mm was estimated. This is principally due to the flooding of the mock-up rather than non-homogenous swelling of the buffer.

No detailed analysis of the impact of an uplift of such a value has been conducted. However, things can be estimated in different ways: absolutely, this value can be considered as significant and could cause problems when inserting the canisters inside the disposal tube, especially since this is 200 m long. On the other hand, it is unlikely that the accuracy of the alignment achieved during the installation of the disposal tube is greater, over a distance of 200 m, than this deviation of 24 mm.

12.6. Conclusions

Numerical simulation of the mock-up, associated with the results of the THM laboratory characterisation programme, has provided strong support for the interpretation and understanding of the THM processes that took place during the experiment. More in-depth numerical investigations would require 3D modelling. However, 1D models can reproduce the overall behaviour of the mock-up.

Overall, with regard to its THM performances, the buffer material fulfilled its role: after four years of hydration and heating, it kept a low hydraulic conductivity and high thermal conductivity. Although the target value of the swelling pressure was not reached (4 MPa) due to the collapse under wetting, all initial physical gaps were filled. Optimised swelling could be obtained by regulating the dry density and managing the initial physical gaps.

The movement measured in the central tube is mainly due to the flooding of the mock-up during the initial hydration phase rather than non-homogenous swelling of the buffer.

It is difficult to draw conclusions on the degree of saturation reached by the buffer material. The analysis of the water intake volume suggests that the mock-up was fully saturated. Numerical simulations without taking into account the presence of joints also indicated full saturation. Conversely, measurements of the degree of saturation performed during dismantling indicated that the buffer was not saturated. However, experimental artefacts could be present. Detailed investigation of the water transfer mechanism is still necessary. In any event, in the case of an actual disposal, the significant value of the thermal conductivity associated with the rapid filling of the initial physical gaps would make feasible the installation of waste before saturation is reached.

With regard to the PRACLAY Experiment, it is recommended that the small-scale laboratory characterisation programme and numerical simulations need to be enhanced. Indeed, laboratory tests under well-controlled conditions are extremely useful in identifying and quantifying processes within a short period of time for the material to be used in the in-situ experiment. Numerical modelling taking into account the different mechanisms can lead to a better

understanding of the experiments and allow discrimination of the coupling between processes and detection of dependencies among them.

13. Behaviour of the concrete segments

A concrete ring, consisting of six segments, was installed inside the mock-up to verify the performances of the measuring instruments that were to be installed in and around the concrete PRACLAY gallery lining.
Although it was not a priority objective of the OPHELIE experiment, the presence of the concrete ring also provided a good opportunity to verify the evolution of the mechanical properties of the concrete after having been subjected to different pressure and temperature conditions and in contact with a saturated medium.

13.1. Evolution of the mechanical properties of the concrete segments: results

13.1.1. Overview of the different tests

The "Laboratoire du Génie Civil" of UCL (Université Catholique de Louvain-La-Neuve, Belgium) conducted the following tests on cores taken from the segments:

- compressive strength (uni-axial) according to the Belgian standard NBN B15-220;
- tensile strength through splitting (Brazilian Test) according to NBN B15-218;
- elastic modulus under compression according to NBN B15-203.

After sampling, the cores were stored at 20°C and > 90% RH. For the last five days, the samples were stored under water.

13.1.2. Original specifications

The specifications and original strength properties are listed in the following two tables.

Table 13-1: Specifications of the concrete.

group	8D5
strength class ($C_{fck\ cyl}$ / $f_{ck\ cub}$)	C 50/60
$f_{ck\ cub}$	60.00 N/mm²
cement type	III R (furnace type, early strength)

The values from Table 13-2 are related to cubic test samples (standardized dimension of 150 mm). When comparing them with the values obtained from cylindrical samples, the form factor needs to be taken into account. The standardized height of the test cylinder is 300 mm, and in this case, the standard stipulates:

$$f_{c\ cub\ 150} = 1.265\ f_{c\ cyl\ 150\ /\ 300}.$$

The dimensions of the cylinders were about 105 mm in diameter and 93 mm in height (except A2 and B5, which were about 230 mm in height).

Table 13-2: Original strength characteristics (according to manufacturer's quality control, 1997).

Batch	f7d [N/mm²]	fn (final) [N/mm²]
1997/04/28	52.00	69.55
1997/05/05	57.80	72.65
1997/05/13	59.10	74.00
1997/05/16	48.00	64.65

13.1.3. Sampling

Three segments were sampled; a non-exposed (reference) segment (labelled 'A') and two exposed ones (labelled 'B' and 'C' – Figure 13-1, BOTTOM LEFT).

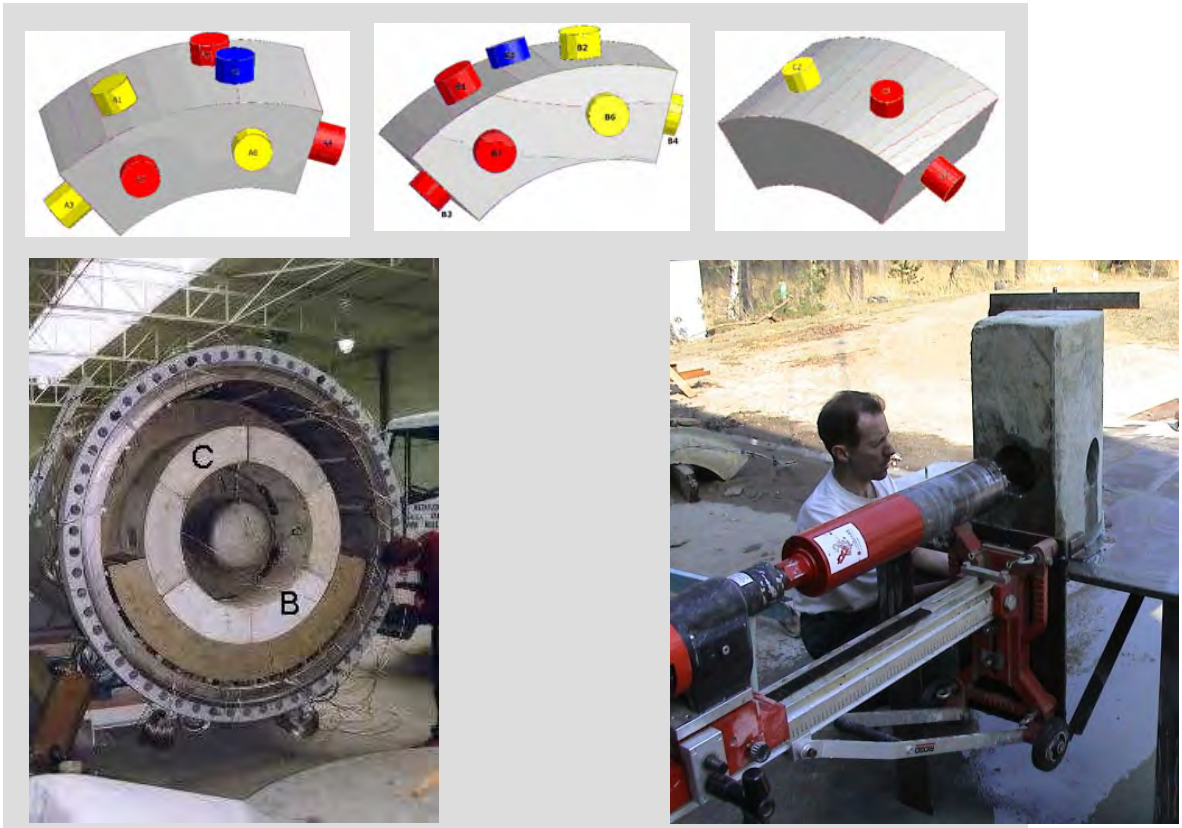

Figure 13-1: Schematic position of the cores of the three segments (TOP) - red: compressive strength measurements, yellow: tensile strength measurements and blue: elastic modulus measurements. Position in the mock-up of concrete segments B and C (BOTTOM LEFT). Sampling operations (BOTTOM RIGHT).

Coring was performed with a "RIGID" drilling machine (Figure 13-1, BOTTOM RIGHT), equipped with an "ADAMAS" coring tool with a OD/ID diameter of 112/105 mm.

The part of the core to be tested was selected in such a way as to avoid the influence of the steel rebar.
Figure 13-1 TOP shows a schematic representation of the core locations.

13.1.4. Compressive and tensile strength results

Figure 13-2 represents the test results. The segments have not suffered from the mock-up conditions.

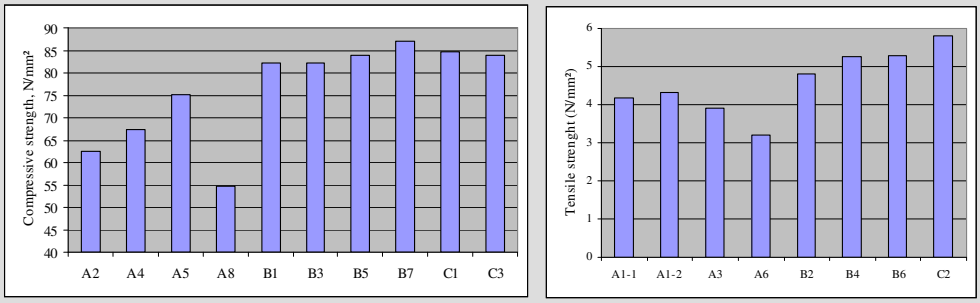

Figure 13-2: Evolution of the compressive (LEFT) and tensile (RIGTH) strengths. The samples of segments B and C (exposed to the mock-up conditions) show a higher strength.

13.1.5. Elastic modulus Ec

Because the determination of E_c is somewhat complicated, the standard also provides a formula, based on the $f_{c\,cyl}$ value:

$$E_c = 9\,500\ \sqrt[3]{8 + f_{c\,cyl}}$$

This formula gives a fairly good estimate of the actual value, as shown in Table 13-3.

Table 13-3: Calculated elastic modulus corresponds well with the measured one.

Sample	fc cyl [N/mm²]	E_c (calculated) [MPa]	E_c (measured) [MPa]
A2	62.4	39 220	38 330
B5	84.0	42 880	43 700

13.2. Conclusion

From a mechanical point of view, the concrete has not suffered from the mock-up conditions. The saturated environment (and maybe the elevated temperature) during the “end” of curing period (during one year) has improved the strength of the concrete.

It must be pointed out that these tests were carried out at ambient temperature. To assess the strength of the concrete under in-situ conditions (about 90°C), which would give a better idea of the mechanical behaviour of the gallery lining, a mechanical test at such a temperature

would be very relevant. It would also provide the data needed to interpret the strain gauge data (lining deformation, chapter 11) more accurately.

14. Conclusions

The OPHELIE mock-up was a full-scale simulation in terms of diameter over a length of 5 m of a section of a disposal gallery of the SAFIR-2 design, the reference design valid in the 90's, as far as buffer material and the disposal tube were concerned.

The OPHELIE experiment was originally planned as a preliminary test for the on-site PRACLAY Experiment as planned at the time. The key objectives were to verify the robustness and performance of the sensors, to develop a buffer material and to verify certain practical aspects relating to its implementation and hydration process. The mock-up also provided a unique opportunity to investigate the coupled thermo-hydro-mechanical behaviour of the buffer material subjected to conditions as similar as possible to the actual ones on a large scale.
The results of the OPHELIE experiment made it possible to satisfy all of the initial objectives and to provide answers to questions that still remained unresolved at the time.

Although not anticipated in the OPHELIE experiment's initial objectives, it highlighted chemical and microbiological processes which were potentially detrimental to the corrosion resistance of the metal elements. Considering the role of the central tube in an actual disposal, these processes could jeopardize the long-term safety of the disposal system. These processes are also detrimental to the sensors' corrosion resistance and therefore, in the case of the PRACLAY Experiment, to obtaining the parameters and information required for the success of the experiment.

These observations were part of the reasons which led ONDRAF/NIRAS to decide in 2001 on an in-depth review of the concept and design of the engineered barriers and, as a result, to adapt the design and objectives of the PRACLAY Experiment. The new concept for high-level waste and spent fuels disposal, called the Supercontainer concept, is based on the principle of the 'Self Containment Concept' which consists of installing the overpack in an environment with favourable chemical conditions in terms of corrosion resistance. This environment is concrete in the case of the Supercontainer concept.

14.1. Development and implementation of the buffer material

The material developed during the initial experiment phase, a mixture of betonite FoCa (60 wt.%), sand (35 wt.%) and graphite (5 wt.%), satisfied more or less (evolution of the swelling pressure, see below) to all the requirements that had been fixed prior to its development.

Although it remained an expensive process, the OPHELIE experiment also showed that it was possible using a "semi-industrial" technique to manufacture a significant quantity of blocks robust enough to be manipulated and observing the strict tolerances established, whether they were of a dimensional type or relating to the physicochemical properties of the material. These strict dimensional tolerances, associated with the initial physical gap of 36 mm located around the buffer allowed for an accurate manual placement of the blocks in a relatively confined space representative of a disposal gallery. It should, however, be noted that while this manual installation would have been acceptable for the PRACLAY Experiment (length 30 m), it could

be more problematic in the case of an actual disposal considering the tens of kilometres of gallery to be filled in a restricted and uncomfortable space (bulky presence of the disposal tube) in terms of working conditions. Furthermore, the time required to install the buffer material (around an hour per section of 13 cm thick) would probably not have been adequate with regard to the operation timing of the disposal galleries. An automated system would have to be developed.

14.2. Hydration process and thermo-hydro-mechanical behaviour of the buffer material

The hydration process of the buffer material was not homogeneous. The initial joints between blocks, rings and sections before being sealed constituted preferential hydration paths (channel effect). It is likely that the presence of the hydrophobic, graphite 'film' on the surfaces between blocks in the same section, due to the manufacturing process of the blocks, amplified this channel effect and consequently the role of the joints in this hydration process. The joints between blocks, although perfectly sealed remain identifiable during dismantling of the model.

It is difficult to draw conclusions on the degree of saturation reached by the buffer material. Both the analyses of the water intake volume and the numerical simulations suggest that the mock-up reached saturation after about 850 days. Conversely, measurements of the degree of saturation performed during dismantling indicated that the buffer was not saturated. However, experimental artefacts could be present (expansion of the material just after sampling, drying of the samples, …). More detailed investigation of the water transfer mechanisms within the buffer may prove necessary. In any event, in the case of an actual disposal, the significant intrinsic value of the thermal conductivity (even for a non-saturated material) associated with the rapid filling of the initial physical gaps would have enabled the installation of waste before saturation of all the material is reached.

Overall, from a thermo-hydro-mechanical point of view, the buffer material fulfilled its role: it kept, as required, a hydraulic conductivity lower than $4\ 10^{-12}$ m/s and a thermal conductivity higher than 2.5 W/mK. The swelling capacity, although producing a swelling pressure lower than expected, was sufficient to fill all initial physical gaps and to obtain perfect contact with the central tube and the liner, thus optimizing heat transfer.

An extended thermo-hydro-mechanical laboratory characterization programme could highlight the intrinsic properties of the material explaining the weaker than expected swelling pressure during the experiment (between 1.5 and 2 MPa while a value of 4 MPa was expected). Firstly, the "yielding" stress for plastic deformation of the material decreases upon hydration and heating. Secondly, the material possesses a "collapse" potential upon hydration when approaching saturation due to the reorganisation of the micro-structure that may induce a decrease in stress. However, it should be noted that the swelling always remained dominant as proved by the absence of voids within the mock-up. An optimal swelling pressure could be obtained by regulating the dry density of the blocks and distributing the initial physical gaps in a more homogeneous way.

Numerical simulations with 1D models using the parameters derived from the laboratory characterisation programme provided strong support for the interpretation and understanding of the thermo-hydro-mechanical processes that took place during the experiment. This allowed to reproduce the evolution of the swelling pressure, of the temperatures as well as the hydration process. More in-depth numerical investigations would require 3D models.

With regard to the PRACLAY Experiment, it is recommended that the small-scale laboratory characterisation programme on Boom Clay and numerical simulations need to be enhanced. Indeed, laboratory tests under well-controlled conditions are extremely useful in identifying and quantifying processes within a short period of time. Numerical modelling taking into account the different mechanisms can lead to a better understanding of the experiments and allow discrimination of the coupling between processes and detection of the dependencies among them.

14.3. Mineralogical evolution of the buffer material

The mineralogical changes observed in the exposed buffer material were very limited. The main modifications concerned the presence of gypsum on the buffer contact with the central tube, on the interface with the stainless steel liner, on the periphery and in the joints between blocks. The ubiquitous presence of gypsum crystals indicates that the redox conditions were generally still oxidizing in the centre of the mock-up and inside the bentonite blocks.

14.4. Chemical and microbial behaviour of the mock-up and influence on the metal components

Although, the OPHELIE mock-up was not designed to study the chemical and microbial evolution of the OPHELIE mock-up, important observations with potential implications for the metallic corrosion studies, the long-term monitoring, the design of the PRACLAY in-situ Experiments and the design of a future repository have been made.

The large scale of the mock-up has enabled the comparison between the composition of the squeezed pore water and the mineralogy of the solid phase. It made possible to obtain evidence of both the driving force and the effect of the movement of the solutes in the buffer material exposed to a temperature gradient.

The OPHELIE experiment highlighted the existence of at least three processes potentially detrimental to the corrosion resistance of the metal elements:

- an enrichment process in chlorides towards the central tube associated with a depletion in species known to inhabit corrosion in chloride-containing solution such as bicarbonate or sulphate. Chloride concentrations up to 1g/L have thus been measured in contact with the central tube presenting a concern for its corrosion by pitting. Such a concentration was never previously considered for the corrosion studies. Two mechanisms could explain this enrichment process without it being possible to conclude which one actually acted or which one was predominant: advective transport of salts by a water front migrating

through the unsaturated buffer during the hydration phase or the diffusion of solutes in a temperature gradient;

- the presence of microbial activity in the water of the hydration system pointed out the presence of dissolved sulphides and, in some samples, thiosulphates, and was confirmed by microbiological analyses which revealed the presence in high concentrations of sulphate-reducing bacteria, thiosulphate-reducing bacteria and methanogenic bacteria. The conditions encountered by the hydration system, namely the presence of free water and free space associated with an even temperature and the presence of nutrients (dissolved sulphate notably from the gypsum and dissolved organic carbon 'renewed' thanks to the convection loops and organic matter potentially released by defective Glötzl cells) have allowed sulphate-reducing bacteria to grow. The large amounts of dissolved organic carbon measured in the water could have contributed to fuelling microbial activity. The source could be the organic matter naturally present in the FoCa clay or hydrocarbons (a mixture of gasoline and oil) released by defective Glötzl cells as observed during dismantling operations. Limiting free space in a disposal is therefore required as much as possible. No stringent conclusion can be drawn from the microbial analyses performed on the initial and exposed solid buffer samples. Tests performed by two laboratories with different techniques yielded contradictory results;

- A relatively low pH value (5 instead of 8.5 for the fresh $NaHCO_3$ water used to hydrate the mock-up) preventing or more or less limiting the formation of a protective passivation layer on the surface of the metal elements. One of the causes of this low pH is amongst others the high content of dissolved CO_2. The source of CO_2 remains unclear. Two mechanisms can be suggested: production by microbial activity or decarboxylation by thermal stress of the natural organic matter present in FoCa clay.

These conditions are probably the origin of the corrosion problems observed on some sensors. On the other hand, no significant signs of corrosion could be detected on the AISI 321 central tube in contact with the bentonite. The resistance of the AISI 304 used as liner for the steel jacket was barely lower. It exhibited a corrosion resistance exceeding initial expectations: corrosion spots were only detected in places with technological artefacts such as welding points. These problems could be avoided in the future by applying appropriate techniques. The most striking observation in terms of corrosion in the mock-up was certainly the general corrosion of the AISI 316L hydration tube #7. A defective relative humidity sensor was discovered not far from this tube and it is highly probable that the electrolysis induced by the direct current applied to this sensor for several years was the cause of this spectacular corrosion. Nevertheless, the favourable behaviour of these varieties of stainless steel has to be confirmed over a longer period of time.

It should be noted that the absence of an in-depth knowledge of the initial chemical conditions and the initial conditions of the material limits the interpretation of the results obtained.

14.5. Performance of the monitoring equipment

The lessons learnt from the instrumentation programme will be taken into account within the framework of the PRACLAY Experiment. Except for thermocouples, a large number of sensors installed inside the mock-up failed during the operational stage of the experiment. For some of them, the failure occurred quite rapidly. This may have to do with the design of the sensors themselves, the cable and its connection to the sensor, or with the installation. Most critical was the water tightness of the sensors and cables. Corrosion seemed to be the worst enemy in this critical area.

Another issue was the temperature range of the sensors. Several sensor types could not cope with the prevailing temperatures in the mock-up.

Besides the loss of data, the OPHELIE experiment has shown that the failure of sensors can also jeopardise the performances of the engineered barriers (e.g., galvanic/electrolytic corrosion as mentioned above, or contamination by hydrocarbons) as observed in the mock-up. For the PRACLAY Experiment, an extended preliminary selection of the sensors followed by a detailed test programme including corrosion aspects will be necessary to guarantee the long-term reliability of sensors in harsh conditions with elevated temperatures and pressures.

14.6. General/practical lessons from the experiment – project management

The objectives of the OPHELIE mock-up were considerably extended during the experiment and the associated information that has been acquired is significant. This shows the interest in maintaining sufficient flexibility over the course of an experiment as long as this does not have a negative impact on the initial objectives established. However, it should be kept in mind that the analysis and interpretation of results arising from an extension of the programme during the experiment may suffer from a lack of knowledge about the initial conditions specified, these aspects not having originally been anticipated.

During the preliminary phase of the OPHELIE experiment, the initial objectives for the mock-up were established and described in a relatively general way, without specific criteria and in various different documents. This has sometimes resulted in difficulties when trying to assess these objectives. In order to avoid this difficulty for the PRACLAY Experiment, it is recommended that a document is drafted at the beginning of the experiment presenting all the various objectives initially assigned to the experiment, their type (demonstration, process, understanding, communication, …) and the criteria, if possible quantifiable, which would allow the success or failure of each objective to be assessed. Establishing a hierarchy of importance between the objectives and a risk assessment for each separate objective should facilitate the decision making process, whether that is in the event of a problem during the experiment or in the case of adding objectives not initially considered.

List of abbreviations

AES: Atomic Emission SPectrometry

Andra: Agence Nationale pour la gestion des déchets radioactifs (France)

ATLAS: Admissible Thermal Loading for an Argillaceous Storage (HADES, Belgium)

BACCHUS: BACkfill Control experiment with Hydration for the Underground Storage of radioactive waste (HADES, Belgium)

BBM: Basic Barcelona Model (THM model)

BET: Brunauer Emmett Teller

BGS: British Geological Survey (United Kingdom)

CACTUS: CharActerization of Clay under Thermal loading in Underground Storage (HADES, Belgium)

CEA: Commissariat à l'Energie Atomique

CEC: Cation Exchange Capacity

CERBERUS: Control Experiment with Radiation of the BElgian Repository for Underground Storage (HADES, Belgium)

CFG: Companie Française de Géothermie (Marseille, France)

CIEMAT: Centro de Investigaciones Energéticas, Medioambientales y Tecnológicas (Spain)

CNRS: Centre National de la Recherche Scientifique

COGEMA: COmpagnie GEnérale des MAtières nucléaires

DAC: Department Advice Committee (of SCK•CEN Waste and Disposal Department)

DSC: Differential Scanning Calorimetry

EB: Engineered Barrier experiment (Switzerland)

EBS: Engineered Barrier System

EC: European Community

EdF: Electricité de France (France)

EIG EURIDICE: Economic Interest Grouping - European Underground Research Infrastructure for DIsposal of nuclear waste in Clay Environment

ESDRED: Engineering Studies and Demonstration of Repository Designs (EC project)

ESEM: Environmental Scanning Electron

FEBEX: Full-scale Engineered Barrier Experiment (Spain)

FTIR: Fourier Transform Infra-Red spectroscopy

GID: Glading Incidence X-ray Diffraction

HADES: High Activity Disposal Experimental Site

HLW: High Level Waste

HM: Hydro-mechanical

ILW-LL: Intermediate Level Waste – Long-Lived

ICP: Inductively Coupled Plasma

ICP-MS: Inductively Coupled Plasma – Mass Spectrometry

LC: Loading Collapse

LEM: Laboratoire Environnement et Minéralurgie (CNRS Nancy)

LOFC: List Of Fabrication Control

MIC: Microbiologically Influenced Corrosion

MIP: Mercury Intrusion Porosimetry

MPB: Methane-Producing Bacteria

MS: Mass Spectrometry

NF-PRO: Near Field PROcesses (EC project)

OM: Optical Microscope

ONDRAF/NIRAS: Organisme National de Déchets RAdioactifs et des matières Fissiles enrichies/ Nationale Instelling voor Radioactief Afval and verrijkte Splijtstoffen

OPHELIE: On-surface Preliminary Heating simulation Experimenting Later Instruments and Equipment (Belgium)

PHEBUS: PHEnomenology of hydrological transfer Between atmosphere and Underground Storage (HADES, Belgium)

PRACLAY: PReliminAry demonstration test for CLAY disposal (HADES, Belgium)

RC: Respository Component

RD&D: Research, Development and Demonstration

RESEAL: REpository SEALing in argillaceous clay (HADES, Belgium)

SAC: Scientific Advisory Committee (of EURIDICE)

SAFIR 2: SAfety and Feasibility Interim Report 2

SAMRA: Service Analyse et Migration des RAdioéléments

SCC: Stress Corrosion Cracking

SCK•CEN: StudieCentrum voor Kernenergie/Centre d'Etude de l'énergie Nucléaire

SEM-EDS: Scanning Electron Microscope - Energy Dispersive Spectrometry

SRB: Sulfate-Reducing Bacteria

TEM: Transmission Electron Microscopy

TGA: Thermo-Gravimetric Analyses

THM-C: Thermo-Hydro-Mechanical – Chemical

TOC: Total Organic Carbon

UCL: Université Catholique de Louvain-La-Neuve (Belgium)

URF: Underground Research Facility (see also HADES)

URL: Underground Research Laboratory

VOC: Volatile Organic Carbon

XRD: X-Ray Diffraction

XRF: X-ray Fluorescence Spectroscopy

XPS: X-ray Photoelectron Spectrometry

Appendixes

Appendix 1 Design and composition of the mock-up metallic structure

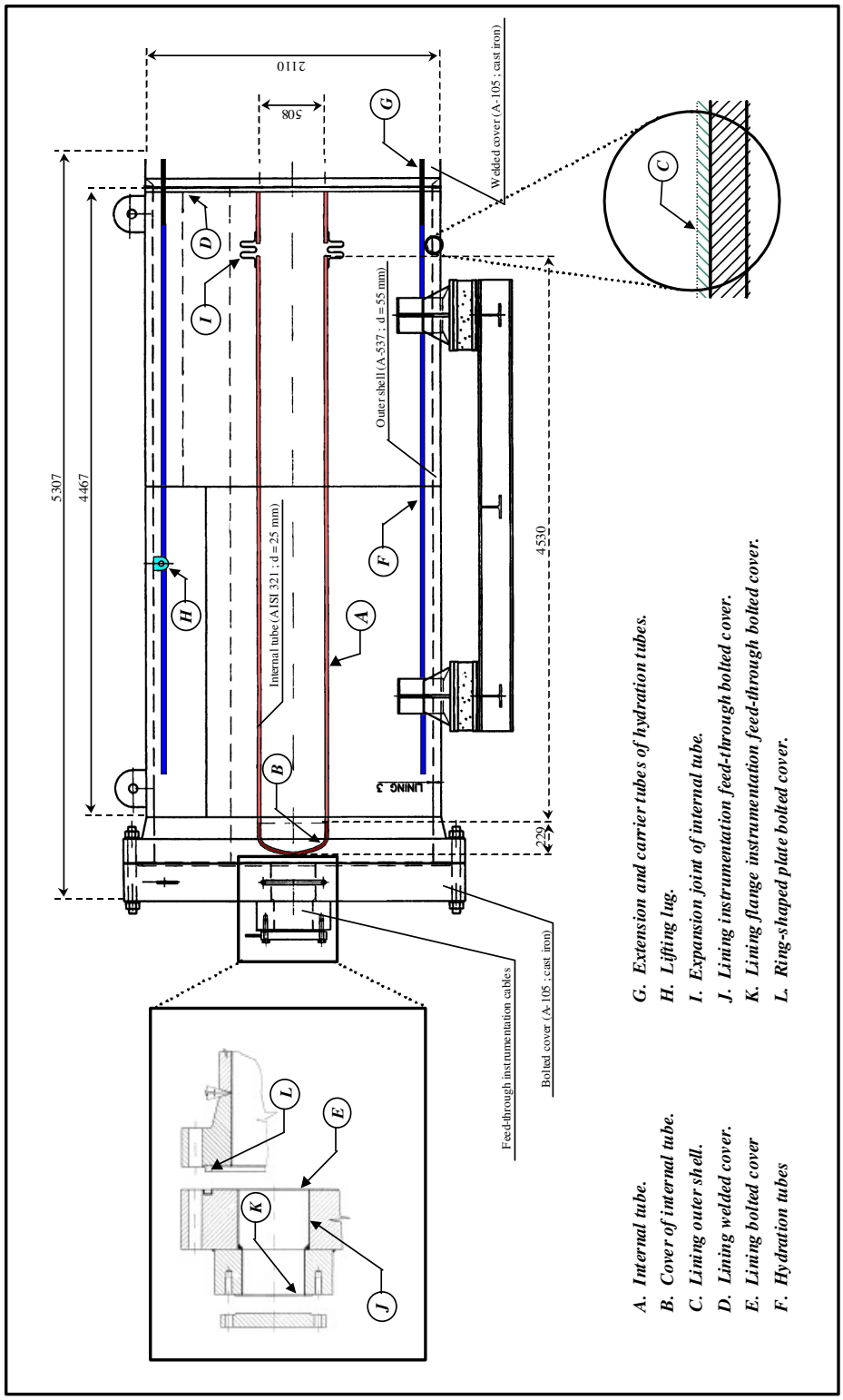

Figure A1-1: Schematic drawing of the OPHELIE mock-up with indication of the various metallic components.

Id.	Component	Supplier	AISI	Fe	C	Mn	P	S	Si	Cr	Ni	Mo	Ti	N
A[1]	Internal tube	SPARTAN REDHEUGH	321	bal	0.040	1.15	0.024	0.0031	0.53	17.01	9.10	-	0.318	0.0126
B[1]	Cover of internal tube[4]	AVESTA	321	bal	0.040	1.44	0.029	0.001	0.56	17.62	9.15	-	0.39	0.01
C[1]	Lining outer shell[3]	ALZ	304	bal	0.045 0.044	1.30 1.36	0.033 0.031	0.008 0.008	0.50 0.41	18.12 18.18	8.70 8.70	- -	- -	0.025 0.025
D[1]	Lining welded cover	ALZ	304	bal	0.044	1.36	0.031	0.008	0.41	18.18	8.70	-	-	0.025
E[1]	Lining bolted cover	ALZ	304	bal	0.045	1.30	0.033	0.008	0.50	18.12	8.70	-	-	0.025
F[2]	Hydration tubes		316L	bal	≤0.03	≤2.00	≤0.045	≤0.03	≤0.75	16.0-18.0	10.0-14.0	2.00-3.00	-	≤0.10
G[2]	Carrier tubes of ***F***		316L	bal	≤0.03	≤2.00	≤0.045	≤0.03	≤0.75	16.0-18.0	10.0-14.0	2.00-3.00	-	≤0.10
H[2]	Lifting lug for ***A***		304L	bal	≤0.03	≤2.00	≤0.045	≤0.03	≤0.75	18.0-20.0	8.00-2.00	-	-	≤.010
I[1]	Expansion joint of ***A***	KRUPP	316Ti	bal	0.045	1.32	0.027	<0.003	0.34	16.76	10.60	2.04	0.47	-
J[1]	Lining instrumentation feed-through bolted cover[4]	ALZ	304	bal	0.045	1.30	0.033	0.008	0.50	18.12	8.70	-	-	0.025
K[1]	Lining flange instrumentation feed-through bolted cover[4]	ALZ	304L	bal	0.021	1.23	0.025	0.003	0.35	18.05	10.01	-	-	0.030
L[1]	Ring-shaped plate bolted cover	AVESTA	304L	bal	0.016	1.56	0.026	0.000	0.55	18.24	10.10	-	-	0.05
M[2]	Strain tubes and protective sheath		304	bal	≤0.08	≤2.00	≤0.045	≤0.03	≤0.75	18.0-20.0	8.00-10.5	-	-	≤0.10

[1] composition from certificate provided by the supplier.
[2] average composition from *Stahlschlussel*.
[3] the material for the lining of the outer shell originates from two different batches (heats).
[4] these components have been in contact with a mixture of quartz sand and bentonite porewater (saturated with concrete).

Table A1-1: Chemical composition of the OPHELIE mock-up's metallic components.

Appendix 2 Establishment of the thermal conditions

The temperature conditions to be applied in the OPHELIE mock-up were studied in 1995 and 1996 by SCK•CEN (Verstricht and Bernier, 1997). The approach was to first consider the thermal conditions of the in-situ PRACLAY Experiment, which was regarded as the reference case. Simulating different mock-up configurations and scenarios made it possible to gain further insight into the steady state (temperature distribution in the mock-up) and transient (external temperature variations, power failure) thermal behaviour of the mock-up. In the end, this resulted in a set of thermal design parameters for the mock-up, including thermal insulation.

A2.1 Simulation of the thermal conditions of the PRACLAY Experiment

Based on the test hypotheses and a 2D axisymmetric configuration, the temperature evolution of the PRACLAY Experiment was first simulated. The simulations were based on a heated length of 20 m, with a linear thermal power of 450 W/m applied through a central heating tube for a period of three years, and followed by a cooling period of two years. These conditions were fixed by ONDRAF/NIRAS in 1992, based on different thermal calculations in order to obtain adequate representativeness with respect to the expected repository case (Van Cauteren, 1990 and 1991). This representativeness applied in particular to the temperatures developed in the near field (radial distance of 1.70 m to the gallery axis), and involved a scaling up of the actual thermal power of the COGEMA canisters after 50 years of cooling time (350 W/m) with almost 30 %. Through this scaled up power the maximum temperatures in the clay are obtained after a heating period of three years (at constant power), compared to the 10 years that would be needed in the case of the actual repository. For its own thermal calculations, SCK•CEN applied two different finite difference codes, FLAC (Itasca Consulting Group, 1995) and HEAT2R (Blomberg, 1994), and these were compared with the semi-analytical results from ONDRAF/NIRAS. All results aligned very well with each other, as can be seen in Figure A2-1.

The simulations focused on the thermal conditions at the buffer material/lining interface. They showed a temperature increase of 105 °C after three years of heating. The temperature gradient in the buffer material itself stabilises fairly quickly – after only two weeks it had reached 90 % of the steady state value of 49 °C (for a thermal conductivity of 2.0 W/mK). The absolute buffer material temperatures then only depend on the slow increase at the outer boundary.

A2.2 Thermal design of the OPHELIE mock-up

With the design of the steel structure of the mock-up at hand, it was possible to make a thermal simulation of the mock-up itself.

The simulations first concentrated on the boundary conditions of the mock-up structure to ascertain whether thermal insulation was needed. Heat loss by convection and radiation were examined. The heat transfer from the mock-up to the ambient air was strongly influenced by radiation, and depended strongly on the ambient temperature. The heat transfer by convection

was difficult to assess: different empirical approaches were mentioned in the literature, with different results. The main conclusion was that the external boundary condition should be applied through thermal insulation, complemented with temperature control through heat tracing cables. This would furthermore also allow compensating for variations in the ambient temperature.

After having defined the boundary conditions, the heat diffusion inside the mock-up was studied in more detail. The simulations started with an analytical solution (transient heating of a hollow cylinder), which is considered a reference case for comparison with numerical simulations. Both the insulated and non-insulated conditions were simulated.

The numerical simulations allowed simulating the detailed internal mock-up configuration, taking into account the actual design of the mock-up (with e.g. the concrete segment ring). The simulations provided a better view of the actual temperature field, and more specifically its uniformity, as it was expected that e.g. the heavy end covers would influence temperatures quite significantly. Also the effect of using insulating materials inside the mock-up, such as PTFE or insulating concrete, to obtain a more uniform temperature field, was explored.

The results of the simulations indicated that temperatures in the mock-up would be lower due to the limited length, and due to the disturbance of the end covers. The thermal design therefore indicated a thick insulation at the end covers, complemented with external heating by self-regulating heating tape, concentrated at both ends (covers). The external temperature regulation would also eliminate the problem related to the estimation of the heat transfer by natural convection to the ambient air. A literature study revealed different (empirical) formulas for this convective transfer, leading to a broad range of estimates.

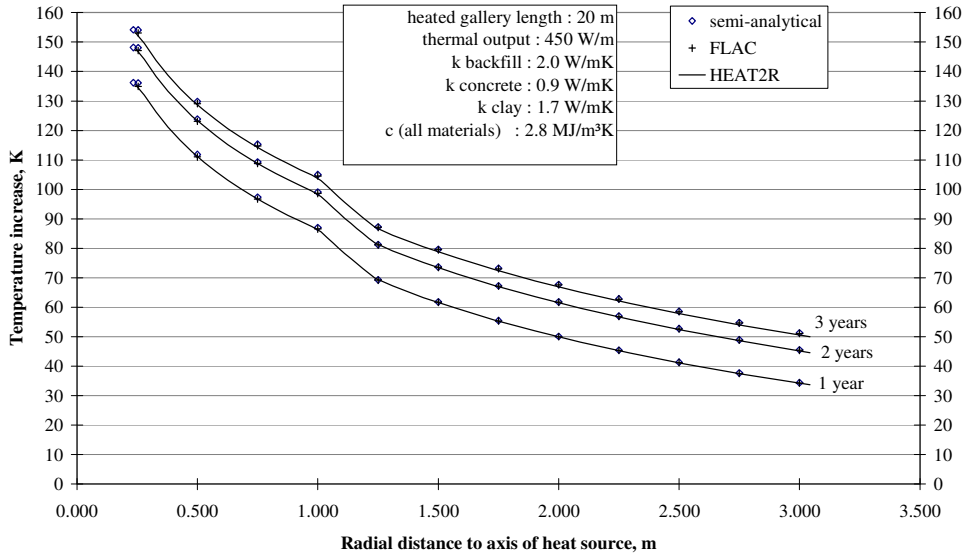

Figure A2-1: The in-situ reference case of the heating was used to define the boundary conditions for the mock-up experiment.

The effect of two disturbing factors was also investigated: variations of the ambient temperature, and power outages. Temperature variations of the ambient air only have a significant impact if they persist beyond several days. Seasonal variations, however, seemed quite probable. Power variations on the other hand affect the temperatures in the mock-up more significantly – a power failure disturbs the temperature field along the central tube within hours.

Appendix 3 Positions of the internal sensors

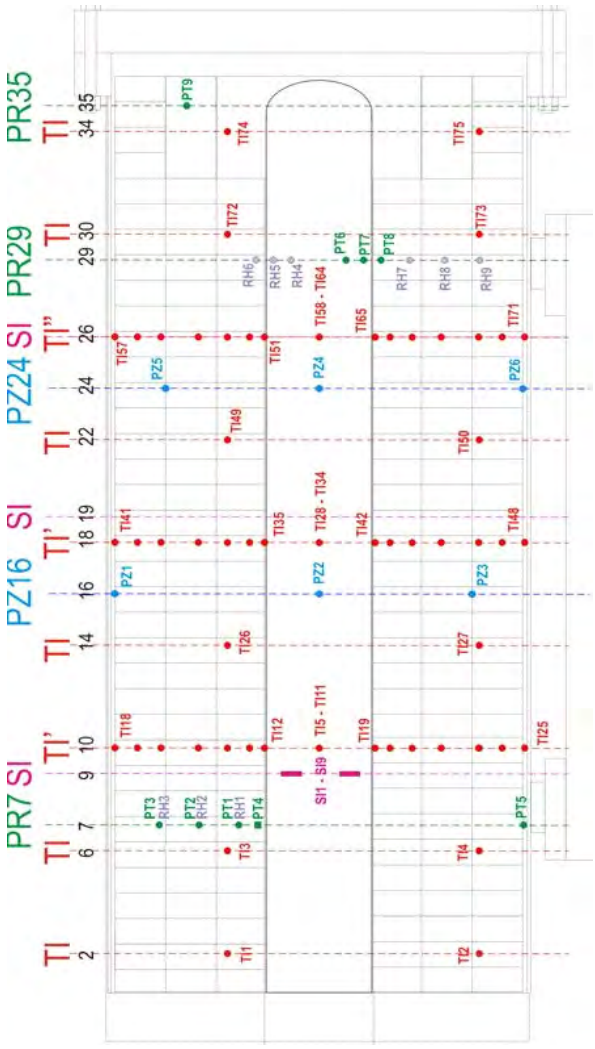

Figure A3-1: Schematic view of the longitudinal section of the OPHELIE mock-up with positions of the different types of sensors (PZ for piezometer, RH for humidity sensor, PT for total pressure cell, TI for thermocouple and SI for internal strain gauge).

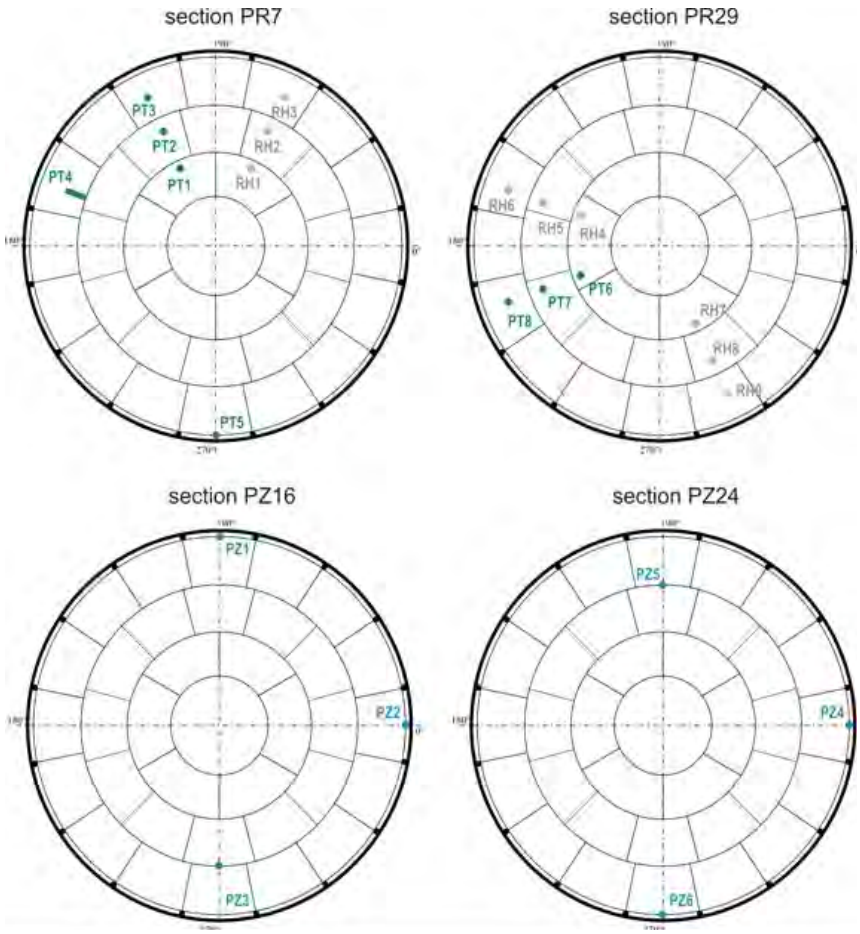

Figure A3-2: Planar position of piezometers, total pressure cells, relative humidity cells for sections #7, #16, #24 and #29.

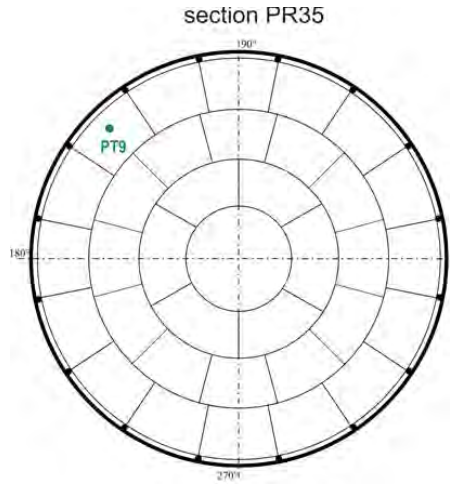

Figure A3-3: Planar position of total pressure cell PT9 for section #35.

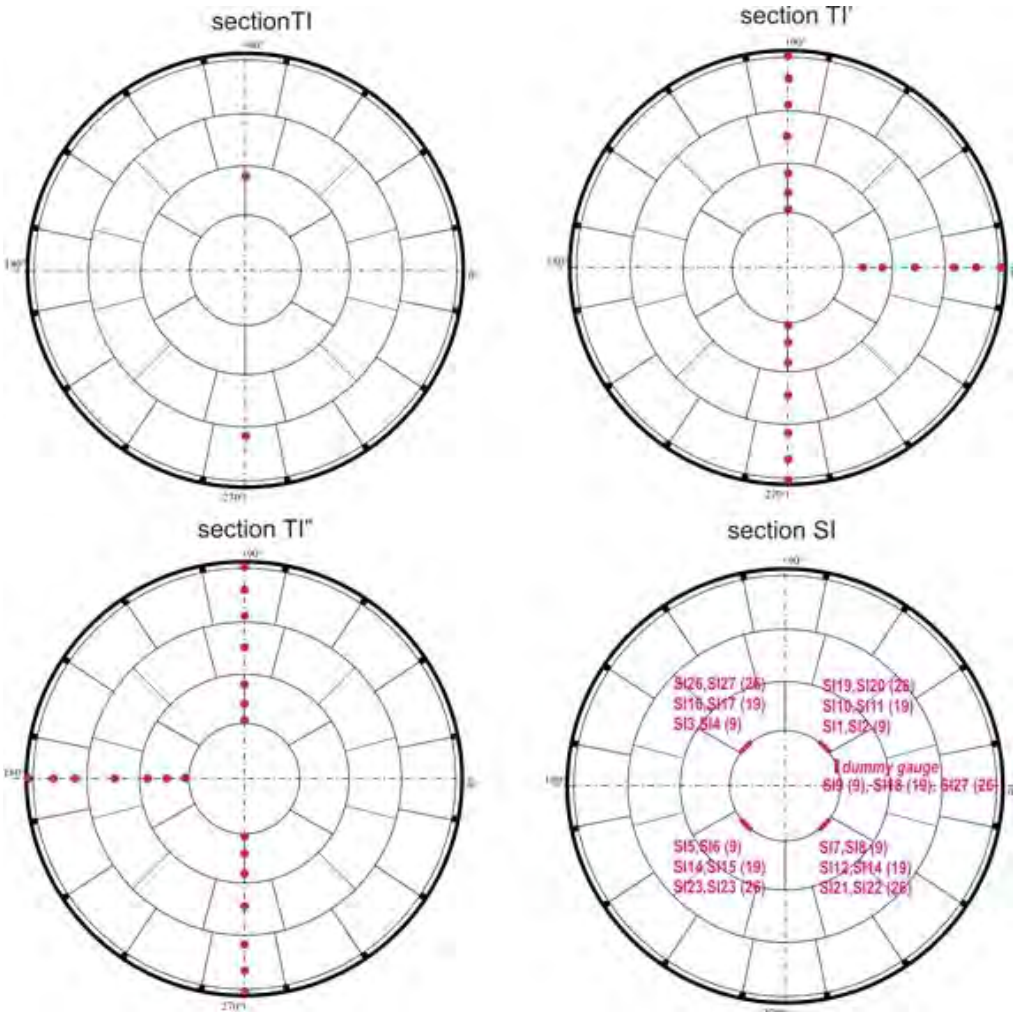

Figure A3-4: Planar positions of thermocouples and internal strain gauges.

Appendix 4 Properties of the buffer material

This appendix outlines the properties of the buffer material. It includes the information related to the mineralogical and pore water composition, and the intrinsic physico-chemical and thermo-hydro-mechanical (THM) properties measured during various stages of the experiment.

A4.1 Mineralogical composition of the FoCa clay

The mineralogical composition of FoCa clay (FoCaPr batch) analysed by CEA is presented in Table A4-1.

Table A4-1: Mineralogical composition of the FoCa clay.

Mineral	Formula	Total rock wt.%
Interstratified, mixed layer kaolinite/smectite	—	80
Kaolinite (pure)	$Si_2Al_2O_5(OH)_4$	6
Quartz	SiO_2	6
Goethite	FeO(OH)	6
Hematite	Fe_2O_3	0.2
Calcite	$CaCO_3$	1.4
Gypsum	$CaSO_4 \cdot 2\ H_2O$	0.4

Two types of clay minerals were identified in the CEA analyses (Lajudie et al., 1995): an interstratified clay kaolinite/smectite (mixed layer) representing the major clay mineral (80 wt. %) and a small proportion of kaolinite (6 wt. %). More detailed analyses on smectites (Jullien et al., 1999) indicated two populations of smectites: montmorillonites and beidellites.

Table A4-1 also clearly indicates the presence of goethite (6 wt. %) and hematite (0.2 wt. %) in FoCa clay, probably resulting from oxidation of pyrite initially present. Indeed, no special precautions had been taken to protect FoCa clay from oxidation caused by oxygen from the air. Moreover, the clay was stored at the surface for an undetermined period of time before being dried in an oven at high temperature in direct contact with the burner flames. So, if pyrite was still initially present in the clay formation at the outcrop in the open pit, it should have been strongly oxidized during surface storage and industrial handling operations.

No pyrite could be detected in the mineralogical analyses: the pyrite content was likely below the limit of detection of X-ray diffraction, or it also escaped at the detection of scanning electron microscope. So, according to analyses, the industrial FoCa clay product should in principle not contain any appreciable residual amount of pyrite. However, results of the fluid analyses (Charlton et al., 2004) and mineral phases (Raynal and Pétronin, 2003) showed important contents in total sulfur in the mock-up. These results were not consistent with the composition of the initial material determined by CEA analyses (Raynal and Jullien, 2001).

As regards the smectite, the following structural formula has been proposed by Michaux:

$$\mathbf{Ca_{0.2}(Al_{1.75}Mg_{0.15}Fe_{0.15})(Si_{3.6}Al_{0.4})O_{10}(OH)_2}$$

The iron in the above formula is strictly Fe^{III}. This formula was determined after Raman spectrometry analyses that exclude Fe^{II} in the clay.

A4.2 Physico-chemical and THM properties of the buffer material: results of the laboratory characterisation programme

The initial and exposed materials were subjected to laboratory characterization programmes which occurred in several phases: before the operational stage in the scope of the material development, during and after the operational stage to gain a better insight into the behaviour of the material observed during operation.

Table A4-2: Characterization programme on the initial and exposed material.

Tests			Initial material		Exposed material	
			Labo.	Reference	Labo.	Reference
T	λ (thermal conductivity)		CEA	Dardaine et al, 1996 Gatabin and Rodrigues, 1999	CEA	Gatabin and Touzé, 2003
H	k_{w0} (hydraulic conductivity.)		CEA	Gatabin and Rodrigues, 1999	CEA CIEMAT	Gatabin and Touzé, 2003 Villar, 2004
	$k_{r,w}$ (relative perm.)		CEA	Gatabin and Touzé, 2003		
	Water retention		CEA UPC	Gatabin and Touzé, 2003 Romero, 2004		
M	Swelling pressure		CEA	Gatabin and Touzé, 2003		
	Oedom.	Sat.	ULB	Huergo, 2004	ULB	Huergo, 2004
		s,T cont.	UPC	Romero, 2004		
	Triaxial	Sat.	ULg	Charlier et al., 2003	ULG	Charlier et al., 2004
		s,T cont.	UPC	Romero, 2004		

A4.2.1 Fundamental physical-chemical properties and microstructure

The tests for establishing the physico-chemical properties were conducted by CEA (Gatabin et al., 1999) and UPC (Romero, 2004). Table A4-2 summarizes the basic physico-chemical properties of the initial blocks, where ρd represents the dry density, w the gravimetric water content, n the porosity, Sr the saturation degree, WL the liquid limit, and IP the plasticity index.

Table A4-3: Physico-chemical properties of the initial material

ρ_d	W	N	S_r	W_L	Ip
≅ 2.10	*≅ 7.70*	*≅ 0.21*	*≅ 72*	*94*	*65*

Mercury Intrusion Porosimetry performed by UPC on the as-compacted state mixture clearly revealed that the material presents a double porosity structure. The pore size density function

(Figure A4-1) displays two pore modes at approximately 19 µm and 19 nm. The largest pore mode corresponds to the inter-aggregate porosity between clay aggregates, while the lowest pore mode is associated with the intra-aggregate porosity inside clay aggregates which represents about 40 % of the total pore volume.

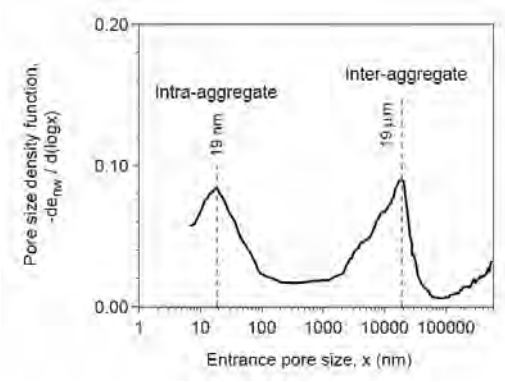

Figure A4-1: MIP test data for as-compacted mixture.

A4.2.2 Fundamental thermal properties

The measured average value of the thermal conductivity of the initial blocks state was about 2.5 W/mK (Sr = 72 %). Despite its high intrinsic thermal conductivity (thanks to the addition of graphite), the effect of the water content/saturation was still significant. It could reach values as high as 3 W/mK at full saturation and with a similar porosity than that of the initial compacted state. The measurements on exposed material confirmed this dependence (Gatabin and Touzé, 2003).

A4.2.3 Fundamental hydraulic properties

Hydraulic conductivity

Hydraulic conductivity was determined in different laboratories on both the initial and exposed materials compacted at different densities. Both CEA and CIEMAT used the permeability cells (direct controlled–gradient method, Villar, 2004, Gatabin and Touzé, 2004) while UPC derived the parameters using primary consolidation data (indirect method, Romero, 2004). Measurements were also performed at different temperatures. The values obtained are plotted in Figure A4-2. The following observations were made:

- at a given temperature, the hydraulic conductivity of both the initial and exposed materials is exponentially related to the dry density, which is one of the most important influencing factors. The hydraulic conductivity of the exposed material is slightly higher than for the initial material;
- at higher temperatures, the hydraulic conductivity values are much greater than at ambient temperature for equivalent dry density. This not only has to do with the change in water viscosity but also with the modification of the microstructure upon heating (pore size redistribution). In fact MIP indicated that, at constant porosity, the intermediate pore size that emerges on saturation (unstressed) clearly increases with the temperature (Figure A4-3). This thermal enhancement of the intermediate porosity causes an increase in the

amount of water and the cross-sectional area available for water to flow, which can explain the increase in hydraulic conductivity;

- the salinity of permeant probably influences hydraulic conductivity. The difference between the CEA values and those from CIEMAT may be attributed to this influencing factor apart from the minor difference in temperature. Actually, the permeant used by CIEMAT presents some salinity (OPHELIE water with 1170 mg/l of $NaHCO_3$). CEA used demineralised water.

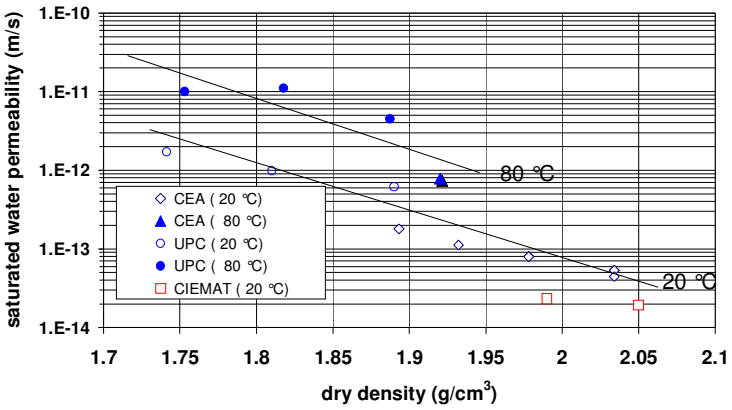

Figure A4-2: Evolution of hydraulic conductivity with dry density.

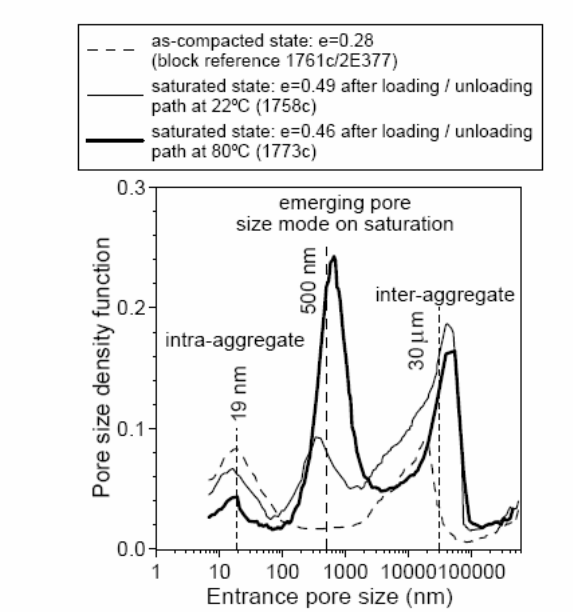

A4-3: Change in pore size density functions on wetting, heating and loading for the as-compacted and saturated states and at two different temperatures (22 °C and 80 °C).

Relative hydraulic conductivity

The hydraulic behaviour of unsaturated soil implies a variation in hydraulic conductivity based on saturation/suction. This is often expressed in relative hydraulic conductivity (ratio between the value in the unsaturated state and the value at saturation). Figure A4-4 shows the relative hydraulic conductivity of the buffer material as a function of the suction (Gatabin and Touzé 2003). It shows that the permeability decreases significantly with saturation/suction.

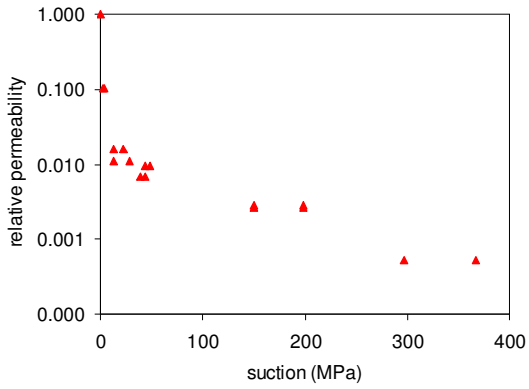

Figure A4-4: Relative permeability of buffer material (unstressed condition, at 20 °C)

Water retention properties

Water retention capacity is an important hydraulic property when dealing with the coupled THM behaviour of an unsaturated material. This is often expressed in the water retention curve, which is the water content or saturation as a function of the suction level. For the measurements performed on both the initial and exposed materials, CEA used different saline solutions to impose different suction levels on samples, while UPC used the SMI transistor psychrometers (Woodburn et al. 1993) to measure the total suction of the material. All retention curves are obtained under unstressed conditions (Figure A4-5).

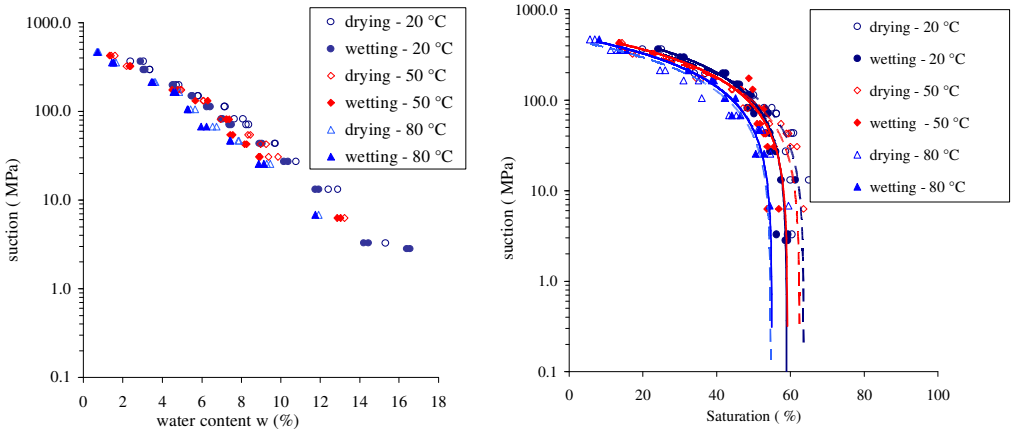

Figure A4-5: Water retention curves at different temperatures.

The following observations were recorded:

- at ambient temperature, the main drying/wetting curves show small hysteresis appearing at a water content above 4 %. Hysteresis evidences irreversible changes in water content along the drying-wetting cycles. Different mechanisms were cited (Nitao and Bear 1996) for this non-irreversible behaviour. With low water content, the irreversibility is related to hysteresis, if it exists, in the chemical potential. With a water content above a certain limit (4 % for the buffer material), hysteresis is mostly governed by the instability of the interfaces between the gas and liquid phases inside the macro pores;
- at a very high suction level (≥150 MPa) and lower water content (w ≤ 4 %), the temperature has no effect on the water retention capacity. This water content limit

probably corresponds to the water bonded to the solid crystals, on which the temperature (at least up to 80 °C) has no effect;

- temperature decreases the water retention capacity;
- temperature seems to decrease the hysteresis. This may point to the modification of the microstructure of the material at high temperature. The enhanced intermediate pore size as observed by MIP yields more of a homogeneous pore size distribution (Figure A4-3);
- at unstressed condition, it is very difficult for the material to reach total saturation due to its high swelling capacity. With a suction level of around 3 MPa, the saturation reaches only about 60 %.

Difference between initial and exposed material

Water retention curves for initial and exposed materials are plotted in Figure A4-6. The following aspects can be observed:

- the exposed material shows a lower water retention capacity for the suction levels lower than 150 MPa. No difference for suction levels greater than 150 MPa (w < 4 %) was observed. This corresponds with the aforementioned water retention mechanism;
- the exposed material seems to present less pronounced hysteresis. This corresponds with the observed temperature effect;
- the exposed material presents smaller swelling/shrinkage capacity upon wetting/drying paths: for the same suction level, the saturation of the exposed material is higher than that of the initial material, despite the lower water content. The exposed material is more rigid than the initial material. This aspect was confirmed by the odometer tests.

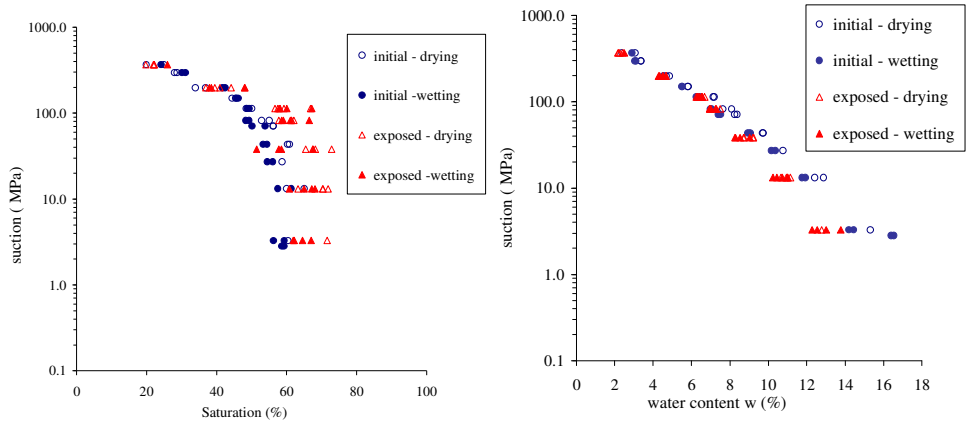

Figure A4-6: Water retention properties for initial and exposed materials

A4.2.4 Fundamental hydro-mechanical properties: swelling pressure

The swelling pressure refers to the pressure reached at full saturation under constant volume conditions when hydrating a swelling material. It is an important parameter for charactering the swelling capacity of a material. The swelling pressure of both the initial and exposed materials was determined by CEA using a fixed cell frame at ambient temperature. The test results

indicate that the swelling pressure (Ps) is related to the dry density of the material (ρ^d). An empirical formula was obtained for the buffer material (Dardaine, et al. 1996; Gatabin and Rodriques, 1999):

$$log\ P_s = -\frac{16.95}{\rho_d} + 9.16$$

The difference between the measured values and the fitting curve (Figure A4-7), which increases with the dry density, is mainly due to the non-homogeneity of the samples, especially on the FoCa clay fraction.

The swelling pressures obtained according to the suction-controlled odometer tests performed by UPC (wetting under different loads) are in agreement with the results of CEA.

The swelling pressure of the exposed material seems to be governed by the same swelling pressure/dry density relationship than the initial material. This agrees with the mineralogical analysis, which indicated that the mock-up condition did not modify the mineralogical composition (chapter 8).

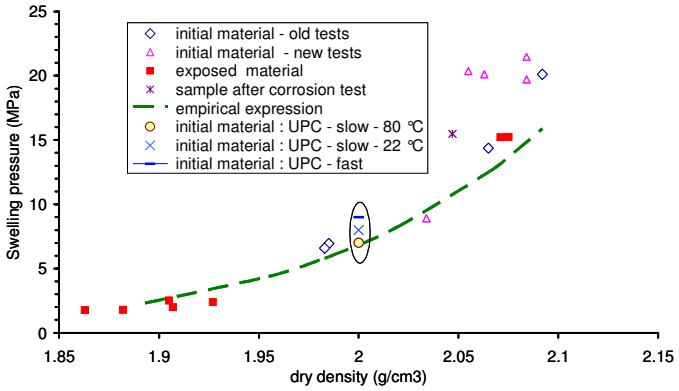

Figure A4-7: Evolution of the swelling pressure with the dry density.

Results of the suction and temperature controlled odometer tests

The purpose of the odometer tests was to study the compressibility parameters for load changes at different suction levels and temperatures (pre-consolidation stress and pre/post-yield compressibility), as well as the compressibility parameters for suction level changes at different vertical net stresses and temperatures.

Test protocols

The unsaturated odometer tests were conducted using combined axis translation (for low suction levels) and vapor equilibrium techniques (for higher suction levels) for suction controlling (Figure A4-8).

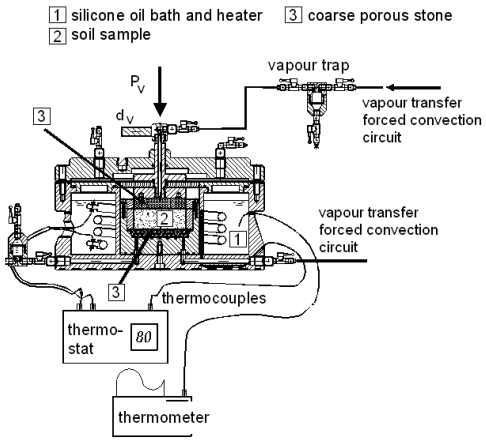

Figure A4-8: Temperature and suction-controlled odometer cell.

The mechanical behaviour of the unsaturated material under odometer conditions without lateral stress measurements is described by two independent stress variables: the vertical net stress (σv-ua) and suction ψ or s (where σv is the total vertical stress, ua the air pressure). Odometer tests included two series of test paths at two different temperatures, 22°C and 80°C (Figure A4-9):

- loading/unloading tests at constant suction level from 0 (saturated state) to 6 MPa;
- drying/wetting tests at constant vertical net stress from 1 to 5 MPa. At the end of the tests, samples were flooded at a constant vertical stress starting from a suction level of 92 MPa to study the expansive/collapse behaviour of the mixture.

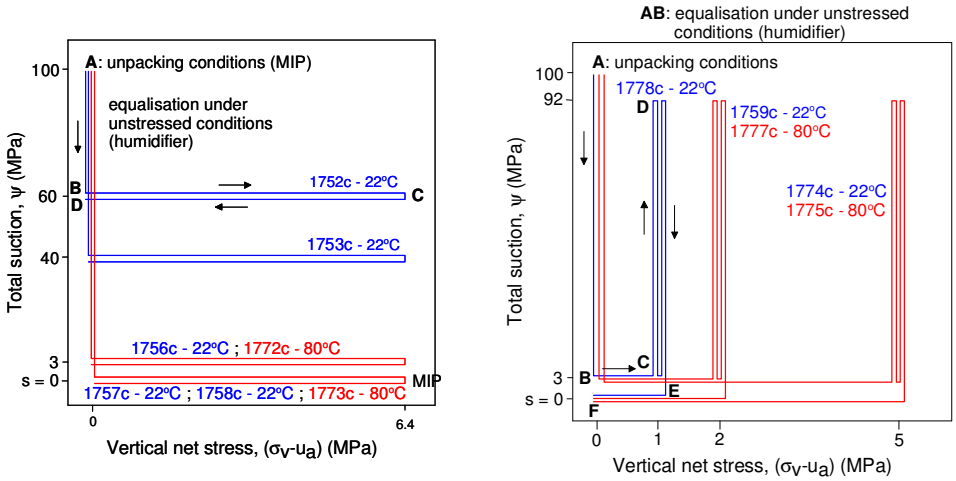

Figure A4-9: Controlled suction level paths for odometer tests. Loading/unloading paths (LEFT) and wetting/drying paths (RIGHT).

Loading/unloading paths

Loading/unloading results in terms of variation of volumetric strain with vertical net stress are shown in Figure A4-10. A higher compressibility on loading is systematically observed at lower total suction levels. The compressibility against loading increases continuously with increasing net stress, proving that the transition towards yielded states is a gradual process. The temperature seems to decrease the compressibility (so increasing the stiffness) at a constant suction. This effect of temperature on the compressibility was confirmed by the odometer tests on the exposed material. Figure A4-11 shows that the exposed material presents greater stiffness.

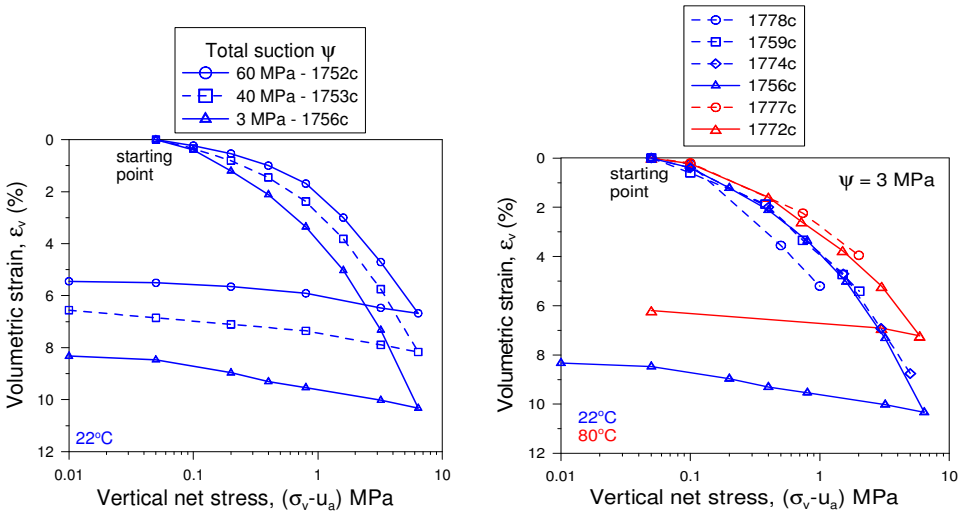

Figure A4-10: Loading/unloading paths at different total suction levels and temperatures.

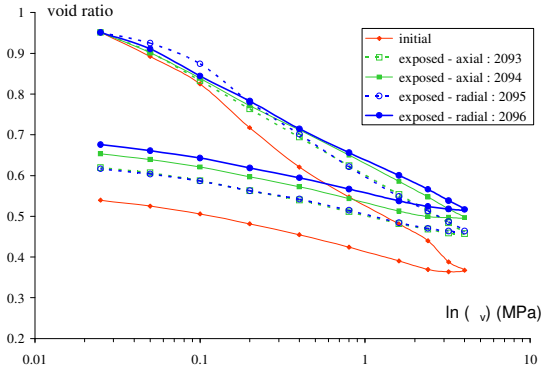

Figure A4-11: Compressibility of initial and exposed materials.

Drying/wetting paths

Volume changes with isothermal drying/wetting cycles under constant applied load and different temperatures are presented in Figure A4-12 (LEFT). The test results indicate that the compressibility for changes in suction decreases considerably with the increase of applied net vertical stress. The overall variation pattern of the compressibility parameter for suction changes, defined as $de/\delta ln(\psi+u_{atm})$, where e is the void ratio and u_{atm} the atmospheric pressure, in function of the applied vertical stress is shown in Figure A4-12 (RIGHT). Temperature

effects are not clearly identified, but they seem to be reflected in a slightly higher stiffness under smaller applied stresses.

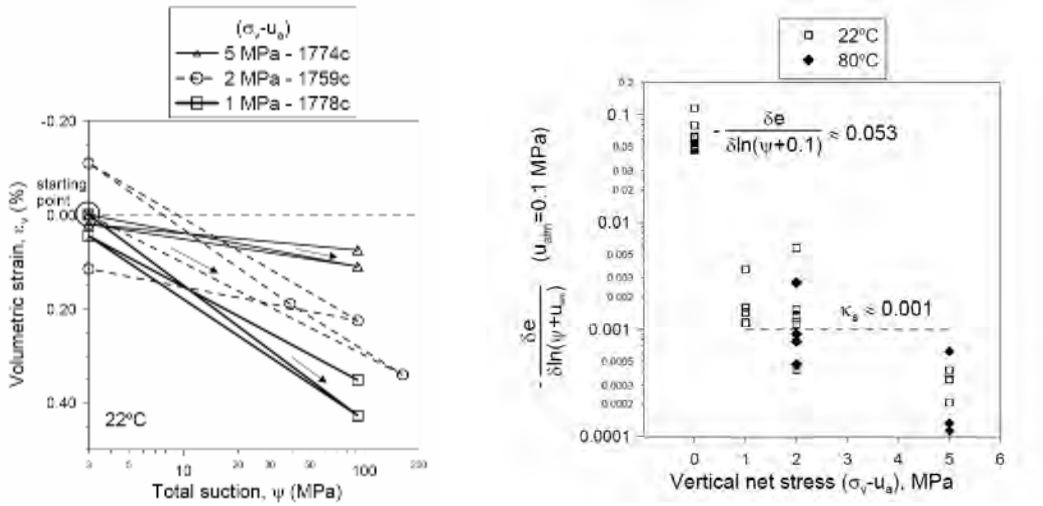

Figure A4-12: Drying/wetting results at different vertical net stresses and temperatures. The LEFT figure represents the volume changes while the RIGHT figure represents the compressibility parameters for suction changes.

Zone of potential collapse on wetting

The loading/unloading curves shown in Figure A4-10 display clear irreversible features, a yield stress under saturated conditions of approximately 0.4 MPa was identified at 22°C, and a slightly lower value of 0.3 MPa at 80°C, which are very low values for such a highly compacted material. The yielding stresses determined at different suction levels and temperatures plotted on a net stresses-suction level plane define the Loading Collapse (LC) yielding curve which is illustrated in Figure A4-13. Interpretation of the observed (very) low yielding stresses requires advanced constitutive frameworks: a double structure model (Alonso et al. 1990, Alonso et al. 1999). The temperature effect on the yielding stresses has been incorporated in Figure A4-13. The reduction of the yielding stresses with the temperature is due to thermal softening (Hueckel & Borsetto 1990).

According to the BBM conceptual model (Alonso et al. 1990), the activation of the LC on wetting allows the reproduction of the occurrence of irreversible collapse strains when suction decreases at high confining stresses. As shown in Figure A4-13, maximum efficiency in generating collapse is concentrated in the zone in which the LC curve is very sensitive to suction changes ($\psi < 3$ MPa). Suction reduction paths in the range $\psi > 3$ MPa cannot drag the curve and induce the occurrence of irreversible collapse strains. For the estimated LC yield locus for the as-compacted state, which was positioned to match the static compaction stress, collapse will probably occur for (σv-ua) > 2 MPa and $\psi < 3$ MPa. The continual decreasing of the swelling pressure observed in the mock-up was probably due to this collapse behaviour of the buffer material.

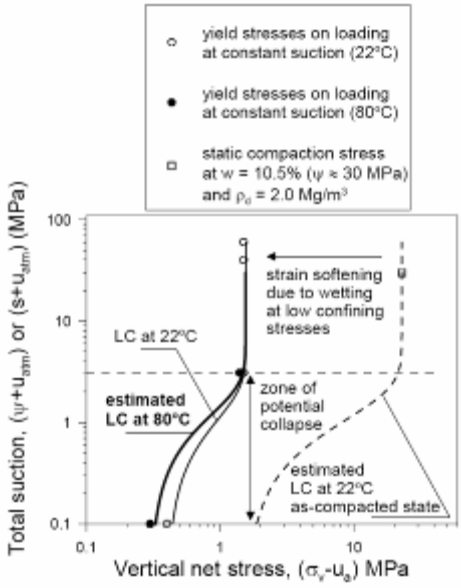

Figure A4-13: Loading/collapse yield locus for different temperatures.

Results of the suction controlled triaxial tests

The purpose of the triaxial tests was to study the variation of the shear strength parameters at different suction levels (apparent cohesion and angle of friction), as well as the change in the stiffness of the material at different suction levels and confining stresses. Attention was also focused on the volume change response (contraction/dilatation) during shearing at different suction levels and confining stresses.

The controlled suction triaxial cell is illustrated in Figure A4-14. Combined axis translation (for low suction levels) and vapour equilibrium techniques (for higher suction levels) were used to control the suction level.

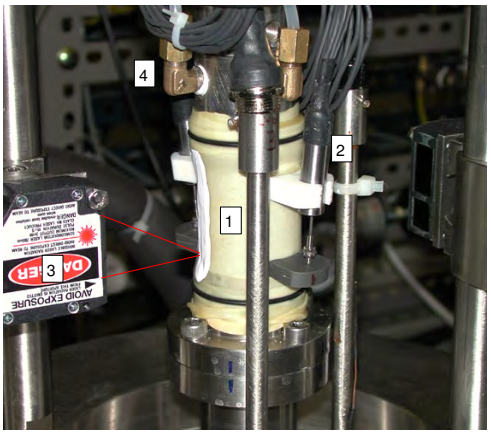

1: specimen ϕ38 mm – h38 mm

2: LVDT (axial)

3: electro-optical laser system (radial)

4: air, vapor and water pressure lines

Figure A4-14: Controlled suction triaxial cell.

Figure A4-15 TOP and BOTTOM LEFT shows a deviator stress q versus axial ε_1 or shear ε_s strain for specimens at various suction levels (total suctions ψ = 60 and 20 MPa, and matric suctions s = 0.3 and 0 MPa) and initial isotropic net stresses (varying from p_0 = 0 to 2 MPa). The peak strength envelope and parameters are presented in Figure A4-15 BOTTOM RIGHT. The shear strength clearly increases with the suction level.

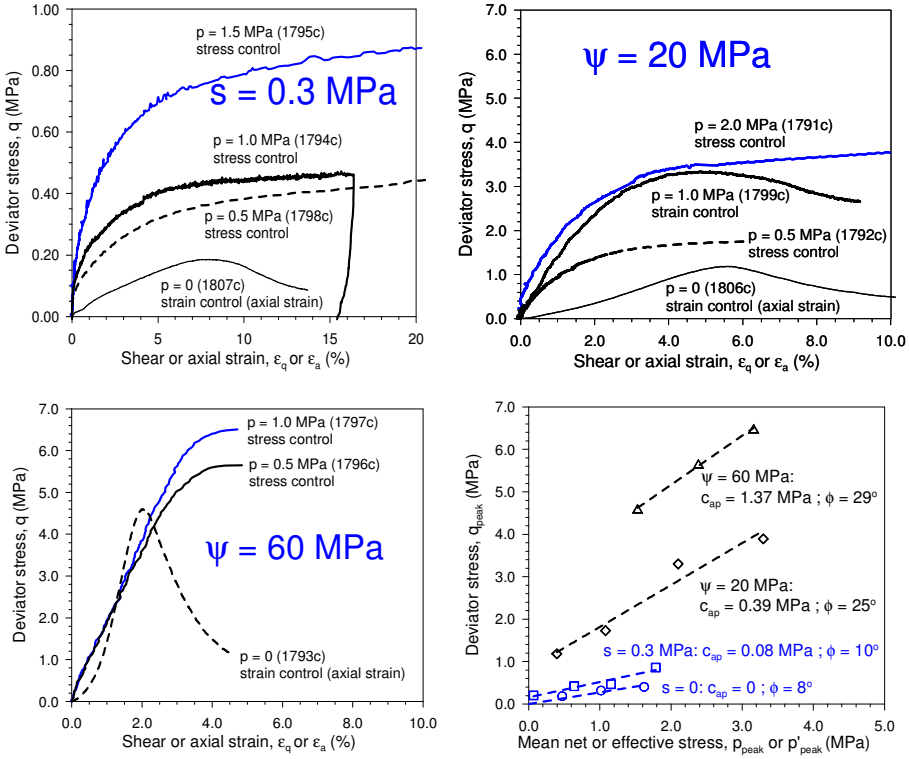

Figure A4-15: Stress-strain curves at different suction levels (TOP and BOTTOM LEFT). Peak strength envelopes at varying suction levels (BOTTOM RIGHT)

Another parameter of interest is the axial stiffness measured for different combinations of confining pressures and suctions. From the stress-strain curves, the Young's modulus was calculated as a secant value E = Δq/Δεa, where εa is the axial strain. Secant modulus measured from the beginning of shearing to 0.05 and 0.10 % axial strain were plotted against the initial mean net stress p0 and at different suction levels in Figure A4-16. The relationship largely depends on the confining pressure. Increasing suction levels also have a significant impact on the stiffness of the material, but there seems to be a leveling off where the stiffness becomes more or less constant at values of $\psi \geq 20$ MPa.

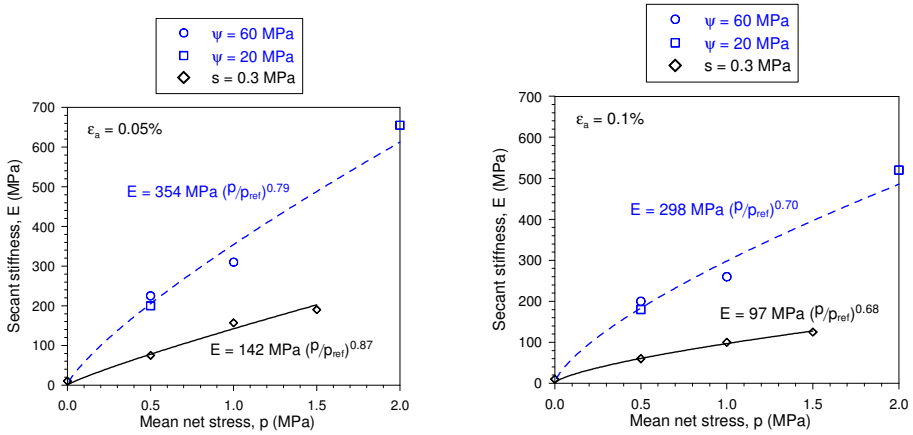

Figure A4-16: Secant stiffness on axial compression at different axial deformations.

References

Chapter 1

ONDRAF/NIRAS (2001), SAFIR-2, Safety Assessment and Feasibility Interim Report 2, Report NIROND 2001-06E.

Chapter 2

ONDRAF/NIRAS (1997), The PRACLAY Demonstration Test, Report NIROND 97-06, Brussels, June 1997.

Chapter 3

Aerts, K. (1997), Constructiedossier, reference manufacturer WN8273, COEK Engineering N.V., Geel, Belgium.

Bergmans G. (1996), Technische Specificatie, internal note ST25236, SCK•CEN, Mol, Belgium.

Brosemer D., Verstricht J. & Bergmans G. (1996), PRACLAY – Prijsaanvraag van 12.02.1996 voor het vervaardigen van het drukvat van de PRACLAY-maquette – Proces-verbaal van het onderzoek van de offertes, internal note 96/DBr/av/N-023 B, EIG PRACLAY, Mol, Belgium.

Dereeper, B. (1998), Project PRACLAY: Tracing and isolation of the mock-up, Technical Note 1998/C073068/BDe/N-54, SCK•CEN, Mol, Belgium.

Van Cauteren L. (1996), Aims of the PRACLAY mock-up, ONDRAF/NIRAS, Note 96-0225, Brussels, January 1996.

Verstricht J. (1995), PRACLAY Mock-up – Concept and Instrumentation, internal report 95/C073060/JV/mvo/R-148, SCK•CEN, Mol, November 1995.

Verstricht J. & Dereeper B. (1999), Project PRACLAY - Mock-up Ophelie: technical specifications, Topical report, SCK•CEN report R-3312, Mol, February 1999.

Chapter 4

Dardaine M., Lajudie A. & Zingarelli V. (1994), Essai de démonstration PRACLAY : 1ère phase – Rapport final. Rapport Technique RT DESD/94.114, CEA, April 1994.

Dardaine M., Mesbah A., Gatabin C. & Zingarelli V. (1996), Essai de démonstration PRACLAY : 2eme phase – Rapport final. Rapport Technique RT DESD/96.139, CEA, Mars 1996.

Dardaine M. & Gatabin C. (1996), Maquette destinée à l'étude du comportement initial de la barrière ouvragée après remplissage des vides d'assemblages. Projet PRACLAY – Phase 3. Note Technique N.T. SESD/96.53, CEA Saclay, Gif-sur-Yvette, December 1996.

Gatabin C. & Dardaine M. (1997) Projet PRACLAY - Fabrication de la Barrière Ouvragée destinée à la maquette OPHELIE. Procès-Verbal d'essais SESD-97.01.01, CEA, Gif-sur-Yvette, France.

Gatabin C. & Rodrigues S. (1999) Projet PRACLAY, maquette OPHELIE : Données complémentaires concernant la barrière ouvragée. Note Technique SESD-99-56, CEA, Gif-sur-Yvette, France.

Neerdael, B., Meynendonckx, P., Voet, M. The Bacchus backfill experiment at the Hades underground research facility at Mol, Belgium (Bacchus 1), Final Report, European Commission, EUR 14155 EN, 1992

ONDRAF/NIRAS (1991b), The PRACLAY Demonstration Test – Scope and Status, Report NIROND 91-10, Brussels, November 1991.

Van Cauteren, L. & Van Miegroet J. (1995), Internal Note. ref. JMG/BG/94-7829/7830 from 15 Sept 1995. ONDRAF/NIRAS, Brussels.

Van Miegroet, J., Matériaux de remblayage et d'obturation pour l'évacuation géologique / discussion et recommandations. Internal note 91-0311, ONDRAF/NIRAS, April 1991.

Chapter 5

Dereeper B. (1998, a). Project PRACLAY : Mock-up interim thermal pulses report. Note 1998/C073068/BDe/N-43, SCK•CEN, Mol, March 1998.

Dereeper B. (1998, b). Project PRACLAY - mock-up interim report: Starting of the heating phase. Note 1998/C073068/BDe/N-91, SCK•CEN, Mol, October 1998.

Dereeper B., Verstricht J. (2000 a), The PRACLAY project – Mock-up OPHELIE: data report Dec. 1997 – Dec. 1998, Progress report, ESV PRACLAY GIE report BD/00-165, Mol, February 2000.

Dereeper B., Verstricht J., De Cannière P., Kursten B. (2000 b), The PRACLAY project – Mock-up OPHELIE: data report Jan. 1999 – Jun. 2000, Progress report, ESV PRACLAY GIE report BD/00-351, Mol, November 2000.

Dierckx, A. (1997), Recipe for Boom Clay water, SCK•CEN, Mol, Belgium.

Noynaert L., Beaufays R., Labat S., Meynendonckx P. and Verstricht J., "Projet PRACLAY - Rapport Instrumentation", SCK•CEN report R-2899, 1991.

Verstricht, J. (1996), Mock-up " Ophelie" - Measurement of strains on the confining structure and on the bolts, Technical Report 96/C0730760/JV/mvg/R-95, SCK•CEN, Mol, Belgium.

Verstricht J. (1998 a). Project PRACLAY : Mock-up – interim hydration report. Note 98/C073068/JVe//N-33, SCK•CEN, Mol, March 1998.

Verstricht J. (1998 b). Maquette "Ophelie" – uitwendige verwarming van de maquette. Note 98/C073068/JVe/mvg/N-94, SCK•CEN, Mol, October 1998.

Chapter 6

Dereeper B., Verstricht J., De Bruyn D., Moerkens K., De Cannière P., Kursten B., and Gens R. (2001a) PRACLAY project – Mock-up OPHELIE: dismantling (version 0). ESV EURIDICE GIE report BD/01-230, Mol (Belgium), April 2001.

Dereeper B., Verstricht J., Li X.L., De Bruyn D., Moerkens K., De Cannière P., Kursten B., and Gens R. (2001b) PRACLAY project – Mock-up OPHELIE: dismantling (version 1). ESV EURIDICE GIE report BD/01-230, Mol (Belgium), October 2001.

Dereeper B., Verstricht J., Li X.L., Moerkens K., De Cannière P., Kursten B., and Gens R. (2002) PRACLAY project – Mock-up OPHELIE: dismantling (version 2). ESV EURIDICE GIE report BD/01-230, Mol (Belgium), April 2002.

ONDRAF/NIRAS (2003). EBS architecture for disposal of Cat. B and C waste in Boom Clay. Progress report on activities between October 1st 2001 and December 31st 2002. Report NIROND 2003-01, Brussels (Belgium), February 2003.

Chapter 7

Raynal J. et Jullien M. (2002). Projet PRACLAY: Expertise minéralogique de la maquette Ophélie, compte rendu du démantèlement, parts 1 and 2 (pictures). Note Technique NT SAMRA 02-056. CEA Centre de Cadarache, Saint-Paul-Lez-Durance (France), Decembre 2002.

Chapter 8

Beaucaire C. et Pitsch H. (2003). Compte rendu succinct d'observations microscopiques faite après le démantèlement de la maquette Ophélie: présence de sulfures de fer. IRSN (France).

Jullien M., Pozo C., Latrille C., Papillon F., Gatabin C., Habert B., Raynal J., Poinssot C., Bataillon C. (2000). Evolution d'une barrière ouvragée sous gradient thermique, expérience in-situ de Stripa, comportement du fer et du silicium dans l'argile FoCa. Note technique CEA NT SESD 99-49.

Karnland O., Sandén T., Johannesson L-E., Eriksen T.E., Jansson M., Wold S., Pedersen K., Motamedi M., and Rosborg B. (2000). Long-term test of buffer material. Final report on the pilot parcels. SKB TR-00-22. Swedish Nuclear Fuel and Waste Management Co., Stockholm, Sweden.

Poinssot C., Jullien M., and Pozo C. (1997a). Du gradient thermique comme moteur de la migration et des transformations minéralogiques. Rapport Scientifique du CEA, Direction du Cycle du Combustible, CEA-R-5801, 196-203.

Poinssot C., Toulhoat P., and Goffe B. (1997b). The influence of thermal gradients on the long-term evolution of the near-field environment of high-level nuclear wastes disposal. 21st Material Research Society Symposium, Davos. 506, 431-438.

Pozo C., Jullien M., Poinssot C. (1997). Evolution of an engineered barrier under thermal gradient during the Stripa experiments: influence of the clay texture on the element transfers. 21st Material Research Society Symposium, Davos.

Pozo C. et Petronin J.-C. (2003). Projet PRACLAY – Expertise microscopique de la maquette Ophélie: caractérisation des interfaces entre matériaux d'un anneau représentatif. Note Technique NT SAMRA 03-043. CEA Centre de Cadarache, Saint-Paul-Lez-Durance (France),

Raynal J. et Jullien M. (2001). Projet PRACLAY. Démantèlement de la maquette Ophélie: caractérisation du matériau initial. Note Technique NT SAMRA 01-0056. CEA Centre de Cadarache, Saint-Paul-Lez-Durance (France),

Raynal J. et Petronin J.-C. (2003). Projet PRACLAY – Expertise minéralogique de la maquette Ophélie: caractérisation d'un anneau représentatif. Note Technique NT SAMRA 03-045. CEA Centre de Cadarache, Saint-Paul-Lez-Durance (France),

Chapter 9

Battaglia F. (2004) Pore water Chemistry (PC) experiment: microbial and particle characterisation in the borehole water. BRGM/RP-52226-FR. Public document with restricted access. TN 2003-23. BRGM. Jan 04. TN2003_23.pdf.

Beaucaire (2003) Short report on the preliminary results obtained by scanning electron microscopy (SEM) on the buffer materials exposed to 5 years heating inside the OPHELIE mock-up. Mention of the presence of small neoformed pyrite crystals. IRSN Report.

Brock T.D., Madigan M.T., Martinko J.M., and Parker J. (1997) Brock Biology of microorganisms. 986 pp. Eight Edition. International edition. Prentice Hall International, Inc. ISBN 0-13-571225-4. See p. 555: A focus on microbial file deep underground.; p. 573: section 14.15 Biogeochemical cycles: sulfur; and p. 575: section 14.16 Biogeochemical cycles: iron.

Cave M.R., Reeder S., Entwistle D.C., Blackwell P.A., Trick J.K., Wragg J., and Burden S.R. (1998) Extraction and analysis of pore-waters from bentonite clay. Technical Report No. WI/98/9C, British Geological Survey, Keyworth, Nottingham.

Charlton B.D., Reeder S., Entwisle D.C., Cave M.R., Shaw R., and Taylor H. (2004) Extraction and characterisation of interstitial pore-waters from SCK/CEN OPHELIE mock-up. British Geological Survey, Keyworth, Nottingham. Commissioned Report CR/04/001. 17 pp.

Cross M.M., Manning D.A.C., Champness P.E., Worden R.H. and Bottrell S.H. (1998) Experimental and isotopic determination of the kinetics and mechanisms of Thermochemical Sulphate Reduction (TSR) reactions at reservoir conditions of pressure and temperature. Mineralogical Magazine 62A, Part 1, 358-359. Goldsmidth Conference, 1998, Toulouse.

Cross M.M., Manning D.A.C., Bottrell S.H. and Worden R.H. (2000) Experimental determination of the rates and mechanisms of Thermochemical Sulphate Reduction (TSR). Journal of Conference Abstracts 5 (1), 26. EMPG VIII Conference, Bergamo, Italy.

Cross, M. M., Manning, D. A. C., Bottrell, S. H. and Worden, R. H. (2004). Thermochemical sulphate reduction (TSR): experimental determination of reaction kinetics and implications of the observed reaction rates for petroleum reservoirs. Organic Geochemistry 35(4), 393-404.

Daumas S. (2000) Report on the microbial characterisation of the Ophélie mock-up: water samples. Unpublished results.

Daumas S. (2003) Report on the microbial characterisation of the Ophélie mock-up: solid samples. Unpublished results.

Daumas S. (2004) Pore water Chemistry (PC) experiment: microbial and technical assistance and initial characterisation of the Opalinus Clay. Field report. Field campaign from 16 to 25 February 2004. Assistance microbiologique lors de l'expérimentation PC-C: Caractérisation initiale de l'argile (report written in French/English). TN 2004-21 PC-C. CFG Services. Sep 04 TN2004_21.pdf.

De Boever P. (2003a) Preliminary microbiological observations done at SCK/CEN with the OPHELIE backfill samples from section 4 and 32. Progress report, January 2003. SCK•CEN inner report, unpublished document.

De Boever P. (2003b) Enrichment and identification of microorganisms surviving in clay blocks whether after presence in the OPHELIE mock-up or not. Progress report, August 2003. SCK•CEN inner report, unpublished document.

De Boever P. (2004) Microbiological analyses performed in the frame of the dismantlement of the OPHELIE mock-up. Progress report, March 2004. SCK•CEN inner report, unpublished document.

De Boever P., Willekens M., Coninx I. and Mergeay M. (2004) Ophelie dismantlement: microbiological investigations. Analyses performed at SCK•CEN. Presentation made at the Ophelie Day on June 10th, 2004. SCK•CEN inner presentation, unpublished document.

Deniau I. (2002) Caractérisation géochimique du kérogène associé à l'argile de Boom (Mol, Belgique) et évolution sous divers stress thermiques, 213 pp. Thèse. Université Paris VI.

Deniau I. (2004) Étude cinétique et moléculaire des produits gazeux et liquides générés par la matière organique insoluble de l'argile de Boom sous divers stress thermiques. Rapport de synthèse, IRSN, Janvier 2003 – Décembre 2004, 50 pp.

Deniau I., Derenne S., Beaucaire C., Pitsch H., and Largeau C. (2001) Morphological and chemical features of a kerogen from the underground Mol laboratory (Boom Clay Formation, Oligocene, Belgium): structure, source organisms and formation pathways. Organic Geochemistry 32, 1343-1356.

Deniau I., Derenne S., Beaucaire C., Pitsch H., and Largeau C. (2004) Occurrence and nature of thermolabile compounds in the Boom Clay kerogen (Oligocene, underground Mol laboratory, Belgium). Organic Geochemistry 35, 91-108.

Deniau I., Derenne S., Beaucaire C., Pitsch H., and Largeau C. (2005a) Simulation of thermal stress influence on the Boom Clay kerogen (Oligocene, Belgium) in relation with long-term storage of high activity nuclear waste. I – Study of generated soluble compounds. Applied Geochemistry 20, 587-597.

Deniau I., Behar F., Largeau C., De Cannière P., Beaucaire C., and Pitsch H. (2005b) Determination of kinetic parameters and simulation of early CO2 production from the Boom Clay kerogen under low thermal stress. Applied Geochemistry 20, 2097-2107.

Deniau I., Lorant F., Pitsch H., De Cannière P., Beaucaire C., Behar F., and Largeau C. (2006) Molecular and kinetic study of gaseous and liquid compounds generated by the insoluble organic matter (kerogen) of the Boom Clay under various thermal stresses. Final report for the post-doc of Isabelle Deniau. Collaboration between IRSN, ENSCP, IFP, and SCK•CEN with the financial support of ONDRAF/NIRAS.

Deniau I., Devol-Brown I., Derenne S., Behar F., Largeau C. (2008) Comparison of the bulk geochemical features and thermal reactivity of kerogens from Mol (Boom Clay), Bure (Callovo–Oxfordian argillite) and Tournemire (Toarcian shales) underground research laboratories. Science of The Total Environment 389(2-3), 475-485. http://dx.doi.org/doi:10.1016/j.scitotenv.2007.09.013.

Dereeper B. and Verstricht J. (2000) The PRACLAY project – Mock-up OPHELIE: data report Dec. 1997 – Dec. 1998. Progress report, ESV PRACLAY GIE report BD/00-165, Mol, February 2000.

Dereeper B., Verstricht J., De Cannière P., and Kursten B. (2000) The PRACLAY project – Mock-up OPHELIE: data report Jan. 1999 – Jun. 2000. Progress report, ESV PRACLAY GIE report BD/00-351, Mol (Belgium), November 2000. 35 pp.

Descostes M. (2001) Evaluation d'une perturbation oxydante en milieu argileux: Mécanisme d'oxydation de la pyrite. Thèse Université Denis Diderot Paris VII.

Descostes M. et Meier P. (2002) Détermination de la spéciation aqueuse du soufre dans les échantillons provenant de la maquette OPHELIE. Rapport CEA/DEN/DPC/SCPA 2002-35, 20 pp. (report on the analyses of sulfides from the OPHELIE mock-up (capillary electrophoresis, CEA), in French).

Jockwer N. (2002) Analyses of dissolved gases in the water of the OPHELIE mock-up. Microsoft Excel 97 spreadsheet attached to an email sent by Norbert Jockwer on Friday, September 27, 2002 1:51 pm [mailto:joc@grs.de] to Jan Verstricht. Subject: analyses of the dissolved gases.

Jørgensen B.B., Isaksen M.F., Jannasch H.W. (1992) Bacterial sulfate reduction above 100 °C in deep sea hydrothermal vent sediments. Science 258, 1756-1757.

Jullien M., Pozo C., Poinssot C., and Tessier D. (1997) Texture influence on mass transfers and alteration processes in clay barrier. 11th International Clay Conference, Ottawa, 1, A41.

Jullien M., Pozo C., Latrille C., Papillon F., Gatabin C., Habert B., Raynal J., Poinssot C., Bataillon C. (2000) Evolution d'une barrière ouvragée sous gradient thermique, expérience in-situ de Stripa, comportement du fer et du silicium dans l'argile FoCa. Note technique CEA NT SESD 99-49.

King F. and Stroes-Gascoyne S. (1995) Microbially influenced corrosion of nuclear fuel waste containers. In: Proceedings of the 1995 International Conference on Microbially Influenced Corrosion, New Orleans, LA, (May 8-10, 1995).

King F., Kolar M., Stroes-Gascoyne S., Bellingham P., Chu J. and Dawe P.V. (1999) Modelling the activity of sulphate-reducing bacteria and the effects on container corrosion in an underground nuclear waste disposal vault. In: Materials Research Society Symposium Proceedings 556, 1167-1174.

Kjartanson B.H., Stroes-Gascoyne S. and Dixon D.A. (2003) Microbe viability and activity in bentonite-based barriers. Proc. 56th Annual Canadian Geotechnical Conference and 4th Joint IAH-CNC and CGS Groundwater Specialty Conference (Sept. 28-Oct. 1, 2003, Winnipeg).

Kursten B. (2004) Ophelie: analyses of the metallic components. Contribution to the final report of the OPHELIE mock-up. June 2004. 225 pp.

Laitinen T. (2000) Localized corrosion of stainless steel in chloride, sulfate and thiosulfate containing environments. Corrosion Science 42, 421–441.

Lajudie A., Raynal J., Petit J.C., and Toulhoat P. (1995) Clay-based materials for engineered barriers: a review. Scientific Basis for Nuclear Waste Management XVIII, Symposium held October 23–27, 1994, Kyoto, Japan. Materials Research Society Symposium Proceedings 353, 221–230. See p. 223, Table 1: mineralogical composition of the different clays (in %).

Lorant F., Largeau C., Behar F., and De Cannière P. (2008) Improved kinetic modeling of the early generation of CO2 from the Boom Clay kerogen. Implications for simulation of CO2 production upon disposal of high-activity nuclear waste. Organic Geochemistry. Accepted, in press.

Motellier S., Gurdale K. and Pitsch H. (1997) Sulfur speciation by capillary electrophoresis with indirect spectrophotometric detection: in search of a suitable carrier electrolyte to maximize sensitivity. Journal of Chromatography A, 770, pp 311-319.

Motellier S. and Descostes M. (2001) Sulfur speciation and tetrathionate sulfitolysis monitoring by capillary electrophoresis. Journal of Chromatography A, 907, pp 329-335.

Naud J. (2000a) Results of X-ray diffraction analyses made on a grey precipitate isolated from water contained in a plastic tubing connected to the hydration system of the OPHELIE mock-up. Evidence of ZnS (wurtzite). Université Catholique de Louvain (UCL). Analysis report made in September 2000.

Naud (2000b) X-ray diffraction analyses of graphite entering the composition of the M 2 mixture used as buffer material for the OPHELIE mock-up.

Newman R.C., Isaacs H.S., and Alman B. (1982) Effects of sulfur compounds on the pitting behaviour of type 304 stainless steel in near-neutral chloride solutions. Corrosion 38(5), 261-265.

Noynaert L., Volckaert G., De Cannière P., Meynendonckx P., Labat S., Beaufays R., Put M., Aertsens M., Fonteyne A., Vandervoort F. (1998a) The Cerberus Project. A demonstration test to study the near-field effects of an HLW canister in an argillaceous formation. 146 pp. Work carried out under a cost-sharing contract with the European Commission, Nuclear Science and Technology, 4th Framework Program (1990-1994) under contract N° FI2W-CT90-0003B. Final report EUR 18 151 EN.

Noynaert L., Volckaert G., De Cannière P., Van Iseghem P., Kursten B., Sneyers A., Put M., Wang L., Aertsens M., Meynendonckx P., Fonteyne A., Labat S., Vercauter R., Vandervoort F., and Beaufays R. (1998b) The Cerberus Project. A demonstration test to study the near-field effects of a HLW-canister in an argillaceous formation. 168 pp. Final report for the period November 1, 1986 – June 30, 1998. Design Specification 1.2. This study has been performed under cost-sharing contract as part of NIRAS/ONDRAF and of the European Atomic Energy Community's programme on "Management and storage of radioactive waste". SCK•CEN report R-3293. July 1998.

Noynaert L., De Cannière P., De Bruyn D., Volckaert G., Put M., Kursten B., Sneyers A., Van Iseghem P., Beaucaire C., Pitsch H., Bouchet A., Parneix J.C., Samper J., Delgado J., Navarro V., Montenegro L., and Zhang G. (2000) Cerberus project: study of the effect of heat and radiation on the near field of a HLW or spent fuel repository in a clay formation. 160 pp. Work carried out under a cost-sharing contract with the European Commission, Nuclear Science and Technology, 4th Framework Program (1994-1998) under contract N° FI4W-CT95-0008. Final report EUR 19125 EN.

Pedersen, K. (1997). Microbial life in deep granitic rock. FEMS Microbiology Reviews, 20(3), 399-414.

Pedersen, K. (1999). Subterranean microorganisms and radioactive waste disposal in Sweden. Engineering Geology, 52(3-4), 163-176.

Pitsch H. (2005) pCO2 calculations for the organic matter exposed to the thermal stress of the Cerberus experiment. PowerPoint slides in annex to the mission report 04/PDC/R-96 of De Cannière P. et al. on: "Effect of a thermal stress on Boom Clay organic matter. Post-doc of Isabelle Deniau (ENSCP, Paris, Fr). Final meeting held in Brussels on Fri 2004-Nov-19". Kinetic and molecular study of gaseous (CO2) and liquid products generated by the insoluble organic matter of Boom Clay under various thermal stresses. PPT Slides filename: Final_Meeting_IDE_19-11-04_H_Pitsch_Cerberus.ppt.

Pitsch H., Beaucaire C., Béhar F., Lorant F., Deniau I., Largeau C., De Cannière P., and Van Geet M. (2007) Modelling pH evolution in Boom Clay pore water during in-situ heating. In:

Proceedings of the Twelfth International Symposium on Water-Rock Interaction (WRI-12) held at Kunming (Yunnan province, Popular Republic of China) from July 31 to August 05, 2007. http://www.wri12.org/. 4 pp.

Poinssot C., Jullien M., and Pozo C. (1997a) Du gradient thermique comme moteur de la migration et des transformations minéralogiques. Rapport Scientifique du CEA, Direction du Cycle du Combustible, CEA-R-5801, 196-203.

Poinssot C., Toulhoat P., and Goffe B. (1997b) The influence of thermal gradients on the long-term evolution of the near-field environment of high-level nuclear wastes disposal. 21st Material Research Society Symposium, Davos. 506, 431-438.

Pozo C., Jullien M., Poinssot C. (1997). Evolution of an engineered barrier under thermal gradient during the Stripa experiments: influence of the clay texture on the element transfers. 21st Material Research Society Symposium, Davos.

Poulain S. (2006) Caractérisation microbiologique de l'argile à Opalinus du Mont Terri et de l'argilite du Callovo-Oxfordien de Meuse/Haute-Marne. Thesis University of Bordeaux I, (FORPRO n°2006/18).

Poulain S., Sergeant C., Le Marrec C., Simonoff M., and Altmann S. (2007a) Opalinus Clay, an argillaceous formation under evaluation for radioactive waste repository, contains viable, potentially ancient microbial cells. Submitted to Environmental Microbiology (FORPRO n°2006/17 A).

Poulain S., Sergeant C., Le Marrec C., Vesvres M.-H., Vinsot A., Dewonck S., Simonoff M., and Altmann S. (2007b) Autochthonous and colonizing microorganisms in argillaceous underground environments. [Oral presentation: O/09/1]. In Proceedings of: Clays in natural and engineered barriers for radioactive waste confinement – Lille 2007 – 3rd International Meeting. Organised by Andra in Lille (France), 17 – 20 September 2007.

Pourbaix A. (2002) Analyse de prélèvements « Ophélie » et de solutions témoins (sulfures, thiosulfates et sulfites). Rapport Cebelcor co296501ap. Objet: Co.2965. Votre Commande n°2002/000028601. 3 pages sans l'annexe avec le rapport du Professeur Guy Schmitz du 23 août 2002. Première analyse.

Pourbaix A. (2003) Analyse d'un échantillon d'eau pour les sulfures, thiosulfates, sulfites et sulfates par polarographie, chromatographie d'ions et iodométrie. Référence de l'échantillon: PCW/2002-02-23. Praclay mock-up hydration tube #4, valve open. Quantity ~ 1 L. DOC, VITO. Rapport Cebelcor co296503ap. Objet: Co.2965. Votre Commande n°2003/000031607 du 3 mars 2003. 3 pages sans l'annexe avec le rapport du Professeur Guy Schmitz du 26 février 2003. Seconde analyse.

Raynal J. et Petronin J.-C. (2003). Projet PRACLAY – Expertise minéralogique de la maquette Ophélie: caractérisation d'un anneau représentatif. Note Technique NT SAMRA 03-045. CEA Centre de Cadarache, Saint-Paul-Lez-Durance (France),

SAFIR 2 Report (2001) coordinated by De Preter P., Lalieux P. and Cool W. (eds.) SAFIR 2 Report, Safety Assessment and Feasibility Interim Report 2. Four volumes, 13 chapters. ONDRAF/NIRAS, Belgian Agency for Radioactive Waste and Enriched Fissile Materials. NIROND 2001-06 E. December 2001.

Schmitz G. (2002) Report on the analyses of sulfides from the OPHELIE mock-up (polarography made at ULB on 23-Aug-2002). Appendix to Pourbaix A. (2002) Rapport Cebelcor co296501ap. Objet: Co.2965. Analyse de prélèvements « Ophélie » et de solutions témoins (sulfures, thiosulfates et sulfites). Votre Commande n°2002/000028601. Première analyse.

Schmitz G. (2003) Report on the analyses of sulfides from the OPHELIE mock-up (polarography, ion chromatography, and iodometry made at ULB on 26-Feb-2003). Appendix to Pourbaix A. (2003) Rapport Cebelcor co296503ap. Objet: Co.2965. Analyse d'un échantillon d'eau pour les sulfures, thiosulfates, sulfites et sulfates par polarographie, chromatographie d'ions et iodométrie. Référence de l'échantillon: PCW/2002-02-23. Praclay mock-up hydration tube #4, valve open. Quantity ~ 1 L. DOC, VITO. Votre Commande n°2003/000031607 du 3 mars 2003. Seconde analyse.

Starosvetsky D., Khaselev O., Starosvetsky J., Armon R., and Yahalom J. (2000) Effect of iron exposure in SRB media on pitting initiation. Corrosion Science 42, 345–359.

Stroes-Gascoyne S., Pedersen K. and Daumas S. (1996) Factors controlling survival of the microbial population naturally present in clay-based buffer materials under simulated repository conditions. In: Proceedings of the International Conference on Deep Geological Disposal of Radioactive Waste, Winnipeg, MB, (September 13-19, 1996).

Stroes-Gascoyne S., Pedersen K., Daumas S., Hamon C., Haveman S., Delaney T., Ekendahl S., Arlinger J., Hallbeck L. and Dekeyster K. (1996) Microbial analysis of the buffer/ container experiment at AECL's underground research laboratory. Atomic Energy of Canada Limited Report, AECL-11436, COG-95-446.

Stroes-Gascoyne S., Pedersen K., Hamon C., Haveman S., Delaney T., Ekendahl S., Arlinger J., Hallbeck L. and Dekeyster K. (1996) Microbial analysis of the buffer/container experiment at AECL's underground research laboratory. Swedish Nuclear Fuel and Waste Management CO (SKB), Stockholm, Sweden. SKB TR 96-02.

Stroes-Gascoyne S., Pedersen K., Hamon C., Haveman S., Delaney T., Ekendahl S., Arlinger J., Hallbeck L. and Dekeyster K. (1996) Microbial analysis of the buffer/container experiment at AECL's underground research laboratory. Agence Nationale pour la Gestion des déchets Radioactifs, France, ANDRA C RP 0.AEC 96-001.

Stroes-Gascoyne S., Haveman S.A. and Vilks P. (1997) The change in bioavailability of organic matter associated with clay-based buffer materials as a result of heat and radiation treatment. Materials Research Society Symposium Proceedings 465, 987-994.

Stroes-Gascoyne S. , Pedersen K., Haveman S.A., Daumas S., Hamon C.J., Arlinger J., Ekendahl S., Hallbeck L., Gahroni N., Delaney T.L. and Dekeyser K. (1997) Occurrence and identification of microorganisms in compacted clay-based buffer material designed for use in a nuclear fuel waste disposal vault. Canadian Journal of Microbiology 43, 1133-1146.

Stroes-Gascoyne S. and Sargent F.P. (1998) The Canadian approach to microbial studies in nuclear waste management and disposal. Journal of Contaminant Hydrology 35, 175-190.

Stroes-Gascoyne S., Hamon C.J., Vilks P. and Gierszewski P. (2002) Microbial, redox and organic characteristics of compacted clay-based buffer after 6.5 years of burial at AECL's underground research laboratory. Applied Geochemistry 17, 1287-1303.

Stroes-Gascoyne S. and King F. (2002) Microbially influenced corrosion issues in high-level nuclear waste repositories. In: Proceedings of CORROSION/2002 research Topical Symposium Microbially Influenced Corrosion (B. Little Chair), NACE International, Houston TX.

Stroes-Gascoyne S. (2002) Assessment of the likelihood of significant microbial activity in Opalinus Clay. NAGRA Interner Bericht 02-46 (November 2002).

Stroes-Gascoyne S. (2004) Microbial activity in Opalinus Clay. NAGRA Interner Bericht (Submitted).

Stroes-Gascoyne S., Schwyn B., Schippers A., Poulain S., Sergeant C., Le Marrec C., Simonoff M., Altmann S., Nagaoka T., Mauclaire L., Vasconcelos C., McKenzie J., Daumas S., Vinsot A., Beaucaire C., Matray J.M. (2005) Microbial investigations on unperturbed Opalinus Clay samples. Mont Terri Project Technical Note TN-2004-44. June 2005. 130 pp.

Stroes-Gascoyne S., Hamon C.J., Dixon D.A. and Kjartanson B. (2005) Factors affecting microbial activity in compacted clay-based sealing materials proposed for use in a deep geologic repository for used nuclear fuel. Proceedings CNS Waste Management, Decommissioning and Environmental Restoration Conference, May 8-12, Ottawa, Canada (submitted).

Stroes-Gascoyne S., Schippers A., Schwyn B., Poulain S., Sergeant, C. Simonoff M., Le Marrec C., Altmann S., Nagaoka T., Mauclaire L., McKenzie J., Daumas S., Vinsot A., Beaucaire C., and Matray J.-M. (2007) Microbial community analysis of Opalinus Clay drill core samples from the Mont Terri Underground Research Laboratory, Switzerland. Geomicrobiology Journal 24, 1–17. http://dx.doi.org/doi:10.1080/01490450601134275. ISSN: 0149-0451 print / 1521-0529 online.

Toland W.G. (1960) Oxidation of organic compounds with aqueous sulfate. Journal of the American Chemical Society 82, 1911-1916.

Tromans D. and Frederick L. (1984) Effect of thiosulfate on crevice corrosion of stainless steels. Corrosion 40(12), 633-639.

Trudinger P.A., Chambers L.A. and Smith J.W. (1985) Low-temperature sulfate reduction: biological versus abiological. Canadian Journal of Earth Sciences 22, 1910-1918.

Tuttle R.N., and Kane R.D. (Eds.) (1981) H2S corrosion in oil and gas production: a compilation of classic papers. NACE, Houston, TX.

Valcke E., Smets S., Labat S., Van Iseghem P., Godon N., Jollivet P., Jockwer N., and Wieczorek K. (2004) CORALUS-II. An integrated in-situ corrosion test on α-active HLW glass – phase II. Work carried out under a cost-sharing contract with the European Commission, 5th Euratom Framework Programme 1998-2002, Key Action: Nuclear Fission. Contract N° FIKW-CT-2000-00011. Annual Report for the period: October 1, 2003, to September 30, 2004. SCK•CEN Report R-4069. Final report to the European Commission under preparation.

Vandevelde L. and Thomas P. (2000) Results of chemical analyses made on a grey precipitate isolated from water contained in a plastic tubing connected to the hydration system of the OPHELIE mock-up. Presence of Zn. SCK•CEN. Analysis report made in September 2000.

VITO (2000) Report on the GC-MS analyses of volatile organic Carbon (VOC) from water of the hydration system of the Ophélie mock-up (first analyses of aromatic compounds and MTBE by the LMB team).

VITO (2002) Report on the GC-MS analyses of volatile organic Carbon (VOC) from water of the hydration system of the Ophélie mock-up (last analyses of VOC, just before to open the mock-up by the team of Eddy Goelen, Leef Milieu).

Volckaert G., Bernier F. and Dardaine M. (1996a) Demonstration of the in-situ application of an industrial clay-based backfill material (Démonstration de la mise en place in-situ d'un matériau de remplissage industriel à base d'argile) (Bacchus 2). European Commission, Nuclear Science and Technology, fourth R&D programme on "Management and storage of radioactive waste" (1990-1994), Part B, "Underground laboratories". Contract N° F12W/CT91/0098. Final report EUR 16 860 EN/FR. 213 pp.

Volckaert G., Bernier F., Alonso E., Gens A., Samper J., Villar M., Martin-Martin P.L., Cuevas J., Campos R., Thomas H., Imbert C. and Zingarelli V. (1996b). Thermal-hydraulic-mechanical and geochemical behaviour of the clay barrier in radioactive waste repositories (model development and validation). European Commission, Nuclear Science and Technology, fourth R&D programme entitled "Management and storage of radioactive waste" (1990-1994), Part B, "Underground laboratories". Contract N° FI2W/CT90/0033 and N° FI2W/CT91/0102. Final report EUR 16 744 EN. 772 pp. See particularly: solute movement, pp. 251-253. See also Fig. 2.2.2.2 on p. 274: Final chloride concentration (ppm) in the extract at different levels of the alteration cell in experiments of different duration.

Wersin P., Gautschi A., Vinsot A., De Cannière P., Hernan P., Gäbler H.-E., Hamma K., Mahara Y., Gaucher E. & Pearson F.J. (2004) Results from the Pore water Chemistry (PC) Experiment in Opalinus Clay at Mont Terri, Switzerland. In Proc. 11th Symposium on Water-

Rock Interaction WRI-11, Saratoga Springs, NY, R.B. Wanty & R.R. Seal II (ed.), pp. 523-526.

Wersin P., De Cannière P., Pearson F.J., Gaucher E., Höhener P., Eichinger L., Mettler S., Mäder U., Vinsot A., Gäbler H.-E., Hama K., Hernán P. (2005) Results from an in-situ pore water chemistry experiment in Opalinus Clay: evidence of microbially-mediated anaerobic redox processes. Communication at the 2nd International Meeting on "Clays in Natural and Engineered Barriers for Radioactive Waste Confinement" organised by Andra (Andra 2005 International Meeting held in Tours, France, on 14 – 18 March 2005). Tours 2005 Conference | Abstracts of Tours 2005 Conference.

Worden R.H., Smalley P.C. and Oxtoby N.H. (1995) Gas souring by thermochemical sulfate reduction at 140 °C. American Association of Petroleum Geologist Bulletin 79 (6), 854-863.

Xu Y. and Schoonen M.A.A. (1995) The stability of thiosulphate in the presence of pyrite in low-temperature aqueous solutions. Geochimica et Cosmochimica Acta 59, 4605-4622.

Zucchi F., Trabanelli G., Monticelli C., and Grassi V (2000) SCC inhibition of a C-steel in acidic 5 % NaCl solutions in the presence of thiosulphate. Corrosion Science 42(3), 505-515.

Chapter 10

Kursten, B. (2004). OPHELIE, analyses of the metallic components. Internal report. Euridice, Mol (Belgium), 2004.

Chapter 12

Alonso E.E, Gens A. and Josa A. (1990). A constitutive model for partially saturated soils (BBM). Geotechnique, 40, 3, 405-430, 1990

Charlier R., Schroeder Ch., Illing P. (2003). Laboratory tests on Praclay samples. Triaxial and isotropic tests. Technical report. Université de Liège – GeomaC.

Collin F., Li X.L., Radu J.P. & Charlier R. (2002). Thermo-hydro-mechanical coupling in clay barriers, Engineering Geology 64: pp. 179-193

Dardaine M., Mesbah A., Gatabin C. & Zingarelli V. (1996), Essai de démonstration PRACLAY : 2eme phase – Rapport final. Rapport Technique RT DESD/96.139, CEA, Mars 1996.

Gatabin C., Rodrigues S. (1999) Projet PRACLAY, maquette OPHELIE : Données complémentaires concernant la barrière ouvragée. Note Technique SESD-99-56, CEA, Gif-sur-Yvette, France.

Gatabin C, Touzé G. (2003a). Project PRACLAY, Caracterisation du matériau de remplissage, Note technique N.T. DPC/SCCME 03-246-A. CEA, Gif sur Yvette (France), 2003

Gatabin C., Touzé, G. (2003b). Projet PRACLAY : Démantelement de la maquette OPHELIE - Mesures de la conductivité thermique et de la conductivité hydraulique du matériau exposé. Note Technique N.T. SCCME 03-242-A. CEA, Gif sur Yvette (France), décembre 2003.

Gatabin C., Touzé, Van Ravenstyn L. (2003). PRACALY : démantelement de la maquette ophelie compte-rendu du demantelement et mesures de saturation de la barriere ouvragée Exposée. Note Technique NT-SCCME 03-221 (Indice A). CEA, Gif sur Yvette (France), avril 2003

Huergo (2004). OPHELIE report : odometer tests on 2093c,2094c2095c and 2096c. Rapport d'essais. ULB, Bruxelles (Belgique), 2004

Philip, J.R., de Vries, D.A. (1957). Moisture movement in porous materials under temperature gradients. Trans. Am. Geophys. Un., 38: pp. 222-232.

Romero E. (2004). Controlled-suction triaxial and odometer tests on PRACLAY mixture (project report). Belgium, EIG Euridice, 2004.

Villar M.V., Campos R., Aroz J. (2004). Hydraulic conductivity tests in samples from section 20 of the OPHELIE mock-up. Ciemat report. Madrid (Spain), 2003

Xiangling Li, Verstricht Jan, C. Gatabin, E. Romero (2005). Thermal-hydro-mechanical analysis of the Mock-up OPHELIE- Laboratory characterisation and numerical modelling. EURIDICE report.

Appendix 2

Verstricht J & Bernier F. (1997), Project PRACLAY – Thermal modelling of the mock-up OPHELIE, SCK•CEN report P-25, Mol, February 1997.

Van Cauteren, L. (1990), Temperatuurverdeling rond een bergingsgalerij voor warmteagevend radioactief afval. Internal note ref. 90/174. ONDRAF/NIRAS, March 1990.

Van Cauteren, L. (1991), Bepaling van de temperatuurstijging rond de PRACLAY-galerij. Internal note ref. 91-0036. ONDRAF/NIRAS, January 1991.

Itasca Consulting Group (1995), FLAC – Fast Lagrangian Analysis of Continua, Itasca Consulting Group, Minneapolis (MI), USA, 1995.

Blomberg, T. (1994), HEAT2R - A PC-program for heat conduction in cylindrical coordinates r and z. Department of Building Physics, Lund University, Lund, Sweden, 1994.

Appendix 4

Alonso, E.E, Gens, A. & Josa, A. 1990. "A constitutive model for partially saturated soils". Geotechnique, 40, 3, 405-430.

Alonso, E.E., Vaunat, J., & Gens, A 1999. "Modelling the mechanical behaviour of expansive clays". Engineering Geology, 54, 173-183.

Cave M.R., Reeder S., Entwistle D.C., Blackwell P.A., Trick J.K., Wragg J., and Burden S.R. (1998) Extraction and analysis of pore-waters from bentonite clay. Technical Report No. WI/98/9C, British Geological Survey, Keyworth, Nottingham.

Charlton B.D., Reeder S., Entwisle D.C., Cave M.R., Shaw R., and Taylor H. (2004) Extraction and characterisation of interstitial pore-waters from SCK/CEN OPHELIE mock-up. British Geological Survey, Keyworth, Nottingham. Commissioned Report CR/04/001. 17 pp.

Dardaine M., Mesbah A., Gatabin C. & Zingarelli V. (1996), Essai de démonstration PRACLAY : 2eme phase – Rapport final. Rapport Technique RT DESD/96.139, CEA, Mars 1996.

Dardaine M. and Gatabin C. (1996), Maquette destinée à l'étude du comportement initial de la barrière ouvragée après remplissage des vides d'assemblages. Projet PRACLAY – Phase 3. Note Technique N.T. SESD/96.53, CEA Saclay, Gif-sur-Yvette, December 1996.

Gatabin C. and Rodrigues S. (1999) Projet PRACLAY, maquette OPHELIE : Données complémentaires concernant la barrière ouvragée. Note Technique SESD-99-56, CEA, Gif-sur-Yvette, France.

Gatabin C, and Touzé G. (2003a). Project PRACLAY, Caracterisation du matériau de remplissage, Note technique N.T. DPC/SCCME 03-246-A. CEA, Gif sur Yvette (France), 2003

Gatabin C. and Touzé, G. (2003b). Projet PRACLAY : Démantelement de la maquette OPHELIE - Mesures de la conductivité thermique et de la conductivité hydraulique du matériau exposé. Note Technique N.T. SCCME 03-242-A. CEA, Gif sur Yvette (France), décembre 2003.

Gatabin C., Touzé, Van Ravestyn L. (2003). PRACALY : démantelement de la maquette ophelie compte-rendu du demantelement et mesures de saturation de la barriere ouvragée Exposée. Note Technique NT-SCCME 03-221 (Indice A). CEA, Gif sur Yvette (France), avril 2003

Hueckel T., Borsetto M. (1990). Thermoplasticity of saturated soils and shales: constitutive equations. Journal of Geotechnical Engineering, Vol. 116, 1990.

Huergo (2004). OPHELIE report : odometer tests on 2093c,2094c2095c and 2096c. Rapport d'essai . ULB, Bruxelles (Belgique), 2004

Jullien M., Pozo C., Latrille C., Papillon F., Gatabin C., Habert B., Raynal J., Poinssot C., Bataillon C. (2000) Evolution d'une barrière ouvragée sous gradient thermique, expérience in-situ de Stripa, comportement du fer et du silicium dans l'argile FoCa. Note technique CEA NT SESD 99-49.

Lajudie A., Raynal J., Petit J.C., Toulhoat P. (1995). Clay-based materials for engineered barriers: a review. Scientific Basis for Nuclear Waste Management XVIII, Symposium held

October 23–27, 1994, Kyoto, Japan. Materials Research Society Symposium Proceedings 353, 221–230. See p. 223, Table 1: mineralogical composition of the different clays (in %).

Li, X., Verstricht J., Gatabin C. , Romero E. (2005). Thermal-hydro-mechanical analysis of the Mock-up OPHELIE- Laboratory characterisation and numerical modelling. EURIDICE report.

Nitao J.J. and Bear J. (1996). Potential and their role in transport in porous media. Water Resources Res. 32(2): 225-250

Pozo C. et Petronin J.-C. (2003). Projet PRACLAY – Expertise microscopique de la maquette Ophélie: caractérisation des interfaces entre matériaux d'un anneau représentatif. Note Technique NT SAMRA 03-043. CEA Centre de Cadarache, Saint-Paul-Lez-Durance (France),

Raynal J. et Jullien M. (2001). Projet PRACLAY. Démantèlement de la maquette Ophélie: caractérisation du matériau initial. Note Technique NT SAMRA 01-0056. CEA Centre de Cadarache, Saint-Paul-Lez-Durance (France),

Raynal J. et Petronin J.-C. (2003). Projet PRACLAY – Expertise minéralogique de la maquette Ophélie: caractérisation d'un anneau représentatif. Note Technique NT SAMRA 03-045. CEA Centre de Cadarache, Saint-Paul-Lez-Durance (France),

Romero E. (2004). Controlled-suction triaxial and odometer tests on PRACLAY mixture (project report). Belgium：EIG Euridice，2004.

Villar M.V., Campos R., Aroz J. (2004). Hydraulic conductivity tests in samples from section 20 of the OPHELIE mock-up. Ciemat report. Madrid (Spain), 2003

Woodburn J.A., Holden J, Peter P. (1993). The transistor psychrometer: a new instrument for measuring soil suction. Unsaturated Soils Geotechnical Special Publications Nº 39, Dallas. S.L. Houston and W.K. Wray (eds.), ASCE: 91-102.